Development of Novel Models to Study Sub and Post Cellular Uptake of Drugs Following Oral Administration

by

Malaz Yousef

A thesis submitted in partial fulfillment of the requirements for the degree of

Doctor of Philosophy

in

Pharmaceutical Sciences

Faculty of Pharmacy and Pharmaceutical Sciences

University of Alberta

© Malaz Yousef, 2024

Abstract

Given the numerous benefits of oral administration, this thesis investigates two key phenomena influencing the pharmacokinetics and pharmacodynamics of orally administered active pharmaceutical ingredients (APIs): lysosomal trapping and intestinal lymphatic uptake via chylomicrons, with a particular emphasis on the latter.

The absence of a standardized lysosomal fluid composition in pharmaceutical compendia represents a current gap. To address it, a simulated lysosomal fluid was developed by incorporating essential components necessary for lysosomal homeostasis. This new fluid demonstrated superiority over existing commercial fluids, and that was further evidenced by its performance in a basic model for capturing lysosomal trapping. Consequently, this simulated lysosomal fluid could fill the gap for a standardized lysosomal fluid, making it applicable to various pharmaceutical and biomedical uses.

Certain drugs can be packaged within enterocyte-formed lipoproteins known as chylomicrons, which naturally facilitate the absorption of dietary lipids and their transport through intestinal lymphatic uptake rather than the portal circulation. This pathway is particularly important in the context of current drug delivery efforts, which focus on lipid-based formulations for both traditional and novel applications in medication and vaccination delivery. However, it is generally overlooked and there is a need for a standardized lymphatic fluid and representative *in-vitro* models to investigate and quantify intestinal lymphatic uptake *in-vitro*.

This work advocates for considering the intestinal lymphatic uptake and emphasizes the need for further research to optimize lymphatic drug delivery, particularly via chylomicrons. The development of simulated lymphatic fluids, both general and intestinal, marks an advancement

towards creating a standardized fluid for pharmaceutical research. Moreover, the established *in-vitro* model offers a promising platform for evaluating drug lymphatic uptake. This model successfully differentiated between drugs with varying lymphotropic affinities. Various enhancers and inhibitors were investigated, revealing that lymphatic uptake could be increased or decreased accordingly. Pluronic® L-81, a known inhibitor of chylomicron uptake, exhibited an inhibitory effect, likely through a novel biophysical mechanism. Furthermore, the *in-vitro* data suggested that zeta potential influences intestinal lymphatic uptake, leading to corresponding increases or decreases based on the agent used. These novel finding necessitates further *in-vivo* investigation. The model also examined the effects of food that may stimulate lymphatic uptake, distinguishing between oils containing long-chain fatty acids. However, it did not differentiate between long-chain-rich oils and medium-chain-rich oils in terms of lymphatic uptake. Additionally, in a real-world scenario assessing the impact of excipients through the developed model, the lipid-based excipient Labrafil® 2125 CS exhibited a statistically significant increase in the *in-vitro* uptake of cannflavin A in a novel formulation.

First-generation dissolution models with a focus on lymphatic uptake were also created to evaluate pharmaceutical formulations and identify factors affecting intestinal lymphatic uptake through this pathway. These new models incorporated the lymphatic absorption pathway, previously neglected in all existing dissolution tests. They showed their capacity to distinguish between different lymphotropics. In addition, they proved to be superior to the biphasic dissolution test in assessing lipid solubility related to lymphatic uptake via chylomicrons. This represented an important step towards more accurate performance testing for assessing lymph-targeted formulations and delivery systems.

As regulatory submissions increasingly incorporate physiologically based pharmacokinetic (PBPK) modeling, one was developed to simulate intestinal lymphatic uptake after a fatty meal. In the absence of direct simulation algorithms for lymphatic uptake, the model was built by adjusting the metabolic profile of the drug to account for its ability to circumvent first-pass liver metabolism. This occurs when the drug is incorporated into postprandially formed chylomicrons, allowing it to be absorbed through the lymphatic system rather than portal blood passing through the liver.

The developed *in-vitro* models for studying the intestinal lymphatic uptake via chylomicrons would reduce reliance on animal studies, addressing ethical concerns and save time and resources for development of lymph targeted drug delivery. Moving forward, establishing a mathematical framework to correlate these *in-vitro* models with *in-vivo* lymphatic uptake would further enhance their reliability. This could streamline regulatory submissions, potentially accelerating the approval process for new therapies and fostering innovation in drug development. Also, incorporating intestinal lymphatic uptake into existing *in-silico* softwares would enable more accurate predictions of drug behavior and provide a deeper mechanistic understanding of lymphotropic drugs and formulations, ultimately aiding in improved formulation development and facilitating regulatory submissions.

Preface

This thesis is an original work completed by Malaz Yousef under the supervision of Dr. Raimar Löbenberg, and Dr. Neal M.Davies at the University of Alberta and Dr. Nádia Bou-Chacra at the University of São Paulo.

Chapter 2 "Sub-cellular Sequestration of Alkaline Drugs in Lysosomes: New Insights for Pharmaceutical Development of Lysosomal Fluid" has been published as: Yousef M., Le T.S., Zuo J., Park C., Bou-Chacra N., Davies N.M., Löbenberg R. Research in Pharmaceutical Sciences. 2022;18(1):1-15. I designed and conducted the experiments, managed the data collection and analysis, and prepared the manuscript.

Chapter 3 "The Lymphatic System: A Sometimes-Forgotten Compartment in Pharmaceutical Sciences" is a review article published as: Yousef M.**,** Amaral Silva D., Bou-Chacra N., Davies N.M., Löbenberg R. Journal of Pharmacy and Pharmaceutical Sciences. 2021;24:533-547. I was responsible for developing the concept, conducting the literature search, writing the manuscript and creating the figures.

Chapter 4 "Lipoproteins within the Lymphatic System: Insights into Health, Disease, and Therapeutic Implications" is a mini-review published as: Yousef M.**,** Bou-Chacra N., Davies N.M., Löbenberg R. Applied Chemical Engineering. 2023;6(2):2202. I was responsible for developing the concept, conducting the literature search, writing the manuscript, and creating the figures.

Chapter 5 "Understanding Lymphatic Drug Delivery through Chylomicron Blockade: A Retrospective and Prospective Analysis" is an original article published as: Yousef M.**,** Bou-

Chacra N., Löbenberg R., Davies N.M. Journal of Pharmacological and Toxicological Methods. 2024;129:107548. I performed the literature search, wrote the manuscript, and created the figures.

Chapter 6 "Simulated Lymphatic Fluid for *In-Vitro* Assessment in Pharmaceutical Development" has been published as: Yousef M., Park C., Le T.S., Bou-Chacra N., Davies N.M., Löbenberg R. Simulated Lymphatic Fluid for *In-vitro* Assessment in Pharmaceutical Development. Dissolution Technologies. 2022;29(2):86-93. I designed and executed the experiments, collected and analyzed the data, and wrote the manuscript.

Chapter 7 "Development of a Novel *In-Vitro* Model to Study Lymphatic Uptake of Drugs via Artificial Chylomicrons" has been published as: Yousef M., Park C., Henostroza M., Bou-Chacra N., Davies N.M., Löbenberg R. Pharmaceutics. 2023;15(11):2532. I designed and conducted the experiments, gathered and analyzed the data, and wrote the manuscript.

Chapter 8 "*In-Vitro* Predictive Model for Intestinal Lymphatic Uptake: Exploration of Additional Enhancers and Inhibitors" has been published as: Yousef M., O'Croinin C., Le T.S., Zuo J., Park C., Bou-Chacra N., Davies N.M., Löbenberg R. Pharmaceutics. 2024;16(6):768. I was responsible for designing and performing the experiments, collecting and interpreting the data, and preparing the manuscript.

Chapter 9 "Novel First-Generation Dissolution Models to Investigate the Release and Uptake of Oral Lymphotropic Drug Products" has been published as: Yousef M., Park C., Bou-Chacra N., Davies N.M., Löbenberg R. AAPS PharmSciTech. 2024;25(6):187. I designed and performed the experiments, managed data collection and analysis, and drafted the manuscript.

Chapter 10 "Modelling Intestinal Lymphatic Uptake of Halofantrine Post-prandially: Advancements and Implications in Physiologically Based Pharmacokinetic Modelling**"** has been submitted to be published as: Yousef M., Bou-Chacra N., Löbenberg R., Davies N.M. Journal of Pharmacy and Pharmacology. 2024. I designed and conducted the modeling, handled data analysis, and prepared the manuscript.

Appendix 3 "Upholding or Breaking the Law of Superposition in Pharmacokinetics: An Overview**"** has been published as: Yousef M., Yáñez J.A., Löbenberg R., Davies N.M. Biomedicines. 2024;12(8):1843. I performed the literature search, composed the manuscript, and created the figures.

Dedication

Dedicated to my family, dear friends, and the resilient people of Sudan—this work is for you.

Acknowledgements

Above all, I extend my deepest gratitude to Allah for providing unwavering strength and guidance throughout this journey.

This achievement would not have been possible without my exceptional supervisors; Dr. Raimar Löbenberg and Dr. Neal M. Davies. Your wisdom, insight, and vast knowledge have been foundational to the successful completion of this work. I am profoundly thankful for your dedication and the countless hours you invested in providing feedback, offering encouragement, and guiding me through each challenge. Your influence has shaped my journey, and I will carry the lessons learned with me throughout every endeavor I pursue in the future. Thank you for believing in my abilities and for providing innumerable opportunities, allowing me to grow both as a scientist and as an individual. I will always hold you in the highest regard as role models, and I look forward to continuing to learn from your extraordinary legacy as my lifelong mentors.

I would also like to extend my sincere appreciation to my supervisory committee members, Dr. Michael Doschak, for his valuable feedback and unswerving support, and Dr. Nádia Bou-Chacra, for her supervision at the University of São Paulo and the discussions that contributed to this work.

Special thanks to Dr. Khaled Barakat, Dr. Ayman Elkadi, Dr. Afsaneh Lavasanifar, Dr. Arno Siraki, and Dr. Dion Brocks from the University of Alberta for their invaluable knowledge and guidance throughout the courses and beyond. I am also thankful to Dr. Gabriel de Araujo from the University of São Paulo for his significant assistance.

A heartfelt thank you to everyone at both universities whose company made this journey so rewarding. I am especially grateful to Dr. Chulhun Park, Dr. Jieyu Zuo, Dr. Daniela Amaral Silva, Rhannanda Copetti Pivetta, Shengnan Zhao, Tyson Le, and Conor O'Croinin from the University of Alberta, as well as CJ Gao, Rong Ling, and Archana Koul from the Applied Pharmaceutical Innovation (API). In addition, I would like to thank Dr. Megumi Yukuyama, Dr. Mirla Henostroza, and Dr. Aline De Souza, Danielle Redondo, and Cristiano Leão from the University of São Paulo. Your collaboration and indispensable backing have been priceless throughout the way.

To the wonderful community at the University of Alberta's Faculty of Pharmacy and Pharmaceutical Sciences— including all the professors, from whom I had the privilege of learning in various contexts, and the staff— particularly Diseray Schamehorn, our guardian angel— thank you for your usual assistance. To my fellow graduate students, I would name each of you if I could, thank you for your camaraderie and encouragement throughout this journey.

MITACS generousity made this possible (IT24899) and I am deeply thankful to Dr. Shirzad Azarmi from RS Therapeutics for his instrumental help throughout this process. I am also immensely appreciative to the donors and institutions that have recognized and supported my academic journey through various awards and scholarships.

To my lifelong mentors, Dr. Venu Vangala, Dr. Magdi AwadAllah, Dr. Abubakr Nur, and Dr. Zuheir Osman, whose support, encouragement, and belief in me have continually propelled me forward—I am profoundly grateful for your faith and continuous guidance.

To my dearest friends— Samah Mohammed, Manasik Mohammed, Wigdan Salih, and Hamdah Al Nebaihi —you know how deeply I love and appreciate you. And to all my other friends, though space may be limited to have you all, you know my heart is not.

To my mother, Dr. Huda Osman, my first and forever role model, and my father, BGen(R). Abdelbagi Elgelani, who has always believed in me and supported my dreams—thank you for shaping me into the person I am today with your endless love and trust.

To my sister, Maha, my forever friend and backbone, and my brother, Mohammed, whose laughter has been a constant source of joy and comfort—your presence has made this journey like all others in life, way brighter.

And last, but certainly not least, to my husband, Khoubieb Mohammed, my forever professor, my better half, and my steadfast companion through every challenge and triumph—thank you for being my guiding light. I am eternally grateful for your love and support every second of the way.

Table of Contents

List of Tables

List of Figures

List of Abbreviations

Acetoxycycloheximid	ACH
Active Pharmaceutical Ingredients	API
Adenosine Triphosphate	ATP
Apolipoprotein	Apo
Area Under The Concentration-Time Curve	AUC
Biopharmaceutics Classification System	BCS
Colorectal Adenocarcinoma Cells	CaCo2
Diglycerides	DG
Endoplasmic Reticulum	ER
Fatty Acid	FA
Follicle-Associated Epithelium	FAE
Free Fatty Acids	FFA
Gastrointestinal	GI
Gut-Associated Lymphoid Tissue	GALT
High Performance Liquid Chromatography	HPLC
High-Density Lipoproteins	HDL
Intermediate Density Lipoproteins	IDL
Lipoprotein	Lp (a)
Lipoprotein Lipase	LPL
Low-Density Lipoproteins	LDL
Maximum Plasma Concentration	C_{max}

Microfold Cells	M cells
Monoglycerides	MG
Mucosa-Associated Lymphatic Tissues	MALT
Pharmacokinetics	PK
Phosphatidylcholine	PC
Physiologically Based Pharmacokinetic Modelling	PBPK
Pluronic® L-81	PL-81
Polyethylene Glycol	PEG
Polyvinylidene Fluoride	PVDF
Simulated Lysosomal Fluid	SLYF
Sodium Lauryl Sulphate	SLS
Time to reach maximum plasma concentration	T_{max}
Transmission Electron Microscope	TEM
Triacylglycerol	TAG
Triglycerides	TG
U.S. Food and Drug Administration	FDA
United States Pharmacopeia	USP
very low-density lipoproteins	VLDL
Vinca alkaloids	VA

SECTION ONE: GENERAL INTRODUCTION AND OVERVIEW

CHAPTER ONE

Journey of Oral Drugs from Administration to Absorption

1.1 Importance of Oral Drug Administration:

Approximately 84% of the leading pharmaceutical products are delivered via oral administration. They represent a market value of trillions of dollars and exhibit a growth rate of 10% per year (1). This preference for oral drug delivery stems from its numerous advantages over other routes of administration. It provides convenience and ease of administration for patients, promoting better compliance with prescribed treatment regimens. Moreover, being non-invasive, oral drug administration minimizes the risk of complications associated with invasive procedures of parenteral administration such as infections and pain. The cost-effectiveness of oral medications further enhances their appeal. Additionally, the wide range of oral formulations available allows for flexibility in dosing schedules and suitability for different patient populations. Advances in drug formulation technology have also enhanced the bioavailability of oral medications, ensuring optimal therapeutic effects. Additionally, certain oral delivery systems enable targeted delivery to specific sites within the gastrointestinal tract, thereby reducing systemic side-effects (2-4).

1.2 Overview of the Absorption Process of Orally Administered Drugs:

Extensive research over the past couple hundreds of years has been conducted to elucidate the mechanisms underlying drug absorption and transport, and contemporary studies continue to explore these processes to enhance drug delivery and therapeutic efficacy (5-7). Oral absorption refers to the movement of chemical substances from the gastrointestinal (GI) tract, across and through its walls, and into the bloodstream and lymphatic system (8). The absorption of oral medications is influenced by various factors

related to which can be broadly categorized into drug-related (physicochemical properties), formulation-related (dosage form), and biological factors (physiology and pathophysiology of the GI tract) (4, 8).

As drugs move through the GI tract, they have the potential to cross the mucous membranes of various organs (**Figure 1.1**). The stomach, with its smaller surface area and thicker mucus layer, presents a more challenging environment for drug absorption (9). Consequently, most orally administered medications are predominantly absorbed in the small intestine due to enhanced contact time its extensive surface area (250 m^2) and epithelium, which allows for efficient fluid filtration driven by osmotic differences caused by the presence of food (10). In contrast, absorption in the colon is generally limited and highly variable due to the presence of undigested materials, bacteria, and varying water content (8).

To be absorbed, drugs must generally be in aqueous solution and traverse the intestinal epithelium, necessitating passage through cell membranes. Typically, drugs can permeate membranes via passive mechanisms such as diffusion across the lipid bilayer or facilitated diffusion (11, 12), or through active mechanisms like active transport uptake or endocytosis (13). **Figure 1.2** illustrates the different mechanisms of passage across cellular membranes.

Passive diffusion is the predominant mechanism for drug translocation across cell membranes. This process involves the movement of drug molecules from regions of high concentration to regions of lower concentration without requiring energy expenditure (14). Key factors influencing passive diffusion include molecular size, concentration gradient,

lipid solubility, and the degree of ionization of the drug (10). Only unionized free drug molecules are available for diffusion (15). Facilitated diffusion is another form of passive transport where drugs rely on carrier proteins to move along their concentration gradient (16). Yet, this process has a comparatively minor role to play in drug absorption (8).

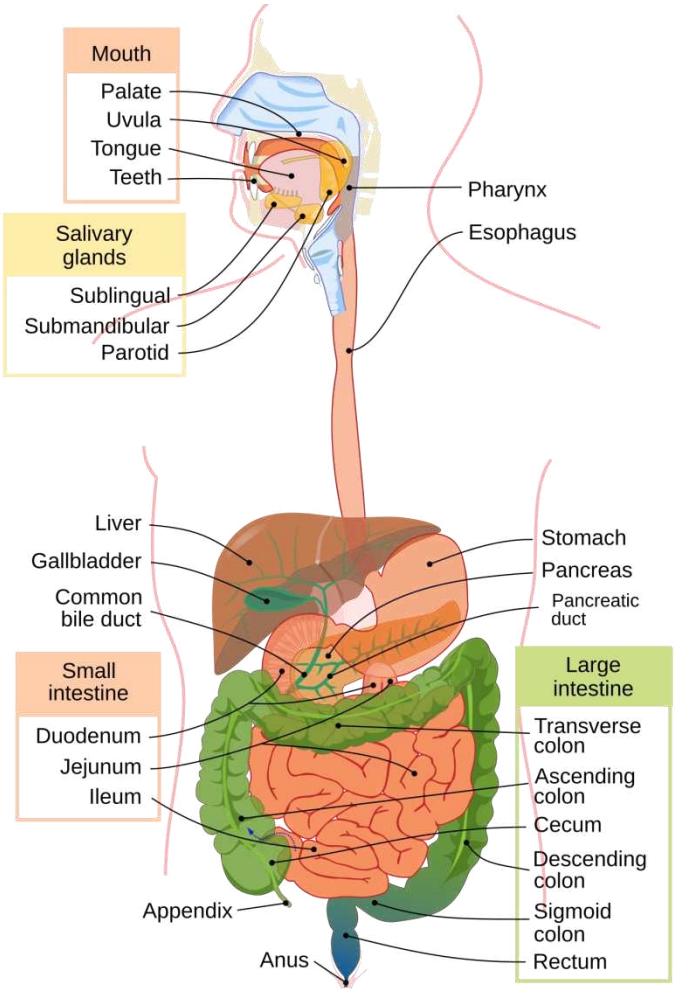

Figure 1.1. Illustration of the gastrointestinal tract and its various organs.

(Available under CC0 1.0 by Mariana Ruiz)

Conversely, active transport requires energy, typically in the form of Adenosine Triphosphate (ATP). Carrier-mediated active transport is crucial for the movement of drugs some of which are structurally similar to endogenous substances. This process involves

specific carrier proteins or pumps within the cell membrane that facilitate the translocation of drugs across the membrane, often against a concentration gradient (8, 17).

There are two primary types of active transport: primary and secondary. Primary active transport uses ATP directly to move ions or molecules. A well-known example is the sodium-potassium pump (Na+/K+ ATPase), which pumps sodium ions out of the cell and potassium ions into the cell, both against their concentration gradients, maintaining essential cellular functions such as membrane potential and volume regulation. In contrast, secondary active transport does not use ATP directly but relies on the energy generated by the electrochemical gradients established by primary active transport. For instance, sodium-glucose co-transporters (SGLTs) in the intestines and kidneys utilize the sodium gradient created by the sodium-potassium pump to bring glucose into cells against its gradient. Similarly, peptide transporters (e.g., PEPT1) use proton gradients to import small peptides (12).

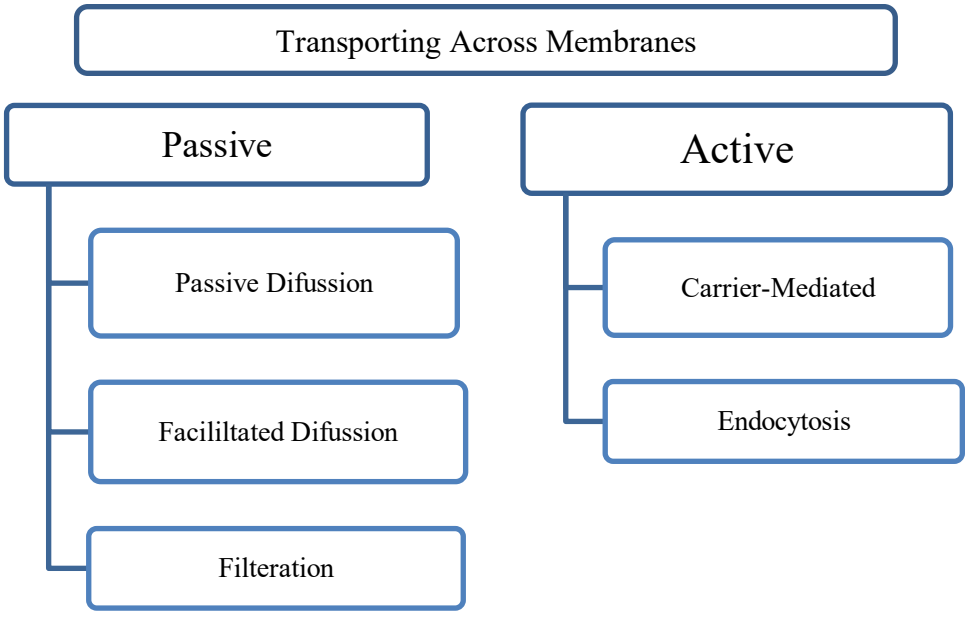

Figure 1.2. Various mechanisms of drugs traversing through cells.

Endocytosis involves the invagination of the cell membrane around a drug molecule, incorporating it into the cell within a vacuole. This can be classified broadly into two forms: pinocytosis, where the cell engulfs extracellular fluid and its contents into large vesicles, and receptor-mediated endocytosis, where specific receptors on the cell surface bind to target molecules, triggering the formation of vesicles that internalize the bound substances (16). Cells can also engulf particles > 500 nm through phagocytosis, although this mechanism is more relevant in histopathology than pharmacology (12).

The aforementioned mechanisms of drug transport can collectively be classified as transcellular, as they involve passing across the cell or enterocyte. However, there is also the paracellular transport pathway to consider. This pathway includes filtration, a form of passive transfer where drugs pass through aqueous channels in the tight junctions between adjacent intestinal epithelial cells. Typically, small, hydrophilic, and ionized drugs utilize this route (10, 12).

1.3 Sub and Post Cellular Uptake of Drugs Following Oral Adminstration:

Whether transcellular or paracellular, the various transport routes mentioned in the previous sections deliver drugs from the apical side to the basal side of the intestinal epithelial layer (18).

The intestinal epithelium is composed of a single columnar layer of cells that separates the lumen from the underlying connective tissue (**Figure 1.3**). This layer includes various specialized cell types: 1) absorptive epithelial cells, also known as enterocytes; 2) paneth cells which protect against microbial infections with their granules containing antimicrobial peptides; 3) mucus-secreting goblet cells; 4) hormone-secreting

enteroendocrine cells; 5) chemosensory tuft cells that play a role in detecting helminth parasites; and 6) M cells (or microfold cells) which mainly uptake and transport luminal antigens to the underlying lymphatics (19-21).

Enterocytes on the apical surface form villi and microvilli (3,000–7,000 microvilli per cell) which provide a large surface area for drug interaction and absorption (1). Direct drug recovery after translocation from the apical to the basal side of the epithelial layer through enterocytes generally occurs for most drugs. However, poor recovery can happen due to various factors, such as metabolism and transporter-mediated efflux back to the lumen (22, 23). One frequent cause of poor recovery is lysosomal trapping (24), which is often attributed to the lipophilicity and basicity of drugs (25). A general overview of this process is provided next:

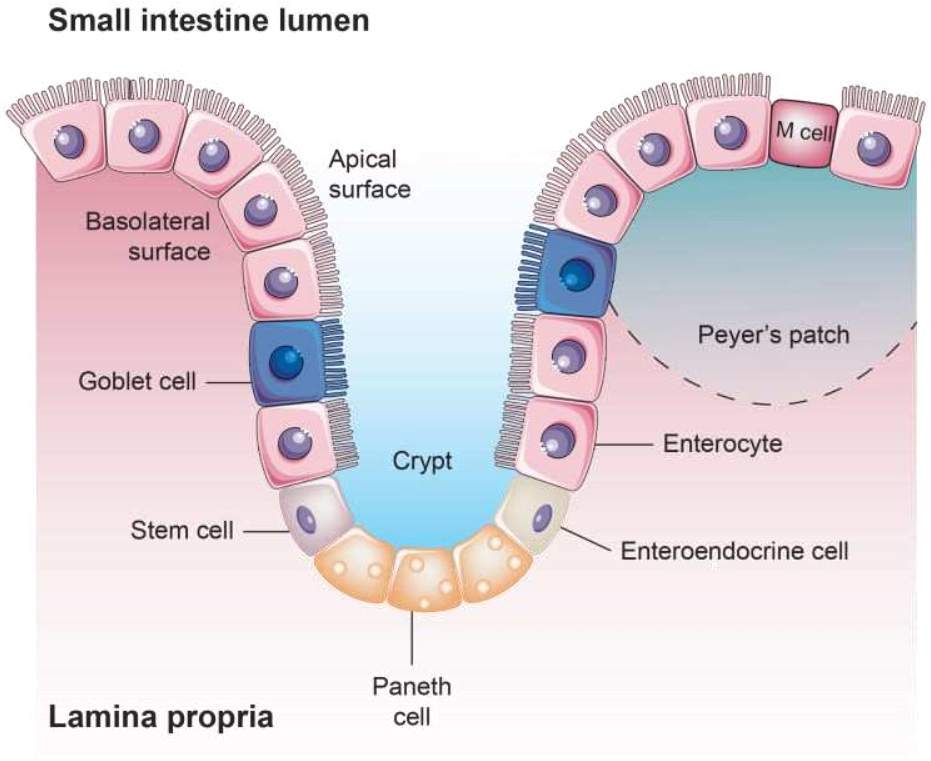

Figure 1.3. Intestinal epithelium and its specialized cells.

1.3.1 Lysosomal Trapping:

Lysosomes are essential for autophagy, degrading damaged organelles and maintaining cellular health (25, 26). They are formed in the rough endoplasmic reticulum (ER), where digestive enzymes are produced. These enzymes are then modified in the Golgi apparatus and tagged for lysosomal transport. Vesicles from the Golgi either fuse with existing lysosomes or mature into new lysosomes (26).

Primary lysosomes are inactive organelles that contain digestive enzymes. They become active when they fuse with vesicles containing material to be degraded, such as endosomes or autophagosomes, forming secondary lysosomes. In this stage, digestion occurs, where lysosomes break down macromolecules and recycle useful components back into the cytoplasm, while waste materials are expelled through exocytosis. Occasionally, undigested material accumulates in lysosomes, forming residual bodies, which may either persist within the cell or be expelled. As lysosomes age, they contribute to cellular aging or are eventually degraded. In some cases, lysosomal rupture can lead to cell death (26).

Lysosomal trapping occurs when a basic compound (lysosomotropic agents, log P ~ 2 – 6, and pKa > 6) (25) enters the enterocyte and subsequently accumulates within the lysosome. Within the acidic environment of the lysosome (pH 4 – 5.5), which is generated by V-type H^+- H+-adenosine triphosphatase (ATPase) pump- the drug molecule undergoes protonation (27). This protonation leads to its entrapment because the ionized form has low permeability across the lysosomal membrane (25, 28, 29). Consequently, drug concentrations in lysosomes can exceed those in the surrounding medium by more than 1000 times (30).

Lysosomal trapping within the enterocytes can considerably impact drug absorption and pharmacokinetics. Oral drugs with ionizable basic centers can become sequestered in the lysosomes of intestinal cells, thereby delaying and/or reducing their availability for reaching the bloodstream. This phenomenon can cause *in-vitro* studies to underestimate the permeability of these drugs, leading to the premature rejection of potentially valuable compounds during the drug discovery process (24). The misestimating of drug permeability due to lysosomal trapping can create discrepancies between *in-vitro* and *in-vivo* data, resulting in poor recovery in permeability assays and incorrect classification of the absorption and clearance characteristics of drugs (24, 31, 32). Consequently, highly permeable drugs might be mistakenly categorized as having low permeability, leading to misguided decisions in drug development and the potential early dismissal of promising compounds (24).

Furthermore, enterocyte lysosomal trapping complicates establishing bioequivalence for immediate-release formulations, as the dissolution rate may not accurately reflect *in-vivo* performance. A study highlighted that traditional *in-vitro* dissolution tests do not correlate well with the pharmacokinetics of dextromethorphan due to lysosomal trapping, which causes a delay in the appearance of the drug in the systemic circulation. Using physiologically based pharmacokinetic modeling (PBPK), it was demonstrated that dextromethorphan is rapidly absorbed into the enterocytes but appears slowly in the plasma because of lysosomal sequestration. The findings suggested that for lysosomotropics like dextromethorphan, dissolution rates are not critical for determining bioequivalence and that a thorough understanding of the mechanistic processes involved in drug disposition is essential for defining clinically relevant product specifications (33).

After being released from the enterocytes, drugs travel through the body to eventually reach the general circulation, where they gain access to cells throughout the body. It is important to note that lysosomotropics may also become sequestered within cells other than enterocytes, which can have several implications.

One major implication is the altered apparent volume of distribution of drugs within the body (34). This is particularly relevant in organs and tissues with a high lysosomal content, such as the liver, kidneys, and lungs, where lysosomally-trapped drugs may accumulate, leading to a higher overall tissue distribution (35, 36). Another implication is the extended half-life of drugs due to lysosomal trapping. Drugs trapped in lysosomes are released slowly as they are gradually transported back to the cytoplasm or excreted through lysosomal turnover, resulting in an extended half-life in the body (37).

Lysosomal trapping also impacts the pharmacodynamics of drugs, potentially increasing their effectiveness if their target is located within lysosomes (38). Conversely, it can reduce their interaction with their intended target if they are sequestered inside the lysosomes (39). Sequestration inside lysosomes can also lead to drug-drug interactions, as drugs that inhibit lysosomal function or affect pH can alter the trapping of other drugs (34, 40, 41). Additionally, it can potentially delay the onset of action, as a significant proportion of the drug is entrapped within the lysosomes and not available for immediate therapeutic activity (33, 42). Consequently, this can result in variable patient responses, as individuals with differences in lysosomal function or pH may exhibit different reactions to drugs affected by lysosomal trapping (42).

The potential toxicity associated with lysosomal trapping is another critical consideration. Excessive accumulation of drugs within lysosomes can disrupt lysosomal

function, leading to cellular toxicity (43). This is particularly relevant for drugs administered at high doses or for prolonged periods. Tissues with high lysosomal content may be more susceptible to drug-induced toxicity due to lysosomal trapping (44, 45).

In addition to lysosomes, there are other organelles within cells that can also play roles in drug accumulation and require further study. These include mitochondria (46), Golgi apparatus (47) and endosomes (48). They contribute to the processes of cellular uptake, trafficking, and drug accumulation. The roles of these organelles can vary depending on the physicochemical properties of the drug, the type of cell, and the specific mechanisms of drug action and transport.

1.3.2 Intestinal Lymphatic Uptake of Drugs via Chylomicrons:

Basic drugs can be trapped within the lysosomes of enterocytes (33). Other drugs may be packaged with triglycerides from ingested long-chain fatty acids, making enterocyte-formed lipoproteins termed chylomicrons through a process involving the endoplasmic reticulum and Golgi apparatus (49, 50).

Chylomicrons are naturally formed to facilitate the absorption of dietary lipids and certain drug entities, typically those that are lipophilic (log $P > 5$) and have a solubility in long-chain fatty acids of ≥ 50 mg/g (51). Studies have demonstrated that additional molecular descriptors, such as the number of hydrogen bond donors and acceptors, polar surface area, melting point, among others also influence the drug-chylomicron association process (52). These drugs might be referred to as lymphotropics throughout this thesis.

After being exocytosized from the basolateral membrane of the enterocytes, the formed drug-packaged chylomicrons are taken up by the intestinal lymph capillaries

(lacteals) rather than entering the portal circulation through blood capillaries (53, 54). This enhances the amount reaching the systemic circulation and improves the bioavailability of highly hepatic extracted drugs susceptible to significant pre-systemic clearance by the liver (55, 56). It will also increase exposure in targets within the lymphatics, leading to favorable therapeutic outcomes for ailments originating or spreading through the lymphatic system, such as cancer, viral infections, metabolic and inflammatory conditions (55, 57-59).

Given the numerous advantages of lymphatic uptake via chylomicrons, several strategies have been employed to enhance drug transport through the lymphatic system using chylomicrons. The administration of drugs in a post-prandial state, particularly with a fatty meal, can facilitate drug transport via chylomicrons, as ingested lipids stimulate their production (60-62). Lipidic pro-drugs have (63) also shown promise in enhancing lymphatic uptake by leveraging chylomicrons for drug delivery (64, 65). Additionally, lipid-based systems especially the nanostructured ones have emerged as promising candidates for drug delivery through the intestinal lymphatics (55, 57, 66, 67).

While food, lipidic prodrugs, and nano-systems can all facilitate drug uptake into lacteals through packing into chylomicrons, nanosystems also enhance drug delivery through the intestinal lymphatic route via alternative entry points. Nano-systems can traverse paracellularly between intestinal epithelial cells, reaching the underlying lamina propria. From there, they can be drained along with excess extracellular fluid as lymph into lacteals (54). Additionally, these nano-systems may be recognized as foreign and taken up by M cells in the gut-associated lymphoid tissue (GALT) within Peyer's patches, ultimately

reaching the mesenteric lymph (68). From there, lymph from all pathways converges and continues its journey until it joins the venous circulation (53).

Drugs delivered through intestinal lymphatics can fulfill the three primary functions of the lymphatic system: maintaining fluid balance by draining excess fluid from the extracellular matrix, defending the body against invading pathogens and foreign bodies, and absorbing ingested dietary lipids (53, 69). However, this thesis will primarily focus on the lipid absorption aspect and the uptake of drugs and xenobiotics through intestinal lymphatics via chylomicrons which will be further detailed in coming chapters.

1.4 Research Questions, Objectives, and Hypothesis:

1.4.1 Research Questions (Identifying Gaps and Exploring Potential Fill-ins):

Due to the considerable advantages of oral administration, this thesis examines two principal phenomena affecting the pharmacokinetics and pharmacodynamics of orally administered active pharmaceutical ingredients (APIs): lysosomal trapping and intestinal lymphatic uptake via chylomicrons. The research primarily emphasizes intestinal lymphatic uptake via chylomicrons, as this critical process is often underappreciated and contains numerous scientific gaps and unanswered questions that warrant further investigation.

Several models have been created to assess and quantify the proportion of potential drug candidates that may be sequestered inside lysosomes. However, the absence of a standardized lysosomal fluid composition in pharmaceutical compendia poses a challenge. Standardization is crucial for achieving consistent and reliable results, enhancing the comparability of studies, and improving the drug development process. Addressing this gap

could be helpful in ensuring that lysosomotropic drugs are evaluated under uniform conditions, thereby providing clearer insights into their potential disposition, efficacy, and safety.

Intestinal lymphatic uptake holds significant importance, particularly with current efforts in drug delivery focusing on lipid-based formulations for both traditional and novel applications in drug and vaccine delivery. Lipids are naturally associated with the chylomicron route of intestinal lymphatic uptake. However, there remains a lack of awareness about this pathway and numerous gaps to be addressed, including the need for a standardized lymphatic fluid and methods for investigating and quantifying intestinal lymphatic uptake.

Reports and studies have often overlooked the absorption route through intestinal lymphatic uptake. This oversight has meant that potential benefits, such as targeted drug delivery, improved bioavailability, and enhanced therapeutic strategies for diseases within or through the lymphatic system, have not been fully explored.

Standardizing lymphatic fluid would serve similar objectives as standardizing lysosomal fluid. Additionally, investigating and measuring drug uptake into the lymphatic system is important for several reasons: it provides a direct assessment of lymphatic drug transport, avoids underestimating total drug absorption, and elucidates absorption mechanisms, thereby clarifying discrepancies in oral bioavailability. Moreover, it evaluates the impact of different formulations and potentially assists in establishing and fulfilling regulatory requirements for the increasing number of lymph-targeted formulations.

1.4.2 Research Objectives:

With the general objective of investigating the subcellular and post-cellular uptake of drugs following oral administration, specifically examining lysosomal trapping and intestinal lymphatic uptake via chylomicrons, the following specific objectives were established:

1. To develop a simulated lysosomal fluid.

2. To increase the scientific community awareness of intestinal lymphatic uptake by providing literature reviews and identifying gaps in existing research.

3. To develop a simulated lymphatic fluid.

4. To create an *in-vitro* model to investigate the oral lymphatic uptake of drugs via chylomicrons and their enhancement or inhibition.

5. To develop first-generation dissolution models to study the release and uptake of oral lymphotropic drugs and address relevant formulation issues.

6. To examine the potential of using *in-silico* models to predict intestinal lymphatic uptake through chylomicrons using a physiologically based pharmacokinetic model (PBPK).

1.4.3 Research Hypothesis:

The central hypothesis of this thesis is that replicating the relevant physiological conditions—specifically within lysosomes and the drug-chylomicron association within enterocytes—will enable the quantification of lysosomal trapping and intestinal lymphatic

uptake, respectively, thereby facilitating the achievement of the stated research objectives. The working hypotheses for these objectives are outlined next.

Hypothesis for Simulated Lysosomal Fluid:

A simulated lysosomal fluid that includes key ions critical for lysosomal function will provide a physiologically relevant medium, supporting studies on drug interactions and potential applications in pharmaceutical and biomedical research.

Hypothesis for Lysosomal Trapping Modeling:

An *in-vitro* two-compartment model mimicking lysosomal and cytosolic environments can effectively replicate the process of lysosomal trapping, allowing for the accurate measurement of the transfer of drugs from the cytosol to lysosomes and determining the proportion that becomes trapped.

Hypothesis for Simulated Lymphatic Fluids:

Simulating lymphatic fluid by reproducing the composition of extracellular fluid and incorporating artificial chylomicrons will accurately mimic both general and intestinal lymphatic environments, respectively, enabling various *in-vitro* pharmaceutical and biomedical applications.

Hypothesis for *In-Vitro* Lymphatic Uptake Model:

A two-compartment *in-vitro* model representing the intestinal lumen and the intraenterocyte environment, along with artificial chylomicrons, will replicate drug movement across the intestinal cell membrane and capture the association of drugs with chylomicrons, reflecting *in-vivo* lymphatic drug uptake through chylomicrons.

Hypothesis for Lymphatic-Focused Dissolution Model:

Adding a lymphatic compartment containing artificial chylomicrons to a dissolution appartus will differentiate and quantify drug distribution through the portal and lymphatic routes, allowing for a detailed understanding of drug transport in the body.

Hypothesis for PBPK Modeling of Intestinal Lymphatic Uptake via Chylomicrons:

Modulating the metabolic kinetics of high extraction lymphotropic (halofantrine) after a fatty meal to account for the portion of the drug incorporated into post-prandial chylomicrons and entering the intestinal lymphatic system will provide an accurate model for predicting the enhanced drug bioavailability and evasion of first-pass metabolism as a result of the lymphatic voyage.

1.5 Thesis Roadmap:

To achieve the stated objectives, the work pursued in this thesis is systematically presented, beginning with the lysosomal trapping component of development of simulated lysosomal fluid. Subsequently, the intestinal lymphatic component was initiated with the literature reviews to establish foundational awareness. This is followed by detailed work related to the simulated fluid, the developed *in-vitro* model, the novel dissolution model, and the *in-silico* modeling, discussed in subsequent chapters.

The appendix sections provide additional insights into the research. Appendix 1 details an initiated *in-silico* project that has the potential to evolve into a comprehensive endeavor, advancing the prediction of chylomicron-mediated intestinal lymphatic transport. Appendix 2 presents an attempt to design a lymphotropic formulation. Appendix 3 explores

a pharmacokinetic principle, specifically superposition, which could be impacted by the intestinal lymphatic uptake and lysosomal trapping. Appendix 4, derived from the insights gained through this project, underscores the need to revisit the Biopharmaceutics Classification System (BCS) to incorporate lipid dissolution alongside aqueous dissolution and permeability.

SECTION TWO: SUB CELLULAR UPTAKE OF ORALLY ADMINISTERED DRUGS THROUGH LYSOSOMAL TRAPPING

CHAPTER TWO

Sub-cellular Sequestration of Alkaline Drugs in Lysosomes: New Insights for Pharmaceutical Development of Lysosomal Fluid

A version of this chapter is published in:

Res Pharm Sci. 2022;18(1):1-15. DOI: 10.4103/1735-5362.363591

Reprinted from Reference (29).

2.1 Introduction:

Inracellular sequestration of drug molecules by various organelles has differential effects on the disposition of xenobiotics which can impart significant alterations to their distribution, efficacy, and safety (28, 70). Moreover, this phenomenon can also yield unintentional targets for molecules which may help in repurposing them for indications that involve initially an off-target site of action (71-73). Previous studies listed lysosomes, mitochondria, and Golgi apparatus as intracellular sites for various drug entities (28, 47, 74). In these investigations we highlight lysosomal trapping, focusing on the structure and function of the lysosomes and the mechanism of "trapping" potential drugs in addition to the therapeutic implications of this phenomenon. We will also detail the various physicochemical and structural properties that candidate molecules possess to be subjected to sub-cellular sequestration in lysosomes and the models used to predict this occurrence**.**

2.1.1 Lysosomes Structure and Function:

Lysosomes are acidic membrane-enclosed organelles (pH 4 - 5.5) (26, 27). They are ubiquitous in cells, yet predominant in the liver, kidney, spleen, and lung (75). Their size can differ in the various tissues, ranging from 0.1 to 1.2 μm (76).

Lysosomes are essential in certain metabolic processes including the digestion of macromolecules and cell fragments, phospholipid turnover, and destroying invading bacteria and viruses (25, 28, 77). Lysosomes play this key role through their array of hydrolytic enzymes (> 60) that function within the acidic environment of the lysosomes, which protects other cell molecules and organelles from being destroyed if these enzymes were able to leak into the cytosol (75, 78).

To maintain their acidic pH, lysosomes depend on proton-pumping V-type ATPase complexes that utilize the energy of ATP hydrolysis in transporting the protons from cytosol into lysosomes (79). As the parallel influx of anions is essential for electro-neutrality, chloride proton anti-porter, known as chloride channel-7 or ClC-7, moves chloride ions into lysosomes to dissipate the trans-membrane voltage (79, 80). Cation efflux into the cytosol has also been reported to play a role in preserving a steady-state pH inside the lysosomes (80).

2.1.2 Mechanism of Lysosomal Trapping:

In 1974 Duve *et al.* first described drug sequestration in the acidic lysosomal vicinity via a process known as lysosomal trapping, lysosomal sequestration, lysosomotropism, acid trapping, or proton pump effect (25, 81, 82). Lipophilic basic drugs were suggested to be the targets for this process (82, 83). However, not all basic drugs have the requisite characteristics to be possible candidates for lysosomal trapping. It is the physicochemical properties of the drugs that determine the accumulation propensity in the lysosomal organelles. Lysosomotropic drugs are termed cationic amphiphilic drugs, referring to their nature being relatively lipophilic (log P ~ 2 - 6) and can bear a positive charge (pKa > 6) (25).

The pH gradient between cytosol (pH 7 - 7.2) and lysosomes represents the driving force for the candidate drugs' deposition into lysosomes (28). Uncharged basic molecules can passively diffuse into lysosomes and their basic group(s) are protonated in the acidic lysosomal vicinity. Ionized charged molecules cannot easily permeate biological membranes, thus the acquired charges reduce the permeability of the molecules across the

lipid bilayer lysosomal membrane back to the cytosol. The equilibrium between the protonated and the neutral forms favors the former and consequently leads to a high fraction of the drug being "trapped" as depicted in **Figure 2.1** (28, 70, 75). The percentage of drugs in the lysosomes can reach up to 70% of the total amount of the drug in the intracellular vicinity (71).

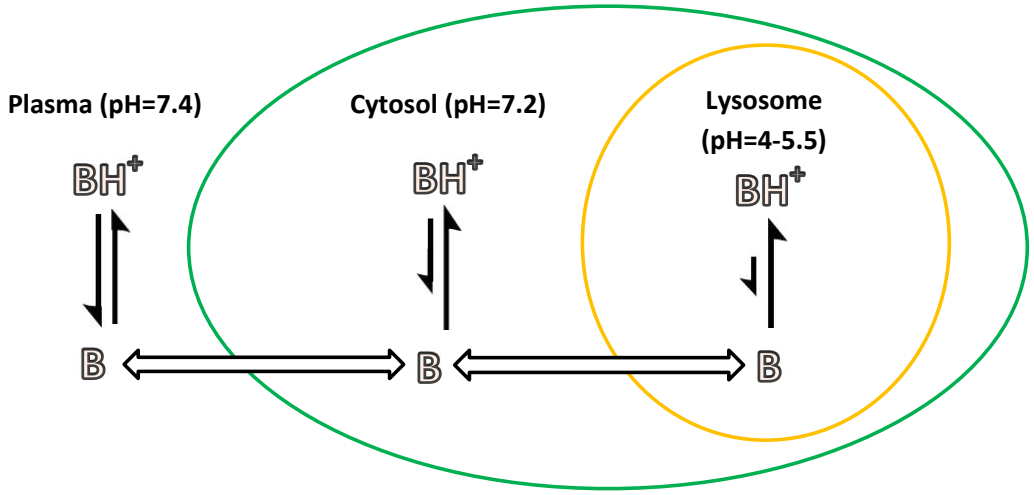

Figure 2.1. Illustration showing the lysosomal trapping of basic drug molecules.

2.1.3 Effects of Lysosomal Trapping:

Drug action and disposition implications of lysosomal trapping mark both the pharmacodynamics and pharmacokinetic properties of drugs (70, 84). For certain molecules, it can be beneficial if the drug target is sequestered inside the lysosomes. Trapping of the antimalarial drug, chloroquine, inside the parasites' lysosome (food vacuole) is fortuitous as this drug binds the heme part of the hemoglobin which is usually metabolized by the parasite to the non-toxic form, hemozoin. Prevention of this process by chloroquine would lead to the death of the parasite in its own waste from the hemoglobin metabolism (38, 85, 86).

Additionally, inhibition of the intra-lysosomal enzyme acid sphingomyelinase is one way through which certain antidepressants elicit their pharmacological action. Thus, lysosomal trapping of fluoxetine and amitriptyline which happens because of their physicochemical properties aids in their pharmacological action as well (87, 88). Lysosomal trapping can also prolong the availability of the drug and in doing so potentiate its activity as seen with the anticancer drug palbociclib and others (73, 89). Palbociclib is an anticancer drug with a mechanism of action that relies primarily on inducing cell-cycle arrest and senescence (90). The process of lysosomal sequestration and release of palbociclib facilitates an increase in the exposure time of the drug and extends the duration of the effect. In addition, the lysosomal trapping of palbociclib can occur in both responsive and resistant cancer cells, the latter effect, however, was found to accumulate and release the drug inducing its paracrine senescence effect (a stable arrest mediated by secreted factors). Moreover, the displacement of palbociclib by other lysosomotropic drugs into the cytosol potentiates its action on cytosolic and nuclear targets (89).

Together with the endosomes (membrane formed-vacuoles), lysosomes play a major role in viral replication (71). Therefore, lysosomotropic drugs have also been investigated to be potentially repurposed and therapeutically utilized for their antiviral properties (91). Several research investigations support the use of lysosomotropic drugs as antiviral agents as demonstrated through *in-vitro*, *in-vivo*, and clinical data. Ebola, Zika, influenza, and even coronavirus are examples of the targets for which lysosomotropic drugs are being investigated (71, 72, 91-93). **Table 2.1** lists examples of different lysosomotropic drugs which have been reported to have antiviral activity.

Nevertheless, lysosomal trapping can also have negative effects on the efficacy of drugs by impeding and decreasing their therapeutic concentration in their intended sites of action. Such effects have been linked to cross resistance of lysosomotropic drugs and might even result in drug resistance as in the case of some anticancer drugs (37, 94, 95). An example of lysosomotropic drug-induced resistance has been reported with sunitinib (25). This cytotoxic agent can trigger lysosomal biogenesis which can result in increased lysosomal sequestration and inadequate target exposure following treatment with lysosomotropic anticancer agents including sunitinib (96). Excessive accumulation of phospholipids as a a result of drug hindrance of their degradation is known as drug-induced

Table 2.1. Examples of some antiviral lysosomotropic agents from various drug classes.

Therapeutic categories	**Compounds**	**References for potential repurposing of the lysosomotropic drug to an antiviral repurposing**
Anti-malarial	(+/-) Chloroquine	(92)
	(+/-) Hydroxychloroquine	(92)
	(+/-) Mefloquine	(97)
	(+/-) Amodiaquine	(98)
	(+/-) Quinacrine	(72)
Psychoactive	Chlorpromazine	(99)
	Clomipramine	(100)
	(+/-) Fluoxetine	(101)
Cardiovascular	Amiodarone	(102)
	(+/-) Verapamil	(102)
Antibiotic	Azithromycin	(103)
Estrogen receptor modulator	Tamoxifen	(104)
	Toremifene	(105)
	Raloxifene	(106)

phospholipidosis (45). Most of the drugs that have been reported to cause this pathological implication (> 50) are lysosomotropic drugs (cationic amphiphilic drugs) (44). Examples of which are collated in **Table 2.2**.

These molecules can be protonated to yield cationic species that when bonded with the phospholipid bilayer of the lysosomal membrane alter its surface charge and subsequently lead to the slowing of phospholipid degradation, which results in their lysosomal accumulation (44, 113).

Table 2.2. Examples of phospholipidosis-inducing lysosomotropic drugs.

Therapeutic categories	Compounds	References
Anti-malarial	(+/-) Chloroquine	(107)
	Chlorpromazine	(108)
Psychoactive	Clomipramine	(109)
	(+/-) Fluoxetine	(108)
	Amitriptyline	(110)
Cardiovascular	Amiodarone	(111)
	(+/-) Propranolol	(112)
Antibiotic	Erythromycin	(108)
	Gentamycin	(107)
Antifungal	(+/-) Ketoconazole	(108)
	Perhexiline	(108)
Estrogen receptor modulator	Tamoxifen	(109)

2.1.4 Models for Lysosomal Trapping:

Models describing the intracellular localization of drugs are not only helpful when it comes to interpreting experiments; they are also useful in rational drug design. Approaches that consider quantitative structure-activity relationships (QSAR) have been

widely used to forecast the movement of molecules within the different intracellular compartments including lysosomes (28). Due to increased interest in lysosomal trapping, several *in-silico* and *in-vitro* models have been proposed.

Fluorescent lipophilic amines such as LysoTracker Red were used to evaluate the lysosomal sequestration in *in-vitro* cell lines including rat and human hepatocytes (25, 70). The compounds that inhibit the fluorescence of these marker compounds in a concentration dependent manner are considered lysosomotropics (70, 114). This method succeeded in predicting many possible lysosomotropic agents yet failed at determining known lysosomotropic drugs like dextromethorphan and labetalol (25).

Nigericin, monensin, and ammonium chloride are known as inhibitors of lysosomal trapping (114). The first two inhibitors interfere with the proton pump presenting in the lysosomes, thus disrupting the pH of lysosomal fluid and ammonium chloride achieves a similar effect by increasing the pH via buffering (25). If the cellular portioning of the tested compounds decreases with the addition of inhibitors, this indirectly confirms categorizing the investigated drugs under lysosomotropic as reported in some papers (25, 84, 115).

Effects of drug trapping on the intralysosomal processes have also been used to predict possible lysosomotropic drugs. The degree of phospholipidosis induction was strongly correlated with lysosomal trapping through a study that involved 47 potential compounds. A similar correlation was undertaken for the phenomenon of lysosomal swelling (116). Inhibition of autophagy can similarly result from lysosomal trapping as previously mentioned and was reported to correlate with the concentrations of drugs accumulating in the lysosomes. However, the study was conducted on a smaller group of

drugs including lysosomotropic drugs such as astemizole, chlorpromazine, and (+/-) chloroquine among others (71, 116-118).

Trapp *et al.* designed an *in-silico* cell model to predict the distribution of weakly basic drug moieties inside the cell. The model is composed of a cell comprising cytosol, lysosome, and mitochondria; each is contained by a membrane and has both an aqueous and a lipid portion. The Fick-Nernst-Planck equation was utilized to calculate the chemical potential-driven flux of the molecules across the electrically charged membranes. It evaluated the ionization status of the different molecules tested via this model. Neutral and ionic molecules across the membrane model were examined for ten model antimalarial drugs whose simulation results anticipated that six of them are optimum for the lysosomal trapping and three were close to the optimum. The results suggested specific physicochemical criteria for potential excellent candidates for lysosomal trapping. These properties included a pKa range of (6 - 10), with a logP of (0 - 3) for monovalent bases, whereas for the bivalent bases, pKa values of below 10 for the higher pKa (pKa 1) and above 4 for the lower pKa (pKa 2) and a LogP of 3 - 6 are optimum for lysosomotropism (28).

Another *in-silico* tool that could potentially predict lysosomal trapping is Membrane Plus™ which is a software developed by Simulations Plus, Inc. (California, USA) for modeling *in-vitro* drugs permeability using different cell types (*e.g.* human colorectal adenocarcinoma cells (CaCo-2), Madin-Darby canine kidney cells (MDCK)) and parallel artificial membrane permeability assay (PAMPA). As there is no reported data on lysosomal trapping using Membrane Plus™, it was used to estimate the lysosomal trapping of the lysosomotropic drugs listed in **Tables 2.1** and **2.2** in addition to other molecules

mentioned throughout the paper (the method is detailed in the Materials and Methods section). The obtained data is depicted in **Figure 2.2**. Some drugs, namely, the four quinolines; (+/-) chloroquine, (+/-) hydroxychloroquine, (+/-) amodiaquine (+/-), and quinacrine had high lysosomal trapping percentages predicted (88.6, 85.4, 74.7, and 88.6, respectively) while the highest percentage for other drugs was 7% for astemizole. Some other well-known lysosomtropics like (+/-) fluoxetine and (+/-) propranolol were not predicted to be trapped in lysosomes to a significant extent and had only 1.7% and 1.9% trapped predicted within lysosomes, respectively. In our attempts to modify the main input parameters (pKa and log P) for the lysosomotropic drug, dextromethorphan, that has been used in some of the reported experiments in this work we could only obtain the percentage of 4.9% predicted by this modeling methodology.

Generally, lysosomes are fragile organelles, which can make it challenging to quantify the compounds trapped inside them (75). The *in-vitro* cellular models avoid the poor recovery challenge and the drug diffusion during sample preparation (119).

They are also superior to the *in-silico* models based on their better resemblance to the *in-vivo* conditions. However, all models have so far been unable to accurately predict every lysosomotropic drug as they depend on indirect methods to quantify the lysosomotropic agents.

The *in-silico* models are at times limited by being incapable of fully replicating what is occurring biologically in the living cells, which is sometimes due to the uncertainty related to the accuracy of the underlying model parameter inputs. Additionally, such models might not consider non-linear processes such as transporter saturation. The effects

of the trapped drugs on the lysosome's membranes, intracellular, and intra-organelle environment properties need to be more holistically integrated into the algorithms or the differential equations that underlie the *in-silico* models. The ionic strength effect on pKa has not been considered in some *in-silico* models and this may affect the accuracy of an important molecular descriptor that determines the lysosomal trapping tendency.

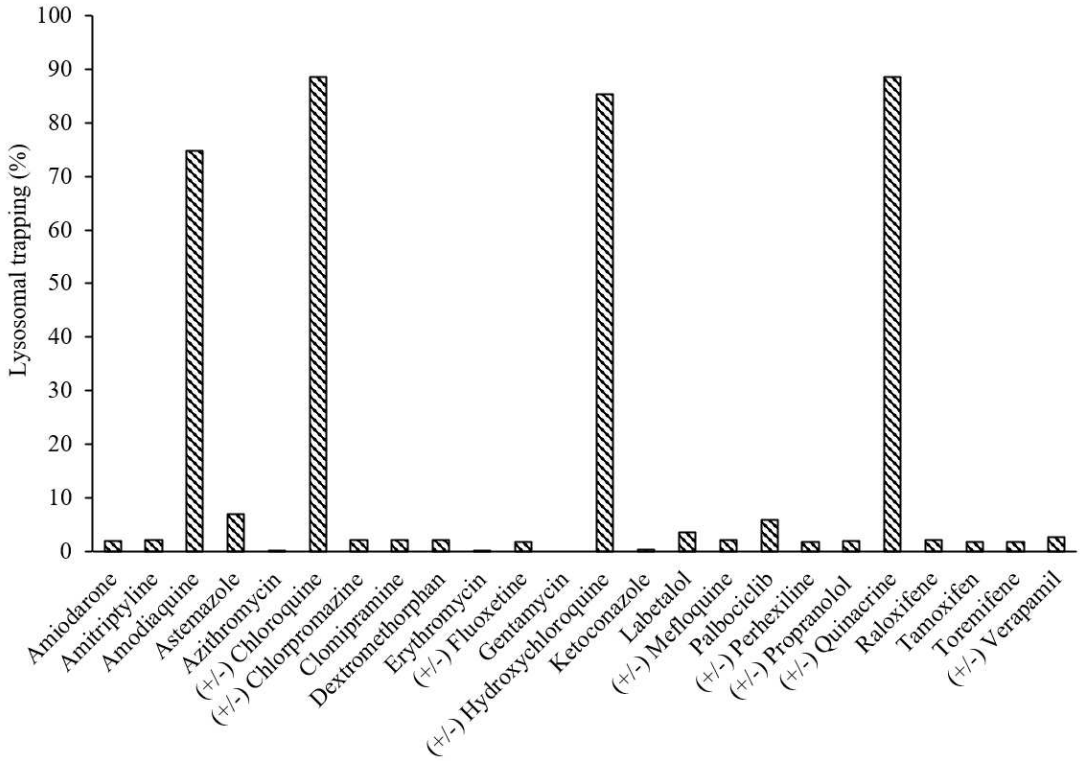

Figure 2.2. Percentage of lysosomal trapping of different lysosomtropic drugs (100 uM) predicted by Membrane Plus™ 2.0 (Simulations Plus, Inc., California, USA) in Caco-2 cells. Default values for the cell model were used with a cytosol pH of 7.22 and lysosomes pH of 4. All properties were calculated by ADMET Predictor 8.1 (Simulations Plus, Inc., California, USA).

2.1.5 Lysosomal Fluid:

In the field of pharmaceutical sciences, lysosomal targeted drug delivery could be designed ab initio for drug therapy and this approach has potential pharmacokinetic and therapeutic benefits. However, there currently is no universally accepted simulated or

artificial lysosomal fluid utilized in the pharmaceutical industry or published by the United States Pharmacopeia. There is at least one commercially available artificial lysosomal fluid sold by Biochemazone (www.biochemazone.com). Biochemazone produces commercially available artificial lysosomal fluid BZ257. This formulation is proprietary although it has been communicated that the use of HCl/acetic acid is employed to maintain acidic pH.

The importance of standardized and physiologically relevant simulated fluids for use in biopharmaceutics and dissolution has been highlighted in many excellent articles and reviews (120, 121). However, there is no mention of a general or optimal lysosomal fluid in these publications for pharmaceutical investigations. The reported lysosomal fluids (artificial lysosomal fluid and phagolysosomal fluid) are categorized under simulated lung fluids (122-126). The former simulated conditions occurring in conjunction with phagocytosis by cells (122), while the latter is a potassium hydrogen phthalate buffered solution that represents the medium inside the phagolysosomes (compartments form after fusion of alveolar macrophages and lysosomes when encountering a foreign particle) (123). **Table 2.3** details the composition of each fluid.

Apart from inhalable formulations investigated with the reported lysosomal fluids, the bioaccessibility of lysosomotropic drugs in preparations intended for other routes of administration must also be considered. Lysosomal sequestration, in general, can demonstrate various therapeutic advantages as illustrated in the earlier section-- "2.1.3 Effects of lysosomal trapping". Additionally, enterocyte and hepatocyte lysosomal trapping can have a profound impact on the pharmacokinetics of a lysosomotropic compound, resulting in a delay in drug input into the systemic vasculature and thus retarded appearance in the plasma (33).

Table 2.3. The concentration of various constituents in artificial lysosomal fluid reported in the biomedical literature.

Compounds	Artificial lysosomal fluid composition (g/L) (122, 124-126)	Phagolysosomal fluid composition (g/L) (123, 126)
Sodium chloride	3.21	6.65
Sodium hydroxide	6.0	
Sodium hydrogen phosphate dibasic	0.071	0.142
Calcium chloride dihydrate	0.128	0.029
Citric acid	20.8	
Trisodium citrate dihydrate	0.077	0.45
Glycine	0.059	0.071
Sodium sulfate	0.039	-
Magnesium chloride	0.05	-
Disodium tartrate sodium tartrate	0.09	-
Sodium lactate	0.085	-
Sodium pyruvate	0.086*	-
Potassium hydrogen phthalate	-	4.085
pH	4.5-5	4.55

*The sodium pyruvate composition is 0.086 g/L according to references No. 64-66 but 0.172 g/L according to reference No. 62. All other ingredients have similar composition across the different references.

Furthermore, ophthalmological lysosomal trapping within the retinal blood barrier has been suggested to be a part of novel transport systems that could safely and effectively deliver candidate drugs to treat retinal dysfunction (127). Development and standardization of a simulated lysosomal fluid (SLYF) would be an essential contribution to pharmaceutical drug and formulation development and aid standardization of *in-vitro* studies for lysosomotropic drugs and their formulations. Based on literature reports on the

principal ions responsible for lysosomal hemostasis and their concentrations (128), a facile SLYF was developed for routine pharmaceutical use. Selected representative drugs that trap within lysosomes were identified using *in-silico* modeling and a review of the literature and solubility and dissolution were examined.

2.2 Materials and Methods:

2.2.1 Materials:

Sodium Chloride (NaCl, CAS: 7647-15-5), potassium chloride (KCl, CAS: 7447-40-7) and sodium acetate (CH_3COONa, CAS: 127-09-3) were obtained from Caledon Laboratories (Ontario, Canada) while the calcium chloride dihydrate ($CaCl_2.2H_2O$, CAS: 10035-04-8) was from Sigma (Steinheim, Germany) and the acetic acid (CH_3COOH, CAS: 64-19-7) was purchased from Fischer Scientific, USA. Distilled water was used for dissolving the reagents. Dextromethorphan hydrobromide (CAS: 6700-34-1) and chloroquine diphosphate (CAS: 50-63-5) were obtained from SigmaAldrich Co. (Missouri, USA) whereas the dextromethorphan soft gel capsules (Robitussin®) were a product of Pfizer (Ontario, Canada) from the lot: DP5155 (Expiration Date: 02/2023).

2.2.2 Using Membrane Plus for Lysosomal Trapping via Caco-2 Permeability Model:

Membrane Plus™ 2.0 from Simulations Plus, Inc. (California, USA) was used to estimate the lysosomal trapping of the potential lysosomotropic. The molecular structure of these drugs was imported into the Caco-2 12-well model. Properties of drugs were predicted by absorption, distribution, metabolism, excretion, and toxicity (ADMET) Predictor 8.1 (**Table 2.4**).

Table 2.4. List of the tested drugs via Membrane Plus™ with their log P and PKa values as predicted by ADMET Predictor 8.1 and used by Membrane Plus™ 2.0 (Simulations Plus, Inc., California, USA).

Drugs	% Of lysosomal trapping	Log P	PKa
Amiodarone	2	6.83	8.96
Amitriptyline	2.1	4.97	8.93
Amodiaquine	74.7	4.95	6.25, 7.95, 10.29
Astemizole	7	5.54	7.97
Azithromycin	0.1	3.39	7.63, 8.72
(+/-) Chloroquine	88.6	5.11	7.25, 9.86
Chlorpromazine	2.1	5.31	8.87
Clomipramine	2.1	5.7	8.87
Dextromethorphan	2.2	3.81	8.91
Erythromycin	0.1	2.3	8.63
(+/-) Fluoxetine	1.7	4.39	9.82
Gentamycin	0	-1.79	7.29, 8.08, 8.9, 9.96
(+/-)	85.4	3.94	7.19, 9.17
(+/-) Ketoconazole	0.4	3.74	6.15
(+/-) Labetalol	3.6	2.54	8.44, 9.66, 11.72
(+/-) Mefloquine	2.1	3.81	8.52
Palbociclib	5.8	1.87	8.96
(+/-) Perhexiline	1.8	6.69	10.1
(+/-) Propranolol	1.9	2.89	9.48
(+/-) Quinacrine	88.6	6.16	7.88, 9.8
Raloxifene	2.2	5.39	8.14, 9.4, 10.08
Tamoxifen	1.8	6.64	8.48
Toremifene	1.8	6.73	8.42
(+/-) Verapamil	2.6	4.45	8.46

The apical compartment of the model was chosen to be filled with 0.5 mL of the drug solution (100 µM, pH = 7.4) while the basolateral one was filled with 1.5 mL of buffer solution (pH = 7.4). The default data for the membrane thickness and pore size were used at a shaking rate of 100. Sampling was done at 0.25, 0.5, 1, 1.5, and 2 h. Default values for the cell model were considered with a cytosol pH of 7.22 and lysosomal pH of 4. The obtained values for the lysosomal trapping percentages for the tested drugs were noted.

2.2.3 Preparation of the SLYF:

The fluid was prepared with the components listed in **Table 2.5**. Components were added successively and dissolved in 70 mL water, and then HCl was used to adjust the pH before completing the volume to 100 mL.

Table 2.5. Simulated lysosomal fluid composition for pharmaceutical investigations.

Reagents	Amount per 100 mL (± 0.1%)
NaCl	0.321 g
KCl	0.0224 g
$CaCl_2.2H_2O$	0.0119 g
Na acetate	0.4046 g
Acetic acid*	0.5 mL
HCl	q.s to adjust the pH (4-5.5)

*Acetic acid volume can be adjusted to be only part of the buffering system and to use the HCl to adjust the pH to the required values.

2.2.4 Analysis of the Developed Lysosomal Fluid and a Commercial Artificial Fluid:

The laboratory-prepared lysosomal fluid (SLYF) and the commercial artificial fluid (BZ257, Biochemazone, Alberta, Canada) were examined for their composition and pH as follows.

2.2.4.1 pH determination:

The pH of the fluids was determined via Fischer Scientific XL20 pH/conductivity meter (Massachusetts, USA).

2.2.4.2 Chemical Analysis:

The lysosomal fluids were chemically investigated using Medica's EasyRA® analyzer (Massachusetts, USA). They were analyzed for their content of potassium (K^+), sodium (Na^+), calcium (Ca^{2+}), and chloride (Cl^-) ions, in addition to lithium (Li^+), magnesium (Mg^{++}), and total protein. After checking and calibrating the system, the probe and the ion-selective electrode were cleaned and the latter was calibrated. A properly calibrated reagent for each component was put with a blank (high performance liquid chromatography (HPLC)- grade water) in the sample holder with 2000 µL samples of the SLYF and the commercial artificial fluids. The required components were selected and the analysis was run for their concentration in blank and fluids samples.

2.2.5 Measuring the Solubility of Dextromethorphan in SLYF and the Commercial Artificial Fluid:

The solubility of the model lysosomotropic dextromethorphan was tested in both fluids using the shake-flask method (129). In brief, the excess drug was weighed into 2 mL samples of SLYF and the commercial lysosomal fluid, then they were shaken at room temperature for 24 h. Subsequently, samples from the supernatant were filtered through 0.45 µm nylon filters before being analyzed at 230 and 280 nm using HPLC C18 (4.6 × 250 mm × 5 µm) column that utilized 60:40 methanol and phosphate buffer (pH = 5.5) as a mobile phase at a rate of 0.8 mL/min for a run time of 10 min.

2.2.6 Measuring the Dissolution and Release Profile of Dextromethorphan from the Commercial Product Robitussin®:

Table 2.6 lists the main components in the liquid-filled dextromethorphan capsules (Robitussin DM Coughgels). *In-vitro* dissolution profiles for this were conducted via VK 7000, USP 711 apparatus by VanKel® (Varian Inc, USA) in 900 mL of 0.1 N HCl, SLYF fluid and 0.05 M phosphate buffer (pH = 7.4), using a USP type I basket method dissolution apparatus. A temperature of 37 ± 0.5 °C and a rotation speed of 100 rpm were maintained according to USP dissolution methods (USP34NF29). Three mL samples were withdrawn over a period of 60 min at predetermined time intervals (15, 30, 45, and 60 min). The filtered samples were suitably analyzed using the HPLC procedure described in the previous section.

Table 2.6. Summary of Robitussin® drug product information obtained from: https: // www. medsafe.govt.nz/Profs/Datasheet/r/robitussinDryCoughcap.pdf.

Drug	Inactive ingredients
Dextromethorphan HBr-15 mg	Allura red AC, brilliant blue FCF, gelatin, macrogol 400, opacode white NSP-78-18022, povidone, propyl gallate, purified water, sorbitol special glycerin blend A810.

2.2.7 Using the Developed Fluid (SLYF) in Predicting Lysosomal Trapping:

Hydrophilic synthetic 0.22 µm polyvinylidene fluoride membranes were first immersed in the developed lysosomal fluid (SLYF) for 10 min and the excess media was removed using absorbent tissues. The membrane was then placed between the two compartments of a horizontal Franz-cell (**Figure 2.3**). The receptor compartment was filled

with 20 mL of the SLYF (pH = 4.21), whereas the donor compartment was filled with 20 mL of the drug solution (1 mg/mL) in phosphate buffer (pH = 7.2). Both compartments were magnetically stirred at 600 rpm throughout the experiment. At time points (1, 2, 3, 4, and 24 h), 400 µL aliquots were withdrawn from the receiver compartment and replaced immediately with an equal volume of fresh receptor medium to maintain a constant volume of the receiving solution. Analysis of both drugs was done using the same HPLC system. For chloroquine, the detection was done at 342 nm using a mobile phase of 60% methanol and 40% acetate buffer (pH = 5.8) that was run at the rate of 1 mL/min for 10 min.

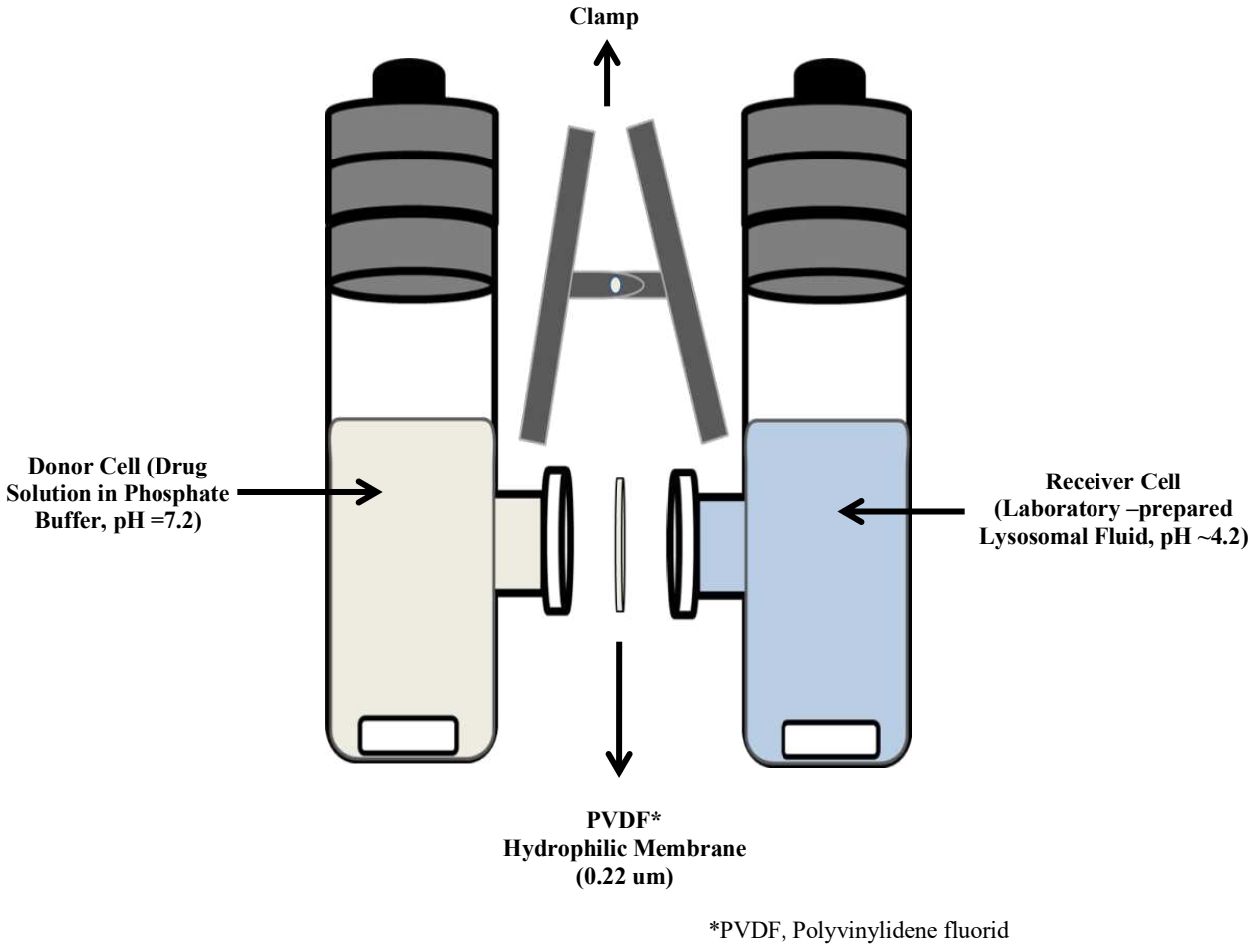

Figure 2.3. Schematic representation of the developed lysosomal trapping apparatus.

2.3 Results:

The pH of the commercial artificial lysosomal fluid was determined to be 7.51, while that of SLYF fluid was 4.2. The chemical analysis of the constituents of both SLYF and the commercial lysosomal fluid for the essential ions for lysosomal function are depicted in **Table 2.7** along with the reported reference values of the tested components. The commercial artificial lysosomal fluid contained only the potassium concentration within the optimum range, while the sodium, calcium, and chloride were all out of range. Moreover, similar to the SLYF fluid, the commercially purchased fluid had no lithium yet contained 1.09 mg/dL of magnesium and a total protein of 2 g/L.

The solubility testing of dextromethorphan in both fluids yielded a clear solution with the SLYF, while the artificial commercial fluid produced a turbid sample with a precipitate (**Figure 2.4**). The average solubility values of the dextromethorphan in the commercial artificial fluid and the SLYF were 1.3 mg/mL and 4.9 mg/mL, respectively (**Figure 2.5**).

Table 2.7. Results of analysis of the simulated lysosomal fluid and a commercial artificial lysosomal fluid using Medica's EasyRA® analyzer (Massachusetts, USA) with the reference values of each component as adopted from literature.

Ions	Amount in the prepared lysosomal fluid (mM)	Amount in the commercial lysosomal fluid (mM ± 5%)	Optimum concentration for lysosomal homeostasis (mM) (69)
Na+	59.08 ± 2.0 √	< 10 X	20-140
K+	3.09 ± 0.06 √	4.24 √	2-50
Ca2+	0.46 ± 0.02 √	1.65 X	~0.5
Cl-	59.1 ± 5.0 √	90.8 X	< 80
pH	4.21 √	7.51 X	4-5.5 (130)

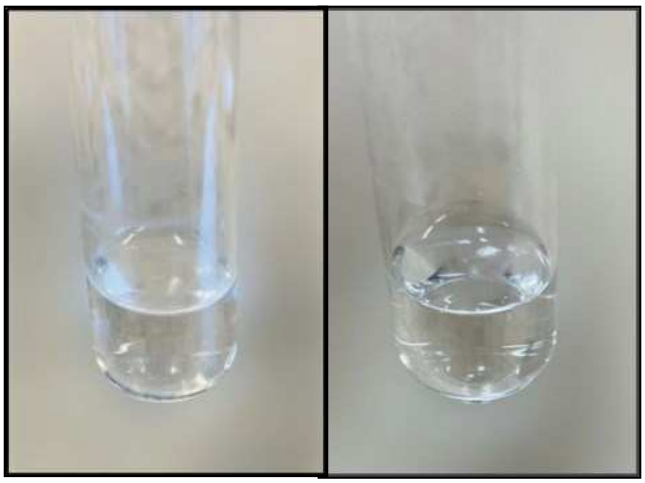

Figure 2.4. Images of samples of the solubility test of the model drug dextromethorphan in the laboratory prepared lysosomal fluid (SLYF) where it fully dissolved (right) and in the commercial artificial counterpart where the fluid was turbid with a precipitate formed (left).

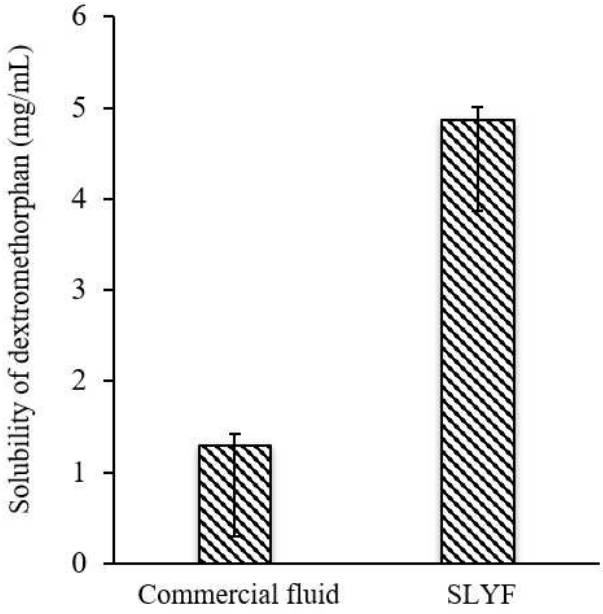

Figure 2.5. Solubility of dextromethorphan in SLYF and in the commercial artificial fluid. Data are presented as mean ± SEM, n = 3. SLYF, laboratory-prepared simulated lysosomal fluid.

Figure 2.6 depicts the drug's rate and extent of release different in the three dissolution media; 0.1 N HCl, SLYF, and phosphate buffer (pH = 7.4). The highest release values were in 0.1 N HCl (> 97%) followed by SLYF (72.6%) and then the phosphate buffer in which only about 32% of the drug was released into. Using SLYF in the

developed model to assess the lysosomal trapping of both chloroquine and dextromethorphan revealed that throughout the experiment the rate and extent of chloroquine release into the lysosomal compartment were higher than the other one as seen in **Figure 2.7**.

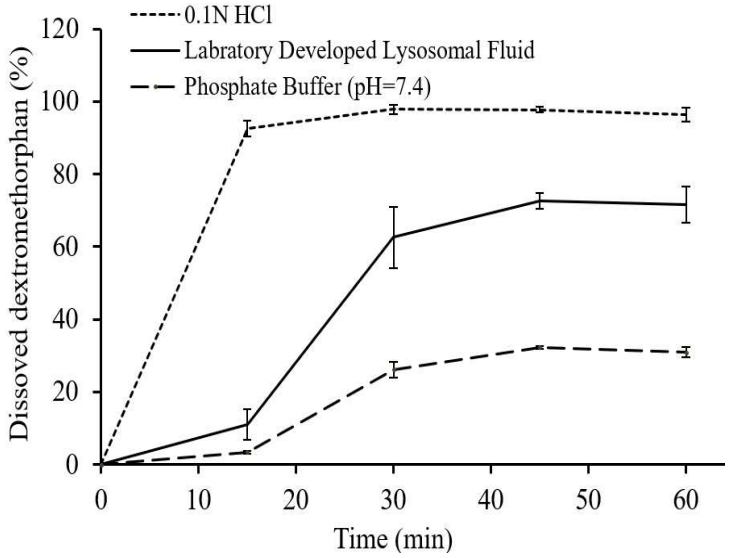

Figure 2.6. Dissolution profile of dextromethorphan performed on the commercial product Robitussin in 0.1 N HCl, developed simulated lysosomal fluid (SLYF), and phosphate buffer (pH = 7.4). Data are presented as mean ± SEM, n = 3.

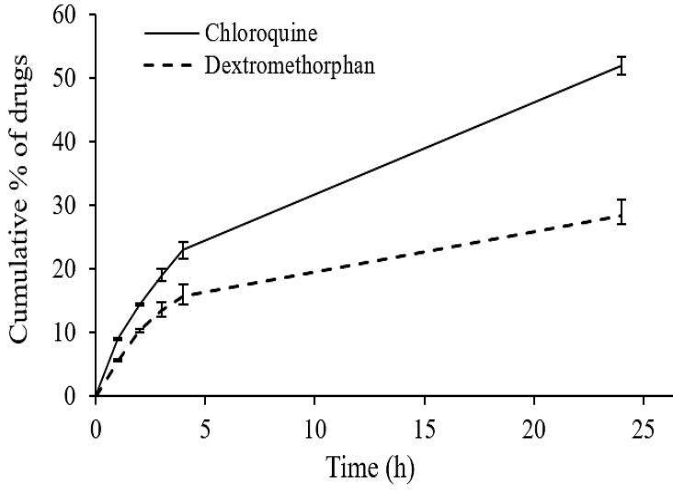

Figure 2.7. Cumulative percentage of tested lysosomtropics ((+/-) chloroquine and dextromethorphan) in the receiver compartment of the model using the developed simulated lysosomal fluid (SLYF). Data are presented as mean ± SEM, n = 3.

2.4 Discussion:

Lysosomal ionic hemostasis is crucial for its function. Sodium (Na^+) and potassium (K^+) ions are essential for determining lysosomal membrane potential that in turn affect the movement of the different ions across the lysosomal membrane and regulate lysosomal acidification. Calcium ions (Ca^{2+}) efflux also contributes to lysosomal acidification and is linked to the fusion of lysosomes with other cellular parts. Chloride ions (Cl^-) are critical counter ions for the chloride proton antiporter which is the main mean that maintains the acidic environment inside lysosomes. The optimal range of these ions inside lysosomes is listed in **Table 2.7**. In addition to the mentioned ions, micromolar deposits of other ions including iron (Fe^{3+} and Fe^{2+}), zinc (Zn^{2+}), and copper (Cu^{2+}) are also found in lysosomes to be provided to the cell when required (128).

For SLYF preparation, only ions that are essential for the lysosomal internal hemostasis were selected. Sodium, potassium, and calcium chlorides were used to provide their corresponding chosen ions (Na^+, K^+, Ca^{2+}, and Cl^-). The equipped buffering system contained acetate and acetic acid (buffering range = 3.5-5.5) (131). In addition to the acetic acid playing a part in decreasing the pH, HCl was used to adjust the pH to the required value.

The pH of the commercial fluid does not reflect the pH inside the lysosomes that should be maintained within 4 - 5.5 (28). Yet, the pH of SLYF does reside within the range. Additionally, the results showed that concentrations of all SLYF components complied with reported data in the literature, unlike the commercial fluid in which only potassium values were optimized.

The improved solubility of the selected model drug in the SLYF could be attributed to the pH of the fluid (4.21) and the pKa of the drug (9.8) (132). However, the discrepancy in the solubility data poses a challenge when considering pharmaceutical or biochemical tests using simulated or artificial biological fluids such as the lysosomal fluid. It is also of special importance for the optimal dissolution conditions of lysosomotropic drug entities and their formulations.

Dextromethorphan's rate and extent of release were different in the three dissolution media examined. The pH can be one factor to the faster release of the basic drug (pK_a 9.85) in the 0.1 N HCl (pH = 1) than the SLYF fluid (pH = 4.2) and the phosphate buffer (pH = 7.4). Fluid composition could also be another factor affecting dissolution. However, even after 45 min, it was only the 0.1 N HCl medium that passed the acceptance criteria for the dextromethorphan dissolution testing of not less than 75% in 45 min in the specified dissolution medium. Other reports indicated the success of the different dextromethorphan dosage forms including capsules to pass the dissolution test in various media *e.g.* 0.1 N HCl, acetate buffer (pH= 4.5), and simulated intestinal fluid (SIF, pH = 6.8) (133, 134).

The developed lysosomal fluid also showed its usefulness in the model used to predict the lysosomal trapping of the two lysosomotropic; (+/-) chloroquine and dextromethorphan. The model was designed in a way to replicate the movement of drugs from the cytosol to lysosomes by having two compartments filled with representative media; a donor compartment in which the drug was dissolved in a phosphate buffer with a pH of 7.2 and a receiver one containing the simulated lysosomal fluid (pH = 4.21). The release profile into the receiver compartment which is an indicator for the lysosomal

trapping demonstrated that chloroquine appeared in the SLYF at *e.g*. a greater rate and extent than dextromethorphan. That observation is reflected by physicochemical molecular descriptors of both drugs, namely the pKa and the log P which would favor chloroquine (pKa = 7.29 and 10.32 and LogP = 3.93) lysosomal trapping over that of the dextromethorphan (pKa = 9.85 and Log P = 3.49) (81). Using this developed SLYF fluid as an *in-vitro* model to evaluate additional lysosomotropic or potentially lysosomotropic drugs.

2.5 Conclusion:

The importance of lysosomes to drug action and disposition is well known. Several *in-vitro* models have been developed to assess lysosomal trapping and quantify the proportion of potential candidates that will be sequestered inside lysosomes. However, there is no standardized composition for lysosomal fluid. Therefore, we developed a lysosomal fluid with the basic components required for lysosomal hemostasis (SLYF fluid) and compared it to a commercial artificial lysosomal fluid. The laboratory-prepared fluid (SLYF fluid) complied with the reported data on the pH and the concentration of the lysosomal components. The obtained result helps fill the void with a lysosomal fluid that can be used to examine various factors related to pharmaceutical product performance including dissolution, solubility, and disposition which are relevant and necessary parts of drug and product development. Preliminary data from the developed fluid and model with dextromethorphan and (+/-) chloroquine suggest the pharmaceutical utility of this developed methodology. The obtained results and model system could be adapted to enable investigating the sequestration of drugs in other cellular organelles using a similarly developed experimental design approach.

SECTION THREE: POST CELLULAR UPTAKE OF ORALLY ADMINISTERED DRUGS THROUGH LYMPHATIC UPTAKE VIA CHYLOMICRONS

CHAPTER THREE

The Lymphatic System: A Sometimes-Forgotten Compartment in Pharmaceutical Sciences

A version of this chapter is published in:

J Pharm Pharm Sci. 2021;24:533-547. DOI: 10.18433/jpps32222

Reprinted from Reference (56).

3.1 Overview and Major Milestones:

About 20-30 litres of plasma are propelled daily out the arterioles into the interstitial spaces of the body tissues. Of this volume, about 90% is reabsorbed back through the venules (135). The remaining fluid is drained back to the circulation via the lymphatic vessels. These vessels, in addition to other tissues and organs, form the lymphatic system (135-137).

The lymphatic system primarily maintains fluid homeostasis but also plays a pivotal role in transporting dietary fat and lipophilic molecules and entities from the intestine to the bloodstream. Moreover, it is involved in all immunological processes and numerous diseases and metabolic disorders which will be discussed later in this review (51, 138, 139).

It was Thomas Bartholin who first gave the term lymphatics to this system in 1652 (140). Nevertheless, the earliest recognition of the lymphatic system dates to the 4th century B.C.E. by Hippocrates and Aristotle (141). Throughout the following centuries, the importance of the lymphatic system with respect to health was largely overlooked. It was not until 1622 when this system regained recognition and was described by the Italian physician Gasaro Aselli who found the intestinal lymphatic vessels, that he called "lacteals" while dissecting a dog's abdomen (142). Aselli's work was published in 1627 after his death, and that was one of the many landmark discoveries in the 17th century; the golden era for lymphatic system research (142, 143).

Again, key gaps in knowledge about various aspects of the lymphatic system remained understudied for a long time afterwards (143). Yet, three decades ago, the lymphatic system started gaining more scrutiny and interest. Advances in science have led

to the salient understanding of the role of lymphatics and its link to numerous diseases (143, 144). Major milestones in lymphatic system research spanning centuries are summarized in **Table 3.1**.

Table 3.1. Milestones in lymphatic system discovery and research throughout different eras.

Year	Marks related to lymphatic system
460-377 B.C	Hippocrates recognized some lymph nodes in various body areas containing a "fluid absorbed from the tissues" (141).
300 B.C **	Aristotle's detection of a lymphatic vessel. He described them as "fibres" between nerves and veins (141).
1622	Discovery of gut lymphatics by the Italian Physician Gaspare Aselli. He called them ''venae albae aut lacteae'' or (lacteals) (142).
1651	The French Physician Jean Pecquet described the thoracic duct and its valves. He also recognized that gut lymphatics empty into the cisterna chyle and not the liver as previous anatomists claimed (145).
1652-1653	Thomas Bartholin, a Danish anatomist, coined the term lymphatic for the first time which appeared in his book "vasa lymphatica." He also confirmed the findings of Pecquet and illustrated that lymph from the intestine flows till it reaches the thoracic duct and that from the liver also do so separately (140).
1744	Description of the morphology and function of the lymphatic valves by the Dutch botanist and anatomist Frederik Ruysch (145).
1784-1787	Paolo Mascagni demonstrated the lymphatic network of the entire body (146).
1869	Arnold Heller noted the first description of lymph propulsion, observed in collecting lymphatic vessels in the guinea pig mesentery (147).
1992	Discovery of the growth factor/receptor system and related findings by Kari Alitalo, his team, and other international teams (143).
2015	Discovery of the brain lymphatic system by a team led by Drs. Antoine Louveau and Jonathan Kipnis from the University of Virginia School of Medicine (148).

3.2 Structural Organization of the Lymphatic System:

The fluid surrounding body's cells is termed the interstitial fluid. When this fluid enters the lymphatic system, it is referred to as "lymph." It does so through the blind-ended lymphatic capillaries, which are sometimes termed, the initial lymphatics. From there, lymph drains into the collecting vessels, which passes through at least one, but usually several lymph nodes distributed throughout the body. Collecting vessels merge into grander trunks which empty into the ducts. Finally, the ducts return the lymph into the venous circulation, completing the circuit of fluid transport (51, 135, 137).

3.2.1 Lymphatic Vessels:

3.2.1.1 Lymphatic Capillaries:

Lymphatic capillaries, initial or terminal lymphatics are commonly interlaced with the capillaries in the connective tissues of various parts of the body except for bones and teeth (149, 150). These are blind-ended structures that are a one cell-thick layer of thin-walled endothelial cells (151). These cells are 10-60 μm in diameter and possess a unique oak leaf shape (150, 152). They have a discontinuous or absent basement membrane acting as primary valves and overlapping button-like junctions (**Figure 3.1**) (153).

Anchoring fibres tie the initial lymphatics to the extracellular tissue matrices (154, 155). These elastic filaments protect the initial lymphatic from collapsing under high tissue pressure. They also sense the pressure in the intercellular space and signal the opening of the flap-like junctions for drainage of the lymph (152, 156).

3.2.1.2 Lymphatic Precollectors:

They are lymphatic vessels built of an endothelial layer of cells (152, 157). In regions close to the initial lymphatics, the endothelial cells of the precollectors still retain the oak leaf shape. The closer proximity to the collecting lymphatic vessels, the endothelial cells acquire a rhombic form like that of the veins (139, 158).

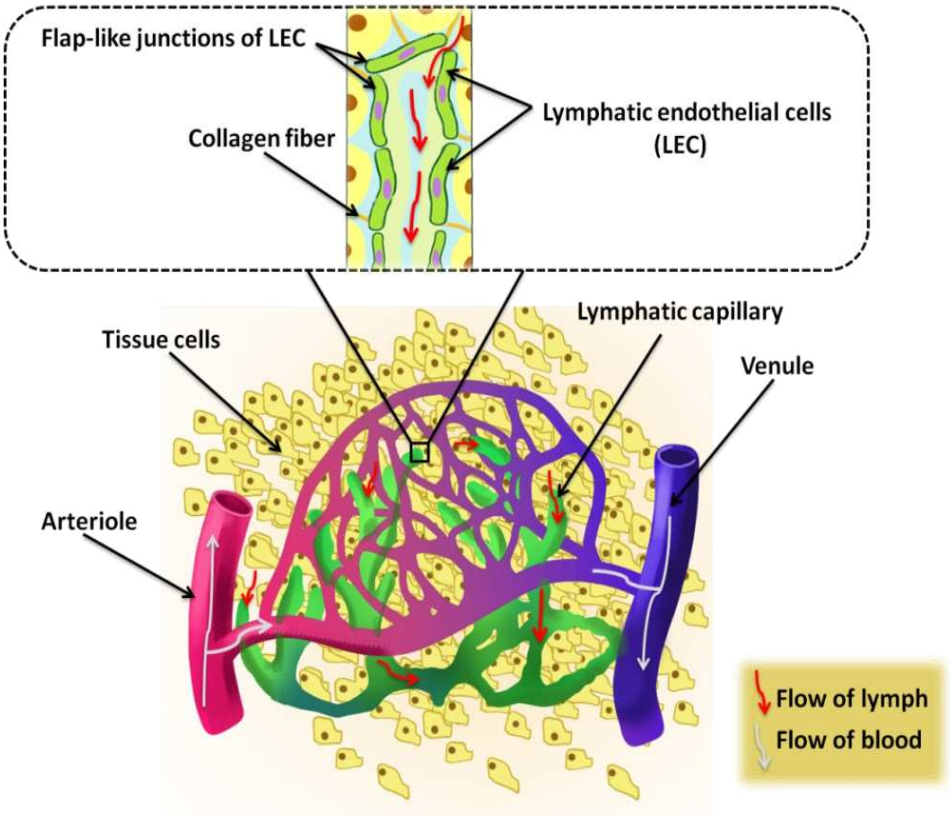

Figure 3.1. Illustration showing the lymphatic capillaries interlaced with the blood capillaries. Network (bottom). The lymphatic capillaries or the initial lymphatics (top) are closed-ended vessels, composed of a single layer of epithelial cells having flap-like junctions in between that serves as valves allowing the interstitial fluid to be drained into the lymphatics. These capillaries are anchored through filaments to the surrounding tissue which help them withstand the high pressure without experiencing a collapse.

These vessels resemble the initial lymphatics in having no smooth muscle layer. Yet, they differ from them in having structured valves within, which are termed secondary valves. The valves here serve in preventing backflow into initial lymphatics (139). Having no smooth muscle layer, lymphatic precollectors rely on the inflow and outflow pressures of individual segments in pushing the lymph forward (137).

3.2.1.3 Collectors:

The next structural vessel organizations in the lymphatic system are the collecting lymphatics. The walls of which are composed of an endothelium layer encircled by a smooth muscle cell layer and a layer of collagen fibres; the adventitia (159).

These lymphatic vessels get thicker as they merge. A new feature of these lymphatic vessels is the microcirculation or the ‘’vasa vasorum’’ that delivers oxygen and nutrients to larger collectors (160). Moreover, the secondary valves here play structural and functional roles. They prevent lymph retrograde movement and also divide the collecting vessels into chambers (137, 159). Each chamber forms a contractile unit called the lymphangion, meaning “lymph heart”. Contraction of lymphangions together with the proper functioning of the valves ensures the smooth unidirectional flow of lymph even against gravity in a standing posture (161).

Usually, many collectors drain into a lymph node, and typically but not always one collecting vessel exits the node. The former is the pre-nodal or the afferent lymphatics and the latter is one of the post-nodal or the efferent lymphatic vessels (162).

3.2.1.4 Trunks:

Structurally, they are the larger counterparts of the lymphatic collectors (162). But functionally, there are some differences; in humans they funnel into two major ducts that return lymph back into the venous circulation. Two major trunks; the intestinal and the lower lumber, drain into a sac-like structure called the cisterna chyli, located at the base of one of the ducts; the thoracic duct (53, 137). Other major trunks (jugular, subclavian and broncho mediastinal) drain directly into ducts (163) as shown in **Figure 3.2**.

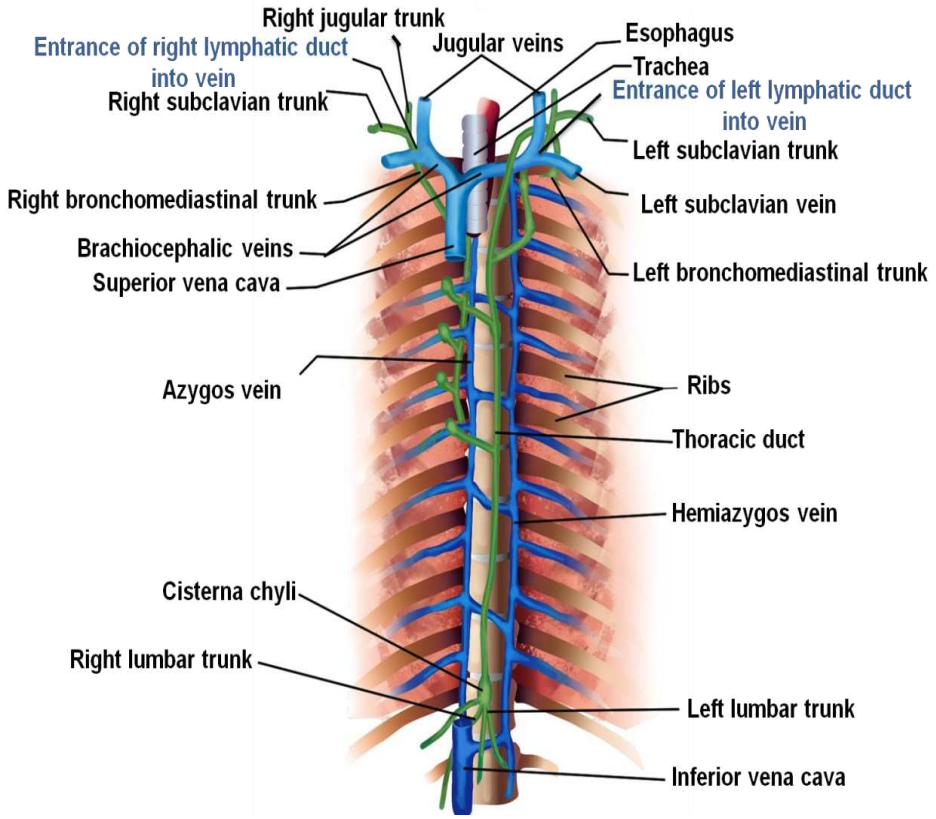

Figure 3.2. Major lymphatic trunks and ducts in the human body. The intestinal and the lower lumber trunks empty into the cisterna chyli, before draining into the thoracic duct. Whereas the jugular, subclavian and broncho mediastinal trunks funnel directly into the duct located on their side. The right lymphatic duct drains lymph into the junction between the right jugular and subclavian veins, whereas the thoracic duct empty into the junction of the same veins on the left side. Modified from (162) with permission.

3.2.1.5 Ducts:

The last part of the lymphatic network is the ducts. Eventually, the larger vessels merge into the lymphatic trunks, that empty into the venous circulation via the right lymphatic duct and the thoracic ducts (136) as depicted in **Figure 3.2.**

The right lymphatic duct is formed from the merger of the right jugular, the right subclavian, and the right bronchomediastinal trunks (162). It receives lymph from the right sides of the head, thorax, and right upper limb and drains into the junction of the right subclavian and right internal jugular veins (164). Lymph from the remaining parts of the body get through the thoracic duct into the junction of the left subclavian and left internal jugular veins (165). It is built of smooth muscle fibres and has a valvar system to prevent lymph backflow and blood reflux at the point where it meets the venous system (165, 166). Summary of the order of lymph flow through the lymphatic network and the structure of each vessel is illustrated in **Figure 3.3.**

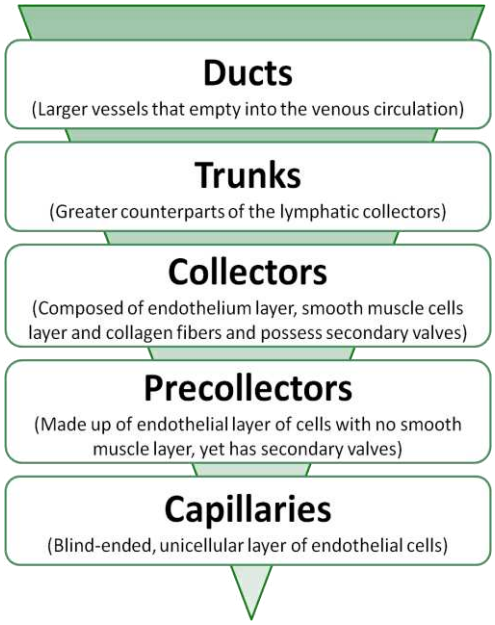

Figure 3.3. Lymphatic network of vessels starting from capillaries and ending with ducts.

3.2.2 Lymphatic Tissues and Organs:

The lymphatic tissues and organs are grouped as primary and secondary based on their functional roles (162). The primary lymphatic organs are the sites of lymphocyte formation and acquisition of immunocompetency and include the red bone marrow and the thymus (162, 167).

The secondary lymphatic organs are where immune responses occur. Lymphatic nodes, spleen and lymphatic follicles are members of this group (167). The first two (the lymphatic nodes and the spleen) are classified as organs because they possess an outer capsule of connective tissue, unlike the lymphatic nodules which lack it and as a result are considered tissues (162). There are numerous lymphatic nodules found within the mucous membranes lining the respiratory, gastrointestinal, and urinary tracts, termed mucosa-associated lymphatic tissues (MALTs) (168). Clusters of these nodules can be found in the tonsils and in the ileum of the small intestine these are referred to as Peyer's patches (169). Out of these different lymphatic organs and tissues, lymph passes only through the lymph nodes which will be detailed next.

3.2.2.1 Lymphatic Nodes:

Lymphatic nodes resemble immunosurveillance units, which functionally serve in filtering the lymph and mounting immune responses against detected antigens (139). These nodes are bean-shaped lymphoid organs placed throughout the body, most prominently near the mammary glands and in the axillae and groin. Lymph nodes range between 1 to 25 mm in length and are divided structurally into two major parts, capsule, and parenchyma (**Figure 3.4**). The capsule is a dense fibrous tissue that runs towards the interior of the node

forming partitions called the trabeculae. The parenchyma has two distinct sections: the cortex and the medulla (167, 170).

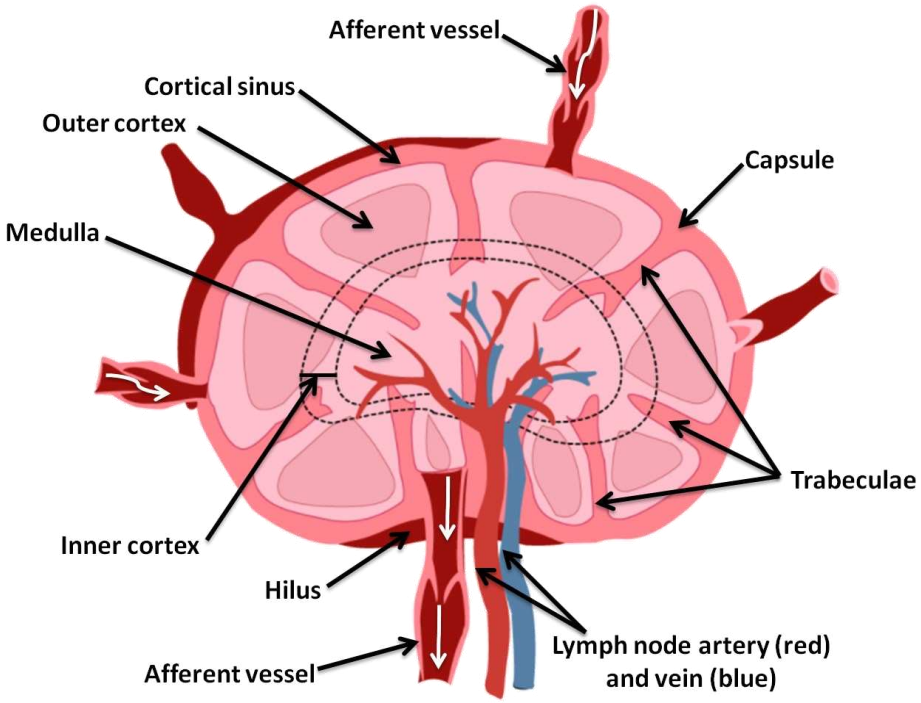

Figure 3.4. Structure of the lymph node. It is composed of the capsule and the parenchyma. The parenchymaencompasses the cortex and the medulla. The cortex is divided into outer and inner parts. The former contains the primary and the secondary follicles. The secondary follicles differ from the primary ones in having a germinal centre (activated B cells with dendritic cells and macrophages) surrounded by a condensation of B cells. Moving inwards there will be T cells and macrophages in the inner cortex, and antibody-secreting plasma cells with the macrophages in the medulla.

The outer cortex houses lymphatic follicles or nodules. There are two types of lymphatic nodules: primary and secondary nodules (171, 172). The former consists of B cells surrounded by a loose network of dendritic cells. Upon encountering an antigen, the macrophages or the dendritic cells stimulates the development of the secondary nodules by the activation of the B cells which are bounded by cortical dendritic cells and macrophages

form what is termed a germinal centre. Surrounding this centre there is a condensation of B cells, forming the outer part of the secondary nodule (172).

There are no lymphatic nodules in the inner cortex; instead, there are T cells and macrophages that migrate from other parts of the body. The macrophages cause the proliferation of T cells to combat antigens. The activated T cells do not reside in the lymph node but rather travel where there is antigenic activity (173).

Cells in the medulla are the antibody-secreting plasma cells that proliferate from the activated B cells in the outer cortex, in addition to the macrophages (162, 174).

Lymph drains into the nodes via the afferent vessels entering the nodes through its convex side. It follows a certain path crossing the sinuses within the node then exits through the efferent vessels emerging from the hilum (a depression on the concave part of the lymph node) (175). Cells might get into nodes with the lymph or through special blood vessels termed high endothelial venules (HEVs) (51).

3.3 Intestinal Lymphatic System:

The intestines are a part of the gastrointestinal organ system and a region in the body that exhibits unique morphology and function of the lymphatics that is not encountered anywhere else. Here the lymphatic system besides drawing out excessive fluids and mounting immunological responses, which are the roles of the lymphatics throughout the body, also facilitates the absorption of dietary lipids through its special lymphatic capillaries; the lacteals (65, 69). In addition, there are several vitamins and food nutrients that use this system to access and enter the systemic circulation.

Structurally, the intestinal lymphatics start with the lacteals, found in the intestinal villi. The lacteals funnel into pre-collecting and collecting vessels located in the mesentery, which in turn drain into the cisterna chyli at the posterior end of the thoracic duct (69).

As illustrated in **Figure 3.5**, lacteals range between 60 and 70% of villi length and are encircled by a mesh of blood capillaries and smooth muscle fibres. A cytoplasmic extension or filopodia is usually attached to the lacteal tip demonstrating the state of regeneration that the lacteals can undergo (53).

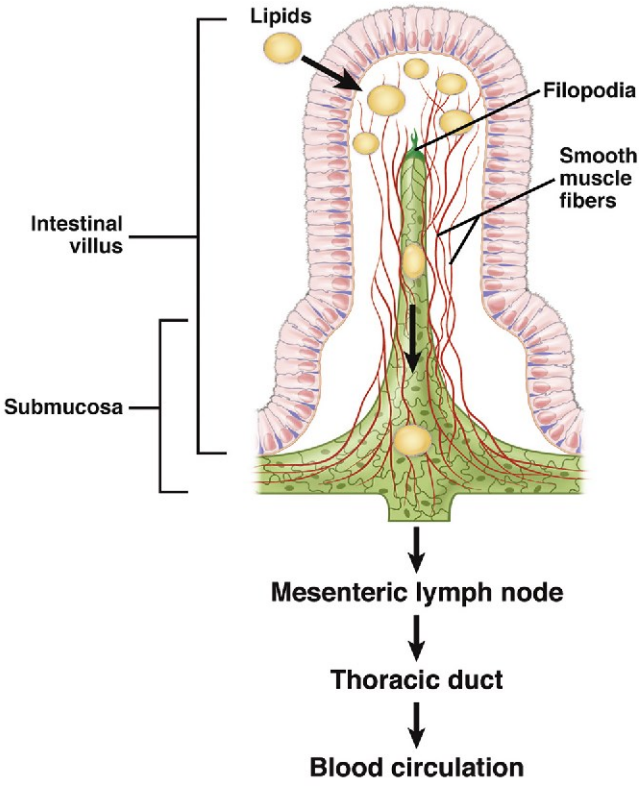

Figure 3.5. Structure of the intestinal lymphatic capillary (the lacteal). It constitutes nearly two thirds of the villi length and is surrounded by network of blood capillaries and smooth muscle fibres. It might have a cytoplasmic extension called filopodia, which indicates the state of active regeneration of the lacteals on which it appears. Lacteals play a vital role in up-taking absorbed lipids and draining them through the mesenteric lymph node into the thoracic duct before they enter into the systemic blood vasculature. Adopted from (53) available under CC BY-NC-ND license.

The discontinuous button-like junctions between lymphatic endothelial cells of the lacteals indicates their functioning in lymph uptake. However, the transition to zipper-like cellular junction in the collecting lymphatic vessels reflects less permeability and the better containment that these vessels must prevent the leakage while transporting lymph (151). Cellular junctions of lacteals were also linked functionally to the chylomicron's entry into the lacteal (176).

Chylomicrons are the form into which lipids and lipophilic components are assembled to be up taken by the lacteals (177). Following their absorption, dietary lipids are hydrolysed into fatty acids and monoglycerides, then re-esterified to triglycerides in the endoplasmic reticulum of the enterocyte's apical membrane (53, 69). The triglycerides, cholesterol, cholesteryl esters, phospholipids, and the apolipoprotein (178) are packaged into chylomicrons and set out from the basolateral membrane of the enterocyte (53). In order to access into lacteals, chylomicrons do not diffuse passively as claimed earlier, but rather are taken up actively through a mechanism involving molecular signalling that is yet to be fully understood (179). However, the vascular endothelial growth factor-A (VEGF-A) has been shown to modulate the cell-cell junctions in lacteals and blood capillaries (180), regulating the lipid uptake process via signalling pathways starting with the binding to the vascular endothelial growth factor receptor-1 (VEGFR-1) and its co-receptor, the semaphorin receptor (NRP1) as depicted in **Figure 3.6** (53).

Lacteals are not the only lymphatic feature present within the intestine. There is another key component there, which is the Peyer's patch. These lymphoid tissues are located within the mucosal lining in the intestine. They compose a gateway for lymphatic

voyage similar to lacteals and are also an immune surveillance site that encounters various ingested immune elicitors like bacteria, viruses and other factors (51, 181).

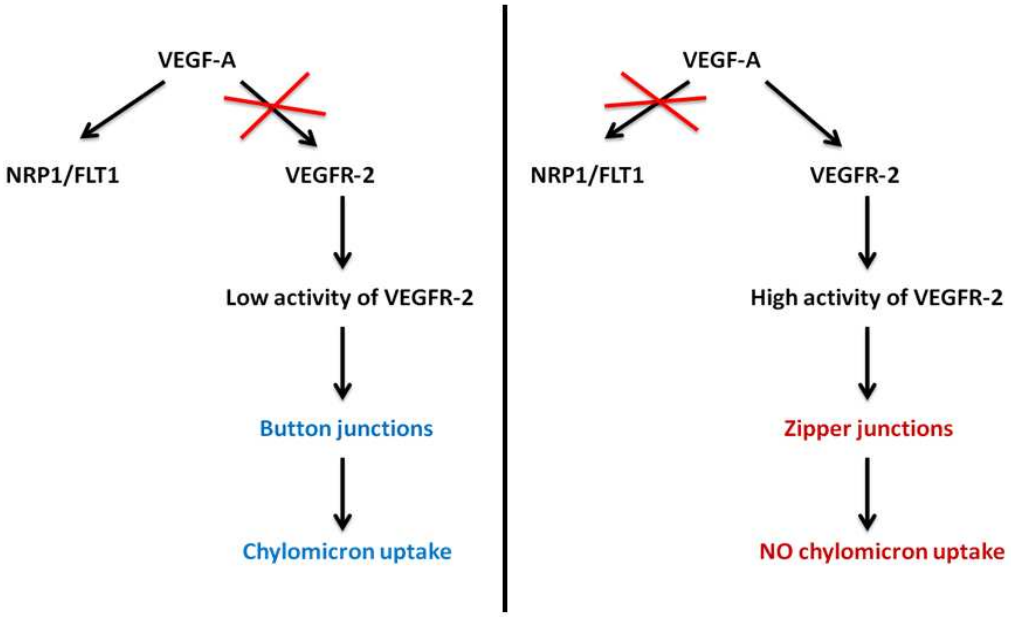

Figure 3.6. Schematic model of cell-cell junctions in lymphatic endothelial cells (LECs) regulating chylomicrons uptake through lacteals. The availability of the vascular endothelial growth factor-A (VEGF-A) for binding the NRP1/Fms-related tyrosine kinase 1 (FLT1) on blood endothelial cells (ECs) results in having the button like junctions between the LECs that enables the chylomicrons uptake into the lacteals. When the opposite is encountered and the VEGF-A binds the vascular endothelial growth factor receptor-2 (VEGF-2) on the LECs, that imparts the tight zipper junctions on the LECs and facilitates the transport rather than the uptake of the chylomicrons into the lacteals.

3.4 Lymphatic System Adding Therapeutic Benefits:

The overall lymphatic function is now thought to be associated with the pathophysiology of various diseases more than initially considered. Thus, lymphatics are an important target site for drugs and their delivery systems used in these conditions, especially lymph resident diseases such as cancer and some viral infections. Moreover, the lymphatic nodes play a central role in generating an immune response, thus they are

considered a crucial target for vaccines (51, 174, 182, 183). For these indications, a new chapter in drug delivery has opened and various formulations have been developed while others are being investigated to target lymphatics through different routes of administration.

Next, the areas of intimacy between the lymphatic system and the pathophysiology of some disorders and diseases are summarized, with the various studies to exploit the lymph targeted delivery to add therapeutic benefits.

3.4.1 Cancer:

Being routes of trafficking through the body, lymphatic vessels are used by the malignant cells to spread. They are preferred over the blood vessels for this mission because of the lymphatic's broader vasculature, lower pressure gradient and higher permeability (184). Usually, the metastases occur in steps, the first of which is the colonization of the sentinel lymph node (51). This can occur through the pre-existing lymphatic vessels or newly formed ones resulting from the induction of tumour secreting growth factors (e.g VEGF-A, VEGF-C and VEGF-D) that stimulate the lymphangiogenesis (formation of new lymphatic vessels) to that node and beyond. Once in the first targeted node (a regional node), disseminating cancerous cells continue to do the same to promote more drainage of the growth factors to the node to aid in invading a distant node using the same strategy (51, 184-187). Other lymphatic markers have also been linked to cancer metastasis such as Prospero Homebox 1 (Prox-1) and Lymphatic Homing Peptide (Lyp-1) (187). Therefore, developing lymphotropic formulations for chemotherapeutic agents and lymphatic biomarkers could enhance their therapeutic outcomes, in terms of target specificity, drug resistance and toxicity.

It has also been delineated that, Lyp-1 is a nano-peptide that binds a specific receptor (p32) which is highly expressed on tumor-related lymphatics, macrophages, and cancer cells (188). The lymphatic targeting of the Lyp-1 achieved via a self-micro emulsifying delivery system (SMEDDS) resulted in decreasing the tumor size in 4T1 Tumor-bearing mice. Concomitant administration of the same peptide with the cytotoxic drug doxorubicin (Dox HCl) exhibited a reduction of the cell viability from 74.3% to 49.6% after 48 hours of incubation in the MDA-MB-231cell line. Thus, lymphotropic delivery of the Lyp-1 can be an effective way to combat tumors (189).

Another example is the cytotoxic anti-cancer agent doxorubicin that has achieved greater antitumor efficacy through a lymphotropic formulation. The subcutaneous administration of liposomal doxorubicin decreased the volume of auxiliary lymph nodes by 56.77% in comparison with the intravenous formulation that caused a 27.08% decrease in auxiliary lymph nodes size using rabbits inoculated with VX2 cells to develop breast cancer. Additionally, this resulted in an increase of the apoptotic cell count by 3.21 and 1.97-fold for the liposomal and the free drug preparations of doxorubicin, respectively. The inhibition of growth and the induction of apoptosis of tumor cells that the liposomal doxorubicin imparted was postulated to lead to higher lymphatic uptake of the developed subcutaneous formulation and the greater drug reaching the regional lymph nodes where metastasis occurs (190).

Moreover, the intravenous and oral administrations of a doxorubicin-quercetin conjugate (DoxQ) demonstrated 5 and ~1.5-fold increase in the area under the curve (AUC) compared with the unconjugated standard drug treatment (Dox), respectively. The volume of distribution at steady state (V_{ss}) imparted with the intravenous DoxQ was 0.138 ± 0.015

where that of the doxorubicin was 6.35 ± 1.06 L/kg in male Sprague–Dawley rats. The oral Dox Q delivery system resulted in double the amount of Dox in the mesenteric lymph fluid than the Dox. The transformed pharmacokinetics and improved oral bioavailability of the DoxQ were attributed to the lymphatic transport of the drug conjugate with the lymphotropic antioxidant flavonoid quercetin (191).

Paclitaxel is used for treating many cancer types, such as breast cancer, lung cancer, ovarian cancer among others (192). Reports on targeted paclitaxel nano-formulations supported its superior chemotherapeutic activity when administered through lymphatics. When incorporated in inhalable solid lipid nanocarriers (SLNs), paclitaxel resulted in tumour cells survival rate of (19.34%) compared with 87% cell viability when free paclitaxel was administered intravenously in a mice lung cancer model. Moreover, the inhalable SLN-paclitaxel showed no toxicity upon prolonged treatment and about 20 times less concentration to inhibit 50% of cell growth (IC_{50}) than intravenously administered paclitaxel (193).

SLNs were also used for the cytotoxic agent etoposide. The study used mice with Dalton's lymphoma to compare the biodistribution of radiolabeled free and nanoparticle-based etoposide through three routes of administration, i.e., subcutaneous, intravenous, and intraperitoneal. Following 24 hour after administration, the subcutaneous route exhibited greater drug uptake by 8-fold and 59-fold than the intraperitoneal and the intravenous ones, respectively. Likewise, subcutaneous administration also showed a relatively low tissue distribution, suggesting lesser systematic side effects of the drug. Therefore, the subcutaneous injection was suggested to be a better route for administering chemotherapeutic drugs targeting lymphatic-related malignancies (194).

Intraduodenal administration of methotrexate solution and SLNs formulations came in favour for the nanoformulations regarding the chemotherapeutic effect as a 10-fold increase in lymphatic drug uptake was reported with drug-loaded SLNs as opposed to the free dug solution using dialysis membrane and rat models (195). Thus, the oral bioavailability of methotrexate can be improved via lipid-based formulations favouring lymphatic transport.

Zara *et al.* also studied oral lymphotropic delivery for cancer drugs using SLNs taking idarubicin as a model drug. The intraduodenally administered formulations of idarubicin showed a 21-fold increase in the area under the plasma concentration time curve compared with the drug solution. Again, the greater biodistribution in the lymphatic system appeared to serve in decreasing the idarubicin concentration in the heart and thus reducing its cardiotoxicity. The 30-fold increase in the elimination half-life of the idarubicin loaded SLNs suggested its potential use as a sustained release delivery system (196).

9-Nitrocamptothecin (9NC) is a potent antitumor agent that is used to treat hepatocellular carcinoma. The liposomal formulation of this drug (9NC-LP) has been shown to demonstrate a greater antiproliferative effect and fewer side effects in a nude mice xenograft model of HepG2 cell line in comparison with the free drug. The higher dose of the 9NC-LP (2.5 mg/kg/d) repressed cancer growth by nearly 87.02% and the lower dose scored 41.66% tumour growth inhibition after three weeks, without any drug-related death. Nevertheless, over half of the animals died on day 14 after administering 2.5 mg/kg/day doses of the free drug. The observed effects with the 9NC-LP systems were attributed to their lymphotropic delivery (197).

Hyaluronic acid (HA) is a natural polymer transported via the lymphatics and when coupled with the chemotherapeutic agent cisplatinum (Pt), it made a successful local pulmonary delivery system with greater platinum concentration in the lung and draining lymph nodes as reported by Xie *et al.* (198). A similar approach was considered with hyaluronan–cisplatin (HA–Pt) nanoconjugate to treat head and neck squamous cell carcinoma (HNSCC). In a developed orthotopic metastatic xenograft model of HNSCC, HA-Pt nanoconjugate achieved complete treatment success for 57% of the female mice whose group also showed significant hindrance of the HNSCC progression in contrast to the standard therapy group ($p < 0.05$) (199).

All previous examples reinforce the importance of lymph-targeted delivery for cancer treatment. However, the lymphatic system is also related to other diseases, as discussed next.

3.4.2 Inflammatory Conditions:

Inflammation is a mechanism of protection against various pathogens and irritants (200). It is characterized by the expansion of both blood and lymphatic networks (angiogenesis and lymphangiogenesis, respectively). Whereas the proliferation of blood vessels exacerbates the inflammation, lymphatics were found to aid in containing the aggravation of this condition (201, 202). The reported mechanistic reasons underlying this was based on the formed lymphatic vasculature acting as clearance conduits, alleviating oedema, and decreasing the levels of pro-inflammatory mediators and immune cells (200). The molecular mechanisms involved in some inflammatory diseases like skin inflammation

(203, 204), inflammatory bowel disease (IBD) (205) and rheumatoid arthritis (RA) (206) and others have been connected to lymphatic biology(200).

Developing delivery systems of lymphangiogenic factors would increase the potential of effective alleviation of inflammatory pathologies. Yet, limited studies are available on this targeted approach. A recent report showed that the antibody-mediated delivery of the vascular growth factor-C (VEGF-C) reduced skin inflammation in two mice models due to its accumulation in the affected tissues and stimulation of the expansion of the lymphatic vascular network (200).

Another study on the lymphatic related effects on inflammation involved the use of the tissue necrosis factor (TNF). It is a pro-inflammatory mediator that was linked to rheumatoid arthritis through its induction of neutrophils which when elevated and impairs the lymphatic pumping and aggravates the inflammation associated with rheumatoid arthritis. A study by Aldrich *et al.* revealed that the intradermal administration of the anti-TNF drug, etanercept, improved lymphatic functioning and reduced the swelling in a rat model of collagen-induced arthritis (CIA) (207).

Intriguingly, many current treatments for inflammatory diseases, such as tocilizumab and infliximab affect lymphangiogenesis (208, 209). These proteins are administered through subcutaneous and intravenous routes and their relatively large size makes at least part of the administered dose to be taken up by the lymphatics (51). Thus, they would exhibit lymph related changes that account for their anti-inflammatory action. Yet, the door is still open for research in treatment options using the lymphatic system-inflammation overlap.

3.4.3 Metabolic Diseases:

Accumulating evidence supports the crosstalk between lymphatics and adipose tissue. The link between lacteal permeability and transport has been already established with adult obesity (176, 210). The disturbance in the signalling pathways modulating the cell-cell junctions of lacteals would result in leakage of fat-rich lymph and its accumulation, leading to diet-induced obesity (176). Insulin sensitivity has also been found to tie with the proper intestinal lymphatics functioning (211). Hyperinsulinemia and inflammation arising from obesity can also affect the lacteals integrity, progressing to deadly complications (53). Nevertheless, there is still an open area of research to dig in here and in other metabolic diseases which were connected to the lymphatic system such as hypertension (212), atherosclerosis (213, 214) and others (51).

In this disease group, there hasn't been translational development of drugs targeting lymphatics for the various indications that have been associated with the lymphatic system yet. Nonetheless, there are drugs that are being used to treat some of these metabolic diseases which have been found to have higher therapeutic efficacy when administrated through delivery systems that favour lymphatic transport. In the aforementioned studies, the reasons behind the better outcome were solely related to the pharmaceutical rather than the pharmacological reasons; with the lymphotropic formulations offering higher bioavailability and preventing the first-pass metabolism. A list of these drugs is in **Table 3.2.**

3.4.4 Infections:

As a system hosting immune surveillance centres and paving immune trafficking pathways throughout the body, the lymphatic system plays a vital role when antigenic invaders enter the body (137). Of special importance are the ones which take advantage of their accessibility to the lymphatics and utilize it to disseminate. Persistent HIV replication was connected to low lymphatic concentrations of the antivirals (215, 216). The list of other infections includes hepatitis (217), Ebola virus and recently the novel human coronavirus, SARS-CoV-2 was added to it (218). This data suggested lymphatics as a therapeutic target that would aid in eradicating certain challenging infections.

One example involves the link of the efficacy of the antivirals in downregulating the replication of the human immunodeficiency virus (HIV) in lymphatic tissue which was revealed to be associated with the lymph node concentration of antiretroviral drugs (219, 220). In support of this contention, the administration of subcutaneous nanoparticles in macaque monkeys indinavir extended the plasma residence times and increased the concentrations of indinavir in the lymph nodes of HIV-2 positive animals. This in turn caused a considerable reduction in the viral RNA load and an incremental increase in the $CD4^+$ T cell count (220).

3.5 Lymphatic System Adding Pharmacokinetic Benefits:

In addition to improving the therapeutic outcomes, lymphotropic delivery can add new possibilities for drugs of low solubility and those that are subjected to the hepatic first-pass effect. Such formulations can increase drug bioavailability, impart higher drug exposure, and lower toxicity by providing a by-pass route of the hepatic circulation to

enable greater systemic access (51, 182). **Table 3.2** summarizes various studies that reported lymphotropic formulations used to improve the therapeutic effects for different indications by enhancing the pharmacokinetics profile of drugs.

Table 3.2. Lymphotropic formulations of drugs targeting various ailments.

Formulation	Drug	Main Indication	Remark	Reference
SMEDDS	Halofantrine	Antimalarial	Lymphatic uptake of the SMEDDS formulation reached 27.4%	(221)
	Valsartan	Antihypertensive	The AUC for the SMEDDS was 607 ng h/mL/hr in comparison to 445.36 and 1.36 h for market formulation	(222)
Microemulsion/ SMEDDS	Raloxifene	Osteoporosis Agent	*In vitro* intestinal permeability studies demonstrated that the microemulsion exhibited significantly higher permeation (90%) compared to the plain drug suspension (41.06%)	(223)
Liposomes	Cefotaxime	Antibiotic	Bioavailability of liposomal cefotaxime was approximately 2.7 times higher than that of the aqueous solution	(224)
	Tobramycin	Antibiotic	The AUC of tobramycin in SLN ~120-fold greater than that following IV administration of tobramycin solution	(225)

SLNs	Clozapine	Antipsychotic	Higher SLN bioavailability than that of the suspension	(226)
	Carvedilol	Antihypertensive	SLNs had higher uptake to the CaCo-2 cells than the drug solution owing to higher lymphatic transport	(227)
	Nimodipine	Prophylaxis of stroke and hypertension	SLNs conducted in male Albino Wistar rats showed 2.08-fold increase in relative bioavailability than that of drug solution, when administered orally	(228)
	Silymarin	For liver disorders	Greater bioavailability and lower hepatotoxicity noted with the SLNs of silymarin compared with commercial product	(229)
Niosomes	Rifampicin	Antibiotic	46.2% of the drug was taken into the lymphatic when the noisomes were administered intraperitoneal route in comparison with 13.1% for the drug solution through the same route	(230)
NLCs	Vinpocetine	For cerebrovascular disorders	The C_{max} for vinpocetine-loaded NLCs was also significantly higher than for the vinpocetine suspension. The area under the curve for the vinpocetine-loaded NLCs was 3.2-fold greater than that of the vinpocetine suspension	(231)

Testosterone	Hormone replacement	The lymphatically transported testosterone undecanoate accounted for between 91.5 and 99.7% of the systemically available ester	(64)

* SMEDDS = Self micro emulsifying drug delivery system, SLNs = Solid lipid nano-particles, NLCs = Nano-structured lipid carriers, AUC= Area under the curve, C_{max} = Maximum plasma concentration.

3.6 Requirements for Lymphotropic Formulations:

Formulations for lymphatic drug delivery, whether for targeting a lymph related disease condition or getting through the lymph to the general circulation- all have certain general requirements that affect their performance. These formulations include lymphophilic emulsions, microemulsions, self-emulsifying and self-micro emulsifying drug delivery systems. Additionally, numerous nanoformulations (e.g., polymeric nanoparticles, nanostructured lipid carriers, solid lipid nanoparticles and others) have also been considered (144, 184, 187).

Nano-sized formulations are found to be superior to actively target lymphatics, especially those which are lipid-based (184). Such formulations are better candidates for lymphatic drug delivery. However, the uptake of these formulations into the lymphatic conduits depends on some factors, such as the route of administration (51). The intravenous administration of cytotoxic agents is reported to result in limited tumour uptake of the drug due to a faster clearance by the phagocytic system (232). An example of such effect has been encountered with the etoposide (Section 3.4.1). In addition, the intradermal route may enhance the lymphatic uptake in comparison with the intramuscular and the subcutaneous routes because of the elevated interstitial pressure and faster flow of lymph within the skin

than in other interstitial sites (233). Likewise, other features such as the particle size, surface charge, hydrophobicity and types of lipids used also affect the lymphatic voyage (184, 187).

The molecular weight, partition coefficient, triglycerides solubility are the main criteria considered for drugs incorporated in lymphotropic formulations (184, 187). Other factors like surface area polarity and pk_a have also been reported to play a role in drug-chylomicron association and thus the intestinal lymphatic uptake (54).

Requirements for both drugs and formulations targeting lymphatics are summarized in **Table 3.3**.

Table 3.3. Criteria for drugs and formulations designed for lymphotropic delivery.

	Factor	Criteria Favouring Lymphatic Transport	Notes/Comments	Reference
Formulation	**Type of lipid**	- Medium chain triglycerides (e.g., Caprylic triglycerides) - Long chain triglycerides (such as the ones in corn oil, olive oil, peanut oil and soybean oil)	The long chain triglycerides support the lymphatic uptake more than the medium chain ones	(234)
	Carrier's Charge	Negative (Zeta potential <-30 mV)	Negatively charged particles shows higher uptake into the lymphatics than neutral (zeta potential between +10 to -10 mV) and positive (zeta potential >+30	(235-237)

		mV) counterparts. However, highly negatively carriers can extend the retention period of in the lymph nodes	
Nano-particle's size	10-100 nm	This is the optimal range for the lymphatic transport, however sizes greater than 100 nm can still provide lymphatic voyage, however at a slower rate	(238)
Hydrophobicity	High	The higher the hydrophobicity of the formulation, the higher the lymphatic uptake	(51)
Emulsifier concentration	< 1.5 % v/v	Concentrations higher than 1.5% v/v tend to decrease the lymphatic uptake	(227)
Molecular weight	> 16,000 Daltons	Molecules of sizes < 10,000 Daltons are readily taken by blood capillaries rather than lymphatics	(239)

Drug	**Triglyceride solubility**	> 50 mg/mL	-	(240)
	Log P	> 5	**-**	(240)

3.7 Conclusion:

Over the last two decades, the functional importance of the lymphatic system in a wide range of diseases has become more evident. Thus, the lymphatic system itself is arising as a potential drug targeting avenue that could enhance the therapeutic outcome of such conditions. There are many studies that have focused on cancer and metastasis and the lymphatic system, however, translational studies on the lymphotropic formulations for therapeutic purposes is still in their infancy for many other disorders including inflammatory and metabolic ones in addition to various infections. Moreover, lymphotropic formulations have been linked to improved bioavailability and pharmacokinetic profiles especially for drug species liable to the first-pass metabolism. Optimized lymphatic targeted drug delivery requires a thorough understanding of the physiology of this system. Therefore, future studies would focus on understanding the detailed mechanisms of the entry and voyage of the lymph and mimicking the endogenous behaviour of lymph transported materials.

CHAPTER FOUR

Lipoproteins within the Lymphatic System: Insights into Health, Disease, and Therapeutic Implications

A version of this chapter is published in:

Appl Chem Eng. 2023;6(2):2202. DOI: 10.24294/ace.v6i2.2202

Reprinted from Reference (178).

4.1 Introduction:

Lipoproteins are complex particles that consist of a hydrophobic core of non-polar lipids surrounded by a hydrophilic membrane made up of phospholipids, free cholesterol, and apolipoproteins (241). These lipoproteins are responsible for various functions such as the absorption and transport of dietary lipids, the transport of lipids from the liver to peripheral tissues, and the reverse transport of lipids from peripheral tissues to the liver and intestine. They also play a role in removing toxic compounds such as bacterial endotoxin from areas of infection (241-245). The lymphatic system works in conjunction with lipoproteins to absorb and transport dietary lipids. Additionally, it plays a vital role in regulating body fluid levels, maintaining the balance of fluids throughout the body. Furthermore, the lymphatic system contributes to the body's defense against infections (56). The relationship between lipoproteins and the lymphatic system have significant implications for the pathophysiology of various diseases.

4.2 Lipoprotein Classes:

Plasma lipoproteins are classified into seven classes based on size, lipid composition, and apolipoproteins. These include chylomicrons, chylomicron remnants, very low-density lipoproteins (VLDL), VLDL remnants which are termed intermediate density lipoproteins (IDL), low-density lipoproteins (LDL), high-density lipoproteins (HDL), and lipoprotein (a) (Lp (a)) (244). Some recognize only four to five main categories, including chylomicrons, LDL, VLDL, HDL, or chylomicrons, VLDL, IDL, LDL, and HDL, respectively, with the rest being grouped under these categories (chylomicron remnants with chylomicrons, and Lp (a) with LDL) (246-248) (**Figure 4.1**)

and **Table 4.1**). NMR continues to be commonly employed for structure elucidation and quantification of chemical mixtures. However, its exceptional sensitivity to the size and density of macromolecules made it highly valuable in the sub classification of major lipoproteins (249).

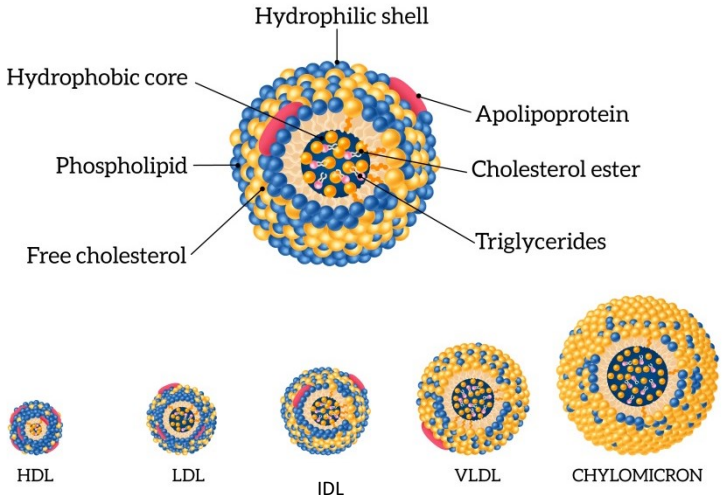

Figure 4.1. Structure of different lipoprotein classes.

HDL: high-density lipoprotein; LDL: low-density lipoprotein; IDL: intermediate-density lipoprotein; and VLDL: very low-density lipoprotein.

Table 1 summarizes the composition of the main lipoproteins categorized based on their buoyant densities.

Table 4.1. Properties (density and size) and major components of main lipoprotein classes.

Lipoprotein	Density (g/mL)	Size (nm)	Major lipids	Major apoproteins
Chylomicrons	<0.930	75–1200	Triglycerides	Apo B-48, Apo C, Apo E, Apo A-I, A-II, A-IV
VLDL	0.930–1.006	30–80	Triglycerides	Apo B-100, Apo E, Apo C
IDL	1.006–1.019	25–35	Triglycerides cholesterol	Apo B-100, Apo E, Apo C
LDL	1.019–1.063	18–25	Cholesterol	Apo B-100
HDL	1.063–1.210	5–12	Cholesterol phospholipids	Apo A-I, Apo A-II, Apo C, Apo E

4.3 Role of Various Lipoproteins in Transporting Drugs, Vitamins, and Xenobiotics:

Lipoproteins, such as low-density lipoprotein (LDL) and high-density lipoprotein (HDL), play a role in transporting various drugs, vitamins, and xenobiotics within the lymphatic system (250, 251). Cholesterol is a component of all lipoproteins and is transported within the lymphatic system to and from cells and tissues by LDL and HDL, respectively (252). Fat-soluble vitamins, including A, D, E, and K, are transported within the lymphatic system in association with lipoproteins such as LDL and HDL (250). Some xenobiotics, such as polychlorinated biphenyls (PCBs) and dioxins, are lipophilic and being transported within the lymphatic system in association with lipoproteins such as LDL and HDL (253). However, not all drugs, vitamins, and xenobiotics are transported in the same way within the lymphatic system, and the extent to which they bind to and are transported by lipoproteins can vary. The presence of these substances in the lymphatic system can also impact its functioning and overall health.

Chylomicrons, also known as cyclic lipoproteins, play a pivotal role in transporting dietary lipids, such as triglycerides and cholesterol, from the small intestine to various parts of the body. They also facilitate the absorption of fat-soluble vitamins, including A, D, E, and K (56). Notably, chylomicrons are crucial for drug absorption since they have the ability to transport lipophilic drugs that would otherwise have poor absorption through the gastrointestinal tract. Lipophilic drugs, characterized by their ability to dissolve in lipids, can be absorbed through the same mechanisms as dietary lipids (254).

When lipophilic drugs are ingested, they become incorporated into chylomicron particles during their formation in the intestinal cells. Subsequently, these chylomicrons

enter the lymphatic system and are transported to the bloodstream, facilitating the distribution of drugs to target tissues (177, 254).

The absorption of drugs via chylomicrons can be influenced by various factors, including the size of the chylomicron particles, the drug dosage, and the dietary lipid intake (53, 56). The size of chylomicron particles can impact the rate and extent of drug absorption. Larger particles are typically cleared more slowly from the lymphatic system, leading to prolonged drug exposure and potentially higher bioavailability. Additionally, the dosage of the drug can affect its absorption through chylomicrons. Higher doses may saturate the transport capacity of chylomicrons, resulting in lower absorption rates and potentially increased variability in drug exposure. Furthermore, an individual's dietary lipid intake can influence drug absorption via chylomicrons. Consuming a high-fat meal can enhance chylomicron formation, thereby increasing drug absorption. Conversely, a low-fat meal may reduce chylomicron formation and subsequently decrease drug absorption (54). Therefore, understanding the role of chylomicrons in drug absorption is crucial for optimizing drug delivery and improving therapeutic outcomes.

4.4 Role of Chylomicrons in Drug Absorption:

Chylomicrons are large lipoproteins that are rich in triglycerides and are formed in the intestinal cells or enterocytes from dietary lipids. The main structural protein in chylomicrons is apolipoprotein 48, although some enterocytes also form Apo B-100 chylomicrons. Other apolipoproteins that can associate with chylomicrons include A-I, A-II, A-IV, C-I, C-II, C-III, and E (177, 244, 254, 255).

Triglycerides from food are hydrolyzed into free fatty acids (FFA), diglycerides (DG), and 2- monoglycerides (2-MG) as they pass through the gastrointestinal tract and reach the small intestine. In enterocytes, these hydrolysis products are re-esterified and packaged into chylomicrons (53, 54). The formation of chylomicrons begins in the endoplasmic reticulum (ER), where Apo B-48 is transported across the ER membrane by the microsomal triacylglycerol transport protein (MTP). In the ER lumen, Apo B-48 associates with phospholipids, mainly phosphatidylcholine (PC), and some triacylglycerol (TAG) to form pre-chylomicrons, which are then transported to the Golgi apparatus for glycosylation and association with other apolipoproteins. The transport vesicles then bud off from the Golgi apparatus and fuse with the basolateral membrane of enterocytes to release the chylomicrons into the lamina propria (248, 255-257). The intestinal lymphatic capillaries take up chylomicrons and deliver them to the venous circulation via the thoracic duct (54).

Chylomicrons play a crucial role in delivering nutrients to muscles and adipose tissues, facilitated by their interaction with lipoprotein lipase (LPL). This enzyme, found in muscle and adipocytes is anchored to the capillary endothelium near these tissues. The activation of LPL relies on Apo C-II, which is present on the surface of chylomicrons.

When activated, LPL hydrolyzes the triglycerides in chylomicrons, breaking them down into free fatty acids that can be taken up by adjacent muscle cells and adipocytes for energy or storage (258, 259). Additionally, some of the free fatty acids released from chylomicrons bind to albumin and are transported to other tissues (259).

As the triglycerides in chylomicrons are hydrolyzed by LPL, the chylomicrons reduce in size and transform into chylomicron remnants. During this process, these remnants acquire Apo E and transfer their apolipoproteins, including Apo A and Apo C, to other lipoproteins, mainly HDL. The transfer of Apo C-II from chylomicrons to HDL decreases the ability of LPL to further break down triglycerides. However, it's essential to note that another apolipoprotein, Apo C-III, plays a significant role in regulating lipid metabolism by inhibiting LPL's action. Apo C-III acts as a potent inhibitor of LPL activity, resulting in reduced hydrolysis of triglycerides in chylomicrons and other lipoprotein particles. Consequently, this inhibition leads to impaired lipolysis and delays the clearance of chylomicron remnants from the circulation (259-261).

Moreover, Apo C-III's interference goes beyond LPL inhibition. It also affects another critical process in lipoprotein clearance, which involves Apo E. Apo E is essential for the uptake of chylomicron remnants by the liver, achieved through interactions with specific receptors on hepatocytes. However, Apo C-III can compete with Apo E for binding to lipoprotein particles, reducing the availability of Apo E and subsequently interfering with efficient lipoprotein clearance (260). The chylomicron remnants, with Apo E still present, bind to various hepatic receptors, including the LDL receptor, Low-Density Lipoprotein Receptor-Related Protein (LRP), and the co-receptor syndecan-4, and are taken up by hepatocytes. The cholesterol in these particles is then used by hepatocytes to produce VLDL, bile acids, or secreted into the intestine with bile (244, 261-263).

As we have explored the essential role of lipoproteins, especially chylomicrons, in facilitating the delivery of drugs from the small intestine through the lymphatic system to the bloodstream, it becomes imperative to further investigate the relationship between

lymphatic conduits and lipoproteins in the context of how these conduits influence lipoprotein dynamics and their potential applications in therapeutics. By shedding light on these mechanisms, we can uncover valuable insights that enable us to optimize lipoprotein-based drug delivery systems and identify new therapeutic targets.

4.5 The Impact of Lymphatic Conduits on Lipoprotein Dynamics and Therapeutic Potential:

The role of lymphatic conduits in maintaining fluid balance is crucial as they drain excess interstitial fluid from the body back into the bloodstream. These conduits also serve as the entry point for different macromolecules, including lipoproteins, on their journey to the bloodstream. Recent studies have highlighted the significance of the lymphatic journey of lipoproteins, which has a direct impact on various physiological processes (54, 264). For example, acute exposure to low-density lipoprotein (LDL) has been linked to an increase in the frequency of contraction of collecting lymphatic vessels and subsequent lymphatic flow (265). This finding suggests that LDL may modulate lymphatic function, which could have implications for fluid homeostasis and the transport of other macromolecules via lymph. Moreover, the removal of cellular cholesterol through peripheral lymph high-density lipoprotein (HDL) is believed to play a critical role in completing the journey of peripheral tissue cholesterol to the liver (266). This function is particularly important near the heart, as lymph mediated HDL trafficking from artery walls has been shown to decrease the size of atherosclerotic plaques (267). In the context of atherosclerosis, the accumulation of low-density lipoprotein (LDL) within the arterial wall leads to the formation of plaques. These plaques consist of lipids, immune cells, smooth muscle cells, and connective tissue (268). Further studies are needed to elucidate the underlying mechanisms and explore the

therapeutic implications of lymph-mediated HDL trafficking in the context of atherosclerosis and cardiovascular health.

Deficiencies in lymphatic function can have direct effects on lipoprotein profiles and related physiological processes. For example, decreased levels of plasma HDL and its related protein and lipid have been documented upon lymphatic diversion (269). Similarly, increased levels of plasma very low-density lipoprotein (VLDL) and LDL have been linked to lymphatic vessel dysfunction in mouse models of atherosclerosis (266). Elevated plasma LDL and decreased HDL levels are major risk factors for the metabolic syndrome, which is associated with atherosclerosis, obesity, increased blood pressure, and glucose intolerance (270).

The intestinal lymphatic system is a promising route for delivering drugs with poor solubility and bioavailability. Examples of drugs and formulations delivered via the intestinal lymphatic system include lipophilic drugs such as cyclosporine, which is used to prevent organ rejection in transplant patients. Oral administration of cyclosporine in a self-emulsifying drug delivery system (SEDDS) improved its bioavailability by promoting lymphatic uptake (240). Another example is the anti-cancer drug paclitaxel, which has low solubility in water and poor oral bioavailability. Oral administration of paclitaxel in a lipid-based formulation improved its absorption and lymphatic uptake, leading to increased efficacy against cancer (271). Additionally, lipid-based formulations have been used to deliver peptides and proteins via the lymphatic system. For example, insulin has been incorporated into lipid-based formulations and shown to enhance its lymphatic transport and reduce its degradation (272). Overall, the intestinal lymphatic system has shown promise as a delivery route for a range of drugs and formulations.

4.6 Conclusion:

While significant progress has been made in unraveling the intricacies of lipoprotein trafficking and remodeling within the lymphatics, there remains a considerable amount of unknowns regarding the detailed mechanisms and factors that regulate these processes. The gaps in our understanding present an opportunity for further exploration and research. By delving deeper into these processes, we have the potential to advance our knowledge, identify novel therapeutic interventions, and pave the way for innovative approaches to tackle a wide range of diseases associated with lipoprotein dysfunction and lymphatic related diseases.

CHAPTER FIVE

Understanding Lymphatic Drug Delivery through Chylomicron Blockade: A Retrospective and Prospective Analysis

A version of this chapter is published in:

J Pharmacol Toxicol Methods. 2024;129:107548. DOI: 10.1016/j.vascn.2024.107548

Reprinted from Reference (592).

5.1 Background:

5.1.1 Overview of the Lymphatic System:

The lymphatic system, an integral component of the circulatory system, comprises a complex network of lymphatic vessels, tissues, and organs (56). Its organs encompass the bone marrow, thymus, lymph nodes, and spleen (51). Within the lymphatic tissues are lymphatic follicles situated in the mucous membranes lining the respiratory, gastrointestinal, and urinary tracts, collectively termed mucosa-associated lymphatic tissues (MALTs) (168). These nodules form aggregates in structures like the tonsils and the ileum of the small intestine, known as Peyer's patches (54).

The lymphatic system serves several key functions, including maintaining fluid balance, transporting dietary lipids and fat-soluble vitamins, and regulating the immune responses (51, 54). Unlike the closed cardiovascular system, where the heart pumps blood throughout the body, the lymphatic system operates as an open-ended network without a central pumping organ (56). Lymph, a clear to white fluid, flows through lymphatic vessels, carrying excess fluid and other substances from tissues back to the bloodstream, thus, serving as an intermediate between the tissues and the vasculature (264).

Each day, approximately 90% of the plasma propelled into the interstitial space by arterioles is reabsorbed into venules (135). The remaining fluid is subsequently drained through the lymphatic system. The entrance into the lymphatic vasculature is facilitated through initial lymphatic capillaries featuring flap-like junctions, aiding in the removal of excess fluid, along with macromolecules, cells and waste products, from the interstitium (137). Subsequently, the lymph travels through various lymphatic vessels, including

lymphatic collectors that merge into larger trunks, and ultimately emptying into lymphatic ducts. These ducts then return lymph to the venous blood circulation (135, 137).

Within the intestinal region, the lymphatic capillaries known as lacteals exhibit distinctive structure and function (69). These specialized vessels play a key role in absorbing dietary lipids, fat-soluble vitamins, and other xenobiotics (177, 264). Situated in the intestinal villi, lacteals channel into pre-collecting and collecting lymphatic vessels found in the mesentery. These vessels, in turn, drain into the cisterna chyli located at the posterior end of the lymphatic duct (thoracic duct) that connects to the venous blood (53).

5.1.2 Lymphatic Drug Delivery:

Before, the significance of the lymphatic system was primarily functional; and related to its role related to immunity, maintaining fluid balance and transporting lipids. However, recent progress in understanding the lymphatic system, along with its crucial involvement in numerous diseases, immune regulation, and cancer spread, has led to new insights. These advancements have prompted the exploration of novel approaches to develop vaccines, drugs, and drug delivery systems tailored to enhance delivery into or through the lymphatic system (51, 54, 56).

Lymphatic targeted delivery offers many advantages, such as increased drug exposure, especially following oral administration, and an increased concentration of the drug in the lymphatic system (51, 273). When a drug is orally administered, it has been presumed to predominantly absorb in the small intestine and enter the venous circulation through the hepatic portal vein, potentially leading to losses of highly metabolized drugs in the liver. However, drugs entering intestinal lymphatics bypass the liver and its first-pass

effect, potentially leading to increased oral bioavailability (53, 273). Moreover, targeting lymphatics can boost therapeutic efficacy by concentrating the drug in the lymphatics, minimizing potential non-specific tissue uptake and off-target toxicities to other tissues (182, 184).

Drugs accessing the intestinal lymph utilize three main pathways: firstly, absorption occurs through a transcellular route, closely associated with the triglyceride core of chylomicrons; secondly, drugs can pass through microfold cells (M cells) located in the lymphatic Peyer's patches; and thirdly, there's a paracellular route, potentially facilitated by absorption enhancers (55, 234). These pathways converge, guiding drugs into the mesenteric lymph, which then progresses to empty into the thoracic duct. From there, it enters the junction of the left subclavian and left internal jugular veins, merging with the venous blood supply in the superior vena cava before finally reaching the right atrium of the heart (135, 136). In contrast, drugs entering the bloodstream from the small intestine via the portal blood undergo hepatic first-pass metabolism in the liver before joining the venous circulation through the inferior vena cava (274). Subsequently, all blood follows the same route in the well-known heart-lung-heart cycle. Starting from the right atrium, the blood is propelled to the right ventricle, then in the first pass to the lungs for pulmonary oxygenation. From the lungs, the oxygenated blood and drug within it returns to the left atrium and is subsequently pumped to the left ventricle. Finally, the left ventricle propels the oxygen-rich blood and drug throughout the entire body for action, disposition and subsequent elimination (275) as seen in **Figure 5.1.**

Considering all the pathways through which orally administered drugs access the systemic circulation, the following general bioavailability (F) equation, describing the

amount reaching the systemic circulation, falls short in clearly accounting for and incorporating the lymphatic component (276).

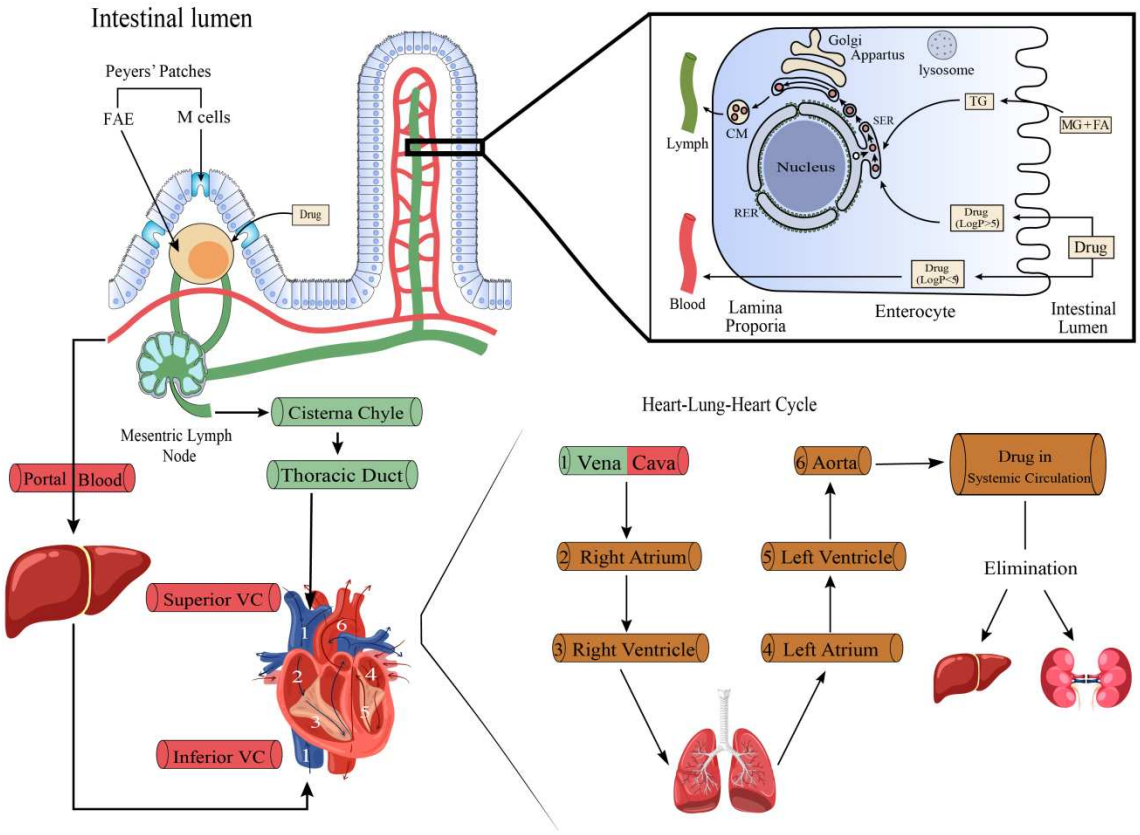

Figure 5.1. Journey of drugs from the intestinal lumen to the systemic circulation. Transcellular drug absorption can occur through both portal and lymphatic pathways. Drugs with low lipophilicity (log P < 5) are absorbed into enterocytes before entering the portal blood circulation. These drugs then travel to the liver, after which they get into the right atrium through the inferior vena cava, and complete the heart-lung-heart cycle, ultimately entering the systemic blood. Lipophilic drugs (log P > 5) are typically packaged into chylomicrons within enterocytes. As these chylomicrons enter the lamina propria, they are taken up by intestinal lymphatic vessels (lacteals) that funnel into lymphatic vessels in the mesentery. This flow drains into the cisterna chyli at the posterior end of the thoracic duct, leading to the junction of the left subclavian and left internal jugular veins. Drugs then enter the right atrium through the anterior vena cava, undergoing the heart-lung-heart cycle before reaching systemic blood. From the 1. vena cava, blood gets the 2. right atrium, then it moves into the 3. right ventricle before making its initial journey to the lungs for pulmonary oxygenation. After being oxygenated in the lungs, the blood, along with any

accompanying medication, flows back to the 4. left atrium. It is then propelled into the 5. left ventricle, which in turn pumps the oxygen-rich blood and medication though the 6. aorta to the entire body for various actions, disposition, and eventual elimination. Additionally, another main intestinal lymphatic pathway involves drugs passing through M cells of Peyer's patches in the intestinal lumen, reaching the mesenteric lymph and joining the previously described flow until entering the general systemic vascular circulation.

$$\mathbf{F = F_{absorbed} \times F_{gut} \times F_{liver}}$$

Where:

F = Fraction of the drug reaching the systemic circulation (bioavailability)

$F_{absorbed}$ = Fraction of the drug absorbed into the intestinal cells

F_{gut} = Fraction of the drug escaping gut decomposition, metabolism, or loss into feces

F_{liver} = Fraction of the drug escaping first-pass metabolism by the liver

For a drug with multiple absorption pathways, the bioavailability equation becomes more complex. F is the total bioavailability, which is the fraction of the administered drug that reaches the systemic circulation from all relevant pathway inputs. It must be expressed as the sum of the individual bioavailabilities through each pathway (**Figure 5.2**).

A simplified version of the equation would be:

$$F = F_1 + F_2$$

Where:

F_1 and F_2 are the individual bioavailabilities through each pathway and each is a fraction of the drug absorbed through a specific pathway (portal and lymph, respectively).

The lung is a first-pass organ that may or may not extract drugs before reaching the systemic circulation, therefore, fraction of the drug escaping the first-pass metabolism by the lung (F_{lung}) should be considered and recognised as well and may not be negligible and should not be overlooked.

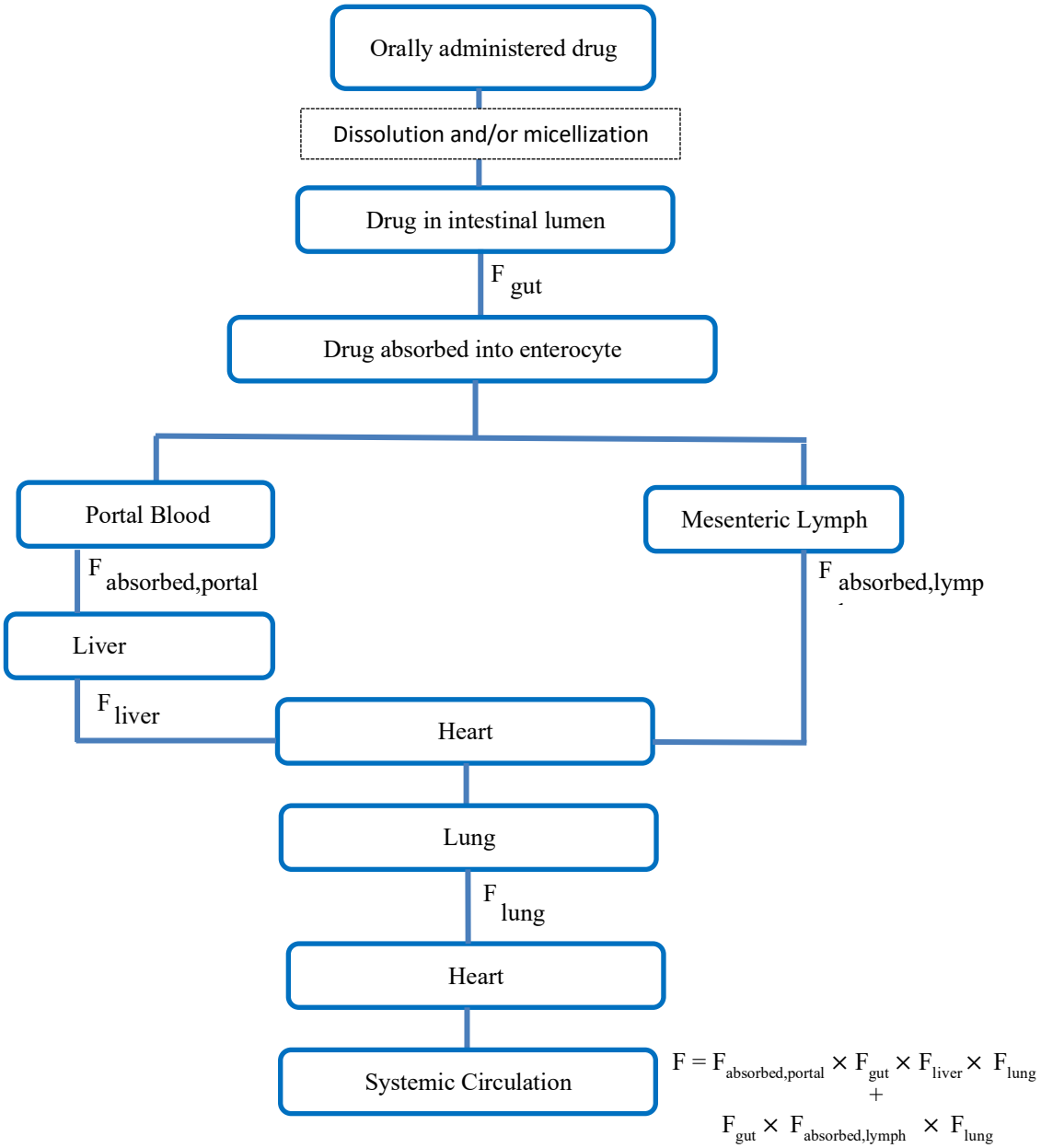

Figure 5.2. Illustration of movement of orally administered drugs until reaching the systemic circulation and the impact of that on the description and quantification of bioavailability.

Consequently, the bioavailability of the drug through the hepatic portal system (F_1) can be represented by the equation:

$$F_1 = F_{absorbed,portal} \times F_{gut} \times F_{liver} \times F_{lung}$$

Where:

$F_{absorbed,portal}$ = Fraction of the drug absorbed from the enterocyte into the hepatic portal blood.

Additionally, the bioavailability of drug through the lymphatic system (F_2) can be represented by the equation:

$$F_2 = F_{gut} \times F_{absorbed,lymph} \times F_{lung}$$

Where:

$F_{absorbed,lymph}$ = Fraction of the drug absorbed through the intestinal lymphatics. This encompasses the various mechanisms of intestinal lymph absorption, such as chylomicron uptake, passage through M cells, or the paracellular pathway.

When both absorption pathways (portal and lymph) are combined together, the equation will be:

$$F = F_{absorbed,portal} \times F_{gut} \times F_{liver} \times F_{lung} + F_{gut} \times F_{absorbed,lymph} \times F_{lung}$$

If negligible lung extraction on the first pass is assumed, then the equation reduces to:

$$F = F_{absorbed,portal} \times F_{gut} \times F_{liver} + F_{gut} \times F_{absorbed,lymph}$$

This equation assumes independence between the pathways meaning the absorption through one pathway does not affect the absorption through the other. Thus, if there is negligible lymph absorption the equation could be reduced to:

$F = F_{absorbed} \times F_{gut} \times F_{liver}$

Conversely, if a drug is targeted to be absorbed solely through the lymphatic pathway and not able to be absorbed through the hepatic portal system:

$F = F_{gut} \times F_{absorbed,lymph} \times F_{lung}$

In light of the above discussion and taking into consideration pre-systemic losses in the gut, liver, and lungs, another comprehensive general equation would be as follows:

$F = \text{Drug Input x } F_A \times (1\text{-}E)$

$F = \text{Drug In x } F_A \times (1\text{-}E)$

Where by:

Drug in = Sum of drug input into the body

F_A = Drug absorption into the body through all pathways

E = Extraction or loss across all first-pass organs and metabolically active tissue or fluid including gut, liver and, lung etc.

The primary route for the absorption of lipophilic drugs (LogP > 5 and a solubility of > 50 mg per g in long-chain triglycerides) - is through the intestinal lymphatics via the chylomicron pathway. These drugs are likely to be preferentially absorbed into the

intestinal lymphatics because of their ability to incorporate with chylomicrons (59, 277, 278). If the desired drug fails to meet these criteria, there are alternative strategies to get it into the chylomicrons. This can be achieved by adjusting its lipophilicity, employing a lipid-based drug delivery system, or creating a lipophilic prodrug (138, 278, 279). For a lipophilic prodrug, the original drug is chemically bonded to a lipophilic component through a linker that can be readily broken down within the body (279). Additionally various drug delivery systems have been utilized to target the lymphatic system (**Table 5.5**) including numerous nano-formulations (54, 138, 273, 278, 280, 281).

5.2 Lymph Blockage Models:

Scientists have used diverse methods to explore and quantify intestinal lymphatic uptake. *In-vitro* models, such as the $CaCO_2$ cellular model and other cellular models, along with models involving chylomicron association, have been reported (52, 282). *In-vivo* methods include the lymphatic cannulation method and the lymph blocking method (184, 283).

This review specifically delves into lymph-blocking models, where the focus is on studying the transport of drugs through the lymphatic system by impeding the production or secretion of chylomicrons from enterocytes. The study of the pharmacokinetics of a drug can demonstrate reduced systemic exposure of a substrate, typically a drug, following the administration of a chylomicron inhibitor compared to when a chylomicron inhibitor is not administered and this provides experimental evidence that suggests absorption, may be at least partially, through the lymphatic route. A typical pharmacokinetic profile will demonstrate that without chylomicron blockade a drug is absorbed over time and reaches a

maximum concentration (C_{max}) and its pharmacokinetics can be followed with serial concentration-time points (**Figure 5.3**, solid line). Upon the administration of a chylomicron blocker before the drug and formulation in question a reduction in both maximum concentration (C_{max}) and the area under the concentration-time curve (AUC) and a shorter time to maximum concentration (T_{max}) will also be apparent depending on the extent of input through the slower lymphatic route to the systemic circulation with the reduction between the two experimental conditions over time representing lymphatic absorption of the drug (**Figure 5.3**, dashed line).

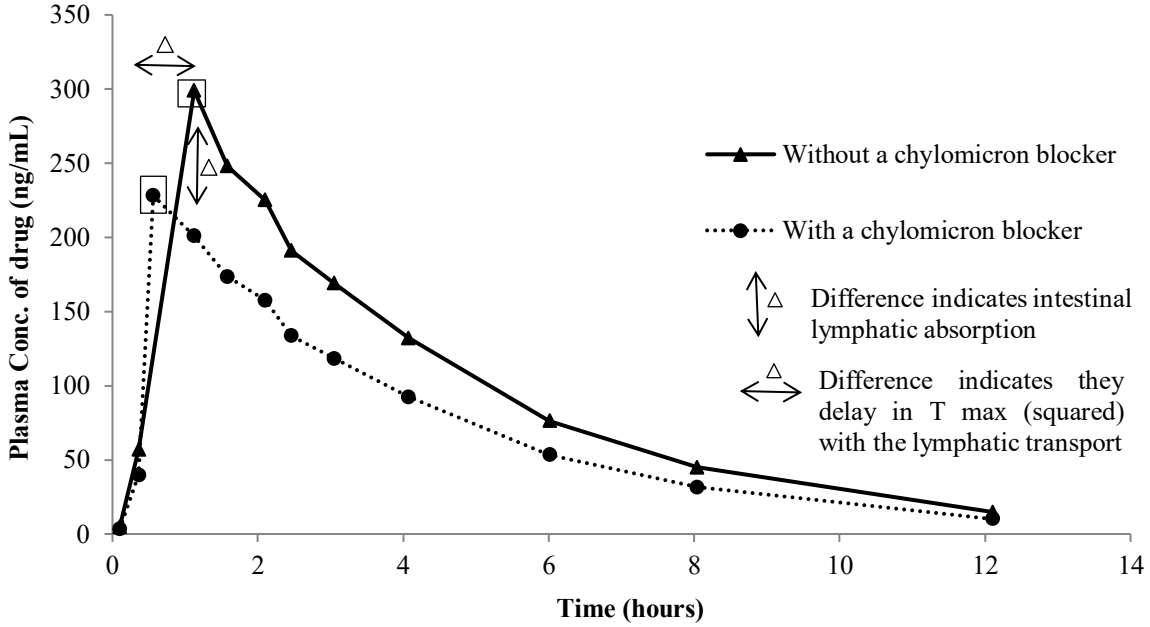

Figure 5.3. Hypothetical graph of drug plasma concentration time profile with and without chylomicron blocker for a drug subjected to intestinal lymphatic absorption.

As previously demonstrated in *in-silico* simulations the total concentrations of drug in the circulating blood are the sum of the drug entering from each of the two pathways (i,e. lymphatic and portal). The drug absorption constant into the intestinal lymphatics (ka_{lymph})

is assumed to be slower and as there is additional processing required within the enterocytes for drug uptake into the mesenteric blood. Contrarily, the drug absorption constant into the portal circulation (ka_{portal}) is of a higher value (284). For low, moderate and high E drugs, there are increases in T_{max} with increases in $F_{absorbed,lymph}$. It should follow that with lymphatic blocking and decreases in $F_{absorbed,lymph}$ a corresponding reduction in T_{max} should also be apparent in comparative pharmacokinetic studies.

We identified 48 studies in the literature that provide such data to determine an effect on T_{max} with a chylomicron inhibitor. In all of these studies whether the drug was high medium or low E (extraction) in the model was never mentioned. Furthermore, the effect on T_{max} was not reported nor discussed in 13 of these studies (285-298). Consistent with the *in-silico* study, findings and pharmacokinetic theory it was reported but not clearly discussed that a reduction in T_{max} occurred with the use of chylomicron blockers was apparent in six studies (299-304). Moreover, it was noted that the T_{max} following administration of a blocker fell within the same range as the animals that did not receive the blockers in some of these reports. There was no apparent effect on this pharmacokinetic index (T_{max}) observed in 24 of the different drugs examined in these studies (287, 305-327). Contrary to pharmacokinetic theory it was evident that treatment with a chylomicron blocker led to a longer T_{max} in at least four studies (328-331), however, no discussion, or explanation was put forth for these findings. There was a discussion regarding the T_{max} of cinacalcet where an unfamiliar rise in the levels of cinacalcet in both serum and tissues was observed in animals pre-treated with cycloheximide (chylomicron blocker), approximately 20 hours after administering the drug. The late increase in cinacalcet concentrations was suggested to be due to either delayed absorption from the gastrointestinal lumen, because

of significantly reduced gastrointestinal motility, or impaired elimination imparted by cycloheximide (306). The toxicological manifestations of cycloheximide and its route of administration and dose are likely to be factors responsible for augmented T_{max} effect findings in several studies (332).

Chylomicrons are spherical particles that consist mainly of a core comprising about 84% triglycerides and around 7% cholesterol, enveloped by a monolayer composed of nearly 7% phospholipids, ~2% cholesterol, and 2% proteins (264). Typically, dietary lipids undergo encapsulation into chylomicrons within the cytoplasm of enterocytes before being absorbed by lacteals (333). The triglycerides from ingested lipids undergo hydrolysis by lipases, breaking down into monoglycerides and fatty acids prior to reaching the duodenum. Once inside the enterocytes, long-chain fatty acids ($C \geq 12$) and monoglycerides are re-esterified in the rough endoplasmic reticulum forming primordial lipoprotein particles (**Figure 5.4**). These particles include a protein component (apo B) connected with a phospholipid monolayer. Simultaneously, the smooth endoplasmic reticulum facilitates the synthesis of large triglyceride-rich droplets. The final step in chylomicron biosynthesis is core expansion, characterized by the merging of the primal lipoproteins with the big triglyceride-rich droplets. Subsequently, the chylomicron is transported to the Golgi apparatus for packaging and secretion which occurs through an exocytosis process (49, 50).

To investigate intestinal lymphatic uptake via the chylomicron flow blockade approach, various models have been developed and implemented to target the various steps of chylomicron formation and secretion. The data collection method is outlined below, and

the various models are presented in **Figure 5.5**, with detailed explanations provided in the subsequent sections.

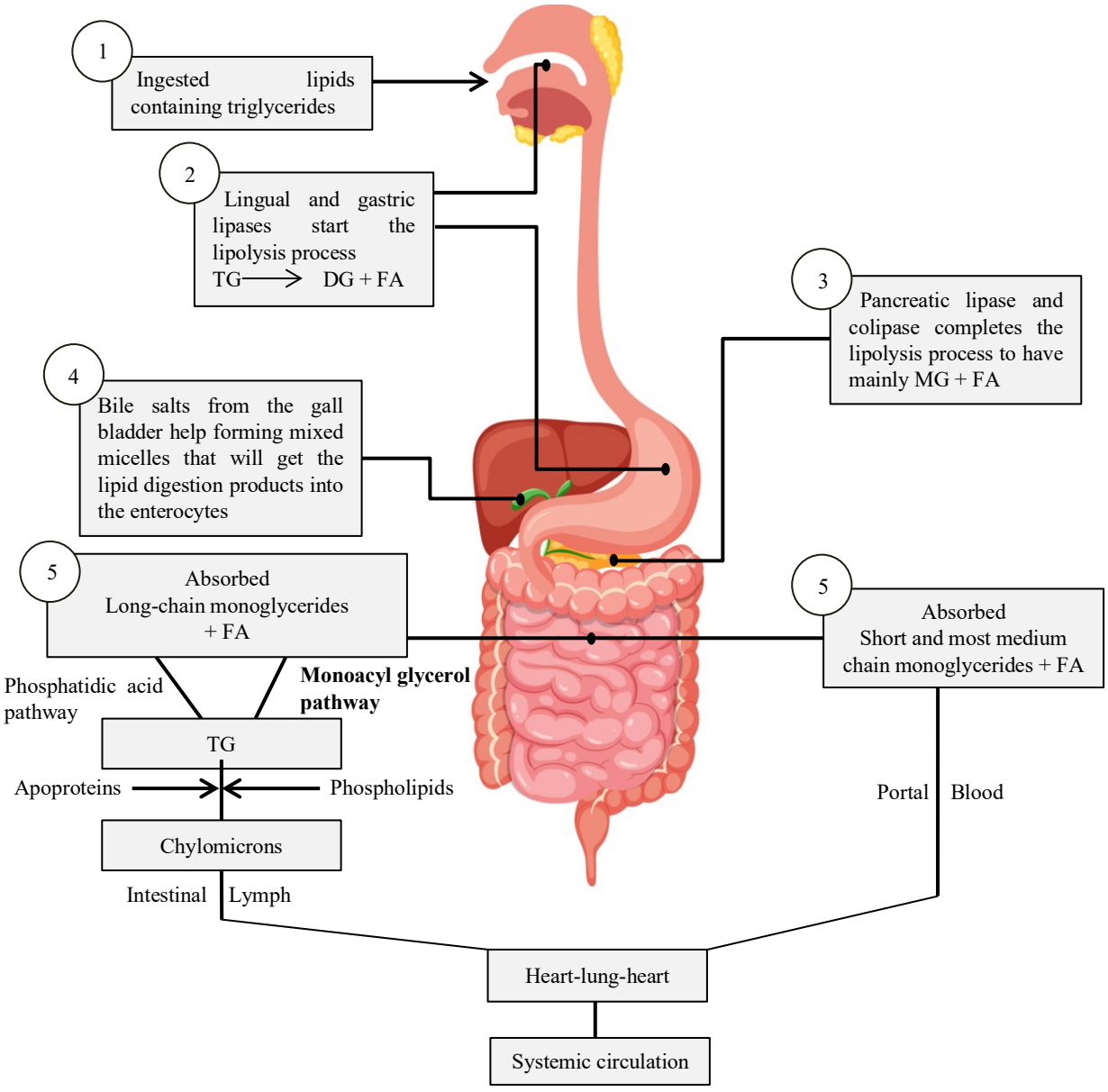

Figure 5.4. Demonstration of the steps involved in the digestion and absorption of ingested triglycerides.

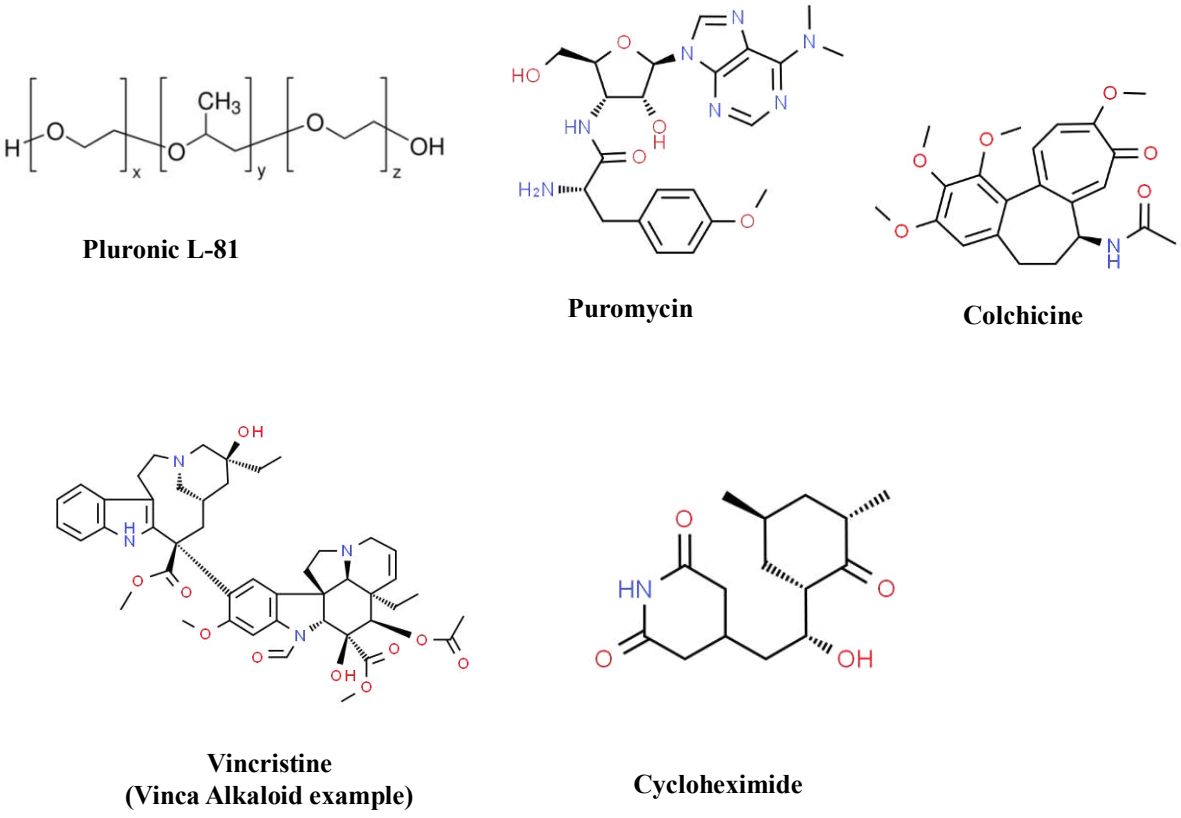

Figure 5.5. Structure of the different chemical substances used in chylomicron blocking models to study intestinal lymphatic transport of drugs. Pluronic® L-81 structure shows the polyoxyethylene-polyoxypropylene-polyoxyethylene (EO_3-PO_{43}-EO_3) triblock structure. The image is available under Creative Commons licence through the link: https://en.m.wikipedia.org/wiki/File:Pluronic_P-123_structure.png. The link was accessed December 1, 2023. Structures of puromycin, colchicine, vincristine and cycloheximide were obtained from Chemspider available under the IDs: 388623, 5933, 5758, and 5962, respectively. The website (https://www.chemspider.com) was accessed on December 1, 2023.

5.2.1 Methods:

The data were gathered through a thorough literature review using the PubMed, Web of Science, and Scopus databases. The utilized search strategy included keywords such as "intestinal lymphatic uptake", "chylomicron blocking agents", "pharmacokinetics",

"Pluronic® L-81", "puromycin", "vinca alkaloids", "colchicine", and "cycloheximide". Boolean operators were employed to combine these terms for a comprehensive search. Articles were selected based on their relevance to the topic, particularly those providing data on the effectiveness and toxicity of blocking agents on chylomicron-mediated lymphatic absorption. The inclusion criteria also focused on studies offering pharmacokinetic data and discussing experimental and clinical implications.

5.2.2 Pluronic® L-81 Model:

Pluronic® L-81 (PL-81) is a liquid non-ionic surfactant with a molecular weight of 2750 g/mol, and it remains in a liquid state at room temperature. Comprising polyoxyethylene-polyoxypropylene-polyoxyethylene block copolymers, PL-81 features hydrophilic moieties (polyoxyethylene) at both ends of the hydrophobic chain (polyoxypropylene). The composition includes 10% hydrophilic residues and 90% hydrophobic ones (334, 335). Synthesized through the controlled addition of propylene oxide to the two hydroxyl groups of propylene glycol, PL-81 finds applications as a defoaming agent in dishwashing, metal cleansing, water treatment, and paper processing (336).

In the late seventies of the last century, Bochenek *et al.* discovered that certain non-ionic detergents had an impact on the absorption of lipids and cholesterol. The influence of these agents was found to be connected to their physicochemical properties. Among these detergents, those containing 90% hydrophobic components, such as PL-81, were the most effective in inhibiting lipid absorption. The study demonstrated that adding a hydrophobic detergent to a high-fat, high-cholesterol diet resulted in reduced levels of cholesterol and

triglyceride in the serum. Additionally, this effect was correlated with a decrease in body weight. The observation that 0.5% PL-81 lowered plasma cholesterol and triglyceride levels, liver cholesterol, and body weight in rats on a high-fat, high-cholesterol diet sparked considerable attention to it (337).

Support for the impact of PL-81 was evident in further investigations. In a particular study, male Sprague-Dawley rats (200-250 g) were administered lipid emulsions containing labeled triolein [^{3}H]-triolein and labeled [^{14}C]-cholesterol, with or without PL-81 for the experimental and control groups, respectively. The observed accumulation of absorbed lipids in the enterocytes of the experimental group suggested that PL-81 hindered the assembly and/or secretion of lipoproteins from intestinal mucosal cells. The study also demonstrated the reversible nature of the effect of PL-81, as the animals regained their lipid transport ability 24 hours after discontinuation of PL-81 input (338).

In another study conducted by the same group, the rate of intestinal transport of absorbed lipid into lymph was investigated using a lipid emulsion containing [^{3}H]-triolein. The study employed intraduodenal infusions of various doses of PL-81 to evaluate its potential inhibitory effect on lipid transport, and the kinetics of this inhibition were determined. Infusing PL-81 at 0.25 mg/h showed no effect, while infusions at 0.5 and 1 mg/h led to a decrease in intestinal lipid transport. The inhibition occurred rapidly, with a half-life of 69 minutes for the 0.5 mg/h dosage and 35 minutes for the 1 mg/h dosage. This hindrance of lipid transportation resulted in the accumulation of lipids in the mucosa, as evidenced by both radiochemical and morphological observations (336).

Consistent with earlier discoveries, the intraduodenal infusion of four categories of intestinal lymph fistula rats with [^{3}H]-triolein, and 1 mg/h of PL-81 resulted in a decrease in lipid transport by the small intestine. The study also determined that the position of the hydrophilic moiety and the hydrophilic-to-hydrophobic ratio in PL-81 play a crucial role in its action, as evidenced by a comparison with two other pluronics (PL-25R1 and PL-84) (339).

Other evidence regarding the impact of PL-81 was gathered through the infusion of intestinal lymph fistula rats with a lipid emulsion containing [1-^{14}C]-oleic acid. In this experiment, rats received a dose of 1 mg/h of PL-81. Both chemically and radioactively assessed lymphatic triacylglycerol output showed suppression in the experimental rats compared to the controls. In the following stage of the investigation, the time required for the appearance of very low-density lipoproteins in control rats and chylomicrons in PL-81-treated rats was determined in the central lacteal. In control rats, the average appearance time was 10.8 minutes, whereas in PL-81-treated experimental rats, it was 16.2 minutes. This difference in appearance time supported the theory that chylomicron and very low-density lipoprotein are segregated during packaging in enterocytes, and PL-81 selectively inhibits the formation of chylomicrons (340).

Based on the findings reported in the studies until the late 1980s, it was revealed that PL-81 disrupted the secretion of chylomicrons and could potentially reduce the formation and stability of luminal triglyceride-rich lipid droplets (339, 340). In the early 1990s, PL-81 was identified as a hydrophobic surfactant that impedes intestinal chylomicron secretion at the pre-Golgi level, while leaving triacylglycerol uptake and re-esterification unaffected (341, 342). To explore the impact of this inhibition, Black *et al.*

conducted a study on newborn female piglets. They subjected the piglets to 24-hour intraduodenal infusions of either low-triacylglycerol or high-triacylglycerol diets, with or without the addition of PL-81. Subsequent evaluations included the assessment of apo-lipoproteins (apo B-48, A-I, and A-IV) synthesis and content, along with apo B-48 and A-IV mRNA levels in the small intestine. The introduction of PL-81 to the high-triacylglycerol infusion led to a decrease in jejunal apo B-48 content, synthesis, and mRNA levels below basal levels. The typical increase in apo A-I synthesis caused by triacylglycerol absorption was negated in both the jejunum and ileum. Although dampened, the expected elevation in jejunal apo A-IV synthesis and mRNA levels with triacylglycerol absorption persisted with PL-81 treatment (342). Upon further investigation, it was discovered that the stimulation of apo-lipoprotein (apo A-IV) synthesis and secretion is not coordinated with lipid uptake into the enterocytes or cellular triglyceride content. Rather, it is probable that the processes associated with the packaging and release of chylomicrons are responsible for the elevation in apo A-IV synthesis and secretion. This aligns with the results obtained with PL-81, suggesting that the inhibition of chylomicrons would not impact apo A-IV (341). Instead, its impact seems to be selective, primarily affecting apo B-48 (342).

In another study, the impact of PL-81 on chylomicron composition was examined. The experiment involved intraduodenal infusion of PL-81 at a constant rate of 1.0 mg/hr, in combination with mixed micellar solutions or saline, in mesenteric lymph fistula male Sprague Dawley rats (250-350 g). The interference disrupted trans-epithelial lipid flux during fat absorption, causing the entrapment of exported lipids within enterocytes and resulting in cytosolic and endoplasmic reticulum lipid accumulation, with the Golgi region

remaining unaffected. It reduced mesenteric triglyceride, phospholipid, and total cholesterol secretion. Although there were only negligible changes in chylomicron composition, a slightly higher phospholipid/triglyceride ratio was noted. The chylomicron apo-lipoprotein pattern showed almost no alterations. As a result, the study concluded that PL-81 led to a substantial decrease in chylomicron formation without major compositional alterations (343).

PL-81, employed as a chylomicron blocker, has found application in numerous studies. Some have delved into the intestinal lymphatic transport of endogenous substances (344, 345). In the studies relevant to this work, PL-81 served as a blocking agent to investigate *in-vivo* xenobiotics lymphatic transport (**Table 5.1**). In one study, a lipophilic model molecule-vitamin D3- was utilized for this purpose. Using this model, male Wistar rats (300-325 g) were given an intraduodenal infusion of Lipofundin® emulsion, consisting of 20% w/v medium and long-chain triglycerides in a 1:1 ratio, with or without PL-81. The PL-81 concentration in the Lipofundin® emulsion was 1 mg/mL, and the infusion rate was set at 1 mL/h. Four hours after initiating the infusion, the animals received an oral gavage of vitamin D3 (0.5 mg/kg). The chosen PL-81 dose demonstrated efficacy in inhibiting the intracellular transport of chylomicrons. Nonetheless, it was noteworthy that the intraduodenal infusion of the emulsion without PL-81 also marginally decreased the area under the concentration-time curve of vitamin D3. This reduction was attributed to the additional lipid load provided by the emulsion, leading to an overall decrease in vitamin absorption. Moreover, vitamin D3 absorption in the PL-81 model showed a good correlation with the mesenteric lymph duct cannulation model, emphasizing the crucial role

of packaging the lipophilic molecule into the chylomicron in the cascade of lymphatic absorption (254).

Also, in male Wistar rats weighing 200–250 g, the administration of 5 mL/kg PL-81 resulted in decreased concentrations of ß-carotene and its cleavage product, vitamin A, in both plasma and liver. The observed effect was hypothesized to occur through the modulation of ß-carotene uptake into enterocytes and/or its secretion into the lymph. That modulation was attributed to the known inhibition of chylomicron synthesis by PL-81 and the prevention of the conversion of ß-carotene into vitamin A within enterocytes (346).

Table 5.1. Studies of *in-vivo* xenobiotics lymphatic transport using Pluronic-81® (PL-81) as a chylomicron blocking agent.

Species	PL- 81 Dose and timing	Xenobiotics Tested by the Model	Reference
Male Wistar rats (300-325 g)	Intraduodenal infusion of Pluronic L-81 (1 mg/h) given 4 hours before the drug	Vitamin D3	(254)
Male Wistar rats (200-250 g)	5 mL/kg Pluronic L-81was added to diet containing ß-carotene	ß-carotene	(346)

In 2016, a study utilizing PL-81 demonstrated that co-administering lipids can enhance intestinal lymphatic uptake through chylomicrons. The investigation focused on determining whether the lymphatic uptake of the triglyceride (TG) mimetic pro-drug (1,3-dipalmitoyl-2-mycophenoloyl glycerol, 2-MPA-TG) depended on the presence of exogenous lipids. Conducted in male Sprague-Dawley rats (280-320 g), the study revealed an increase in the lymphatic transport of 2-MPA-TG (2 mg dispersions) when administered with higher quantities of lipids. A comparison between groups with and without the

chylomicron blocker (2 mg of PL-81) demonstrated a strong correlation ($R^2 = 0.99$) in the recovery of 2-MPA-TG in the lymph. Over 97% of the pro-drug was associated with chylomicrons, as evidenced by the inhibition of lymphatic transport when PL-81 was present, highlighting its inhibitory effect on the transportation of 2-MPA-TG through the lymphatic system (347).

In contrast to certain models and inhibitors that may carry the risk of systemic side effects and irreversible tissue damage, as will be discussed in detail next, PL-81 appeared to be devoid of visible side effects. Consequently, the PL-81 model has proven to be an effective approach to hinder the secretion of chylomicrons from the enterocyte. This interference is achieved by a conformational change of apo B and disrupting droplets through the destabilization of their surface, thereby affecting the core expansion process (339, 340, 348).

The absence of observed adverse effects aligns with the characteristics of PL-81. It selectively disrupts the chylomicron assembly while leaving the digestion, and absorption of triglycerides and cholesterol unaffected. This was demonstrated by the oral d-xylose loading test (254). The absorption of d-xylose involves both active and passive processes and has been used to evaluate the absorptive function of the intestine (349). Furthermore, the inhibition induced by PL-81 can be promptly reversed by discontinuing its administration (338, 341). The noted reversible inhibition of PL-81 aligns consistently with findings observed both in the *in-vivo* rat model and the *in-vitro* CaCo2 cellular model (347).

Our group published a recent study that documented the use of PL-81 in an *in-vitro* setting to inhibit the intestinal lymphatic uptake of drugs. The research explored this phenomenon in an *in-vitro* model utilizing artificial chylomicrons. The study findings indicated that concentrations of PL-81 at ≥ 1% effectively inhibited the uptake. The results showed that PL-81 exerted its effect through a mechanism involving the surrounding/coating of artificial chylomicrons, preventing the drug from being packaged into the Intralipid® chylomicrons (350).

5.2.3 Puromycin Model:

The antibiotic, puromycin, has also been investigated as a chylomicron-blocking agent. In 1963, the potential of puromycin as a protein inhibitor was investigated. Puromycin was administered intraperitoneally at a rate of 75 mg/kg per hour for 5 hours. The findings indicated that puromycin could induce clinical and biochemical protein alterations in rabbits, rats, and mice (351).

However, the use of puromycin as a lymph blocker can be traced back to Sabesin and Isselbacher in 1965. In that study, female Sprague-Dawley rats weighing 180 to 200 g experienced a 24-hour fasting period before receiving intraperitoneal injections of puromycin. Dissolved in a buffered salt solution, puromycin was delivered via a regimen of hourly injections, initially at a dose of 2.5 mg over 4 hours, followed by five subsequent injections, each containing 1 mg. Following the administration of the fourth injection by one hour, the animals were intubated with 1.5 mL of corn oil, and euthanasia occurred 2, 4, and 6 hours later. Under these conditions, rats accumulated triglyceride within the intestinal

cells and failed to develop normal post-prandial hyperlipemia due to impaired chylomicron formation (352).

In 1969, Redgrave and Zilversmit investigated the impact of puromycin on fat absorption using various approaches. Female Holtzman and Sprague-Dawley rats weighing 200-225 g were infused with a lipid mixture equivalent to 63.7 μmoles of triolein to examine the effect of puromycin on lymph flow and fat absorption. The lipid mixture was infused through lymph fistula and duodenal cannula preparations, while puromycin (2 mg/mL dissolved in the same buffered salt solution as used in the previous study) was administered intraperitoneally. During puromycin administration, lymph flow remained constant, and the hourly output of triglycerides in puromycin-treated animals was lower than in control animals, although the concentrations in both groups were comparable. For the assessment of oral fat absorption, female Sprague-Dawley rats (180-200 g) were intraperitoneally injected with puromycin. Initial 6-hour infusions (2.5 mg each hour) were followed by 1 mg each hour until the end of the experiment. After the fifth injection, rats received 1.5 mL of corn oil containing [^{14}C]-linoleic acid via a stomach tube. Puromycin at this dosage caused liver triglyceride accumulation, moderately suppressing protein synthesis. Gastric emptying delay in the puromycin group indicated no inhibition of chylomicron formation or transport at this dose, challenging the conclusion of Sabesin and Isselbacher (353).

In the same year, another study investigated the metabolic comparison of short and long-chain fatty acids, along with triglycerides, in rats. The study distinguished between control and puromycin-treated groups. In Fisher-strain female rats weighing 150-175 g, puromycin was administered hourly at a rate of 2.75 mg/h for four doses. Subsequently, a

continuous puromycin infusion was maintained at a rate of 1.1 mg/h throughout the study. The study observed the hindrance of long-chain fatty acid absorption into the thoracic duct lymph, particularly in the form of chylomicron triglycerides, due to puromycin supporting the findings of Sabesin and Isselbacher (354).

Linked to the previous studies, an examination of the impact of puromycin on the apo-lipoproteins of chylomicrons revealed intriguing findings. This agent, known for prematurely ending protein translation, led to the secretion of incompletely synthesized apo B polypeptides as lipoprotein particles by HepG2 cells incubated with puromycin (355). Additionally, a separate study involving similar cells treated with puromycin suggested that the length of apo B might play a role in determining the size of lipoproteins during biosynthesis, potentially influencing the chylomicrons produced during puromycin treatment (356).

The impact of puromycin on cholesterol absorption in male and female Wistar strain rats (200-300 g) with indwelling catheters in the left thoracic lymphatic duct revealed important findings (357). Following the protocol outlined earlier (352), the administration of puromycin led to a decrease in cholesterol absorption, accompanied by inhibition of simultaneously administered fatty acid absorption. In male rats subjected to the same treatment, a reduction in cholesterol absorption was observed, yet it had no impact on the absorption of fatty acids. Despite the reduced lipid absorption observed in puromycin-treated animals, there was no accumulation of cholesterol or fatty acids in the intestinal mucosa, regardless of gender. The study proposed that the altered lymph production in fed animals treated with the protein synthesis inhibitor puromycin was attributed to delayed

gastric emptying rather than the lymph blockage effect of the substance (357) which is a conclusion similar to that of Redgrave and Zilversmit (353).

However, Miura *et al.* in 1979 reported another study supporting Sabesin and Isselbacher in which they observed a disruption in lipid transport due to impaired chylomicron formation resulting from the effects of puromycin. In the male Wistar rats (350-400g) used in that study, puromycin demonstrated a block in lipoprotein formation in intestinal cells and a reduction in the lymphatic absorption of [1-^{14}C]-linoleic acid (358).

Literature reports provide evidence of the ability of puromycin ability to block intestinal chylomicrons, as illustrated in various studies (352-354, 358). Additionally, some investigations suggest that the delay in lymph uptake, previously attributed to the chylomicron-blocking effect of puromycin, may be linked to delayed gastric emptying (353, 357). The Miura *et al.* study (358) shed light on a potential explanation for these discrepancies. Their research indicated that the impact of puromycin on the lymphatic transport of fatty acids is influenced by the type of fatty acids being transported. Puromycin seemed to exert more effect on the lymphatic uptake of highly unsaturated fatty acids. This specificity was critical according to that study, as more unsaturated long-chain fatty acids are prime candidates for chylomicron packaging. The effect of puromycin appeared to be targeted specifically at chylomicrons, as opposed to other lipoproteins like very low-density lipoproteins (VLDL), which transport less unsaturated fatty acids. Still, further studies are essential to investigate the detailed effects of puromycin and the mechanism by which it blocks chylomicrons. Currently, there are no reports on whether puromycin inhibits chylomicron exocytosis from enterocytes or targets other phases of chylomicron formation, such as intracellular movement or the re-esterification of fatty acids. Besides,

conducting studies on the inhibition of intestinal lymphatic uptake of xenobiotics would contribute valuable data for this model. It would also enable an exploration of its potential advantages and disadvantages when compared to other chylomicron-blocking agents.

5.2.4 Colchicine Model:

Colchicine is derived from the *Colchicum autumnale* plant and has a history of being used for joint pain since at least 1500 BCE (359). Despite its use for thousands of years, clinical and experimental interest in the mechanism of action and the toxicological data of colchicine can be traced back to 1950s.

In 1954, Sternberg and Ferguson conducted a toxicology study on colchicine using Wistar rats and cats. Rats, evenly divided by sex and weighing 90 to 150 g, received either a single intravenous dose or intraperitoneal doses administered five times weekly. The intraperitoneal doses started with non-toxic amounts and doubled weekly until significant mortality occurred. For the single intravenous dose in rats, 4 mg/kg was administered to 31 rats, with sacrifice occurring seventeen hours after administration. In ten rats, repeated injections started at 0.1 mg/kg/day and increased to 1.6 mg/kg/day in the fifth week, with sacrifice during the fourth and fifth weeks. Cats received a single intravenous dose varying between 0.5 or 5 mg/kg per cat, and they were sacrificed after eight to twenty-four hours. Repeated doses in four cats started at 0.025 mg/kg/day and increased to 0.2 mg/kg/day in the fourth week, with sacrifice during the third and fourth weeks (360).

Upon further investigation, it was found that the LD_{50} of colchicine in Sprague-Dawley female rats weighing approximately 200 g was 1.6 mg/kg when administered through intravenous injections at dosages ranging from 0.25 to 2.0 mg/kg (361). This

closely aligned with the previously reported value by Sternberg and Ferguson (360). Death did not occur until around 8 hours after administering the drug dose. Rats displayed symptoms including lethargy, diarrhea, loss of appetite, and others, at doses equal to or greater than 0.5 mg/kg. Consequently, it was decided to utilize the 0.5 mg/kg dose of colchicine for further metabolic investigations (361).

In 2007, the oral toxicity of colchicine was assessed through a single gavage administration (10, 20, or 30 mg/kg body weight) in young, mature male and female Sprague-Dawley rats. Colchicine toxicity resulted in progressively more severe, dose-related clinical signs in both male and female rats. The observed signs encompassed mortality, decreased body weight, and reduced feed intake in the days immediately following dosing, followed by recovery in surviving animals. Gender-related discrepancies in the toxic reaction to colchicine were observed between male and female rats, with female rats displaying twice the susceptibility to the lethal effects of colchicine compared to their male counterparts. The calculated oral LD_{50} for saline-pretreated female rats was 26 mg/kg body weight, while for saline-pretreated male rats, it was 51 mg/kg (362).

The elucidation of the effects of colchicine gained prominence in the 1970s. In 1974, Stein and colleagues investigated the regulation of secretory processes in the liver by conducting an intraperitoneal colchicine injection study, using female and male Albino rats weighing around 200 grams from the Hebrew University strain. Two colchicine doses, 0.5 mg/kg and 5.0 mg/kg, were administered. The study specifically investigated triglyceride secretion into the serum, monitoring the process for 90 minutes following the injection of Triton WR 1339 and [^{14}C]-palmitic acid. Triton WR 1339, also known as tyloxapol, is a substance known to inhibit the catabolism of lipoproteins and was utilized to showcase the

action of colchicine in non-Triton-treated rats. Triton WR 1339 interferes with the hydrolysis of chylomicrons and VLDL, causing a linear increase in serum levels of triglycerides and inhibiting their removal from circulation. The release of triglyceride was reduced to approximately 20-30% of control values. The impact of colchicine on serum triglyceride levels was observed to be independent of Triton WR 1339 presence, demonstrating similarity in both males and females, as well as in fed and fasted rats. Since the intestine contributes only about 10% of serum triglyceride in fasted rats, the researchers concluded that colchicine primarily affected the liver. The dose-dependent effect of colchicine was reversible 6-7 hours after injection of 0.05 mg/100 g body weight after 270 minutes. Non-secreted triglyceride accumulated in liver cells within secretory vesicles. The study also observed a noticeable reduction in microtubules and a slight increase in microfilaments. It was suggested that microtubules play a role in regulating the release of lipoproteins into the bloodstream by preserving the structural arrangement of the cell membrane, which is crucial for fusion with secretory vesicles (363).

More than a year later, a study delving into the influence of colchicine on intestinal chylomicrons employed female Sprague-Dawley rats weighing between 230 and 250 grams. Intraperitoneal injections of colchicine (0.5 mg/100 g of body weight) were administered one hour before the consumption of a margarine emulsion (1 g in 2 mL of saline). During the following hours, this group did not display the elevation in plasma triacylglycerol levels observed in the control group. The impact of colchicine became more pronounced when the experiment followed the prior administration of Triton WR-1339. Colchicine-treated rats also displayed a five-fold increase in triacylglycerol in the proximal jejunum. These results supported the colchicine disrupts the intracellular phase of fat

absorption, proposing the involvement of the microtubular-microfilamentous system in releasing chylomicrons from intestinal cells into circulation. The same study investigated the potential general toxic effects of colchicine on the intestine using a D-xylose absorption test. The results indicated that the 3-hour urine excretion of xylose in controls (6.9 ± 0.5 mg/3 h) and treated rats (7.9 ± 1.6 mg/3 h) did not exhibit statistically significant differences. The comparable xylose absorption capacity of controls and colchicine-treated rats suggested that the colchicine dose in this experiment did not induce a general toxic effect on the intestinal mucosa (364). In the same year, Glickman *et al.* investigated the impact of colchicine on the lymphatic transport of oleic acid, suggesting again a potential involvement of microtubules in the mechanism. The study, conducted in Male Holtzman rats (250 to 300 g) with indwelling mesenteric lymph cannulas, revealed that animals treated with colchicine (0.5 mg per 100 g) exhibited delay and reduction in the lymphatic absorption of [^{14}C]-oleic acid. The findings pointed towards a potential role of microtubules in intestinal lipid transport particularly in chylomicron secretion (365).

Additional studies in subsequent years supported the earlier findings. In one study involving male Wistar rats weighing 300-350 g, a decrease in lymphatic transport was observed after administering colchicine via intraperitoneal injection (5 mg/kg). This pre-administration preceded the administration of a 5 mL mixed micellar solution containing [1-^{14}C]-linoleic acid. The administered lipid showed a slower transit to the lymphatics, mainly in the form of free fatty acids. Colchicine was reported to act by inhibiting microtubule function through its binding with tubulin, leading to the predominant presence of triglycerides as chylomicrons, whose release was hindered from intestinal epithelial cells in colchicine-treated animals. Thus, this resulted in an increased abundance of free fatty

acids rather than triglycerides as lipids were transported from epithelial cells into the lymphatics (366).

In a different investigation using an intraduodenal pulse injection of [^{14}C]-oleic acid, the administration of colchicine at a dose of 0.5 mg/100g in female Albino rats (200-250 g) was found to have no impact on the uptake of fatty acids by the intestinal mucosa. However, it had contrasting effects on fatty acid esterification, promoting their integration into triglycerides rather than phospholipids. Additionally, colchicine led to the buildup of endogenous diglycerides, triglycerides, and cholesterol esters within the intestinal epithelium. Ultra-structural and morphometric analyses showed a reduction in visible microtubules and a displacement of the smooth and rough endoplasmic reticulum and Golgi apparatus. Also, microvilli were observed at the lateral plasma membrane of enterocytes following colchicine treatment (367).

The colchicine model was utilized to investigate the impact of chylomicrons on the lymphatic absorption of various drugs (**Table 5.2**). For instance, male Wistar rats weighing 230-270 g received an intravenous dose of 5 mg/kg colchicine to study vitamin D3 absorption. In this experiment, rats were administered a soybean oil emulsion containing vitamin D3, prepared using either milk fat globule membrane (MFGM) or Tween 80 as emulsifiers. In colchicine-untreated rats, the cumulative percentage of vitamin D3 absorbed in lymph at 12 h post-dose was 19.2% and 13.8% for MFGM and Tween 80 emulsions, respectively. This absorption decreased to 2.05% and 2.23% in each case when rats were treated with colchicine (368).

In a succeeding study, Dahan and Hoffman extended the findings of previous researchers by administering colchicine to rats through intraperitoneal injection (5 mg/kg). One hour post-injection, male Wistar rats (300-325 g) received oral gavage of vitamin D3. Colchicine substantially reduced the intestinal absorption of vitamin D3, resulting in a relative bioavailability of 12.5% compared to the control group. Markedly, the vitamin D3 elimination rate constant increased from 0.04 ± 0.005 in the control to 0.08 ± 0.0009 after colchicine treatment. The elimination half-life of vitamin D3 from the plasma in both control and colchicine-treated animals was 15.5 (± 0.9) h and 8.6 (± 1.7) h, respectively (254). Eighteen hours after the colchicine dose, rats displayed lethargy and began to die, as had been seen in earlier studies (360, 361). A lower colchicine dose (2.5 mg/kg) did not create adequate inhibition of lipid transport and proved to be as fatal as the higher one. Results from the d-xylose loading test indicated impaired d-xylose concentrations in colchicine-treated animals compared to other groups, implying a degree of toxicity to the absorptive function of the intestine after colchicine treatment (254).

Following this, Iwanaga *et al.* examined the intestinal absorption of Solvent Green (SG) 3, a model poorly water-soluble compound, using colchicine. They orally administered SG to male Wistar rats (300–350 g) with inhibited chylomicron synthesis, achieved by pre-treatment with intravenous colchicine at 5 mg/kg one hour before the administration of SG and its lipid-based formulations. These formulations included a soybean oil emulsion and a self-microemulsifying drug delivery system (SMEDDS). Colchicine effectively impeded the intestinal absorption of SG across all tested lipid-based formulations, indicating that SG was absorbed from the intestine through a lymphatic route (285).

Table 5.2. List of studies investigating colchicine as a blocker of lymphatic uptake via chylomicrons for various xenobiotics.

Species	Colchicine Dose	Colchicine Pre-treatment Timing hours	Xenobiotics Tested with the Model	Reference
Male Wistar rats (230-270 g)	IV injection (5 mg/kg)	1	Vitamin D3	(368)
Male Wistar rats (300-325 g)	IP injection (5 mg/kg)	1	Vitamin D3	(254)
Male Wistar rats (300-350 g)	IV injection (5 mg/kg)	1	Solvent Green 3	(285)
Female Sprague-Dawley rats (200-220 g)	IP injection (5 mg/kg)	1	Docetaxel	(299)
Female Sprague-Dawley rats (220-250 g)	IP injection (5 mg/kg)	_	Paclitaxel	(300)

*Abbreviations: IV = Intravenous, IP = Intraperitoneal

Moreover, in 2016, Valicherla *et al.* developed self-emulsified drug delivery systems loaded with Docetaxel (D-SEDDS) to enhance both the oral bioavailability and antitumor properties of the drug. To assess the intestinal transport of D-SEDDS following oral administration, they utilized the colchicine model in female Sprague Dawley rats (200-220 g). After intraperitoneal colchicine administration (5 mg/kg), the C_{max} of D-SEDDS experienced an 8.69-fold decrease, dropping from 125.5 ± 2.5 to 14.44 ± 4.72 ng/mL. Furthermore, the $AUC_{0-\infty}$ exhibited a reduction of over 10-fold, decreasing from 260.23 ± 51.8 to 11.29 ± 1.03 h·ng/mL (299).

Similarly, Meher *et al.* recently used the same approach by formulating a silica-based solid self-emulsifying drug delivery system (Si-PTX-S-SEDDS) to encapsulate

another anticancer agent, paclitaxel (PTX). The goal was to enhance the oral bioavailability of PTX and address challenges associated with conventional delivery systems. Using the colchicine model in female Sprague Dawley rats (220–250 g), the study aimed to elucidate the transport mechanism of the developed formulation. The results revealed a 4–6-fold decrease in oral bioavailability in colchicine-treated animals, highlighting the involvement of chylomicrons in the oral absorption of the Si-PTX-S-SEEDS formulation in rats (300).

Research on colchicine as a lymph-blocking agent has centered on its toxicity, role as a microtubule inhibitor, and relevance in investigating the lymphatic absorption of formulations designed for this route. Additionally, studies have delved into the pharmacokinetic profile of colchicine within a practical dose range (1-10 mg/kg) in rats (369). The chylomicron-blocking effect of colchicine is primarily linked to its ability to disrupt the secretion of chylomicrons from enterocytes, thereby impeding their uptake into intestinal lymphatics. However, the exact extent and duration of inhibition by colchicine remains unclear despite these efforts. In studies examining the lymphatic uptake of xenobiotics, the reported dose of colchicine was 5 mg/kg, a dose deemed effective in blocking lymphatic uptake when administered intravenously and intraperitoneally, but also potentially associated with toxicity. Although the analytical feasibility for lower oral and intravenous doses of colchicine in the rat model (0.1 mg/kg) has been documented (370), the low doses (0.1 to 0.5 mg/kg) were not found to be effective in blocking the lymphatic uptake (371). Even higher intraperitoneal dose of 2.5 mg/kg has been reported to be ineffective in blocking chylomicrons (254). Further exploration of lower doses using different routes of administration would support the reported data and assess the potential use of lower effective doses, if feasible.

5.2.5 Vinca Alkaloids Model:

Vinca alkaloids (VA), first extracted in the 1950s by Canadian researchers Robert Noble and Charles Thomas Beer from the Madagascar Periwinkle plant, *Catharanthus roseus*, have a rich history of use in Ayurveda and traditional Chinese medicine. Yet, the connection between VA and cancer was established following animal studies that revealed fatalities attributed to septicemia and leukopenia (372).

Initial investigations into VA centered on their hypolipidemic effects. Swiss/H-Riop outbred male mice (30 to 35 g) were subjects in experiments designed to explore the serum lipid-lowering properties of VA, both in normal mice and those with ascites tumor-induced hyperlipidemia (Ehrlich, NK/Ly). Administered through intraperitoneal injections ranging from 0.2 to 5 mg/kg, VA demonstrated a rapid and reversible reduction in serum lipid levels following a single, non-toxic dose. The dose-dependent increase in the serum lipid-lowering effect showed the same changes in serum lipid and lipoprotein composition across all doses. Vinca alkaloids were observed to decrease levels of neutral lipids (triglycerides) and very low-density lipoproteins (VLDL) in the serum. Simultaneously, higher doses resulted in an elevation of total lipid and triglyceride content in the liver. These findings suggested that VA might hinder the release of lipoproteins in the liver by either obstructing active sites of membrane systems (cytoplasmic, Golgi) responsible for secretion or altering the physicochemical properties of the membranes, such as membrane fluidity (373).

An additional study in rhesus monkeys with vincristine and vinblastine revealed a decrease in plasma low-density lipoprotein cholesterol concentrations, accompanied by an elevation in plasma triacylglycerol concentrations. Within 7-10 days post-injection, plasma

lipid levels reverted to normal concentrations. Electron micrograph examinations of hepatocytes in monkeys subjected to the stated VA showcased an accumulation of glycogen particles and a proliferation of smooth endoplasmic reticulum. This coincided with an increase in the number of vesicles containing lipoproteins (374).

Later, one study looked into the effect of intestinal lymphatic blocking in the previously quoted study by Stein *et al.* using colchicine for the same purpose. In that study, female and male Albino rats of the Hebrew University strain weighing 200 g were administered intraperitoneal injections of vinblastine sulfate at doses of 0.1 or 1.0 mg/100 g body weight (equivalent to 1 or 10 mg/kg). Subsequently, they were subjected to intravenous injections of [l-^{14}C]-palmitic acid and Triton WR 1339 at different time intervals. The inhibition of triglyceride secretion into the serum was observed to a reduced extent, with reductions of 19.5% and 57.2% in female rats. The inhibition required a higher dose of vinblastine compared to colchicine. Additionally, the effect of vinblastine lasted for a shorter duration in comparison to that of colchicine, and the inhibition was nearly entirely reversed within 270 minutes (363).

Similar to puromycin, VA were not found to be used in studying the intestinal lymphatic uptake of drugs or formulations. Data regarding more detailed mechanisms of action and related aspects is still lacking as well. However, an intriguing literature finding suggests and involves a group of VA with lipid-lowering effects beyond the well-known drugs vincristine and vinblastine (373). Most of these compounds are commercially available and they can be further explored for their potential chylomicron-blocking effect. **Table 5.3** presents some of these VA, their LD50, and the doses examined for their hypolipidemic effects.

Table 5.3. Some of the vinca alkaloids (VA) that have shown hypolipidemic effects (373).

Vinca Alkaloid	LD 50 (mg/kg)	Doses Studied for the Lipid-Lowering Effect (mg/kg)
Vincristine	4.2	0.2 and 1
Dimethylaminoacetyl-Vincristine	> 200	10
Vinblastine	7.6	1
Penta-hydroxy-Vinblastine	> 200	10
Dimethylaminoacetyl-Vinblastine	> 200	5
Leurosine	29	3
Vinleurosine	90	6
N-Formyl-Leurosine	29	3
Vindoline base	>200	200
Vindoline HCI-salt	~ 280	50 and 200
Desacetyl-Vindoline	>200	10
Catharantine	>200	20
Velbanamine	>200	3 and 10

5.2.6 Cycloheximide Model:

Acetoxycycloheximide (ACH), derived from *Streptomyces albulus* cultures, has been recognized for its inhibitory effects on transplanted tumors and demonstrated toxicity to yeast, mammalian cells in tissue culture, and intact animals since the 1960s. Concurrently, research has explored the impact of this antibiotic on the inhibition of [^{14}C]-amino acid incorporation into tissue proteins. The blockade of protein synthesis by ACH was found to induce a syndrome marked by various symptoms and eventual death. Toxicity

was observed across various animals, including female Albino rabbits at a dose of 0.5 mg/kg, female mongrel dogs at doses ranging from 2 to 4 mg/kg, and mice (Carworth CF-1 strain) and rats (Wistar strain) at 5 mg/kg. Actidione-cycloheximide or cycloheximide, though described as less toxic to intact mammals but closely related to ACH, exhibited over 90% inhibition of [^{14}C]-amino acid incorporation into rabbit liver proteins when administered intraperitoneally at a dose of 50 mg/kg. The study concluded that cycloheximide can induce clinical and biochemical changes in rabbits, rats, and mice similar to those produced by ACH (351).

Similar to puromycin, the utilization of cycloheximide as a chylomicron lymph blocker has roots in the work of Sabesin *et al.* in 1965. In the previously mentioned study, female Sprague-Dawley rats (180-200 g) were subjected to ACH treatment. The administration of ACH (0.2 mg per kg), followed by 3 hours and 1.5 mL corn oil, resulted in lipid accumulation within the intestinal mucosa, accompanied by low concentrations of plasma triglycerides. Interestingly, the administered corn oil failed to induce the typical post-prandial hyperlipemia, suggesting interference in lipid transport due to impaired chylomicron formation (352).

A few years later, an in-depth exploration of the effect of cycloheximide on protein synthesis unfolded, using a dose of 1.5 mg/kg in male white Wistar rats (160-175 g). This dosage exerted a reduction in hepatic protein synthesis throughout 7 hours. Despite the pronounced decline in protein synthesis, the liver manifested only minimal ultra-structural alterations. These alterations encompassed a partial disorganization of the customary parallel arrays of rough endoplasmic reticulum, with closer proximity of its lamellae to various cytoplasmic organelles, particularly mitochondria. Additionally, the Golgi cisternae

exhibited a near absence of contents, and the vacuoles, which typically contained multiple electron-dense particles in controls, were lacking in the cycloheximide-treated animals (375).

A couple of years later, the same author contributed to a toxicological assessment of cycloheximide conducted in both male and female white Wistar rats weighing 160-175 g. Cycloheximide, prepared at a concentration of 1 mg/mL, was intraperitoneally administered as a single dose ranging from 1.5 to 4.5 mg/kg of body weight. In preliminary dose-response studies, it was found that, among the tested doses, only 1.5 mg/kg of the antibiotic was non-lethal to animals of both sexes. Doses in the range of 3.0-4.5 mg/kg approached or exceeded the LD_{100}, particularly in female rats. Specifically, 3.3 mg/kg was the only dosage within this range where at least one animal of each sex survived the entire 72-hour test period. In addition, both male and female rats exhibited symptoms such as diarrhea, lethargy, and semi-comatose states at the time of sacrifice (376).

Then, the research shifted its focus to investigating the impact of inhibiting protein synthesis on lipid absorption, employing ACH in rats with mesenteric lymph fistulas. Male Sprague-Dawley rats (200-250 g) equipped with indwelling mesenteric lymph cannulas received an intraduodenal infusion of a micellar solution of oleic acid labeled with [^{14}C]-oleic acid. Protein synthesis inhibition was achieved through an intraperitoneal dose of 0.25 mg/kg ACH administered one hour before lipid infusion. A temporary increase in chylomicron size occurred during maximal triglyceride absorption in control animals, while ACH-treated animals exhibited a sustained increase in chylomicron size, lasting up to 4 hours after lipid infusion. The mean recovery of labeled lymph triglycerides was 65% in control animals, compared to 43% in the ACH-treated group. These findings underscored

the role of protein synthesis in the formation and transport of chylomicrons from the mucosal cell into the lymph (377). Following studies by the authors demonstrated that ACH-induced impairment of intestinal protein synthesis was associated with a deficiency in a key chylomicron apo-protein, offering a potential explanation for the observed decline in lipid absorption under conditions of impaired protein synthesis (378). Further investigations provided direct evidence of a substantial decrease in the mucosal content of two major chylomicron apo-proteins, namely apo B and apo A-I, during inhibition of protein synthesis by ACH (379).

In the early studies applying the cycloheximide model to chylomicron blockade, male Wistar rats (200-250 g) with lymphatic fistulas were subjected to protein synthesis inhibitors: cycloheximide (administered intraperitoneally at a dose of 1.4 to 1.6 mg/kg) or acetoxycycloheximide (0.4 mg/kg). Following this, an intraduodenal infusion of a lipid emulsion, consisting of an equimolar blend of monopalmitin, palmitic acid, and [^{14}C]-oleic acid, was conducted. In normal rats, 75% of the introduced radioactivity was recovered in the intestinal lymph 6 hours post-infusion, contrasting with 4.5% in rats treated with cycloheximide. Moreover, in normal rats, 65% of the radioactivity was found in the intestinal lymph 4 hours after infusion, whereas in rats treated with acetoxycycloheximide, only 43% of the radioactivity passed into the lymph. The findings of the study affirmed the inhibitory impact of both cycloheximide and acetoxycycloheximide on the lymphatic absorption of oleic acid (380).

Research using the cycloheximide model to study the lymphatic absorption of drugs began with a study evaluating the intestinal absorption of vitamin D and 25-hydroxy vitamin D [25(OH)D_3]. In that study, male Holtzman rats (250-300 g) were treated with 3

mg/kg intraperitoneal cycloheximide to inhibit chylomicron synthesis. Findings indicated that 53% of vitamin D was found in the chylomicron fraction, in contrast to only 13% of [25(OH)D_3]. Inhibiting chylomicron synthesis with cycloheximide resulted in a 46% reduction in vitamin D absorption but only a 30% decrease in [25(OH)D_3] absorption. Several lipophilic and hydrophilic components were included for comparative analysis. The intestinal absorption of the hydrophobic oleic acid and retinol decreased by approximately 70%, surpassing the reductions observed for vitamin D and [25(OH)D_3]. Interestingly, the absorption of the water-soluble substance phenylalanine remained unaffected by cycloheximide in this experimental system (381).

In succeeding investigations by the same previous group on 1,25-dihydroxy vitamin D_3[1,25$(OH)_2D_3$], a similar approach using cycloheximide to impede chylomicron synthesis did not result in reduced absorption of [1,25$(OH)_2D_3$]. Almost all [1,25$(OH)_2D_3$] was directly released from the intestine into the portal blood, evading the need for chylomicron packaging for transport into the intestinal lymph. Inhibiting protein synthesis did not decrease the intestinal absorption of 1,25-dihydroxyvitamin D; 80.2 ± 7.6% of the absorbed 1,25-dihydroxyvitamin D was observed in cycloheximide-treated rats, compared to 88.6 ± 0.4% in the control animals (382).

In 2005, Dahan and Hoffman extended their exploration beyond the previously detailed PL-81 and colchicine models to include the cycloheximide model for investigating vitamin D absorption. The administration of cycloheximide (3 mg/kg) through intraperitoneal injection before oral gavage of Vitamin D3 in male Wistar rats (300-325 g) exhibited an association with the mesenteric lymph duct cannulation model. This observation implied that the integration of this lipophilic molecule into chylomicrons

played a vital role in its lymphatic absorption. Similar to the PL-81 model and in contrast to the colchicine model at 4-hour time point, the oral d-xylose loading test indicated that, at this dosage, cycloheximide did not affect intestinal absorptive functions, and no adverse effects were recorded (254).

More than 50 distinct experimental studies employing cycloheximide as a lymphatic blocker since 1982 have been identified **(Table 5.4).** Originally demonstrated as a non-invasive chylomicron flow block approach in male Holtzman rats, this method has been extended to include various rat strains, such as Wistar, Sprague-Dawley, Swiss Albino and Carlie Foster rats. Moreover, ICR mice have also been subjects in this model as have both male and female Swiss albino mice. Cycloheximide pre-treatment conducted an hour before administering the drug under study, has been a common approach in various investigations. Attili *et al.* and Alrusahid *et al.* proposed enhanced blocking efficacy when the pre-treatment occurred at 1.5 hours rather than at 1 hour after administration (191, 383). A common dosage used in the cycloheximide model has been 3 mg/kg, although alternative doses have also been explored (305, 332). While the intraperitoneal route is predominantly utilized, other administration routes have also been examined (332). A detailed compilation of reported studies can be found in **Table 5.4**.

Table 5.4. List of literature reports in which cycloheximide was used as a chylomicron blocker.

Species	**Cycloheximide Dose**	**Cycloheximide Treatment Timing**	**Xenobiotics Tested with the Model**	**Reference**
Male Holtzman rats (250-300 g)	IP injection (3 mg/kg)	3 h before administering the drug	Oleic Acid Retinol Vitamin D3 25-Hydroxy Vitamin D3	(381)

Male Holtzman rats (250-300 g)	IP injection (3 mg/kg)	3 h before administering the drug	1,2- Dihydroxy Vitamin D3	(382)
Male Wistar rats (300-325 g)	IP injection (3 mg/kg)	1 h before administering the drug	Vitamin D3	(254)
Male Wistar rats (275-300 g)	IP injection (3 mg/kg)	1 h before administering the drug	Vitamin D3	(286)
Male Sprague-Dawley rats (270-310 g)	IP injection (3 mg/kg)	1 h before administering the drug	Halofantrine	(307)
Male Sprague-Dawley rats (200-250 g)	IP injection (3 mg/kg)	1 h before administering the drug	Candesartan Cilextil	(301)
Male Sprague-Dawley rats (190-230 g)	IP injection (3 mg/kg)	1 h before administering the drug	Sirolimus	(308)
Male Sprague-Dawley rats (220-250 g)	IP injection (3 mg/kg)	1 h before administering the drug	Nimodipine	(328)
Male Sprague-Dawley rats (225-275 g)	IP injection (3 mg/kg)	1 h before administering the drug	Puerarin	(287)
Male Sprague-Dawley rats (300-325 g)	IP injection (3 mg/kg)	1 or 1.5 h before administering the drug	Docetaxel	(383)
Male and Female Charle Foster strain Albino rats (230-270 g)	IP injection (3 mg/kg)	1 h before administering the drug	Praziquantel	(309)
Male Wistar rats (200-250 g)	IP injection (3 mg/kg)	1 h before administering the drug	Acetylpuerarin	(288)

Male Wistar rats (200-250 g)	IP injection (3 mg/kg)	1 h before administering the drug	Terbinafine	(384)
Male Wistar rats (200-220 g)	IP injection (3 mg/kg)	1 h before administering the drug	Carvedilol	(289)
Wister Albino rats (180-220 g)	IP injection (3 mg/kg)	1 h before administering the drug	Diacerin	(310)
Male Sprague-Dawley rats (230-270 g)	IP injection (3 mg/kg)	1 h before administering the drug	Efavirenz	(311)
Male Wistar rats (180-250 g)	IP injection (3 mg/kg)	1 h before administering the drug	Darunavir	(312)
Male Wistar rats (200-300 g)	IP injection (3 mg/kg)	1 h before administering the drug	Lopinavir	(290)
Female Sprague-Dawley rats (200-220 g)	IP injection (3 mg/kg)	1 h before administering the drug	Docetaxel	(299)
Male Sprague-Dawley rats (180-220 g)	IP injection (3 mg/kg)	1 h before administering the drug	Piroxicam	(313)
Male Sprague-Dawley rats (220-250 g)	IP injection (3 mg/kg)	1 h before administering the drug	Huperzine A	(314)
Male Sprague-Dawley rats (250-300 g)	IP injection (3 mg/kg)	1.5 h before administering the drug	Doxorubicin-Quercetin	(191)
Male Wistar rats (180-220 g)	IP injection (3 mg/kg)	1 h before administering the drug	Lopinavir	(295)

Male Wistar rats (200-250 g)	IP injection (3 mg/kg)	1 h before administering the drug	Topotecan	(291)
Male Sprague-Dawley rats (200-250 g)	IP injection (3 mg/kg)	1 h before administering the drug	Berberine	(385)
Male Wistar rats (180-220 g)	IP injection (3 mg/kg)	1 h before administering the drug	Pueraria Flavones	(315)
Male Sprague-Dawley rats (180-260 g)	IP injection (3 mg/kg)	1 h before administering the drug	Canagliflozin	(386)
Male Sprague-Dawley rats (180-220g)	IP injection (3 mg/kg)	1 h before administering the drug	Bacalein	(316)
Male Sprague-Dawley rats (250-300 g)	IP injection (3 mg/kg)	1 h before administering the drug	Bacalein	(317)
Rat Male Sprague-Dawley (230-270 g)	IP injection (3 mg/kg)	1 h before administering the drug	Baicalein	(292)
Wistar rats (~250 g)	IP injection (3 mg/kg)	1 h before administering the drug	Exenatide	(387)
Female Sprague-Dawley rats (180-220 g)	IP injection (3 mg/kg)	1 h before administering the drug	Asenapine Maleate	(293)
Female Sprague-Dawley rats (180-220 g)	IP injection (3 mg/kg)	1 h before administering the drug	Lurasidone	(294)
Female Sprague Dawley rats (190g-230 g)	IP injection (3 mg/kg)	1 h before administering the drug	Raloxifene Hydrochloride	(329)
Female Sprague-Dawley rats (220-250 g)	IP injection (3 mg/kg)	1 h before administering the drug	Paclitaxel	(300)

Male Sprague-Dawley rats (270-330 g)	IP injection (3 mg/kg)	1 h before administering the drug	Nislodipine	(318)
Male Wistar rats (213.5-237.5 g)	IP injection (3 mg/kg)	1 h before administering the drug	Ibrutinib	(319)
Female Sprague-Dawley rats (200-240 g)	IP injection (1 mg/kg)	0.5 h before administering the drug	Raloxifene	(320)
Male Wistar rats (250-280 g)	IP injection (3 mg/kg)	1 h before administering the drug	Quetiapine	(388)
Male ICR mice	IP injection (6 mg/kg)	1 h before administering the drug	(Cy5)-Labeled Insulin	(305)
Male Sprague-Dawley rats (220-250 g)	IP injection (3 mg/kg)	1 h before administering the drug	Andrographolide	(321)
Male and Female Swiss Albino Mice (30-40 grams)	IP injection (3 mg/kg)	1 h before administering the drug	Nintedanib Esylate	(322)
Male Sprague-Dawley rats (220-250 g)	IP injection (3 mg/kg)	1 h before administering the drug	Baicalin	(297)
Male Wistar rats (300-450 g)	IP injection (3 mg/kg)	1 h before administering the drug	Abiraterone and Cinacalcet	(306)
Male Wistar rats (230-270 g)	IP injection (3 mg/kg)	1 h before administering the drug	Mebendazole	(303)
Male Wister Albino rats (250-280 g)	IP injection (3 mg/kg)	1 h before administering the drug	Resveratrol	(323)

Male Wister Albino rats (200-250 g)	IP injection (3 mg/kg)	1 h before administering the drug	Revaprazan	(324)
Male Wistar rats (215-235 g)	IP injection (3 mg/kg)	1 h before administering the drug	Atazanavir	(325)
Male Wistar rats (200-250 g)	IP injection (3 mg/kg)	1 h before administering the drug	Ritonavir	(302)
Rat Male Sprague-Dawley (180–220 g)	IP injection (3 mg/kg)	1 h before administering the drug	Madecassic Acid	(330)
Male Wistar Albino rats (200-250 g)	IP injection (3 mg/kg)	1 h before administering the drug	Gefitinib	(326)
Male Wistar rats	IP injection (3 mg/kg)	1 h before administering the drug	Hydroxymethylnitrofurazone	(296)
Wistar rats (each is 250 g)	IP injection (3 mg/kg)	1 h before administering the drug	Etravirine and Darunavir Ethanolate	(327)
Male Wistar rats (220–250 g)	IP injection (3 mg/kg)	1 h before administering the drug	Efavirenz	(304)
NOD.Cg Prkdcscid Il2rgtm1Wjl/SzJ (NSG) mice (30-35 g)	IP injection (3 mg/kg)	0.5 h or 2 hbefore administering the drug	Niclosamide	(331)
Sprague-Dawley male rats (200 ± 20 g)	IP injection (3 mg/kg)	1 h before administering the drug	Dihydroartemisinin	(298)

Male Wistar rats (200–250 g)	IP injection (3 mg/kg)	1 h before administering the drug	Idarubicin Hydrochloride	(389)

*Abbreviations: IP = Intraperitoneal

Various formulations have been developed to specifically target the intestinal lymphatics as a route of absorption. **Table 5.5** provides examples of the different reported formulations. One recent study showcased the potential of specially formulated nanoparticles as a promising oral delivery system for insulin, employing cycloheximide as a chylomicron blocker. In this investigation, diabetic mice underwent pre-treatment with cycloheximide to explore the lymphatic transport of orally administered nanoparticles. The bioavailability of insulin- and cholic acid-loaded zein nanoparticles with dextran surfaces was significantly reduced by 43% and 49% in formulations A1 and A2, respectively, in the presence of cycloheximide. This suggested that approximately half of the nanoparticles were transported via the lymphatic pathway. Conversely, the bioavailability of a specific A2 nanoparticle formulation decreased by 22% in the presence of cycloheximide. The difference between A1 and A2 nanoparticles in intestinal lymphatic transport indicated that embedded cholic acid played a role in promoting the intestinal absorption of A1 nanoparticles through the lymphatic pathway, a feature lacking in A2 (305).

Table 5.5. Examples of formulations analyzed for their lymphatic uptake tendency through the inhibition models of colchicine and cycloheximide. All studies were done in a rat animal model.

Delivery System	**Compound**	**Reference**
SEDDS	Docetaxel	(299)
	Paclitaxel	(300)
	Resveratrol	(323)

SMEDDS	Solvent Green 3	(285)
	Sirolimus	(308)
	Terbinafine	(384)
	Huperzine A	(314)
	Canagliflozin	(386)
	Asenapine Maleate	(293)
	Bacalein	(292)
	Pueraria Flavones	(315)
	Lurasidone	(294)
	Niclosamide	(331)
SNEDDS	Revaprazan	(324)
	Madecassic Acid	(330)
SNESNS	Diacerein	(310)
S-SNEOFs	Lopinavir	(290)
SLN	Praziquantel	(309)
	Efavirenz	(311)
	Darunavir	(312)
	Lopinavir	(295)
	Topotecan	(291)
NLC	Ibrutinib	(319)
	Mebendazole	(303)
	Hydroxymethylnitrofurazone	(296)
	Atazanavir	(325)
	Gefitinib	(326)
	Ritonavir	(302)

	Etravirine and Darunavir Ethanolate	(327)
ME	Puerarin	(287)
	Piroxicam	(313)
MD	Raloxifene Hydrochloride	(329)
NCs	Docetaxel	(383)
Nanoemulsion	Acetylpuerarin	(288)
	Baicalin	(316), (317)
	Nisoldipine	(318)
Niosomes	Carvedilol	(289)
Nanocrystals	Nimodipine	(328)
Bioactive Chylomicrons	Berberine	(385)
Nanoemulsomes	Andrographolide	(321)
Bioemulsomes	Baicalin	(297)
NMs	Efavirenz	(304)
Cerasomes	Idarubicin Hydrochloride	(389)

Abbreviations:
Self-Microemulsifying Drug Delivery System (SMEDDS), Nanocapsules (NCs), Microemulsion (ME), Solid-Lipid Nanoparticles (SLN), Self-Nanoemulsifying Self-Nanosuspension (SNESNS), Solid Self-Nanoemulsifying Oily Formulations (S-SNEOFs), Self-Emulsified Drug Delivery Systems (SEDDS), Nanostructured Lipid Carrier (NLC), Matrix Dispersion (MD), Nanomicelles (NMs).

A comprehensive examination of the pharmacokinetic profile of cycloheximide and its associated effects and toxicity has been undertaken by Al Nebaihi *et al* to enhance the understanding of its impact. In adult Sprague-Dawley male rats, cycloheximide was administered at 0.5 mg/kg through oral, intraperitoneal, and intravenous routes. The findings showed that cycloheximide exhibited high clearance and volume of distribution, with an oral bioavailability of 0.47 at the 0.5 mg/kg dose. The pharmacokinetics of

cycloheximide was dose- and route-dependent, showing over a 3-fold relative bioavailability after intraperitoneal doses. Cycloheximide also demonstrated low plasma protein binding and minimal urinary excretion. Metabolism appeared to occur through oxidation and glucuronidation. Oral administration of 2.5 mg/kg cycloheximide led to reductions in plasma lipids (24–40%), accompanied by signs of inflammation and increased liver enzymes for a week following the dose. Markers of hepatic function and inflammation were elevated after the oral administration of 2.5 mg/kg. Additionally, cycloheximide was found to induce hepatotoxicity within 2 hours after a single intraperitoneal dose of 5 mg/kg (332).

Another study highlighted an important observation; when the lymphatic absorption pathway is obstructed, the primary route for drug absorption in the intestine is through the portal blood. Consequently, drugs relying on lymphatic transport may undergo hepatic first-pass metabolism when lymphatic uptake is hindered, leading to a reduction in both the rate and extent of drug absorption, reflected in decreased AUC, C_{max} and T_{max}. This phenomenon was evident with abiraterone, as pre-treatment with cycloheximide reduced the rate and extent of its absorption, resulting in a threefold decrease in C_{max} and a twofold decrease in AUC. Although the mean half-life was approximately 2 hours after both oral and intravenous administrations, it appeared to be extended to 18 hours in the cycloheximide pre-treated group. Yet, the specific pharmacokinetic mechanisms underlying this observation, including alterations in the volume of distribution, total body clearance, or both, remained unclear (306). In a similar manner, pre-treatment with cycloheximide modified the pharmacokinetic profile of cinacalcet, suggesting a potential alteration in absorption in this model (306).

Although being the most used chylomicron-blocking model compound, concerns have recently surfaced regarding the potential exaggeration of lymphatic uptake, particularly for drugs with low lipophilicity (log P < 5), when utilizing the cycloheximide model. This issue came to the forefront during a study evaluating abiraterone and cinacalcet using the cycloheximide model. The results may suggest a substantial overestimation of relative bioavailability (28-fold higher for abiraterone and 2.7-fold higher for cinacalcet) compared to the cannulation method, which directly measures drugs from the lymphatic vessel draining the intestinal region (mesenteric lymph duct). In light of these findings, the study concluded that the cycloheximide model may not be suitable for accurately assessing lymphatic transport and advocates for a critical re-evaluation of previously obtained data (306). Further studies would be required to support this claim as there have been other reports supporting the good correlation between chylomicron blocking and cannulation methods (254).

The cycloheximide model is the most extensively studied and applied one among the mentioned chylomicron-blocking models. Various xenobiotics, ranging from peptides like insulin to drugs addressing diverse conditions such as anticancer, antiviral, and hypertensive medications, have been investigated using this model. The advantage of cycloheximide lies in its capacity to block chylomicrons effectively at concentrations (3 mg/kg) without inducing appreciable toxicity, distinguishing it from the antitubular chylomicron blocker, colchicine.

5.3 Outlook and Future Perspectives:

Upon reviewing the literature on chylomicron blockers, in addition to considering the various points discussed in different sections, three specific aspects have surfaced as areas that merit more detailed examination beyond what is covered in the individual sections. These key points are delineated below:

5.3.1 Chylomicron Blockade: An Underappreciated Drug Interaction?

Chylomicron blockers are being used and designed to reduce lymphatic drug absorption experimentally. However, the suitability of cycloheximide for human use is challenged by its toxicity, limiting its application primarily to *in-vitro* and animal experiments (390). Moreover, puromycin, a cytocidal antibiotic, is utilized principally in cell culture experiments when a selective agent is required to eliminate all cells without resistance genes, leaving only specific targets behind (391). PL-81, employed in formulation and drug delivery, has also been identified as a potent anti-obesity drug in animal models (392-394). Nevertheless, clinically, some of these blockers are available and have been used for decades for a number of malignancies. Colchicine, a remedy with a history spanning over a millennium for treating gout, is now being explored for potential applications in dermatological conditions, and cardiovascular diseases, as well as in immunology and oncology (359, 395, 396). Additionally, vinca alkaloids, such as vincristine, vinblastine, vinorelbine, vindesine, and vinflunine, are widely used chemotherapeutic agents. Vincristine and vinblastine, particularly studied in the context of chylomicron blockade, demonstrate clinical availability for its antitumor effects (372, 397).

The hypothesis proposed is that *in-vivo* use of chylomicron blockers may interact with lipophilic xenobiotics, partially absorbed through the chylomicron pathway, resulting in a reduced absorption of the latter. The combination of clinical use of drugs (colchicine, vinca alkaloids) or an excipient (PL-81) inhibiting chylomicron formation or secretion, along with a substrate intended for absorption through the chylomicron pathway, could lead to a reduced T_{max} and a decreased area under the concentration-time curve and consequently less drug available to exert effects. Reports on drug interactions, particularly with colchicine and vinca alkaloids, attribute these interactions to competition and effects related to transporters and enzymes that both inhibitors and concurrently administered drugs interact with (398-402).

However, to the best of our knowledge, there is no documented evidence that PL-81, colchicine, or vinca alkaloids in clinical use have led to a demonstrable reduction in drug concentrations as a result of the chylomicron blockage effect. Several factors may contribute to this lack of support, such as the percentage of PL-81 in formulations potentially not reaching the threshold for inducing chylomicron blockage and subsequent reduction in drug concentration. Additionally, the developed formulations may not have been tested *in-vivo* or even *in-vitro* for the chylomicron blocking effect (335, 393, 403).

Also, formulations of vinca alkaloids still in development may not have be used at effective doses to impart the blockage effect. Furthermore, many formulations are designed to enter the M cells pathway rather than the chylomicron pathway, as will be explained in the next section. Therefore, drugs taken with such formulations may not be affected, as they follow a different pathway to the general circulation (404). Another factor that may obscure the evidence of chylomicron blockage in clinical use is that these agents might not

be suitable for oral administration. For instance, vinca alkaloids, known to have adverse effects and fatalities when administered via routes other than intravenous, prompted the FDA to add a warning to the labeling of vinca alkaloids such as vincristine and vinblastine, advising intravenous administration only (405).

Despite its utilization in various ailments, including gout (406), colchicine also lacks clinical documentation as a chylomicron blocker in humans. Taking it as an example, where a reported dose of 0.5 mg/kg has demonstrated a chylomicron blocking effect in a rat model (363), the Human Equivalent Dose (HED) can be calculated. The HED (mg/kg) calculation follows the method reported in the literature (407), considering the rat as the animal model and using rats with a weight of 200g, falling within the standard weight range specified for the method (90-400 g) (363). The equation is as follows:

HED (mg/kg) = rat dose (mg/kg) × 0.16 = 0.08 (mg/kg)

It is worth mentioning that the oral recommended dose of colchicine in humans is (0.015 – 0.03 mg/kg) (408), and the toxic oral dose in humans is > 0.1 mg/kg (409). Also, it is important to note that the effectiveness of colchicine at the dose specified in the rat model has been questioned in other reports, as mentioned earlier in section (3.3). Likewise, the animal dose was administered intraperitoneally, whereas the recommended and toxic doses specified for humans are for oral tablets. Thus, an effective dose range for various routes of administration of colchicine and other blockers, complemented by additional toxicity studies would be necessary to broaden the applicability of the findings to humans.

5.3.2 Other Pathways for Intestinal Lymphatic Uptake:

As previously demonstrated, in addition to drugs moving between the enterocytes (paracellularly) to get into the intestinal vasculature, they can gain entry into the intestinal lymphatics through two distinct routes: chylomicrons and M cells. While these pathways initially operate independently, they eventually converge into the mesenteric lymph for further transportation (328). Although the inhibitory models discussed earlier primarily target the chylomicron pathway, some drugs can be found in the mesenteric lymph as a result of their uptake through the M cells. Therefore, it is essential to clarify the role of the M cells pathway as well.

M cells play a critical part in transporting antigens and microorganisms to the underlying mucosal lymphoid tissues (Peyers' patches) for antigen presentation (181, 410). They may also transport microparticles or particulates from the intestinal lumen, releasing them at the basolateral side for transport through the mesenteric lymph and, ultimately, the systemic circulation (54). As M cells recognize pathogens by specific ligands on their surfaces, some particles including drugs and vaccines can be engineered to mimic specific ligands, enhancing their uptake through this pathway (411, 412).

Factors influencing drug transport via the M cell pathway are still under investigation. Though, studies have explored the impact of particle size, hydrophobicity, surface charge, and shape on transport through this pathway. Particles measuring 600 and 2000 nm have been reported to undergo transport via the M cell pathway (413). Increasing hydrophobicity has been found to enhance uptake through M cells as studied with rifampicin nanoparticles coated with hydrophobic polymers (414). Studies on the effect of

surface charges on the M cell pathway have different conclusions. In some studies, it has been noted that positively charged particles are more easily taken up by M cells than negatively charged ones, due to electrostatic affinity with intestinal mucus or cell membranes (415). These findings have been documented in a few reports including one with an oral DNA vaccine targeting Peyers' patches (416). Other studies have shown a higher uptake through the M cells for the neutral and the positively charged particles compared to the negatively charged counterparts (417, 418). Also, compared to spherical-shaped particles, rod- and disc-shaped particles achieved a higher extent of lymphatic transport through this pathway (419, 420).

5.3.3 Urinary excretion to quantify the lymphatic uptake:

Pharmacokinetically, plots of cumulative urinary excretion over time are often used to analyze the excretion of a drug through urine. This method involves collecting urine samples over a period of time and plotting the cumulative amount of the drug excreted versus the time of collection. These plots help in understanding the rate and extent of drug excretion from the body (421). They are particularly useful in calculating urinary pharmacokinetic parameters such as the total amount excreted ($A_{e\infty}$) which can be used to determine the bioavailability of drugs (422, 423).

The rate at which the body eliminates drugs through urine correlates directly with the concentration of drugs in the bloodstream. This relationship enables the determination of bioavailability by comparing the quantity of unchanged drug excreted in urine following the administration of test and reference formulations (423). This method is based on the principle that the parameters obtained from the urinary excretion data reflect the absorption

of the drug. However, it is important to note that this approach applies only to drugs that are excreted unchanged in the urine, and the relationship between serum concentration and renal clearance should be established before using urinary excretion data to assess bioavailability (424, 425). Therefore, urinary excretion data can be a valuable tool in assessing the bioavailability of certain drugs, particularly when coupled with plasma level-time data (425). To our knowledge, the use of urinary excretion of drugs has not yet been studied with chylomicron blockers but could be a useful non-invasive alternative approach to study drugs that are absorbed lymphatically and undergo renal excretion (**Figure 5.6**).

The equation for bioavailability (F) when there are two different input pathways (p1 and p2) for a drug into the body, and the numerator is made up of two amounts, one from each pathway, can be expressed as:

$$F = \frac{(Amount\ of\ the\ drug\ excreted\ into\ the\ urine\ via\ p1 + Amount\ of\ the\ drug\ excreted\ into\ the\ urine\ via\ p2)}{\text{Dose of the drug administered}}$$

This equation considers the total amount of the drug excreted into the urine via each pathway and relates it to the dose of the drug administered. It allows for the estimation of drug bioavailability when there are multiple input pathways contributing.

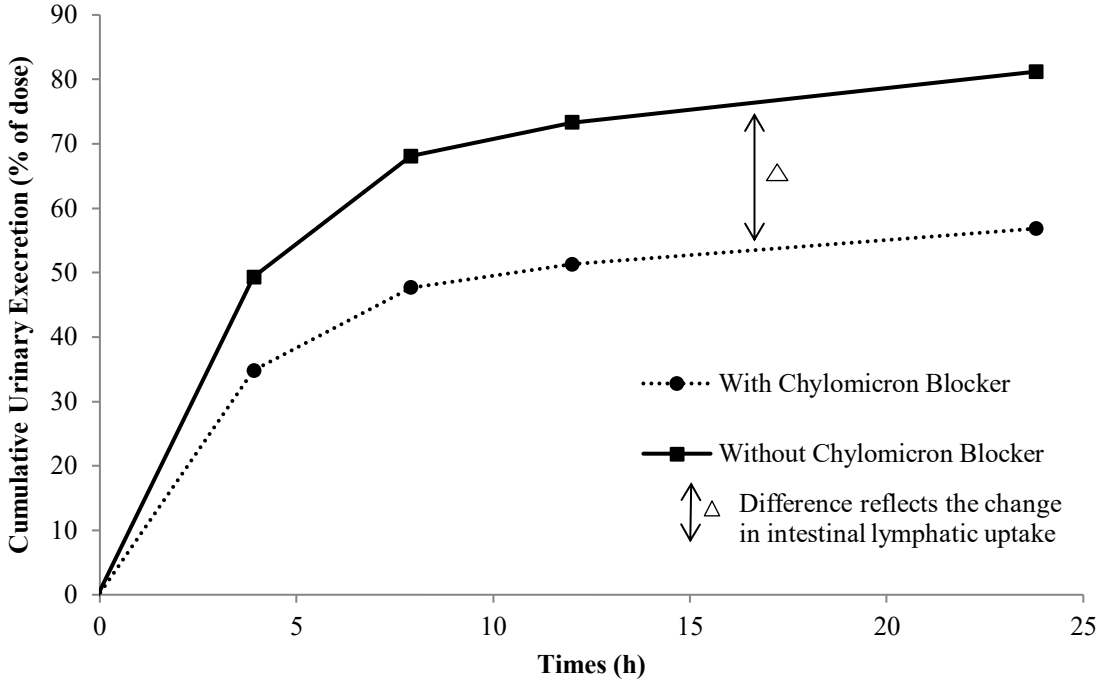

Figure 5.6. Hypothetical graph of drug urinary excretion with and without chylomicron blocker for a drug that can be absorbed through intestinal lymphatics.

5.4 Conclusion:

Numerous xenobiotics have been employed to obstruct the formation and/or secretion of chylomicrons, with the aim of hindering the uptake of associated drugs through the intestinal lymphatic pathway. Since this pathway constitutes a distinct route into the general circulation besides the portal pathway, here we reported a comprehensive pharmacokinetic equation for bioavailability that accounts for this pathway. The same principle when applicable, urinary data can be utilized as a non-invasive alternative to provide insights into the portion of the drug taken up through intestinal lymphatics.

Research in this field dates back to the 1940s, yet essential data for various chylomicron blockers are still lacking. Reported compounds in the literature include PL-81, puromycin, vinca alkaloids, colchicine, and cycloheximide. Among these, PL-81 has stood

out as a compound with a reversible effect and minimal toxicity and can be used *in-vitro*, and *in-vivo* in animals. Additionally, it is unique as it does not function as a protein synthesis inhibitor; instead, it exerts its action by destabilizing the surface of forming chylomicrons. It also disrupts the transport of triglycerides within enterocytes and alters the conformation of chylomicron apo-lipoproteins. PL-81 was tested *in-vitro* using a cellular Caco-2 model and a non-cellular model with artificial chylomicrons. However, no reports were found on its clinical blockage of the chylomicron pathway, attributed probably to the low concentrations used in the formulations, which are likely well below the EC_{50} to induce this effect.

Puromycin and vinca alkaloids (vincristine and vinblastine) have been sporadically reported in the literature, focusing on their toxicity and effects on lipid absorption through chylomicrons. However, documentation on their application in drug intestinal lymphatic uptake is lacking. Moreover, beyond vincristine and vinblastine, other vinca alkaloids have been reported to affect the triglyceride profile and lower their concentrations. Consequently, these alternatives present promising prospects for further investigation as potential agents for blocking chylomicron pathways. Despite the clinical use of vinca alkaloids in many applications, especially as anticancers, their likelihood of being associated with chylomicron blockage in clinical practice is low.

Colchicine and cycloheximide have been the most commonly used chylomicron blockers in the pharmaceutical development of lymphotropic drugs and formulations. The latter is preferred due to its lower toxicity compared to colchicine in animal models, even at concentrations inducing chylomicron blockage. By relying on a reported effective colchicine dose in rats to block chylomicrons and employing allometric scaling, it was

found that recommended doses used in humans might have a similar effect. However, further investigation into the effective and toxic doses of colchicine is required to understand its clinical impact on blocking the chylomicron pathway in humans.

CHAPTER SIX

Simulated Lymphatic Fluid for *In-Vitro* Assessment in Pharmaceutical Development

A version of this chapter is published in:

Dissol Technol. 2022;29:86-93. DOI: 10.14227/DT290222P86

Reprinted from Reference (264).

6.1 Background:

Lymph or lymphatic fluid is a biological fluid derived from the interstitial fluid of parenchymal cells throughout the body. The hydrostatic pressure within the capillary beds results in molecule ultrafiltration from arterioles, which drives some blood components along with proteins into the interstitial space (426). Approximately 90% of the 20–30 liters of the plasma that leaks into the interstitium returns to blood through the capillary venous end, and the remaining fluid is drained back along with other molecules from the extracellular space to the circulation by the lymphatic system in the form of lymph (135, 136). Lymph also carries the invading pathogens and immune cells into lymph nodes where proper immune responses can be mounted (136, 427). Thus, lymph serves in regulating and modulating immune response, thereby affecting some important immunological processes like immune tolerance in the body. Furthermore, lymph has two other main functions – maintaining fluid homeostasis and delivering some nutrients and fat absorption products from the intestine to the general circulation (51).

6.1.1 Lymph Flow:

From the extracellular space, lymph first enters blind-ended lymphatic capillaries, termed the "initial lymphatics." Next, it drains into the lymphatic collecting vessels, then passes through at least one but usually several lymph nodes distributed throughout the body. Collecting vessels merge into larger trunks that empty into lymphatic ducts. Finally, the ducts return the lymph back into the venous circulation at the junction of the jugular and subclavian veins (**Figure 6.1**), completing the circuit of fluid transport (56, 162).

Dietary lipids and highly lipophilic drugs are usually packaged into lipoprotein vesicles (chylomicrons) in the cytoplasm of the enterocytes before being up taken by the lymphatic capillaries (281). Triglycerides of ingested lipids are usually hydrolyzed by lipases into monoglycerides and fatty acids prior to reaching the duodenum. When hydrolysis products enter the enterocytes, long chain fatty acids ($C \geq 12$) and monoglycerides get re-esterified in the endoplasmic reticulum and are assembled into chylomicrons, which then migrate to the Golgi apparatus before being exocytosized into intestinal lymphatics (53, 234).

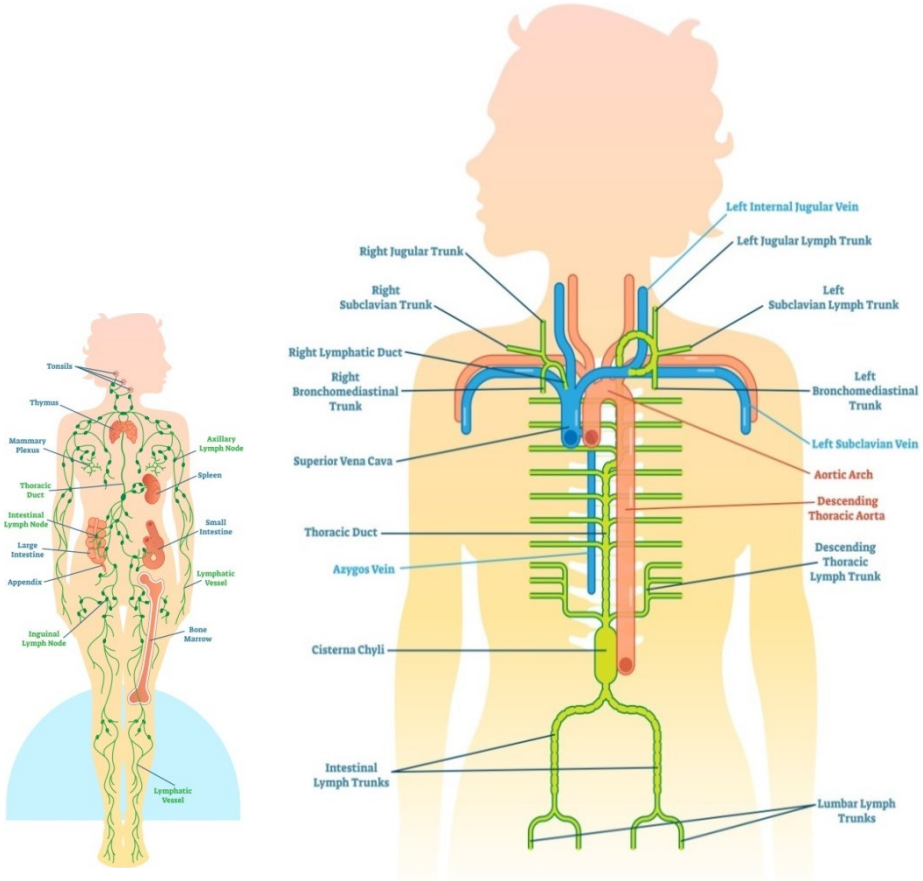

Figure 6.1. Lymphatic system through the body (left). The vessels part of this system starts with the initial lymphatic capillaries that are interlaced with arterioles and venules, then drain into lymphatic collectors and trunks before they empty into the right lymphatic and thoracic ducts, which in turn joins the venous circulation at the junction between the jugular and subclavian veins on both body sides (right).

Lymph flow rate differs among species, within species, and within subjects (428, 429). Ultimately, it is a function of the blood flow through an organ and the proportion of the blood that leaks from the capillaries into the lymphatics (429). Pre-nodal (afferent) lymph flow collected from fasted-state rat individual mesenteric collecting lymphatic vessel is 15 μL/h, and post-nodal (efferent) flow of the total mesenteric lymphatics is approximately 1.3 mL/h (430). In humans, the afferent lymph flow is estimated to be twice that of the efferent, i.e., 8 and 4 L/day, respectively (431). This is attributed to the reabsorption that occurs at the lymph nodes through special blood vessels across. Lymph components can cross into either direction, thus changing the post-nodal lymph rate and composition (135, 432, 433).

6.1.2 Lymph Composition:

Reported studies on lymph composition date back to the late 1920s. In 1932, Heim tested thoracic and cervical lymph of dogs for protein, non-protein nitrogen, urea, uric acid, creatinine, sugar, amino acids, chlorides, calcium, and phosphorus (434). After comparing his results with previously reported data, Heim concluded that the chemical composition of lymph overlaps with that of the plasma. The exception was for protein and its related substances (phosphorous and calcium), which were higher in plasma than in lymph (434). In a study that investigated rat ovarian lymph, the total concentration of protein was estimated to be 53% of the plasma (429). Yet, similar studies in other species have reported higher percentages of total protein concentration in lymph compared to plasma, with the highest level recorded in sheep as 90% (435, 436).

Similarly in humans, the lymph composition was first believed to coincide with that of the plasma as the former was considered a filtrate of the latter. Challenges associated with cannulating lymphatic vessels with collecting only little amounts of lymph for analysis and the low sensitivity and resolution of the analytical instruments were barriers to a thorough analysis of lymph (135, 434). Nevertheless, lymph biology has progressed over years and these hurdles have been resolved. It is now known that pre-nodal lymph has a similar make up of salts, plasma proteins, sugars, and lymphocytes as interstitial fluid. However, the post-nodal lymphatic fluid is more concentrated, having a higher count of lymphocytes and a two-fold higher concentration of the plasma protein (136, 433, 437).

Proteomic analysis revealed that the proteins essential to osmotic pressure maintenance, namely albumin, α1, α2, β globulins, and fibrinogen, in addition to the coagulation factors are higher in plasma than in lymph (438-441). Nevertheless, the lymph is richer in extracellular matrix proteins and intracellular proteins resulting from cellular metabolism, i.e., those released from apoptosis and lipoproteins (442-446). To date, more than 2000 proteins have been identified through protein mapping of lymph derived from various species including human (447). Mapping was mostly done on peripheral subcutaneous and mesenteric pre-nodal lymph; therefore, the full lymph profile is not yet completed (447).

The cellular component averages 12,000 ± 5200 cells/μL in rat mesenteric lymph (430). In human peripheral lymph, there are 162 cells per mm^3, with lymphocytes accounting for up to 96% of all these cells (448). Low concentration of these cells does not appear to affect the bulk properties of the lymph (136).

6.1.3 Simulated Lymphatic Fluid:

In the field of pharmaceutical sciences, lymph-targeted drug delivery can open a new era to medicines and vaccination (51). This approach has relevant therapeutic and pharmacokinetic benefits (69). The intestinal lymphatic transport, in particular, can demonstrate various advantages over portal blood absorption following oral administration of drugs (449). Intestinal lymphatic absorption can aid drugs by shunting away from first pass hepatic metabolism, thus imparting higher bioavailability. Thus, drugs with a high extraction ratio are the most ideal candidates to be delivered via lymphatic fluid. Additionally, intestinal lymphatic delivery can boost efficacy of chemotherapeutic and immunomodulatory agents, with the lymphatic system being primarily involved in cancer metastasis and immune modulation (53, 56, 449). Examples of lymphotropic drugs include carvedilol (227), halofantrine (221), praziquantel (309), docetaxel (383), valsartan (222), among others (184, 187).

The importance of standardized physiologically relevant simulated fluids for use in biopharmaceutic and dissolution studies have been highlighted in multiple articles and reviews; however, there is no mention of standardized simulated lymphatic fluid in these publications (120, 450, 451). Standardization of a simulated clinically or physiologically relevant lymphatic fluid media would be an important and novel contribution to fill the current void this emerging area of drug and formulation development.

Simulated lymphatic fluid can be composed of the components listed in **Table 6.1** (120, 136). The composition of salts in the proposed fluid is similar to that of the extracellular fluid (120). Protein composition is approximated to be less than 0.01 g/mL in

pre-nodal lymph (136). As albumin is a main protein that affects drug binding and pharmacokinetics, it can be added into the simulated lymphatic fluid. It composes nearly 60% of the total protein in lymph and would be used in the concentration of less than 0.006 g/mL (429, 438, 452).

Table 6.1. Concentration of various constituents in lymphatic fluid (120, 136).

Component	General Simulated Lymphatic Fluid (mM)	Intestinal Simulated Lymphatic Fluid or Chyle (mM)
HCO^{3-}	4.2	4.2
K^{+}	5	5
Cl^{-}	148.8	148.8
Na^{+}	142	142
Ca^{+}	2.5	2.5
Mg^{+}	1.5	1.5
HPO_4^{-2}	1	1
SO_4^{-2}	0.5	0.5
Tris(hydroxymethyl)aminomethane	50	50
Hydrochloric acid	45	45
Proteins	< 0.01 g/mL	0.02–0.06 g/mL
Triglyceride fat globules (chylomicrons)	-	> 0.01 g/mL

Lymph derived from the intestine is termed “chyle.” It has a rich protein content (0.02–0.06 g/mL) and a milky color, unlike the clear lymph from other parts of the body (143, 453). The white color is attributed to the fact that this portion of lymph is rich in chylomicrons (141, 454). Chylomicrons are mainly composed of triglycerides as well as phospholipids, proteins, and cholesterol (260).

Intralipid® (Fresenius Kabi Canada Ltd, Toronto) 20% is a commercial product used for providing fats and calories to patients in need of total parenteral nutrition (455). The components of Intralipid® are listed in **Table 6.2**. Interestingly, the components are comparable to those of endogenous chylomicrons, which are used as a main component to simulate intestinal lymphatic fluid (455, 456). The size of globules lies within the range of the chylomicron's; furthermore, it contains the main components that constitute chylomicrons and chiefly affect their drug uptake. The acids present in soybean oil, from which Intralipid® is prepared, resemble the typical acids packaged into the chylomicrons (333, 457). As a consequence, the simulated chyle would be similar to the previously described lymphatic fluid, with a slightly higher albumin level (0.012–0.036 g/mL). As a surrogate for the chylomicron component of lymphatic fluid, Intralipid® has a triglyceride concentration of more than 0.01 g/mL (136, 455).

Table 6.2. Composition of Intralipid® and endogenous chylomicrons.

	Chylomicrons	**Intralipid®**
Size	75–1000 nm (1 μ)	0.5 μ
Components	Triglycerides (~84%)	Soybean oil* (20 g)
	Phospholipidis (~7%)	Egg phospholipids (1.2 g)
	Protein (1-2%)	Glycerol (2.2 g)
	Cholesterol (~7%)	q.s water for injection (100 mL)
	Cholesterol esters (1-2%)	

*Acids in soybean oil include 52% linoleic and 22% oleic in addition palmitic (13%), linolenic (8%), stearic (4%), myristic (< 1%), and other acids (1%).

6.2 Materials and Methods:

6.2.1 Preparation of Simulated Lymphatic Fluid:

For pharmaceutical compounding and preparation of simulated lymphatic fluid, reagents in **Table 6.3** are used. The method of preparation for both general and intestinal lymphatic fluid involves successive addition of the reagents in the specified amounts after each being fully dissolved in 700 mL water, before adjusting to the required pH with 1 M HCl and completing the volume to 1 L (120). If stored at 2–8 °C, simulated general lymphatic fluid is stable for more than 2 months, whereas simulated intestinal lymphatic fluid requires gentle shaking before use if stored under similar conditions and for the same period of time.

Table 6.3. Reagents for preparing simulated lymphatic fluid.

Reagent	CAS number	Amount for 1 L of Simulated Lymphatic Fluid
Sodium chloride	7647-14-5	8.035 g
Sodium bicarbonate	144-55-8	0.355 g
Potassium chloride	7447-40-7	0.225 g
Potassium phosphate dibasic	7758-11-4	0.231 g
Magnesium chloride hexahydrate	7791-18-6	0.311 g
1 M Hydrochloric acid	7647-01-0	39 mL
Calcium chloride dihydrate	10035-04-8	0.292 g
Sodium sulfate	7757-82-6	0.072 g
Tri(hydroxymethyl)aminomethane	7283-04-7	6.118 g
Protein (human serum albumin)	70024-90-7	40 g
Intralipid®	68890-65-3	100 mL

6.2.2 Analysis of Simulated Lymphatic Fluids:

The lymphatic fluids (prepared and a commercial obtained product) were analyzed to compare their composition and properties with the reported data for biological lymph. Variables used for comparison of the fluids included pH, density, chemical content, and solubility.

The pH of the fluids was measured using a Fischer Scientific XL20 pH/conductivity meter. The density of 80 mL-samples of each fluid were analyzed using a Mettler Toledo XPR/XSR-Ana density kit at 25 ± 0.2 °C. The specified amount was placed in the beaker, the sinker was completely immersed, and after ensuring no bubbles adhered to the immersed sinker, the draft shield was closed. After the balance reached stability, the obtained readings were recorded.

Medica's EasyRA analyzer was used to investigate the lymphatic fluids for chemical content, i.e., potassium (K^+), sodium (Na^+), calcium (Ca^{++}), magnesium (Mg^{++}), phosphorus (P^{2-}), iron (Fe^{3+}), and chloride (Cl^-) ions, as well as total carbon dioxide (CO_2), total protein, albumin, and triglyceride concentration. After calibration and a system check, cleaning the probe and the ISE (ion selective electrode), calibrated proper reagents were placed in sample holder with the blank (HPLC grade water) and 100 or 2000 µL samples of the simulated lymphatic fluids (or dilutions of the fluids). The required tests were processed and the acquired results were noted.

Solubility of a lymphotropic drug (rifampicin) a Zwitterion with pKa 1.7 for the 4-hydroxy and pKa 7.9 for the 3-piperazine nitrogen was measured using the shake-flask

method adopted from the literature in the prepared simulated lymphatic fluids and the commercially obtained artificial fluid (129).

6.3 Results and Discussion:

When compared with a commercial artificial lymphatic fluid (Biochemazone), the prepared simulated lymphatic fluids more accurately resembled the composition of biological lymphatic fluid (136, 333). The data are presented in **Table 6.4** for comparison.

The density values of both commercial and laboratory-prepared fluids were within the range reported for biological lymphatic fluid. However, the pH of the commercial fluid (6.98) did not lie within the physiological range reported for lymph collected from the thoracic duct (7.08–7.40) (458). Despite being close to the reported range, this pH could pose a hurdle to using commercial fluid for *in-vitro* drug studies in which the conditions are usually set to mimic those *in-vivo*.

The concentration of Na^{+} in all fluids was less than the reported value in the biological fluid. The lowest concentration was recorded in the artificial fluid, whereas the simulated lymphatic fluids values were closer to the reported physiological value. A similar result was determined with Ca^{++} concentration. The artificial lymphatic fluid had no Cl^{-} and very high concentration of K^{+} and Mg^{++} whereas the values of both in the prepared simulated lymphatic fluids were within an acceptable range compared to biological fluid. All fluids contained a higher concentration of P^{2-} than the reported physiological value; the highest was the artificial fluid by almost 18-fold, and the simulated fluids were higher by approximately 2 and 3 fold for the simulated general and intestinal fluids, respectively. A negligible amount of iron was detected in the simulated intestinal lymphatic fluid,

stemming from the reagents and the Intralipid® used to prepare the fluid. The artificial fluid contained a high concentration of CO_2, unlike the others examined that had no CO_2.

Table 6.4. Comparison of prepared simulated lymphatic fluids, commercial artificial fluid, and biological fluid.

Property or Component	**Commercial Artificial Lymphatic Fluid***	**Simulated General Lymphatic Fluid**	**Simulated Intestinal Lymphatic Fluid**	**Biological Lymphatic Fluid (136, 333)**
pH	6.98	7.4	7.4	7.08 - 7.4
Density	1.007 g/mL	1.006 g/mL	1.005 g/mL	1.005 - 1.016 g/mL
Na+	97.3 mM	135.7 mM	135.7 mM	142 mM
K+	43.5 mM	5.23 mM	5.23 mM	5 mM
Cl-	_	117.4 mM	117.4 mM	148.8 mM
Ca+	0.91 mM	2.51 mM	2.51 mM	2.5 mM
Mg+	3.65 mM	1.45 mM	1.45 mM	1.5 mM
P2-	6.02 mM	1.06	1.06 mM	1 mM (Phosphate) 0.32 mM (Phosphorus)
Fe3+	_	_	0.007 mM	_
CO2	48.6 mM	_	_	_
Albumin	0.002 g/mL	0.005 g/mL	0.021 g/mL	≤ 0.0054 g/mL for general lymphatic fluid 0.012-0.036 g/mL for intestinal lymphatic fluid
Total Proteins	0.004 g/mL	0.005 g/mL	0.04 g/mL	< 0.01 g/mL for general lymphatic fluid 0.02 - 0.06 g/mL for intestinal lymphatic fluid
Triglycerides	0.0009 g/mL	-	0.03 g/mL	> 0.01 g/mL

*Artificial lymphatic fluid was purchased from Biochemazone, Waterloo, Canada (Batch no. BZ-0421A).

All essential amino acids and serum proteins were present in the artificial lymphatic fluid with a total protein concentration of 0.004 g/mL. Albumin concentration was 0.002 g/mL, which coincides with the level of the albumin present in the general biological lymphatic fluid. The prepared simulated fluids only contained the albumin level known to be in the general and intestinal lymph (136). Usually, acidic drug binding in particular can be affected by albumin concentration, thus having an accurate representation of protein concentration in simulated lymphatic fluid is prudent. The presence of other protein moieties in the artificial commercial fluid, although at low concentrations, remains to be determined. The total protein in the simulated intestinal lymphatic fluid indicated that there are other proteins besides albumin. That additional protein was traced back to the soy protein in the soybean oil in Intralipid® (**Table 6.2**).

Triglycerides were found in both the artificial and prepared simulated fluids in different amounts. The artificial fluid had 0.0009 g/mL triglycerides, whereas the simulated general fluid was developed deliberately to have none and the simulated intestinal fluid contained an amount within the stated range of the fat component found mainly in the intestinal lymph (> 1%) (136). The lipids used in the simulated intestinal fluid resemble those incorporated into the chylomicrons and transported through the intestinal lymph, as outlined earlier.

Solubility of rifampicin (pKa 1.7 and 7.9) (459) was found to be 2.49 mg/mL in the artificial lymphatic fluid and 2.62 mg/mL and 3.00 mg/mL in the prepared simulated general and simulated intestinal lymphatic fluids, respectively. The drug solubility in the artificial and the simulated general fluids was nearly the same. Yet, more optimal results

were encountered with the simulated intestinal fluid, which might be attributed to the higher protein and triglyceride content in the simulated intestinal fluid compared to the other two fluids. This result demonstrates that the solubility of a compound can vary in simulated and artificial lymphatic fluids, which is essential when considering pharmaceutical, biochemical, or biological assays using these fluids. Solubility is also important for determining the dissolution profile of lymphotropic drugs and formulations.

6.4 Conclusion:

Lymph-targeted drug delivery can open a new era for development of medicines and vaccines. Further study of lymphatic delivery of molecules is an important aspect of pharmaceutical research and development. Understanding and standardization of simulated lymphatic fluid and its relevance must be considered for optimal drug development research processes. This study reviewed and analyzed simulated general and intestinal lymphatic fluids that proved to be closer in makeup to biological fluid than a commercial artificial lymphatic fluid. These results are a step towards filling the current need for a standardized simulated lymphatic fluid in pharmaceutical investigations.

CHAPTER SEVEN

Development of a Novel *In-vitro* Model to Study Lymphatic Uptake of Drugs via Artificial Chylomicrons

A version of this chapter is published in:

Pharmaceutics. 2023;15(11):2532. DOI: 10.3390/pharmaceutics15112532

Reprinted from Reference (350).

7.1 Introduction:

Most orally administered drugs enter the systemic circulation after absorption from enterocytes in the intestine via the portal vein (234). However, some orally administered lipophilic xenobiotics access the systemic vasculature via the intestinal lymphatic system, offering several advantages for drug delivery (53, 240, 278). Absorption through the intestinal lymphatics enables the drug to reach the general circulation without passing through the liver, which is beneficial for molecules that are prone to first-pass metabolism by the liver (54, 56). Additionally, drug delivery through the lymphatic system can result in higher drug concentrations in the systemic circulation and improve bioavailability, as reported for several drugs (54, 138, 182). The lymphatic route of absorption can be more effective for drugs targeting conditions involving the lymphatic system pathophysiology, including some viral infections, metabolic and inflammatory conditions, hypertension, and solid tumors, among others (51, 56, 184).

Drugs can access the intestinal lymphatics through enterocytes or microfold cells (M cells) in the follicle-associated epithelium (FAE) that overlies Peyer's patches (54, 234, 278). Chylomicrons, which are mainly composed of triglycerides, phospholipids, proteins, cholesterol, and cholesteryl esters, are responsible for transporting drugs across the enterocytes and into the lymphatic system (254, 264). Ingested triglycerides are hydrolyzed by lipases into monoacylglycerols and free fatty acids, which are subsequently re-esterified to triglycerides and assembled into chylomicrons in the endoplasmic reticulum and Golgi apparatus of enterocytes before being exocytosed via the basolateral membrane (53, 234, 278).

There are various methods of enhancing the transport of drugs through the lymphatic system. These include administration of drugs during a postprandial state and the utilization of lipid-based formulations and lipidic prodrugs (54). Lipid-based nanoparticles have emerged as promising candidates for drug delivery. Multiple studies have been dedicated to creating formulations that leverage the potential of the intestinal lymphatics (54, 234, 254, 278). For instance, in a study involving Solid Lipid Nanoparticles (SLNs) loaded with nimodipine, a considerable improvement in bioavailability was observed compared to the drug solution. The bioavailability of nimodipine increased by a factor of 2.08 in male Albino Wistar rats. This enhancement was attributed to the portion of nimodipine carried by the lymphatic system (228).

Another illustration that highlights the harmonious interplay between utilizing a prodrug approach and the influence of food on the transportation of substances through the intestinal lymphatics can be found in the example of testosterone. When administered orally, testosterone exhibited limited effectiveness in treating male androgen deficiency syndromes due to significant initial loss during the first pass through the liver (460). However, studies have indicated that testosterone undecanoate, a prodrug of testosterone, displays higher systemic exposure compared to testosterone administration (64, 461). Furthermore, the exposure to both testosterone and the prodrug was notably greater in individuals who had consumed a meal compared to those who were fasting. This increase in systemic exposure after a meal was correlated with an augmentation in lymphatic transport efficiency. Moreover, the strategic conjugation of testosterone with a lipophilic long-chain ester (undecanoate) led to an elevated androgenic response compared to using pure testosterone. This lipophilic ester was observed to follow the intestinal lymphatic

route, evading the liver and ameliorating the initial pass effect. Once within the systemic circulation, the ester form underwent hydrolysis, liberating the free form of testosterone. Notably, a significant portion—ranging from 91.5% to 99.7%—of the testosterone available within the system was attributed to the testosterone undecanoate that had been transported via the lymphatic system (64). Numerous additional instances of such approaches can be found within various reports and reviews in the existing literature (54, 56, 182, 278).

For investigating lymphatic uptake, researchers have established and employed the mesenteric lymphatic cannulation model, which serves to assess lymphatic transport (283, 462). As intestinal lymph drains, it passes through the mesenteric lymph node en route to the circulation (56). This model facilitates the direct sampling of the mesenteric lymph node, allowing for the quantification of the drug that enters the systemic circulation through its journey in the intestinal lymphatics. While this method simplifies sample collection and measurement, it is important to note that lymphatic cannulation is invasive and comes with inherent limitations. The procedure necessitates intricate surgical steps and may potentially influence lymph flow and vessel pressure gradients, rendering sequential sampling challenging following multiple sessions. Given the interplay of various factors, the overall success rate of lymphatic cannulation tends to be quite low (54).

To circumvent the challenges associated with cannulation procedures, researchers have introduced lymph blocking models by employing specific blocking agents. For instance, the use of cycloheximide, a protein synthesis inhibitor, offers a targeted approach to suppressing the exocytosis and secretion of chylomicrons from enterocytes (463). Moreover, various other inhibitors employing distinct blocking mechanisms, including

Pluronic® L-81 and colchicine, have been utilized for assessing the portion of substances delivered through the intestinal lymph (59).

The *in-vivo* models offer the best evaluation, yet they pose technical challenges, demanding advanced surgical expertise, while also raising ethical concerns regarding human application (54, 184). An alternative approach involves the utilization of *in-vitro* models, incorporating both cellular and non-cellular strategies. Among cellular models, Caco-2 cells are commonly employed, but they come with constraints that include their resemblance to almost colonic rather than small intestinal tissue and the absence of the mucus layer secreted by goblet cells. Moreover, they lack other cell types existing in the human mucosa niche such as M cells (51). Advancement has been achieved through the co-culture of Caco-2 cells with lymphoid cells like Raji cells, which exhibit M cell-mimicking capabilities, or murine-derived lymphocytes (464). Nonetheless, this approach faces limitations due to the excessive presence of M-like cells, possibly leading to an overestimation of experimental outcomes. Consequently, there is a high anticipation for further enhancements or potential alternatives.

Regarding formulations targeted at lymphatic delivery and utilizing lipid-based carriers, the typical progression involves initial vehicle degradation via lipolysis. These degraded components subsequently transition into micellar vehicles, which are then absorbed by enterocytes and reassembled with chylomicrons (234, 278). To evaluate the effectiveness of such formulations, *in-vitro* lipolysis has proven useful. This method estimates the proportion of the drug intended for intestinal lymphatic uptake by quantifying the fraction incorporated into the generated micellar vesicles after the completion of lipolysis (465).

The interaction between drugs and chylomicrons plays a pivotal role in facilitating drug transportation across enterocytes via lipoproteins carried by the lymphatic system. Notably, a direct correlation between drug uptake by isolated chylomicrons and *in-vivo* intestinal lymphatic uptake has been documented across nine lymphotropic compounds. This finding highlights the credibility of using drug-chylomicron association as a reliable indicator for assessing intestinal lymphatic uptake (52, 282).

The aim of this study is to develop a model with the use of artificial chylomicrons (Intralipid®) to investigate intestinal lymphatic uptake. Intralipid® closely mimics the size and composition of natural chylomicrons, as illustrated in **Figure 7.1** (264, 466). To examine the uptake of lymphotropic drugs known to undergo lymphatic absorption, a Franz cell diffusion system was employed. Cannabidiol, halofantrine, quercetin and rifampicin were used as model lymphotropic drugs, and the interaction between these drugs and Intralipid® was explored. This experimental approach allowed for valuable insights into the mechanisms of intestinal lymphatic uptake and its association with Intralipid®. It can be employed as a convenient *in-vitro* physiologically based biopharmaceutical tool for preliminary assessment to anticipate the outcomes of drug delivery through the intestinal lymphatics via chylomicrons.

7.2 Materials and Methods:

7.2.1 Materials:

The following chemicals were used in this study: rifampicin (≤100%, CAS: 13292-46-1) was obtained from EMD Millipore Corp, Burlington, MA, USA; quercetin (≥95%, CAS: 117-39-5), Pluronic® L-81 (PL-81) (CAS: 9003-11-6), cannabidiol (CAS: 13956-29-1), and

1-octanol (99%, CAS: 111-87-5) were from Sigma-Aldrich Co. (Saint Louis, MO, USA); Halofantrine (CAS: 69756-53-2) was from SmithKline Beecham Pharmaceuticals (Brentford, London, UK); Intralipid® 20% was from Fresenius Kabi (Toronto, ON, Canada); and peanut oil product was purchased from a local Edmonton grocery. For HPLC analysis, water (99.9%, CAS: 7732-18-5), acetonitrile (99.9%, CAS: 75-05-8), methanol (99.9%, CAS: 67-56-1), acetic acid (≥99.7%, CAS: 64-19-7) and o-phosphoric acid (85%, CAS: 7664-38-2) were of HPLC grade from FisherFisher Chemical™ (Fisher Scientific, Ottawa, ON, Canada); all other reagents were of analytical grade.

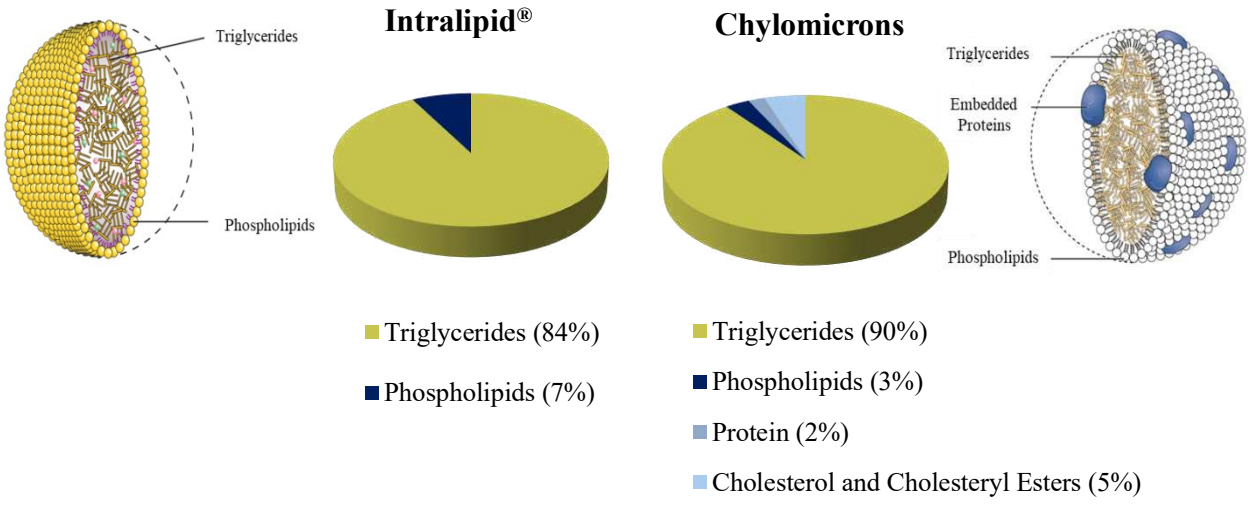

Figure 7.1. Schematic representation of natural chylomicrons (right) and the artificial counterpart (left) demonstrating their resemblance. The schematic representation of the chylomicron on the (right) is available under a cc license at http://cnx.org/content/col11496/1.6 (accessed on 17 September 2023). Intralipid® representation on the (left) was created based on the existing data regarding the structure of Intralipid® (466).

7.2.2 Methods:

7.2.2.1 Franz Cell for Investigating Intestinal Lymphatic Uptake:

The Franz Cell receiver compartment was filled with 12 mL of either Intralipid® or Intralipid® mixed with a potential inhibitor or enhancer and maintained at 37.0 ± 0.5 °C with magnetic stirring at 600 rpm, as shown in **Figure 7.2**. A synthetic 0.22 µm Polyvinylidene Fluoride (PVDF) membrane impregnated with octanol was placed between compartments. For the uptake experiments four model drugs (cannabidiol, halofantrine, quercetin and rifampicin) were used and to capture the inhibition and enhancement effect, rifampicin was utilized. Two mL solutions of the model drugs were added to the donor compartment with the receiver compartment containing either Intralipid® or Intralipid® mixed with an enhancer or an inhibitor. At different time intervals (0–4 h), 0.2 mL samples were withdrawn, extracted, and analyzed for drug content using HPLC with a C18 column (150 mm × 4.6 mm i.d., 5 µm). The column temperature was maintained at 25 °C, and the conditions of analysis for all drugs are listed in **Table 7.1**.

Table 7.1. HPLC analysis conditions for the model lymphotropic drugs.

Model Drug	Mobile Phase	Flow Rate (mL/min)	Detection Wavelength (nm)
Rifampicin	Methanol, Acetate Buffer (pH = 5.8) (60:40)	1.2	254
Quercetin	Methanol, Acetate Buffer (pH = 5.8) (60:40)	1.2	257, 370
Cannabidiol	Acetonitrile, Phosphoric acid (0.2%) (72:28)	1	210, 224
Halofantrine	Methanol, Phosphate Buffer (pH = 7.5) (80:20)	1	210, 259

7.2.2.2 Entrapment Efficiency:

To determine the entrapment efficiency of rifampicin in Intralipid®, a solution of rifampicin was mixed with Intralipid® at a concentration of ~145 mg/mL and stirred for 15 min. Then, 0.5 mL of the mixture was added to an Amicon Ultra-0.5 30 KDa centrifugal filtering unit (Millipore, Sigma-Aldrich, Darmstadt, Germany) and centrifuged at 10,000× g for 10 min. The filtrate was collected and analyzed using HPLC. The sample was then returned to the filtering unit and the process was repeated. The filtrate was collected again and analyzed to determine the entrapment efficiency.

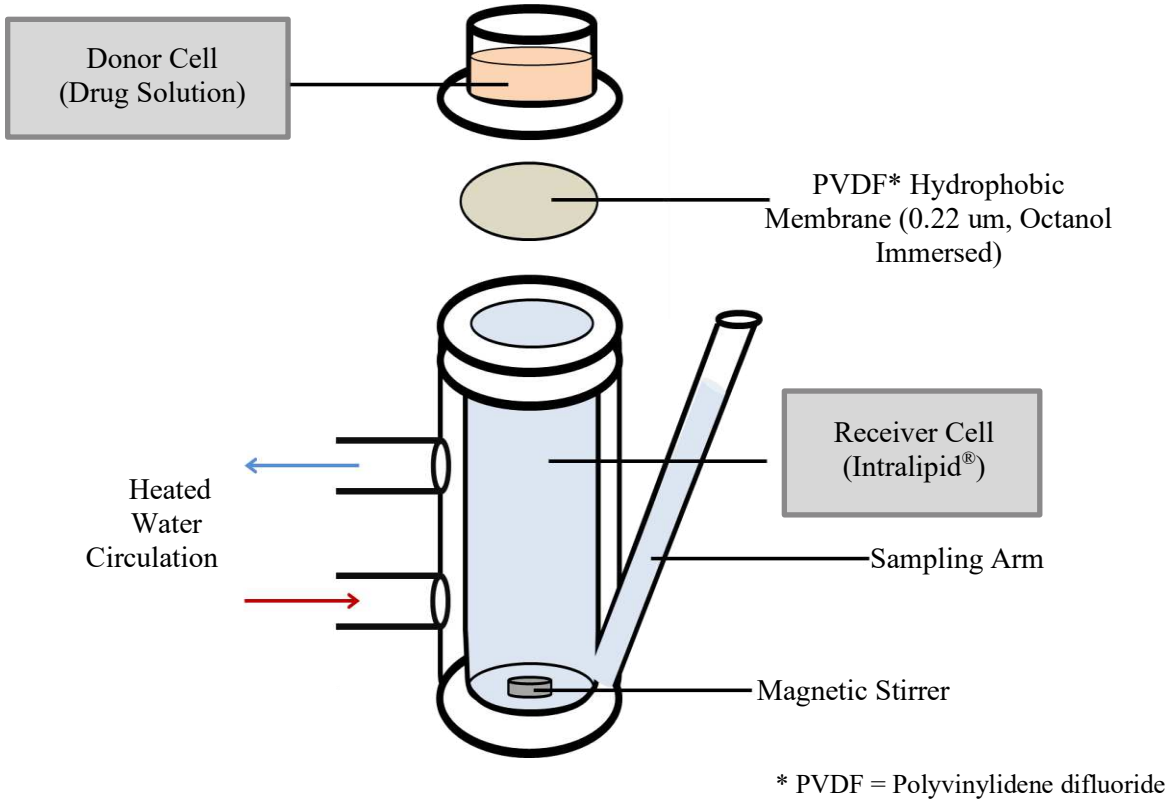

Figure 7.2. Demonstration of the proposed lymphatic uptake model.

7.2.2.3 Characterization of Intralipid®:

7.2.2.3A Measurement of Size of Intralipid®:

The particle size of Intralipid® and Intralipid® mixed with different percentages of Pluronic® L-81 (0.05%, 0.1%, 1% and 10%) were measured using a Malvern Ultra Zeta Sizer (Malvern, UK) at an angle of 173° and 25 °C. This instrument uses 10 mW 632.08 nm HeNe laser, adaptive correlation algorithm, and avalanche photo diode (APD) detector. Samples were analyzed in polystyrene latex cells (DTS0012) for 30 runs in triplicates for each. Results were analyzed using Malvern Panalytical software (version: 2.1.0.15).

7.2.2.3B Morphological Characterization of Intralipid® via Transmission Electron Microscopy (TEM):

The morphology of various Intralipid® samples was studied using transmission electron microscopy (TEM) following a negative staining procedure. A drop of the sample was placed on a 300-mesh, carbon-coated copper grid, the excess solution was removed using blotting paper, and the samples were stained with a drop of 1% phosphotungstic acid for 60 s. The stained samples were dried at ambient temperature and observed with TEM (JEM-1230, JEOL Ltd., Akishima, Tokyo, Japan) at an acceleration voltage of 120 kV.

7.2.3 Statistical Analysis:

Statistical comparisons were performed using GraphPad Prism software version 10.10.3 (GraphPad Software, San Diego, CA, USA). Paired t-tests were employed for comparisons between two groups, while one-way ANOVA was used for multiple groups. A

significance level of α = 0.05 was applied, and in all instances, p-values of less than 0.05 were considered indicative of statistical significance.

7.3 Results and Discussion:

7.3.1 Lymphatic Uptake via the In-vitro Model:

The chylomicron-drug association has proven to be an effective approach for investigating the intestinal lymphatic absorption of drugs (52, 282).Therefore, this *in-vitro* model was developed to replicate this *in-vivo* process. Since certain lipophilic drugs are taken up from the intestinal lumen into enterocytes and subsequently enclosed within chylomicrons (53), the developed model was designed to include a donor compartment, resembling the intestinal lumen, where the drug solution is placed. Additionally, there was a receiver compartment that contains an artificial chylomicron medium, simulating the environment within enterocytes. These two compartments were separated by an octanol-immersed membrane, which served as a representation of the lipophilic cell membrane found in enterocytes (**Figure 7.2**).

The results of the release of various drugs into the receiver compartment of the proposed intestinal lymphatic uptake model are shown in **Figure 7.3** and indicate significant differences (p = 0.0236) among the drugs in terms of lymphatic uptake. Halofantrine showed the highest uptake, with nearly all drugs detected in the artificial chylomicrons compartment after 2 h. Quercetin and cannabidiol showed moderate efficiency in passing through the side of the artificial chylomicrons, while rifampicin was the least available. The entrapment efficiency results suggested the uptake of the drugs into the Intralipid® particles, as none was detected outside.

The examined drugs were individually tested and suggested in previous studies to be lymphatically absorbed. Halofantrine has been extensively investigated for lymphatic transport, as its bioavailability was improved due to lymphatic voyage (467-469), and its superiority over other tested lymphotropics in the proportion traversing into the lymphatics is established (234, 281). Investigative reports on cannabidiol, quercetin, and rifampicin also documented the contribution of lymphatic uptake to their circulating plasma concentrations (277, 470-472).

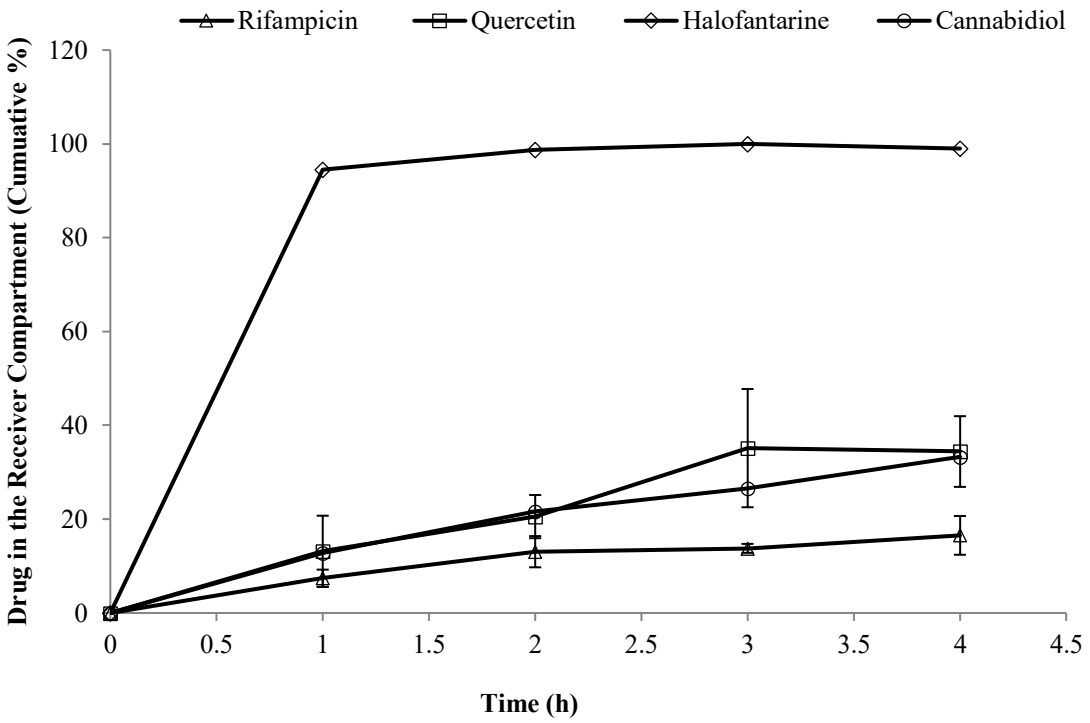

Figure 7.3. Cumulative percentage of tested drugs (cannabidiol, halofantrine, quercetin, and rifampicin) in the receiver compartment of the developed *in-vitro* lymphatic uptake model. Data represent mean ± standard error (SE) (n = 3 for all drugs and 2 for halofantrine). Results showed significant differences ($p < 0.05$) among the drugs regarding their lymphatic uptake.

Halofantrine is a lipophilic antimalarial that has prompted several reports underscoring the impact of lymphatic transport on its overall oral bioavailability. In a specific study utilizing lymph-cannulated rats, the administration of halofantrine in lipidic

vehicles resulted in 15.8% of the drug's journey occurring through the lymphatic system, while the total systemic exposure was documented to be 22.7% of the administered dose (469). A parallel experiment with halofantrine in a lipid-based formulation of long-chain triglycerides yielded values of 5.5% and 12.9% for direct systemic circulation transport and lymphatic transport, respectively. The total bioavailability documented in the study (19.1%) was mostly contributed to by the lymphatic voyage (473). Generally, the absorption of halofantrine from the gastrointestinal tract tends to be inconsistent, but the presence of food can remarkably boost its absorption (by 6–10 times) (474).

The pivotal factor contributing to the better and more consistent oral absorption of halofantrine with food lies in its transit through the intestinal lymphatic system. When halofantrine takes the lymphatic route instead of entering through the portal circulation, it evades the extensive liver metabolism it typically undergoes, aligning with the outcomes reported.

Dietary fats have been found to enhance the oral bioavailability and systemic exposure of quercetin, a potent antioxidant flavonol. This effect is attributed to the increased lymphatic transport of quercetin, which allows it to bypass the initial metabolism in the liver (475, 476). In experiments involving thoracic duct-cannulated rats that received intraduodenal doses of quercetin with soybean oil, the transport of quercetin through the lymphatic system was notably improved (470). Furthermore, other research has indicated that prior exposure to a high-fat diet enhances the effects when quercetin is administered. In a mesenteric-cannulated rat model receiving a dosage of 30 mg/kg of intraduodenal quercetin, the maximum concentration (C_{max}) of quercetin found in the lymph was approximately five times higher than that in the plasma (475).

The non-psychoactive compound cannabidiol has been a subject of research for its potential therapeutic effects in recent decades. The reported bioavailability of cannabidiol has been less than 10% (477, 478). However, cannabidiol is highly lipophilic and has been shown to undergo significant transport through the intestinal lymphatic system when taken orally with long-chain triglycerides (479). In experiments with Sprague-Dawley rats, it was found that co-administering cannabidiol with lipids, as opposed to using lipid-free formulations, increased its systemic exposure by a factor of three. The use of oils containing long-chain fatty acids that are packaged into chylomicrons served as the basis for developing the FDA-approved oral solution of cannabidiol known as Epidiolex®. This cannabidiol oil solution is recommended as an antiepileptic medication for the treatment of Dravet syndrome in children (480).

Rifampicin, a lipophilic bactericidal drug commonly used to treat active mycobacterial infections, faces several challenges, including poor and unpredictable bioavailability and a short biological half-life. These issues can result in subtherapeutic drug levels in the bloodstream and an increased risk of developing multidrug-resistant tuberculosis (MDR-TB) (481, 482). Incorporating rifampicin into lipid-based nano-formulations has been explored as a solution to enhance its oral bioavailability. These nano-formulations help protect the drug from degradation in acidic pH environments, and the lipid component primarily aids in improving absorption through the lymphatic system (483). Researchers have developed solid lipid nanoparticles (SLNs) and niosomes with the aim of enhancing the lymphatic uptake of rifampicin (230, 471).

When analyzing the *in-vivo* data of the tested drugs, direct comparisons and correlations with their *in-vitro* counterparts can pose challenges. The research landscape

reveals variations in drug concentrations, co-administered fats, animal models, and experimental setups for different drugs within the literature. Nevertheless, examining the highest reported fractions of intestinal lymphatic uptake for halofantrine, quercetin, and cannabidiol when co-administered with long-chain fatty acids or meals containing them, a notable pattern emerges. Their order of release in the *in-vitro* model aligns with their respective order *in-vivo*, with halofantrine showing a ten-fold increase in absorbed amount (474), quercetin demonstrating a five-fold increase in plasma concentration when factoring in lymphatic uptake (475), and a three-fold increase in systemic exposure for lipid-based CBD formulations (478). Although direct comparisons may not hold significant meaning, a discernible trend emerges for these three drugs. Conversely, rifampicin lacks sufficient data on intestinal lymphatic uptake with food or long-chain fatty acids, the criteria on which the aforementioned comparisons are based, preventing the establishment of a correlation.

Rifampicin ranked last when using molecular descriptors to correlate the order of the tested drugs with their expected *in-vivo* outcomes. The structures of the different molecules tested, along with their molecular descriptors, are depicted in **Table 7.2.** As reported earlier, the degree of the effect sequence was found to be as follows: hydrogen-binding acceptors (HBA) > polar surface area (PSA) > solubility in long-chain triglycerides (SLCT) > logP > melting point (MP) > logD > molar volume (MV) > density > pKa > molar weight (MW) > freely rotatable bonds (FRB) > hydrogen binding donors (HBD) (52). It has also been suggested that while HBA, PSA, HBD, MP, density, pKa, and FRB negatively affect drug association with chylomicrons, other descriptors increase it.

Table 7.2. Molecular descriptors of tested lymphotropic drugs.

Drug	MW	HBA	PSA	LogP	MP (°C)	Density (g/cm^3)	pKa	HBD	Structure
Rifampicin	822.9	15	220.15*	4.9	183	1.178**	1.7 7.9	6	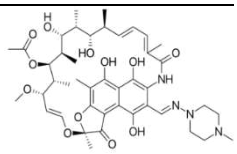
Cannabidiol	314.469*	2*	40.46*	6.3*	66–67#	1.04#	9.13*	2*	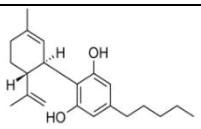
Quercetin	302.23	7	127.45*	1.48	316–318	1.8##	7.17 8.26 10.13 12.30 13.11	5	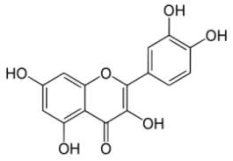
Halofantrine	500.4	5	23.5*	8.9	93–96 and 203–204 (for the hydrochloride salt) **	1.2***	10.05* 14.47	1	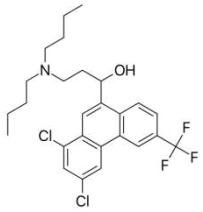

Abbreviations: molecular weight (MW), hydrogen-binding acceptors (HBA), polar surface area (PSA), melting point (MP), and hydrogen binding donors (HBD). Data was obtained from Pub-Chem, if certain data was not found there then DrugBank *, ChemBK **, ChemSpider databases ***. The following sources were also consulted: # https://www.drugfuture.com/chemdata/Cannabidiol.html (last accessed 12 September 2023). ## https://www.chemsrc.com/en/cas/117-39-5_947030.html (last accessed 12 September 2023).

Considering the drugs examined, it can be noted that rifampicin had the highest values for a higher number of factors that can adversely affect release, namely, hydrogen bond acceptors and polar surface area, in addition to molecular weight, molecular volume, and hydrogen bond donors. Although halofantrine did not have the greatest number of proposed factors that aid in drug association with chylomicrons, it had the highest logP

value, which is thought to enable it to penetrate the octanol-immersed membrane more easily than others, aiding in its penetration into the lipophilic core of the artificial chylomicron vesicles. Quercetin and cannabidiol were in between in terms of their release, and this can be justified by the values of their descriptors, which lie in-between rifampicin and halofantrine.

Given that rifampicin exhibited the slowest release, it was selected for further investigation to explore both inhibition and enhancement possibilities.

7.3.2 Inhibition of the Lymphatic Uptake in the In-vitro Model:

Pluronic® L-81 (PL-81) is a non-ionic surfactant consisting of 10% ethylene oxide (EO) and 90% propylene oxide (PO) copolymers arranged in a tri-block structure with the hydrophobic PO component located at the core of the two hydrophilic EO chains (334). PL-81 has been demonstrated as an *in-vivo* inhibitor of fat absorption and chylomicron secretion (254, 484). In the developed *in-vitro* model, when PL-81 was introduced to the receiver compartment medium, a decrease in lymphatic uptake of rifampicin was observed. Altering concentrations of PL-81 resulted in varying degrees of inhibition, with both 1% and 10% causing complete inhibition of release, as shown in **Figure 7.4**.

PL-81 has been proposed to act *in-vivo* to inhibit lymphotropic drug absorption by alternative mechanisms (339). It is thought that it might disturb the stability of the surface of the triglyceride particles, induce their aggregation, and thus prevent the formation of the chylomicron (348), or it might interfere with the transport of triglycerides from the cytosol to the endoplasmic reticulum and consequently inhibit the formation of the triglyceride-based lipoproteins (chylomicrons) (55). It has also been suggested that PL-81 may affect

chylomicron formation by changing the conformation of the associated protein (apolipoprotein) (348).

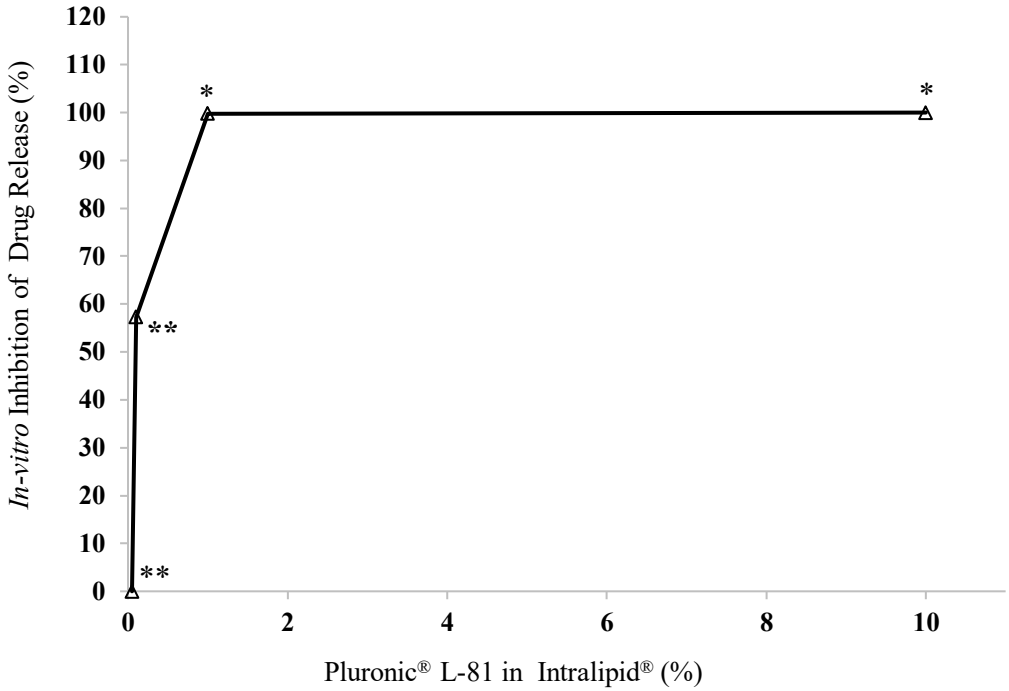

Figure 7.4. The effect of different percentages of Pluronic® L-81 added to Intralipid® on drug release inhibition in the *in-vitro* lymphatic uptake model. Higher concentrations (10% and 1%) were highly effective in imparting the inhibition (* $p < 0.05$). Lower concentration of the Pluronic® L-81 (0.1%) showed inhibition but did not reach statistical significance (** $p > 0.05$). No inhibition was seen with the 0.05% of Pluronic® L-81 as confirmed through statistical analysis (** $p > 0.05$)

The developed model suggested that the concentration of PL-81 plays a critical role in its effectiveness in blocking intestinal lymphatic uptake. In these two concentrations (10% and 1%), there was a statistically significant difference between the sample groups with the inhibitor and the ones without the inhibitor (* $p < 0.05$). While there was inhibition observed with 0.1% PL-81 (57.29 ± 6.25%), no inhibition was observed with 0.05% PL-81. The lack of statistical significance ($p > 0.05$) in both cases indicated that the inhibition observed may not be consistent or substantial enough to be considered significant in the two scenarios, respectively.

Based on the obtained data, there emerged a suggestion that PL-81 might employ an additional, previously undocumented mechanism. This mechanism involves encapsulating Intralipid® particles, thereby preventing the drug from entering the chylomicrons. Pluronic® L-81 is postulated to coat the Intralipid® droplets, as illustrated in **Figure 7.5**. The particle size results demonstrated that without PL-81, the Intralipid® droplets had discrete edges and smaller sizes. But with the addition of 1% and 10% Pluronic®, the particle size increased from 477.86 ± 5.19 nm to 646.9 ± 4.87 nm and 1615 ± 8.1 nm, respectively (p = 0.0424).

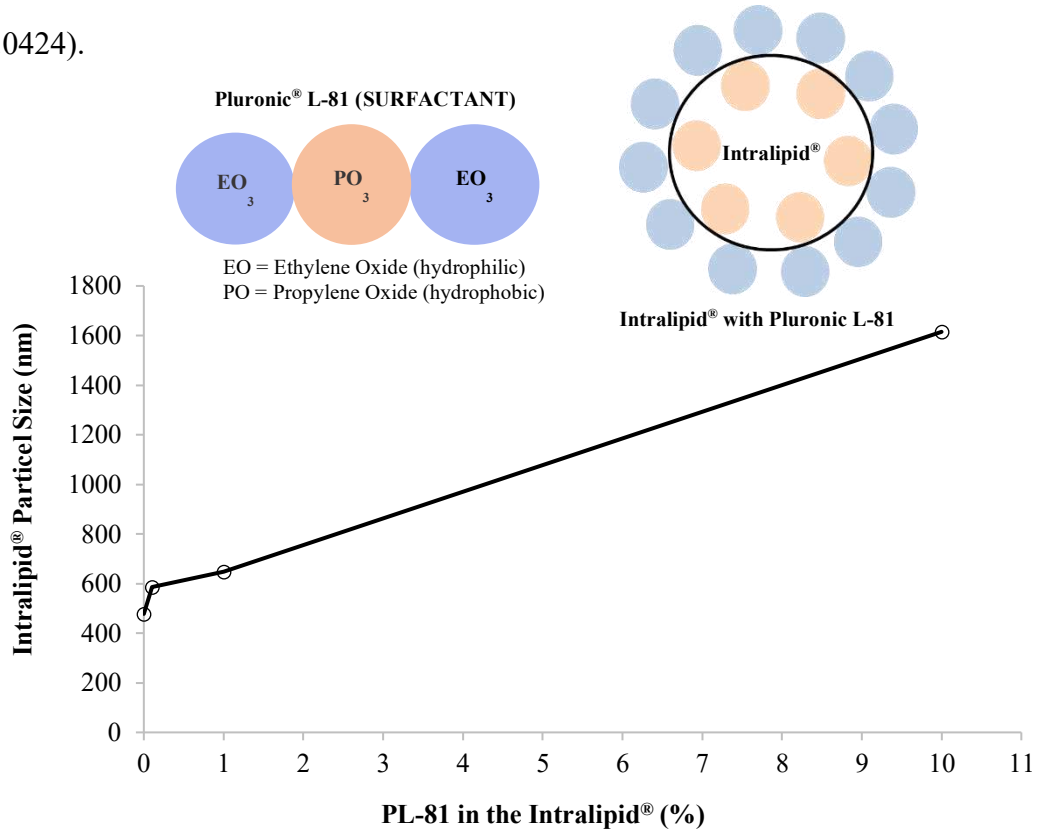

Figure 7.5. Change in the Intralipid® particle size with the varying percentages of Pluronic® L-81 ($p < 0.05$). As the percentage of Pluronic® L-81 increased, the particle size also increased. Specifically, the presence of 0%, 0.1%, 1%, and 10% Pluronic® L-81 within the Intralipid® yielded particle sizes of 477.86 ± 5.19 nm, 585.7 ± 5.06 nm, 646.9 ± 4.87 nm, and 1615 ± 8.1 nm, respectively (mean ± SE), n = 3. It was postulated that Pluronic® L-81 coats Intralipid® particles as shown in the illustration on top.

TEM images in **Figure 7.6** revealed that particles with PL-81 are larger and surrounded by a layer that makes their edges less apparent, with agglomerations of particles enveloped by the same layer also noted.

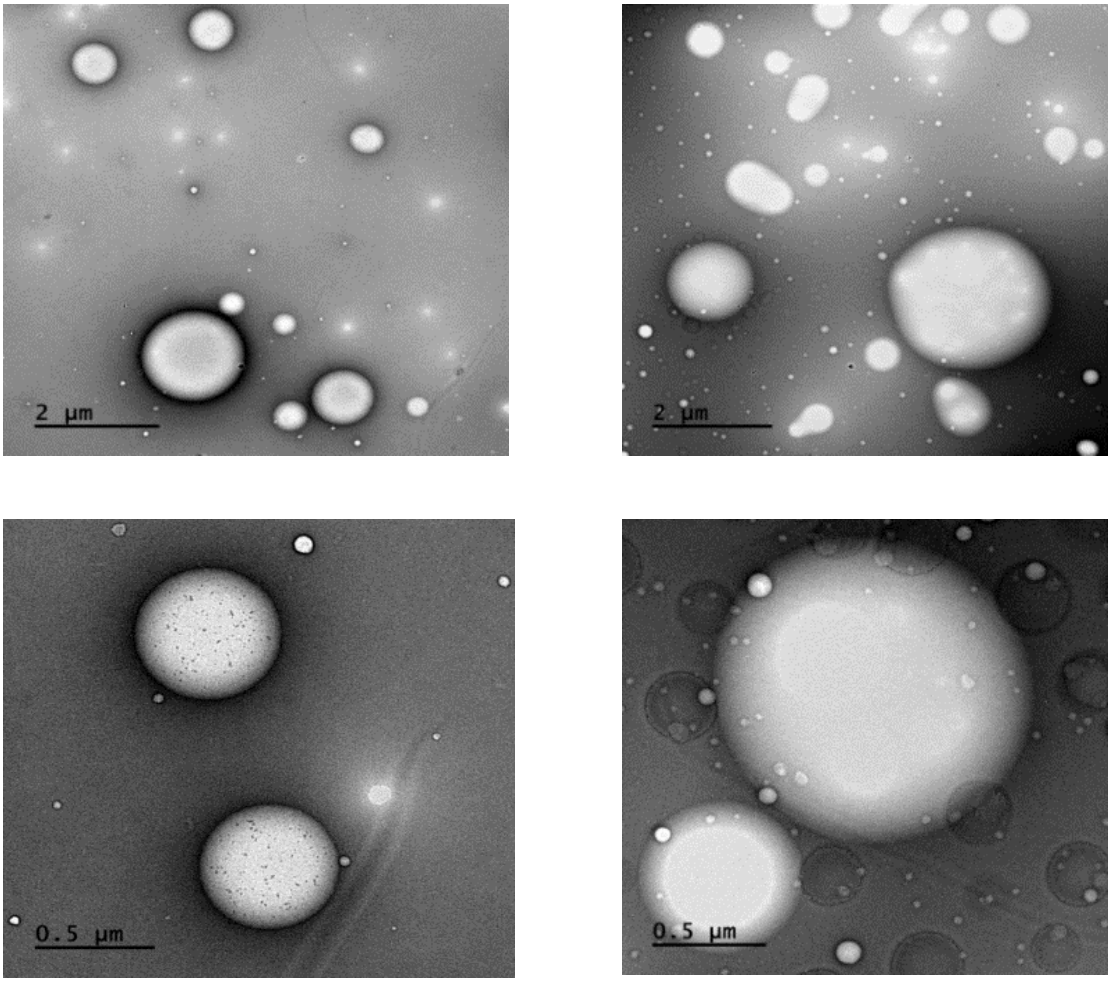

(a) **(b)**

Figure 7.6. TEM images of Intralipid® particles (a) and Intralipid® with 10% Pluronic® L-81 (b) at 10 K magnification power (top) and 40 K magnification power (bottom). The Intralipid® droplets when captured alone (a) had discrete edges and smaller sizes, while in the presence of Pluronic® L-81 (b), particles were larger and surrounded by a layer that made their edges less apparent. Agglomerations of particles enveloped by the same layer can also be noted in the presence of Pluronic® L-81.

7.3.3 Enhancement of the Lymphatic Uptake in the In-vitro Model:

It has been reported that food, especially a high-fat diet, may affect the intestinal lymphatic uptake of drugs (476, 485). The mechanism may involve the increased formation of chylomicrons following a high-fat intake, particularly those providing the appropriate fatty acids or triglycerides to produce chylomicrons (470, 486). The length of fatty acid chains has been determined to correlate with the efficiency of lymphatic drug transport, with longer fatty acids resulting in higher lymphatic uptake. This is attributed to the increased lipophilicity of longer fatty acids, which have a higher affinity to form chylomicrons (469).

Vegetable oils, being rich in triglycerides, have been shown to stimulate chylomicron formation and enhance the oral absorption of some lipophilic drugs suggested to be absorbed via the intestinal lymphatics. For example, a three-fold improvement in the bioavailability of a synthetic cannabinoid (PRS-211,220) was achieved by administering it in a peanut oil solution (487). Sesame oil was also documented to induce lymphatic transport of cannabidiol, resulting in a 250-fold increase in its plasma concentration and a 2.8-fold increase in systemic exposure (478, 479).

When peanut oil was added to the Intralipid® in the receiver compartment, the lymphatic uptake of the tested drug (rifampicin) through this model revealed a considerable improvement ($p = 0.0276$) as seen in **Figure 7.7**. Peanut oil was chosen for two main reasons: it is well-documented to facilitate intestinal lymphatic uptake, and it is composed of a variety of long-chain fatty acids (as seen in **Figure 7.8**) that resemble those found in soybean oil, which help form the artificial chylomicrons (Intralipid®) (66, 273). Soybean

oil contains five main fatty acids, including palmitic acid (10%), stearic acid (4%), oleic acid (18%), linoleic acid (55%), and linolenic acid (13%) (488). The fatty acids with the highest percentages are similar in both peanut and soybean oils, which are linoleic and oleic acids (489).

With the addition of oil, rifampicin was emulsified into the oil droplets of the Intralipid®, creating a rifampicin-carrier area in the receiver compartment, which eventually led to higher rifampicin movement into the receiver compartment.

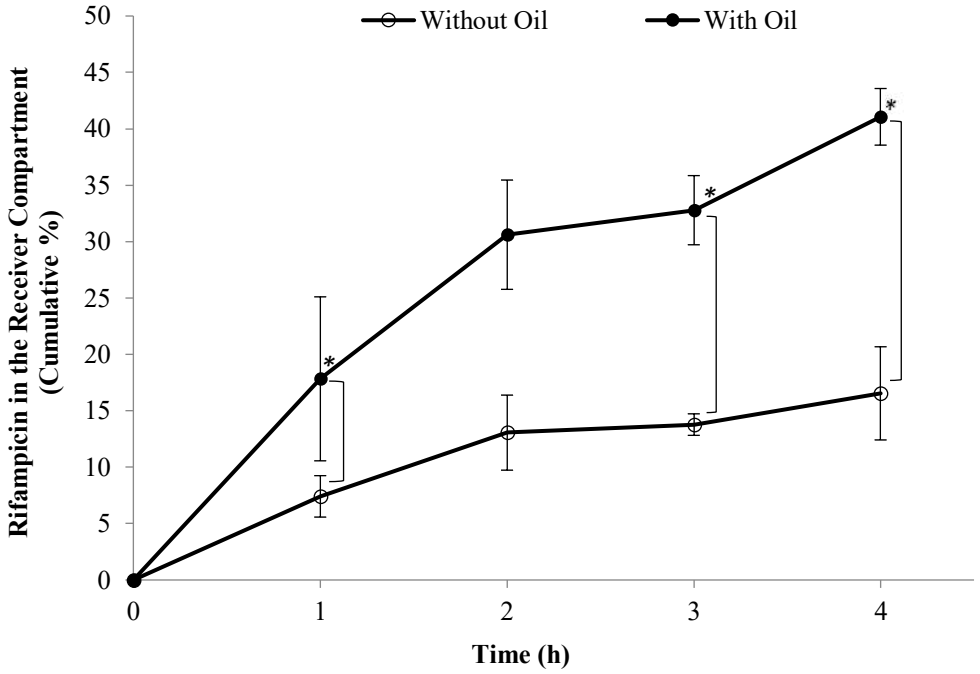

Figure 7.7. Demonstration of the increased *in-vitro* lymphatic uptake of rifampicin via the developed model when peanut oil (2%) was added to Intralipid® ($p < 0.05$). Data represent mean ± SE ($n = 3$). Data at 1, 3 and 4 h demonstrated statistical significance (* $p < 0.05$) between the samples with and without the oil.

Figure 7.9 shows the difference in droplet contrast at both magnification powers; with the added oil, the center of the droplets appears clearer and shinier, indicating that the

oil was emulsified into the center of the Intralipid® droplets. In contrast, without added oil, the centers of the droplets appear rather dull.

While it is important to acknowledge that lipid digestion and incorporation into chylomicrons for absorption are more intricate processes *in-vivo*, as discussed earlier, this approach can still serve as a useful tool for examination. The inclusion of lipolysis would enhance this model and provide a more comprehensive understanding of the effects of oils *in-vitro*.

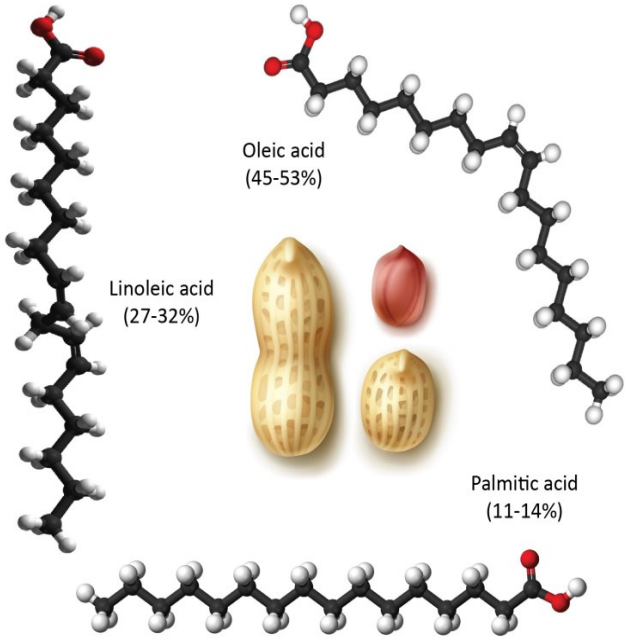

Figure 7.8. Illustration of the main fatty acids in peanut oil. This oil also contains other long-chain saturated fatty acids in small percentages such as arachidic acid (1–2%), behenic acid (1.5–4.5%), and lignoceric acid (0.5–2.5%).

The *in-vitro* model developed in this study, is utilizing a commercial product (Intralipid®), has the potential to become an invaluable tool for pharmaceutical researchers. It offers a means to investigate lymphatic drug transport—a field where conducting *in-vivo* studies in preclinical animal models or clinical trials is challenging.

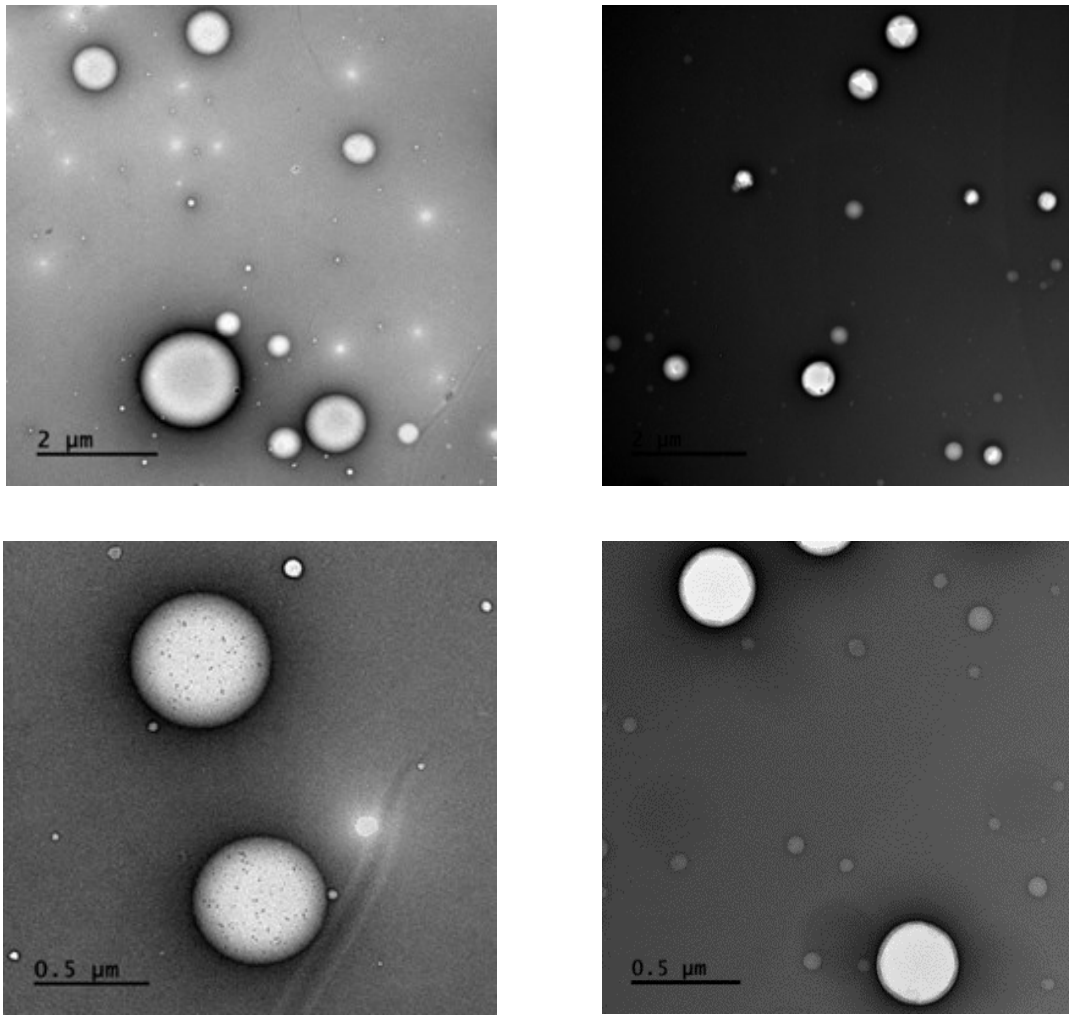

(**a**) (**b**)

Figure 7.9. TEM images showing Intralipid® particles (a) and Intralipid® with 2% peanut oil (b) at 10 K magnification power (top) and 40 K magnification power (bottom). With the incorporation of oil, the centers of the Intralipid® droplets exhibit a distinct clarity and shine, indicating emulsification of the oil into the droplet cores. Conversely, in the absence of added oil, the centers of the droplets appear dull.

This model represents the initial step towards creating a physiologically based predictive tool, which could be further refined to yield more accurate estimations of drug interaction with chylomicrons and subsequent lymphatic transport. Notably, the current *in-*

vitro model does not include a compartment for drug metabolism. This omission warrants discussion, and there is an opportunity to potentially adapt the model by incorporating elements like microsomes to better mirror *in-vivo* conditions. Another adaptation could also encompass lipolysis, which could account for the major intricacies of the lipid gastrointestinal pathway.

7.4. Conclusion:

The developed *in-vitro* model appears to be a valuable tool for investigating and predicting lymphatic drug uptake via chylomicrons and assessing the impact of various excipients on this process. The tested drugs demonstrated different degrees of lymphotropic affinity, which highlights the importance of considering this pathway when designing drug delivery systems. The use of the lymphatic uptake inhibitor Pluronic® L-81 demonstrated its potential to inhibit drug uptake via the lymphatic system by coating the Intralipid® particles, a finding not previously reported. The addition of peanut oil to the Intralipid® in the receiver compartment demonstrated an improvement in lymphatic uptake, suggesting that the model can be utilized to explore the impact of solubility enhancers, novel formulations, and food effects, particularly fat-containing meals that may stimulate lymphatic uptake. Future studies may include exploring the effect of other excipients and formulations on lymphatic uptake as well as investigating the impact of food on lymphatic drug absorption. The model can also be utilized to screen potential lymphatic targeting agents and assess their effectiveness in improving lymphatic drug uptake. In summary, this *in-vitro* model provides a promising platform for evaluating the lymphatic uptake of drugs and their potential for targeted drug delivery.

CHAPTER EIGHT

In-Vitro Predictive Model for Intestinal Lymphatic Uptake: Exploration of Additional Enhancers and Inhibitors

A version of this chapter is published in:

Pharmaceutics. 2024;16(6):768. DOI: 10.3390/pharmaceutics16060768

Reprinted from Reference (62).

8.1 Introduction:

Intestinal lymphatic drug transport has garnered attention in recent times owing to the many potential benefits it presents for drug delivery (53, 54). Following absorption, some drugs pass across the intestinal enterocytes, and during that transit, these drugs associate with the excretory enterocyte lipoproteins, chylomicrons (234). This process underscores the potential and significance of exploiting intestinal lymphatic transport for drug delivery purposes.

Chylomicrons are spherical particles that are composed mainly of triglycerides (85–90%) in addition to phospholipids (7–9%), cholesterol and cholesteryl esters (3–5 and 1–3%, respectively), and apolipoproteins (1–2%) (490). They principally play a role in absorbing and facilitating the systemic distribution of dietary fats and lipophilic vitamins (56). Following digestion, when dietary triglycerides transform into free fatty acids and monoglycerides, a subsequent process of re-esterification occurs inside enterocytes**.** During this phase, the resulting triglycerides are encapsulated within chylomicrons, which serve as transportation carriers into the bloodstream through the lymphatic network (53, 177).

In the context of pharmaceutical applications, specifically lymphatic targeting -or lymphotropic- drugs, these enterocyte-formed chylomicrons offer a unique avenue. By hitchhiking on these carriers, candidate molecules gain entry into the circulation. Using chylomicrons as an approach holds the promise of evading the initial hepatic metabolism, commonly known as the first-pass effect, thereby elevating their bioavailability (51, 56, 254). Alternatively, these drugs could accumulate within the lymphatic system, reaching increased concentrations at lymph node target sites. This concentration enhancement may

translate into a more potent therapeutic impact with reduced off-target toxicity. This aspect is particularly important for compounds with immunomodulatory or anticancer properties, where maximizing their effect within the lymphatic system proves crucial (51, 56).

In a previous study, we presented an *in-vitro* model crafted to predict, inhibit, and enhance lymphatic uptake. Its foundation lies in the interaction of drugs with chylomicrons, a process documented for its predictive abilities of intestinal lymphatic uptake (282, 350). This model consisted of two compartments: a donor compartment containing the drug solution under investigation, and a receiver compartment filled with artificial chylomicron media (Intralipid®) (350). These artificial chylomicrons serve as carriers for the drug molecules and mimic the behavior of naturally occurring chylomicrons in the body. To simulate the *in-vivo* chylomicron blocking effect and suppress drug release in the *in-vitro* setting, Pluronic® L-81 (PL-81) was utilized. This chylomicron-blocking agent, proven effective in both *in-vivo* and CaCo2 cell culture models, demonstrated an inhibitory effect within the *in-vitro* model (334, 336, 348). Moreover, to enhance drug release into the receiver compartment and mimic the lymphatic enhancement, peanut oil was used. This choice stemmed from being the source of the artificial chylomicrons used in the model and was guided by its potential to function as a carrier, facilitating increased drug entry into the receiver compartment (264, 350).

In this study, the aim was to investigate other agents that would enhance or inhibit intestinal lymphatic uptake through the chylomicron pathway. Rifampicin served as the model drug in this study, consistent with the earlier investigation. Additionally, quercetin was used as a second drug to provide further confirmation in some experiments. Additional oils were explored to investigate their impact on enhancing intestinal lymphatic uptake.

Olive, sesame, and coconut oils were chosen for use due to their varying percentages and chain lengths of different fatty acids, which are recognized for their impact on *in-vivo* lymphatic uptake (277, 490). In order to deliver drugs through intestinal lymphatics, various formulation excipients and drug delivery systems have been and are being developed (51, 54). One example of the excipients used is Labrafil®. It consists of mono-di- and triglycerides and PEG6 (MW 300) mono- and diesters of linoleic (C18:2) acid. It is a non-ionic water-dispersible surfactant for lipid-based formulations to solubilize and increase the oral bioavailability of poorly water-soluble APIs (491). A novel formulation of cannflavins was examined in this model system with Labrafil® M 2125 CS being the enhancer. Moreover, the study delved into the impact of zeta potential on either enhancing or inhibiting intestinal lymphatic uptake. For that, racemic chloroquine ($C_{18}H_{26}ClN_3$), and sodium lauryl sulfate ($C_{12}H_{25}NaO_4S$) were utilized. Chloroquine is an antimalarial drug that has been shown to reduce plasma levels of triglycerides and cholesterol (492). At physiological pH, chloroquine carries a positive charge. The hypothesis was to investigate whether this positive charge could influence its interaction with chylomicrons, consequently reducing triglyceride levels and potentially drugs transported through chylomicrons. To further confirm the impact of this charge interaction, sodium lauryl sulfate, an anionic surfactant widely used in pharmaceutical formulations (493), was employed due to its negative charge, which contrasts with that of chloroquine. Both of these substances showed their capability of influencing the zeta potential of artificial chylomicron particles in preliminary experiments. Using the previously developed *in-vitro* model, the study investigated how the addition of these agents to the artificial chylomicron compartment could affect the uptake of model drugs into this compartment.

8.2 Materials and Methods:

8.2.1 Materials:

Rifampicin (≤ 100%, CAS: 557303) was procured from EMD Millipore Corp, Burlington, MA USA; while quercetin (≥ 95%, CAS: 117-39-5); 1-octanol (99%, CAS: 111-87-5); and chloroquine as diphosphate salt (98.5-101.0%, CAS:5 0-63-5) were sourced from Sigma –Aldrich Co. (Saint Louis, MO, USA). Intralipid® (20%) was from Fresenius Kabi (Toronto, ON, Canada). Peanut, olive and sesame oil products were acquired from a local Edmonton grocery, while coconut oil (CAS: 8001-31-8) was from Medisca (Saint-Laurent, Qc, Canada) and sodium lauryl sulphate (≤ 100%, CAS: 151-21-3) was obtained from Caledon Laboratories (Toronto, ON, Canada). Labrafil® M 2125 CS was obtained from Gattefosse (Toronto, ON, Canada) while cannflavin (≥ 98%, CAS: 76735-57-4) was from Cayman Chemical (Michigan, USA).Additionally, synthetic hydrophobic Polyvinylidene Fluoride (PVDF) membranes were from Millipore affiliated with Merck KGaA, Darmstadt, Germany. For HPLC analysis, methanol (99.9%, CAS: 67-56-1), and acetic acid (≥ 99.7%, CAS: 64-19-7) were of HPLC grade and were obtained from Fisher Scientific (Ottawa, ON, Canada); all other reagents were of analytical grade.

8.2.2 Methods:

8.2.2.1 Franz Cell for Studying Intestinal Lymphatic Uptake:

The receiver compartment of the Franz cell was filled with either Intralipid® (20%) alone or Intralipid® mixed with a potential enhancer or inhibitor, totalling 12 mL. Olive, sesame, peanut, and coconut oils were added at a 2% concentration into the Intralipid® in

the receiver compartment to explore their potential as enhancers for uptake in the model. Additionally, 5% (+/-) chloroquine, 2%, 1%, and 0.5% sodium lauryl sulfate were introduced into the receiver compartment containing Intralipid® to investigate the impact on zeta potential. The experimental setup was maintained at a temperature of 37.0 ± 0.5 °C, and magnetic stirring at 600 rpm was employed for fluid agitation. A hydrophobic PVDF membrane, with a pore size of 0.22 μm and impregnated with n-octanol, was positioned between the compartments. Within the donor compartment, 2 mL solutions (1 mg/mL) of the model drugs, rifampicin, quercetin, in methanol and dimethyl sulfoxide, respectively- were introduced. The receiver compartment in various experiments contained either Intralipid® or a mixture of Intralipid® with an enhancer or an inhibitor at specific percentages. Sampling was conducted at various time intervals (0 - 4 hours), involving the withdrawal of 0.2 mL samples. A similar procedure was followed with cannflavin A being in the donor compartment and Labrafil® M 2125 CS added to the Intralipid® in the receiver compartment to investigate the effect of adding Labrafil® to the cannflavin formulation. Samples taken from the receiver compartment were subsequently extracted and subjected to analysis for drug content through Shimadzu HPLC (LC-10AD, Shimadzu Corporation, Kyoto, Japan) equipped with SIL-10A (Shimadzu Auto Injector) and UV-VIS detector (SPD-10AV). Analysis was done via Kinetex™ C18 column (250 mm × 4.6 mm i.d. - 5 μm) from Phenomenex (California, USA) (350). The column temperature was maintained at 25 °C, and specific analysis conditions for all the drugs are in **Table 8.1**. The resulting peak areas were integrated using LabSolutions software (Shimadzu Corporation, Kyoto, Japan). Cannflavin A was detected using the method developed by O'Croinin *et al.* (494). This methodology utilizes electrospray ionization liquid chromatography-mass spectrometry

(LC-MS) analysis to separate and quantify cannflavins using an efficient isocratic elution. The LC-MS system consists of a Phenomenex Luna® 3 µm C18 (2) 100 Å 150 × 4.6 mm (Torrance, CA, USA) column for separation and a single quadrupole mass spectrometry apparatus (Shimadzu, Kyoto, Japan) for quantification of cannflavin A in positive single ion monitoring mode.

Table 8.1. HPLC Analysis conditions for the model lymphotropic drug.

Model Drug	Mobile Phase	Flow rate (mL/min)	Detection Wavelength (nm)
Rifampicin	Methanol, Acetate Buffer (pH=5.8) (60:40)	1.2	254
Quercetin	Methanol, Acetate Buffer (pH=5.8) (60:40)	1.2	257, 370

8.2.2.2 Measurement of the Zeta Potential of Intralipid®:

The zeta potential measurements of both Intralipid® and the Intralipid® mixtures with different agents, specifically (+/-) chloroquine at 10%, 5%, 2.5%, 1.25%, and 0.125% in addition to sodium lauryl sulfate at 2%,1% and 0.5%- were conducted using dynamic light scattering, employing the Malvern Ultra Zeta Sizer (Malvern, United Kingdom). This analysis was conducted at a temperature of 25 °C, using polystyrene latex cells (DTS0012) in triplicates for each sample. The obtained results were analyzed using Malvern Panalytical software (version: 2.1.0.15).

8.2.2.3 Statistical Analysis:

Statistical analysis was conducted using GraphPad Prism software version 10.10.3 (GraphPad Software, San Diego, CA, USA). For comparisons between two groups, paired t-tests were performed or one tailed p-values were determined. A significance level of $\alpha = 0.05$ was applied, and in all cases, p-values less than 0.05 were considered indicative of statistical significance.

8.3 Results and Discussion:

8.3.1. Effect of different oils in augmenting the in-vitro intestinal lymphatic uptake:

Chylomicrons, being lipoproteins rich in triglycerides- primarily derive their triglycerides from dietary sources (254). This emphasizes the significance of diet and lipid-based prodrugs and formulations in promoting the production of chylomicrons (495). Consequently, it would promote the uptake of drugs delivered via such formulations and delivery systems into the intestinal lymphatic system through the chylomicron pathway, ultimately enhancing the bioavailability of potential therapeutic agents (184, 496, 497).

In the quest for these effects, the utilization of oils containing long-chain fatty acids emerged as a prominent strategy. Long-chain triglycerides are primary constituents of chylomicrons (254, 333), therefore, oils rich in long-chain fatty acids, such as sesame oil, olive oil, and peanut oil are frequently employed (277, 469, 498). Typically, long-chain triglycerides undergo re-esterification and become part of chylomicrons, allowing them to enter the lymphatic system. In contrast, medium-chain triglycerides are known to be transported mainly via the portal pathway (498, 499). Few studies have reported that

medium-chain triglycerides appear in human chylomicrons after their oral administration (277, 500). In this study, coconut oil was incorporated, distinguished by its high proportion of medium-chain triglycerides fatty acids (501), to enhance the breadth of comparison with other oils. All other oils are abundant in long-chain fatty acids, recognized for their lymphatic transportation properties. In the assessment of the potential of various oils to enhance intestinal lymphatic uptake as depicted in **Figure 8.1**, distinct patterns of uptake emerged. Coconut oil showcased the most prominent early-stage release effect. Olive oil initially exhibited a lesser magnitude of uptake enhancement than coconut oil, yet towards the later stages of evaluation, it had a similar enhancing effect resulting in a 3.5-fold increase in uptake. Moreover, sesame oil initially exhibited a similar enhancement pattern to that of olive oil. However, its release profile eventually matched that of peanut oil, which demonstrated the least pronounced impact. As previously reported, the addition of peanut oil to Intralipid® resulted in a 1.5-fold increase in lymphatic uptake of rifampicin in the *in-vitro* model (350).

The fatty acid composition of the diverse oils used in this work is detailed in **Table 8.2**. Coconut oil distinguishes itself with an abundance of saturated medium-chain fatty acids, setting it apart from other used oils that are predominantly composed of long-chain fatty acids (49, 501). This specific characteristic renders it the least likely, if at all, to impact lymphatic uptake *in-vivo* (502, 503). However, it also corresponds with the performance of coconut oil when compared to its counterparts *in-vitro*. Its superiority in enhancing the uptake in the *in-vitro* model can be traced to its elevated content of medium-chain fatty acids, which exhibit heightened water solubility in comparison with the other oils (501, 504). This increased water solubility is thought to facilitate the integration of the

oil within the aqueous external phase of Intralipid®. Therefore, coconut oil served as a favorable vehicle for the drug, facilitating its capture within the artificial chylomicron particles within the receiver compartment of the used model.

Table 8.2. Fatty acids composition of the oils investigated to enhance the lymphatic uptake of rifampicin in the developed model.

Fatty Acid	**Length:Saturation**	**% of fatty acid in different oils**			
		Coconut Oil (501)	**Olive Oil (505)**	**Sesame Oil (506)**	**Peanut Oil (507)**
Capric Acid	C8:0	7	-	-	-
Caprylic Acid	C10:0	8	-	-	-
Lauric Acid	C12:0	49	-	-	-
Myristic Acid	C14:0	8	-	-	-
Palmitic Acid	C16:0	8	7.5-20	11-16	11-14
Stearic Acid	C18:0	2	0.5-5	11-16	-
Oleic Acid	C18:1	6	55-83	35-46	45-53
Linoleic Acid	C18:2	2	3.5-21	40-48	27-32
Linolenic Acid	C18:3	-	-	0.5	-
Arachidic Acid	C20:0	-	-	-	1-2
Behenic Acid	C22:0	-	-	-	1.5-4.5

While medium-chain triglycerides are not the primary choice for facilitating intestinal lymphatic transport; however, they do play a significant role in minimizing fluctuations in drug absorption through the lymphatic route (508). When included in lipid formulations designed to promote enhanced intestinal lymphatic uptake, medium-chain triglycerides -when combined with natural oils containing long-chain triglycerides- have demonstrated the ability to improve drug emulsification and micellar solubilization of the tested lipid-based formulation (49). This, in turn, resulted in a more consistent drug concentration within the lymphatic system. Nevertheless, it is worth mentioning that while

the addition of medium-chain triglycerides reduced variability (509), formulations with only natural oil vehicles containing long-chain fatty acids still outperformed in terms of both lymphatic transport and systemic *in-vivo* bioavailability (508, 509).

The effects of the remaining oils, namely olive oil, sesame oil, and peanut oil, aligned with their *in-vivo* behavior in enhancing lymphatic uptake. These oils share a high content of long-chain fatty acids (495-497), including stearic acid (C18:0), oleic acid (C18:1), linoleic acid (C18:2), and palmitic acid (C16:0), which are major fatty acids found in chylomicrons at varying proportions (498). Yet, the degree and type of unsaturation within these fatty acids arise as factors determining their effectiveness in enhancing intestinal uptake. The existing literature emphasizes that vegetable oils containing higher levels of oleic acid and linoleic acid tend to have a more favorable impact on promoting intestinal lymphatic absorption (358, 510). Olive oil and sesame oil, in particular, are abundant in these unsaturated C18 fatty acids (505, 506) and have been documented to enhance both intestinal lymphatic and systemic transport more effectively than other vegetable oils (277).

Similar to what has been reported previously, the resultant findings from this study demonstrated that olive oil performed better than sesame oil in facilitating the transportation of drugs into the receiver compartment. However, it is essential to acknowledge that sesame oil can display variable performance due to its susceptibility to oxidation, a significant concern for oils, especially those rich in linoleic acid (511). Sesame oil, in comparison to olive oil, contains a higher proportion of linoleic acid (**Table 8.2**). Consequently, the observed differences in performance between sesame oil and olive oil may be attributed to the decline in linoleic acid levels caused by potential oxidation

mechanisms. Similarly, peanut oil aligned with its previously reported *in-vivo* performance, which identified it as the least effective in enhancing lymphatic transport among oils containing long-chain triglycerides (277). The reported results may be attributed to the specific composition of this oil, as it contains the lowest percentage of fatty acids known to enhance chylomicron lymphatic transport (507).

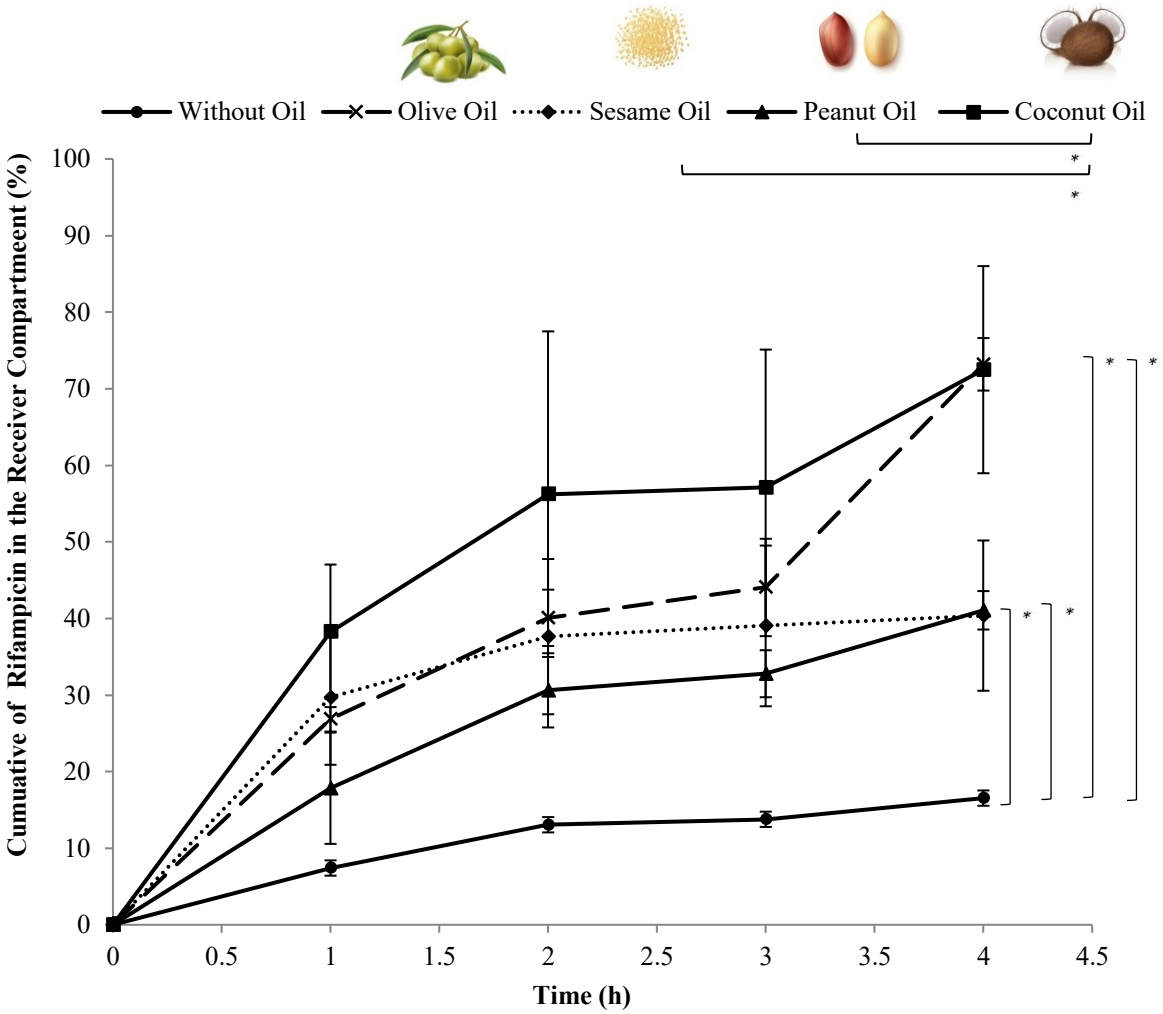

Figure 8.1. Demonstration of the increased *in-vitro* lymphatic uptake of rifampicin via the developed model when 2% of different oils were added to Intralipid®. Data represent mean ± SE (n = 3). * Indicates the statistical significance ($p < 0.05$) between the different groups.

As explained in our previous study (350), incorporating lipolysis or another digestion model into the developed model could address the complexities of the gastrointestinal journey for various fatty acids and co-administered drugs (277, 512). Such an approach would help estimate the implications of the different digestion processes on the absorption of co-administered drugs and coupled with this model may offer additional insight into their potential lymphatic uptake when applicable.

Various lipid-based formulation excipients and drug delivery systems have been and continue to be developed to deliver drugs through intestinal lymphatics (51, 54, 184). To assess the suitability of our *in-vitro* model for formulation development, we examined the uptake of cannflavin A with and without Labrafil®. The results presented in **Figure 8.2** demonstrate the efficacy of the model in studying the impact of formulation excipients on intestinal lymphatic uptake, with Labrafil® enhancing cannflavin uptake.

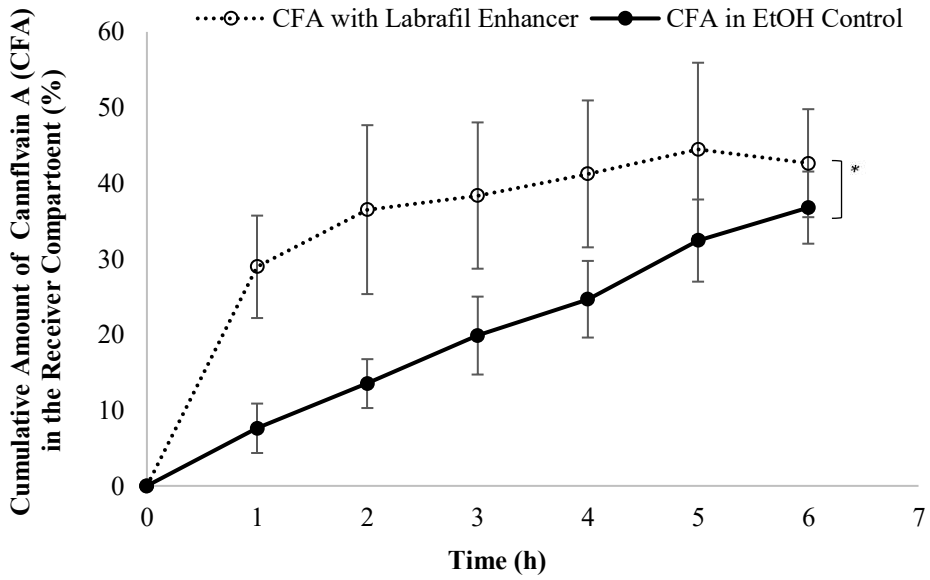

Figure 8.2. Demonstration of the increased *in-vitro* lymphatic uptake of cannflavin A (CFA) via the developed model when Labrafil® 2125 CS (uptake enhancer) was added to Intralipid®. Data represent mean ± SD (n = 6). * Indicates the statistical significance ($p < 0.05$) between the different groups.

8.3.2 Effect of changing the zeta potential of artificial chylomicrons on the lymphatic uptake:

(+/-) Chloroquine is a drug that is primarily employed for malaria prevention and treatment (513). This compound possesses dibasic characteristics, featuring two basic groups corresponding to the nitrogen in the quinoline ring and the diethylamino side-chain nitrogen. These groups possess ionization constants of 8.1 and 10.2, respectively (514). At physiological pH levels around 7.4, (+/-) chloroquine predominantly undergoes ionization in its mono-protonated form, while in lower pH regions of the body, it can transition into its di-protonated state (**Figure 8.3**) (492).

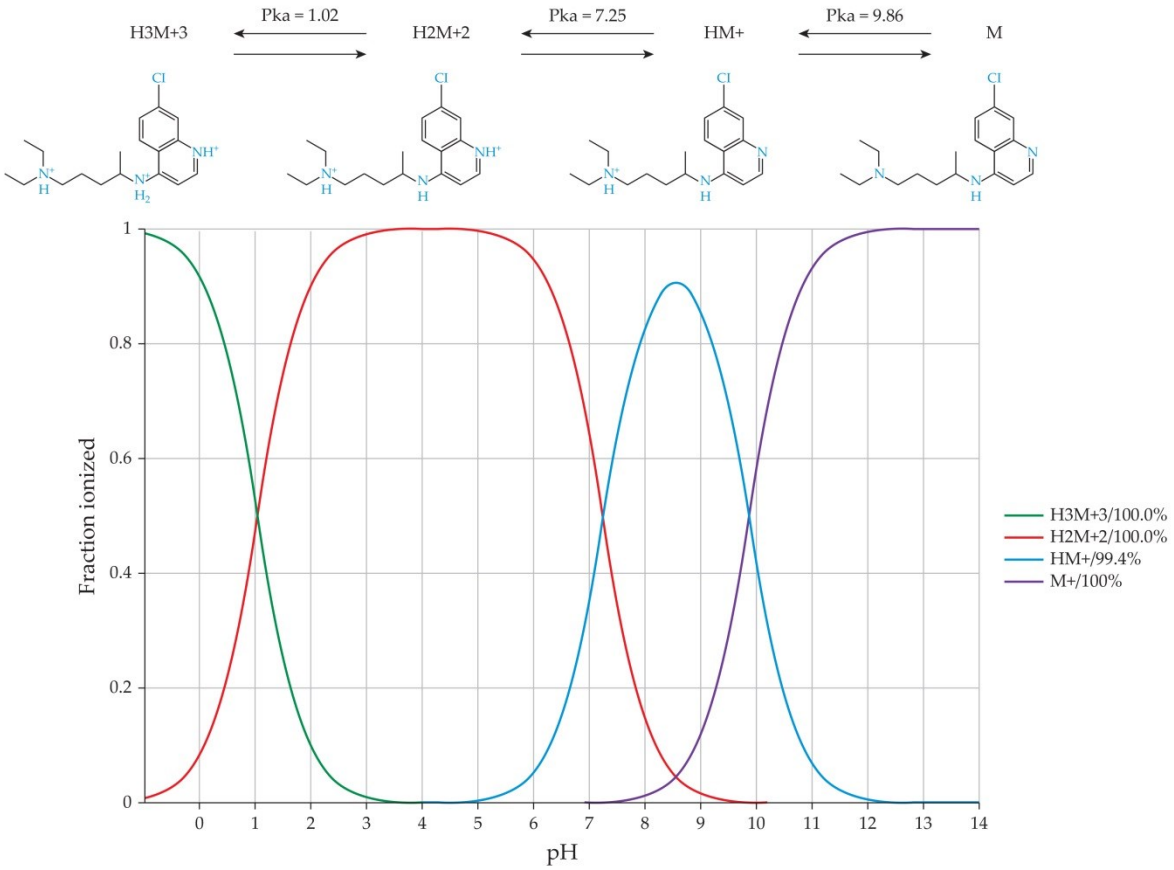

Figure 8.3. Microspecies of chloroquine at different pHs (0-14) showing the ionization behaviour of chloroquine throughout this range of pH values.

As illustrated in **Figure 8.4**, the introduction of 5% (+/-) chloroquine into the Intralipid® within the receiver compartment led to reduction in drug release for both rifampicin and quercetin. Specifically, when (+/-) chloroquine was added, only a mere 0.4% of the release achieved with (+/-) chloroquine was observed for rifampicin. Similarly, with quercetin, the presence of (+/-) chloroquine resulted in approximately 1% of the release that was documented in its absence.

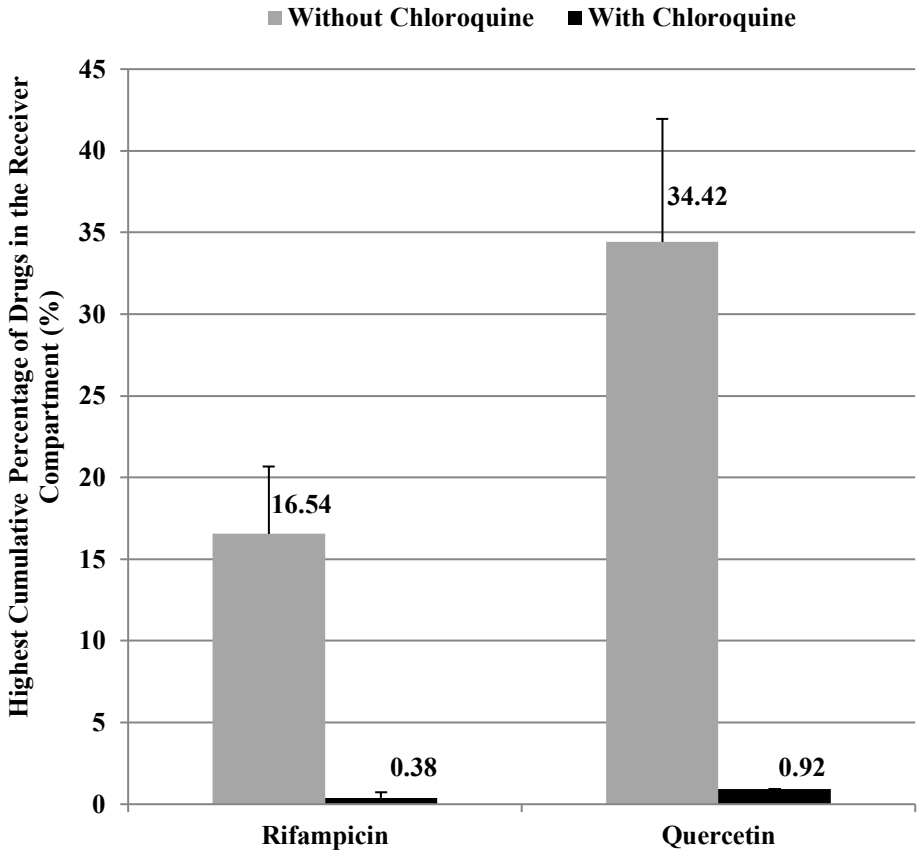

Figure 8.4. Illustration of the differences in the percentage of the *in-vitro* lymphatic uptake of the model drugs; rifampicin (16.54 ± 4.13) and quercetin (34.42 ± 7.53) via the developed model when 5% (+/-) chloroquine was added to the Intralipid® in the receiver compartment of the model. Upon doing that the uptake decreased to (0.38 ± 0.35, $p < 0.05$) and (0.92 ± 0.01, $p < 0.05$) for rifampicin and quercetin, respectively.

This inhibition mechanism is assumed to arise from the positively charged nature of (+/-) chloroquine within the donor compartment. This positive charge might have prompted an interaction with the negatively charged Intralipid® particles, thus impeding the entry of the tested drugs into the artificial chylomicron particles. To validate this hypothesis, zeta potential measurements were conducted for Intralipid® both with and without the addition of (+/-) chloroquine. From **Figure 8.5,** it was evident that as the percentage of (+/-) chloroquine increases, a corresponding rise in the neutralization of the negative charge on Intralipid® occurs. This trend resulted in a reduction of the zeta potential on the Intralipid® particles.

In our previous publication, it was demonstrated how the PL-81 coating encapsulated the Intralipid® particles, thus hindering drug penetration (350). This confirmation was supported by microscopic images, thus it was raised that there might be another biophysical mechanism for PL-81 chylomicron blockage. In this context, the primary objectives are two-fold: first, to determine if the inhibition mechanism of chloroquine relies solely on the presence of the coating, and second, to investigate the potential involvement of zeta potential in this process.

To address the second part, an alternative agent was introduced with the aim of elevating the zeta potential of Intralipid® particles. This part of the experiment was to investigate whether enhancing the zeta potential would translate to an increased *in-vitro* lymphatic drug uptake or not. Thus, sodium lauryl sulphate (SLS) was used to increase the zeta potential to see if that would increase the lymphatic uptake via the used model.

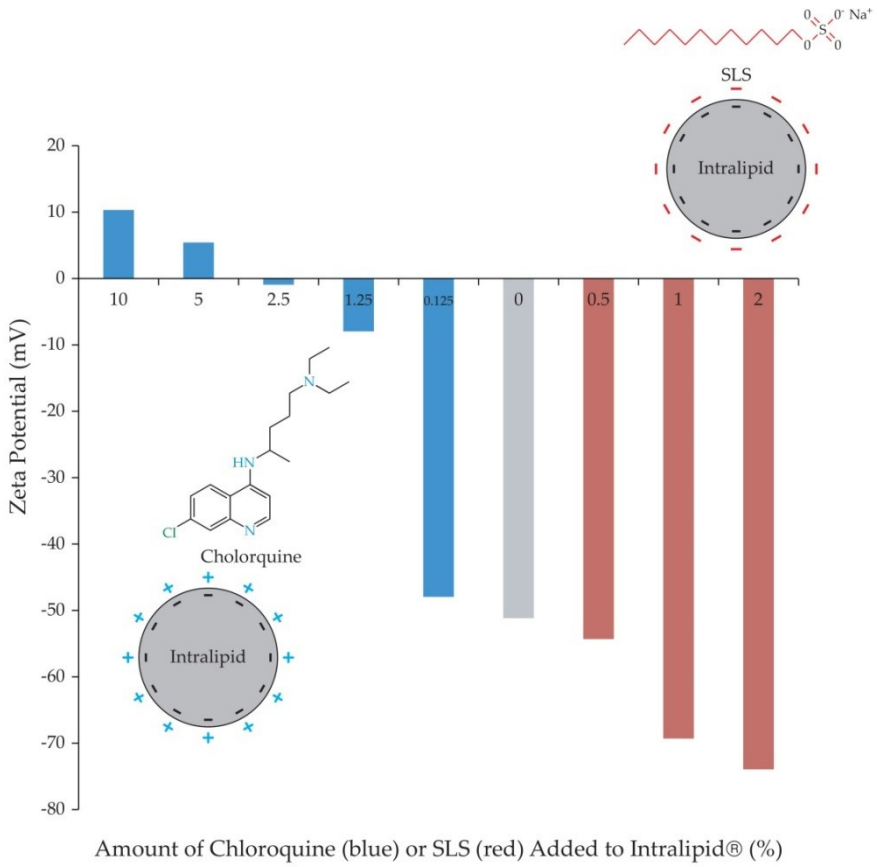

Figure 8.5. Change in the Intralipid® zeta potential with the varying percentages of chloroquine (blue) and sodium lauryl sulphate (SLS, red) expressed as an average of triplicates. The zeta potential of Intralipid® alone is grey.

Sodium lauryl sulfate (SLS) is an alkaline, anionic surfactant with versatile applications. Within pharmaceutical formulations, SLS fulfils various roles including those of an emulsifying agent, modified-release facilitator, penetration enhancer, solubilizing agent, tablet, and capsule lubricant (493, 515). Upon incorporation of SLS within the range of 0.5-2% into Intralipid®, escalation in the zeta potential was observed, as illustrated in **Figure 8.6**. Investigating the impact of varying SLS percentages on the release of rifampicin revealed intriguing insights. At 0.5% SLS concentration, there was almost no change of zeta potential, and also the effect on release remained minimal. Addition of 1% and 2% SLS translated to zeta potential increases of approximately 1.4 and 1.6 times,

respectively. Correspondingly, these SLS levels yielded enhancements of 1.6 and 1.2 times the uptake within the *in-vitro* model.

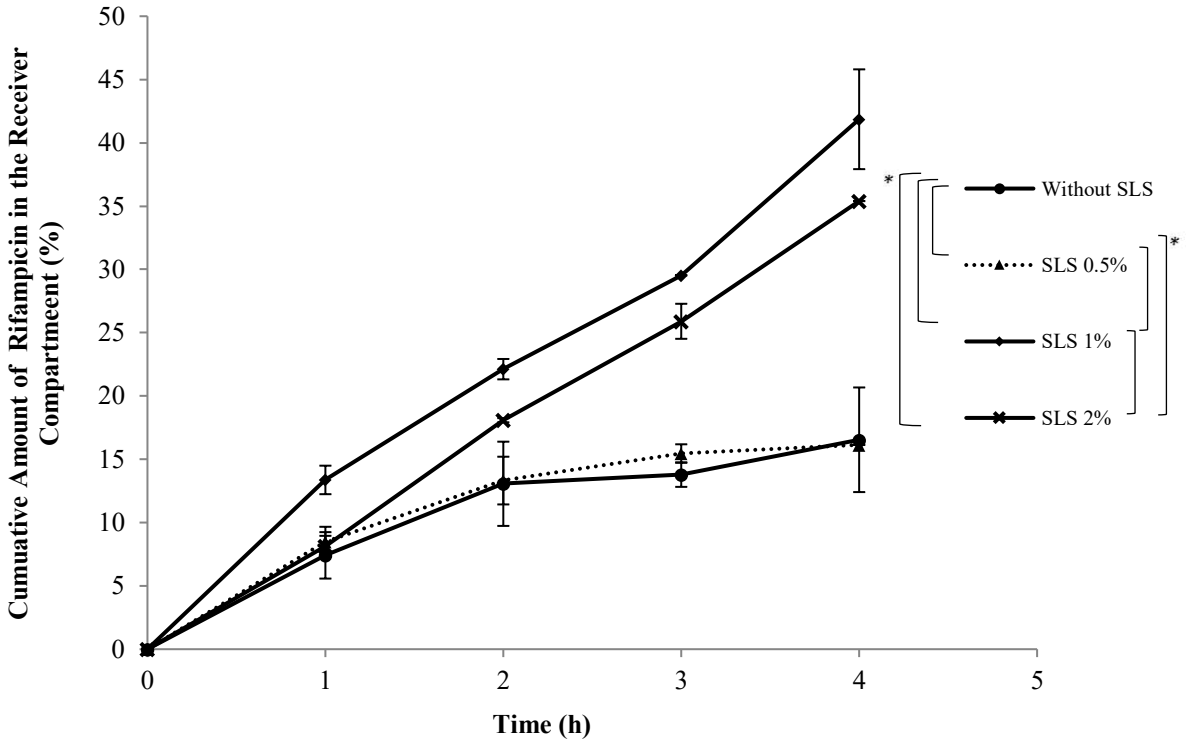

Figure 8.6. Demonstration of the increased *in-vitro* lymphatic uptake of rifampicin via the developed model when different percentages of sodium lauryl sulphate (SLS) were added to Intralipid® in the receiver compartment. * Indicates the statistical significance ($p < 0.05$) between the different groups.

Literature has indicated that SLS may enhance absorption, possibly through a connection with the cAMP system. In this current experimental setup, as there is no cAMP system involved, it is suggested that the effect is physicochemical rather than biological (493). The experiment aimed to test the hypothesis that increasing the zeta potential through the addition of Sodium Lauryl Sulfate (SLS) would enhance uptake in the *in-vitro* model. Still, it is important to note that SLS functions as an anionic emulsifier within the concentration range of 0.5-2.5% (516). Therefore, another potential explanation for the

observed results could be attributed to the emulsifying role of sodium lauryl sulfate. At lower concentrations (0.5% and 1%), SLS would be adsorbed at the oil-water interface, facilitating the uptake of rifampicin into the internal phase droplets. But, as the concentration increased (2%), the interface could have become saturated, indicating an excess of SLS molecules covering the available surface area. Consequently, once the interface reached saturation, the uptake of rifampicin into the droplets became more challenging. As a result, little difference was observed in the latter case (2% SLS) compared to the scenario in which no SLS was added to the medium.

Yet, if only coating was the factor affecting the uptake, SLS would have decreased it similar to PL-81 and which was found to coat the Intralipid® particles and hence impede the rifampicin uptake. The outcomes acquired from this study may potentially imply the existence of an optimal range of sodium lauryl sulphate wherein the uptake enhancement becomes apparent. Nonetheless, these findings underscore the affirmative influence of zeta potential increase on uptake within the *in-vitro* model. Moreover, the precise mechanism through which alterations in zeta potential produce these uptake effects necessitates further comprehensive investigation.

8.4 Conclusion:

In this study, our previously developed *in-vitro* model was utilized to investigate how various agents influence the uptake into artificial chylomicrons (Intralipid®). Typically, long-chain fatty acids facilitate intestinal lymphatic uptake, while medium-chain counterparts are mainly absorbed through the portal pathway. The results showcased the ability of the model to distinguish between oils containing long-chain fatty acids,

particularly olive, sesame and peanut oils. Yet, it did not capture the difference between these long-chain rich oils and medium-chain-rich oil (coconut oil) in terms of lymphatic uptake. The increased uptake observed with coconut oil was attributed to its better emulsification in artificial chylomicron media, due to its composition the medium-chain fatty acids. Moreover, the enhanced uptake of the tested formulation with linoleoyl polyoxyl-6 glycerides emphasized the practical utility of our model in optimizing formulations. Additionally, the findings indicated that adjusting the zeta potential, increasing it with sodium lauryl sulfate (SLS) and decreasing it with (+/-) chloroquine, resulted in corresponding increases and decreases in uptake in the in vitro model. These results underscored the potential influence of zeta potential on intestinal lymphatic uptake in our model. Nevertheless, further research is necessary to explore whether this mechanism holds true *in-vivo*.

CHAPTER NINE

Novel First-Generation Dissolution Models to Investigate the Release and Uptake of Oral Lymphotropic Drug Products

A version of this chapter is published in:

AAPS PharmSciTech. 2024;25(6):187. DOI: 10.1208/s12249-024-02866-y

Reprinted from Reference (593).

9.1 Introduction:

Dissolution testing, as defined by the United States Pharmacopeia (USP), measures the rate and extent of drug solution formation from a dosage form (517). Its fundamental importance was recognized in 1957, when Nelson discovered a correlation between *in-vivo* blood concentrations of oral theophylline salts and their *in-vitro* dissolution (518). Contemporary dosage form dissolution testing has been further developed and refined to aid in the drug development process. It now reflects the suitability of developed formulations in the early stages of product development and allows for the selection of formulations that will advance into *in-vivo* studies. It also serves as a quality control measure and a means of comparison between different commercial products containing the same active pharmaceutical ingredient (bioequivalence assessment) (519). Furthermore, *in-vitro in-vivo* correlations (IVIVC) utilize *in-vitro* data to predict *in-vivo* performance in humans, bridging the gap between pre-clinical and clinical studies (520-522).

There are several types of dissolution apparatus commonly used in pharmaceutical research and development, and the choice of apparatus depends on various factors, including the type of dosage form, pharmacopeial and regulatory requirements, and drug properties (521). The general performance tests monographed in the United States Pharmacopeia (USP) chapters on Dissolution <711> (523), and Drug Release <724> (524) details guidelines and standards for testing pharmaceutical dosage forms, and for solid oral dosage forms, USP type Apparatus 1 and 2 are most frequently used (517). However, these standard dissolution equipment only estimate the aqueous release of drugs from formulations, without reflecting the pathways through which they are absorbed.

Most oral drugs when absorbed intracellularly (active or passive), they pass through the portal vein to the liver before entering the general circulation (525, 526). However, certain drugs can enter the general circulation via the intestinal lymphatics (lymphotropic drugs) instead of simply conventional enteric absorption. These xenobiotics are packaged into triglyceride-rich lipoproteins called chylomicrons and then exocytosized out of the enterocytes to be taken up by the intestinal lymphatics (53, 55). This method of drug absorption and delivery offers several pharmacokinetic and pharmacodynamics advantages, including shunting away from first-pass enteric and hepatic metabolism, potentially higher bioavailability, and increased efficacy of various treatment modalities (54, 56, 138). Yet, quantifying this pathway directly is not possible without measurements in the lymphatic fluid, which requires invasive procedures (264).

In a previous study, we presented an *in-vitro* model crafted to predict, inhibit, and enhance lymphatic uptake. The foundation of the model was based on the interaction of drugs with chylomicrons, a process well-documented for its predictive abilities in assessing intestinal lymphatic uptake (350).

Here we report the first lymph-focused dissolution models. This study aimed to develop innovative first-generation dissolution models that provide a deeper understanding of the release and uptake of oral lymphotropic drugs, thereby enhancing formulation design strategies. In light of the growing number of formulations and delivery systems designed for lymphatic transport, these models also have the potential to eventually contribute to the establishment of bioequivalence guidelines specifically for lymphotropic formulations.

The proposed models consider both pathways through which released drugs may enter the general systemic circulation and incorporate an artificial chylomicron-containing compartment within the dissolution vessel. This compartment adds a lipid dissolution sink for lymphotropic drugs to the setup. By analyzing the media in both the dissolution vessel and lymphatic compartments, the drug content in each compartment can be assessed, providing valuable insights into drug behavior.

9.2 Materials and Methods:

9.2.1 Materials:

Sodium chloride (NaCl, CAS: 7647-15-5), potassium phosphate monobasic (KH_2PO_4, CAS: 7778-77-0), potassium phosphate dibasic (K_2HPO_4, CAS: 7758-11-4), sodium hydroxide (NaOH, CAS: 1310-73-2) and triethylamine (CAS: 121-44-8) were all obtained from Caledon Laboratories (Ontario, Canada). Hydrochloric acid (36.5-38%) was from BDH Inc. (Ontario, Canada) whereas artificial chylomicrons media (Intralipid® (264)) was purchased from Fresenius Kabi Ltd (Toronto, Ontario, Canada). HPLC-grade acetonitrile and o-phosphoric acid (85%) were both products of Fisher Chemicals (Ontario, Canada).

9.2.2 Equipment:

The tools and equipment used in the different experiments included dialysis bags with molecular weight cut-off, MWCO: 12-14 KDa and 45mm-width (Spectra/Por molecular porous membrane tubing SP4) from Fisher Scientific (Ontario, Canada), Amicon Ultra-0.5 30 KDa centrifugal filtering units (Millipore, Sigma-Aldrich, Darmstadt,

Germany), accumet® XL20 pH/conductivity meter (Fischer Scientific, Massachusetts, USA) and density kit (XPR/XSR-Ana) from Mettler Toledo (Ohio, USA). For HPLC analysis, Shimadzu HPLC (LC-10AD, Shimadzu Corporation, Kyoto, Japan) equipped with SIL-10A (Shimadzu Auto Injector) and UV-VIS detector (SPD-10AV) was used. Analysis was performed using Kinetex™ C18 column (250 mm ×4.6 mm×5 µm) from Phenomenex (California, USA), and resultant peak areas were integrated using LabSolutions software (Shimadzu Corporation, Kyoto, Japan).

9.2.3 Preparation of the Dissolution Media:

9.2.3.1 Standard Simulated Gastric Fluid (pH = 1.2) and Phosphate Buffer (pH = 6.8):

USP41-NF36 protocol was employed to prepare the simulated gastric fluid (without enzymes, pH 1.2) and the phosphate buffer (pH 6.8) (p 5754 and 5748, respectively) (517).

9.2.3.2 Modified Simulated Gastric Fluid:

An adapted gastric fluid was prepared by adding 0.9 g of sodium chloride, 3.27 mL of hydrochloric acid and 3.2 g of potassium dihydrogen phosphate to make 1000 mL solution using water. The pH of this solution was attuned to 1.9.

9.2.3.3 Measurement of Density of the Prepared Dissolution Media:

The density of 80 mL-samples of each fluid was measured at a temperature of 25±0.2 °C. The designated amount of fluid was added to the beaker and the sinker was fully submerged. Any air bubbles that adhered to the sinker were removed and the draft shield was closed. Once the balance was stabilized, the readings were recorded.

9.2.4 Measuring the Dissolution of Terbinafine Products Using the Developed Models:

Dissolution of three commercial products of the lymphotropic drug terbinafine was tested using modified USP Apparatus II and IV (**Figure 9.1**). The used products were Terbinafina (Laboratorio Chile, Chile), Apo-terbinafine (Apotex, Toronto, Canada) and Lamisil (Manufactured by Novartis Pharma Productions GmbH, Germay for Novartis Pharma AG, Switzerland). Each product was tested between 4-6 times using each developed methodology. For terbinafine hydrochloride tablets, FDA Dissolution Methods Database calls for 500 mL media, maintained at 37±0.5 °C and stirred at 50 rpm (527). The same conditions were applied in these experiments.

9.2.4.1 Dissolution Testing via Modified USP Apparatus II:

Freshly prepared and degassed media was used (250 mL of modified simulated gastric fluid (pH=1.9)). Dialysis bag containing 5 mL of artificial chylomicrons media was added to mimic lymphatic uptake. Initially, the dialysis bag was attached either to the bottom of the paddle or the paddle shaft. However, a systematic assessment led to determining that the most effective configuration involved placing the dialysis bag within the dissolution media in the vessel of the modified USP Apparatus II. This positioning ensured continuous contact with the media throughout the experiment, enabling valuable comparisons between the Apparatus II and Apparatus IV setups as further illustrated in the following section. Samples were taken from the vessel media at different time points (5, 15, 30, 45, and 60 min). From the dialysis bags, 60-minute samples were taken after the end of the experiment. These samples of 0.2 mL were then diluted with 0.8 mL acetonitrile before being filtered into the HPLC vial for analysis. Also from the bag, 0.5 mL was added to the

centrifugal filtering unit and centrifuged at 10K g for 10 min. The filtrate was collected and analysed using HPLC. The calculated concentrations for the samples were plotted to determine the cumulative percent dissolved over time using DDSolver (528).

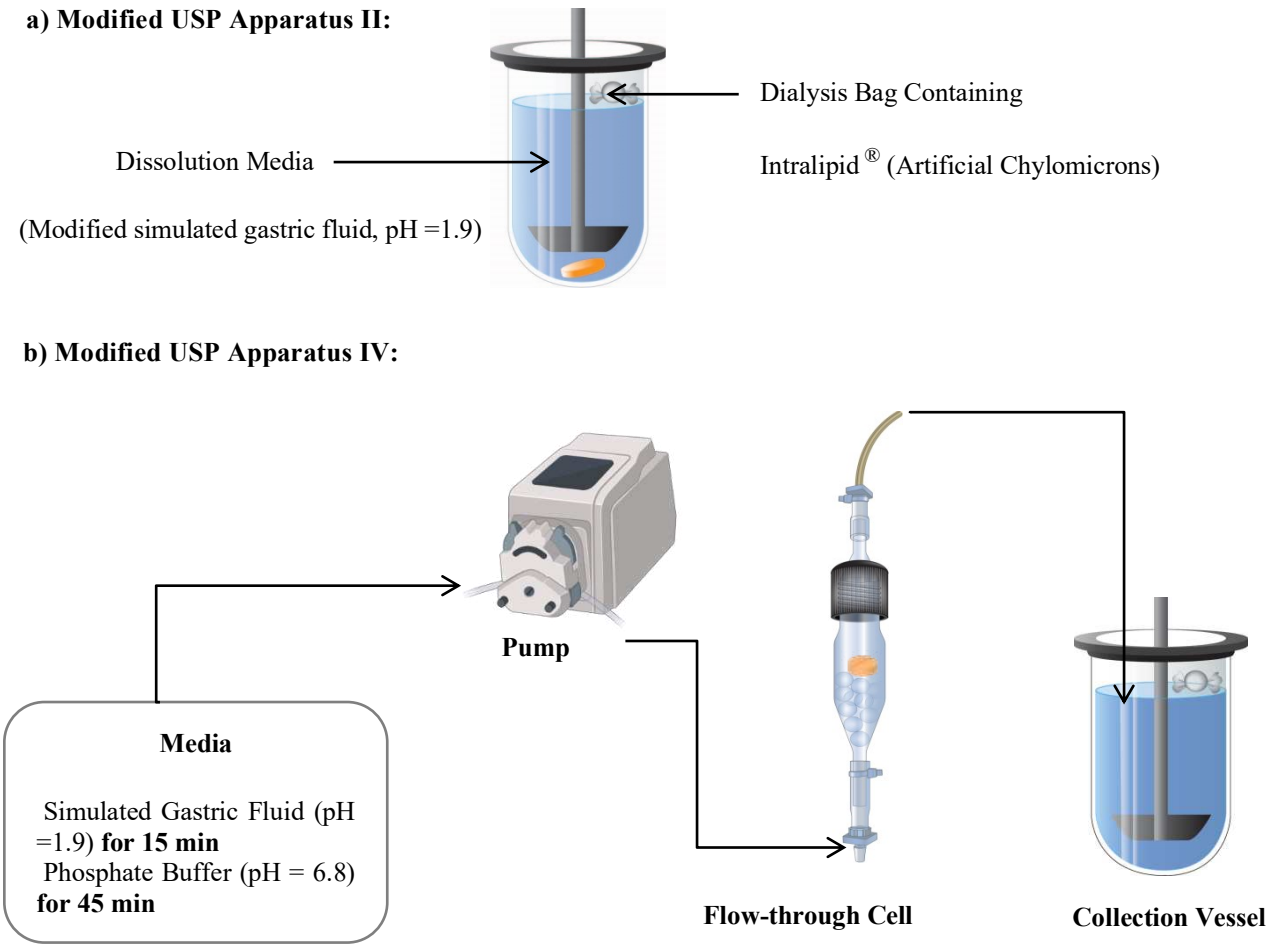

Figure 9.1. Illustration of the a) Modified USP Apparatus II (Top) and b) Modified USP Apparatus IV (Bottom) used to study the dissolution of various commercial products of the lymphotropic drug, terbinafine. To each model a dialysis bag (molecular weight cut-off, MWCO:12-14 KDa and 45mm-width) containing 5 mLof artificial chylomicrons – was added to mimic lymphatic uptake. Part of this illustration was created with BioRender.com.

9.2.4.2 Dissolution Testing via Modified USP Apparatus IV:

This apparatus included a pump that moved the media from a container through a flow cell of 22.6 mm internal diameter. The cell held the dosage form that was placed over 25 glass beads of 1 mm size positioned in the bottom of the cell. The media used for the test were placed in a constant temperature water bath, maintained at 37 ± 0.5 °C and pumped through the cell. The dissolved drug along with any other substances that pass through the flow cell were collected in a vessel comparable to the USP Apparatus II vessel. First, simulated gastric fluid (SGF) was pumped through the cells at a flow rate of 8 mL/min for 15 min. This was followed by phosphate buffer (pH 6.8) at a flow rate of 16 mL/min for 45 min. Upon switching to the second media, dialysis bag containing 5 mL of artificial chylomicrons media was added to the collection vessel. Here, the collection vessel would start filling as the experiment progressed, therefore, attaching the bag to a fixed point (paddle bottom or shaft) would not have provided the consistent media contact that the chosen position did, making it a critical choice for this study. During the dissolution test, 5 mL samples were collected at 5, 15, 30, 45, and 60 min. The media volume was weighed and exact volume was calculated using the previously determined density of the media. Samples from the dialysis bags containing the artificial chylomicrons were collected at the end and processed as described with the apparatus II.

9.2.5 HPLC Instrumentation and Chromatographic Conditions:

The mobile phase was composed of a mixture of acetonitrile and water containing 0.02 M ortho-phosphoric acid and 0.01 M triethylamine (40:60 v/v) and was eluted

isocratically at 25 ºC and a flow rate of 1 mL/min. All samples were injected at 20 µl, and detection was set at 224 and 283 nm.

9.2.6 Statistical Analysis:

All dissolution groups were established with 4-6 independent replicates, and the results are presented as mean ± standard error of the mean (SE). Statistical differences were assessed using an ANOVA test with a significance level of $\alpha = 0.05$, where p-values below 0.05 were deemed statistically significant in all instances.

9.3 Results:

As depicted in **Figure 9.2**, results of performance of the different products in the modified USP Apparatus II demonstrated that terbinafine release into the dissolution media was highest with Lamisil followed by Terbinafina, then Apo-terbinafine (87.90%, 83.17% and 71.68%, respectively). For the lymphatic uptake aspect of the model system, Terbinafina and Lamisil accumulated more drug in the lymphatic compartment than Apo-terbinafine. However, Terbinafina had higher lymphatic uptake than Lamisil (2.58%, 2.32%, respectively). Apo-terbinafine had 1.71% in the lymphatic compartment of this model.

The results obtained from the modified USP Apparatus IV revealed notable differences among the tested products (**Figure 9.3**). Specifically, Terbinafina demonstrated superior release as documented in the collection vessel compared to Lamisil, with both exhibiting significantly higher release than Apo-terbinafine (101.93%, 83.93%, and 11.48%, respectively). A similar phenomenon was observed in the lymphatic compartment,

with Terbinafina exhibiting the highest accumulation in the lymphatic compartment (2.14%), followed by Lamisil (1.16%) and Apo-terbinafine (0.21%).

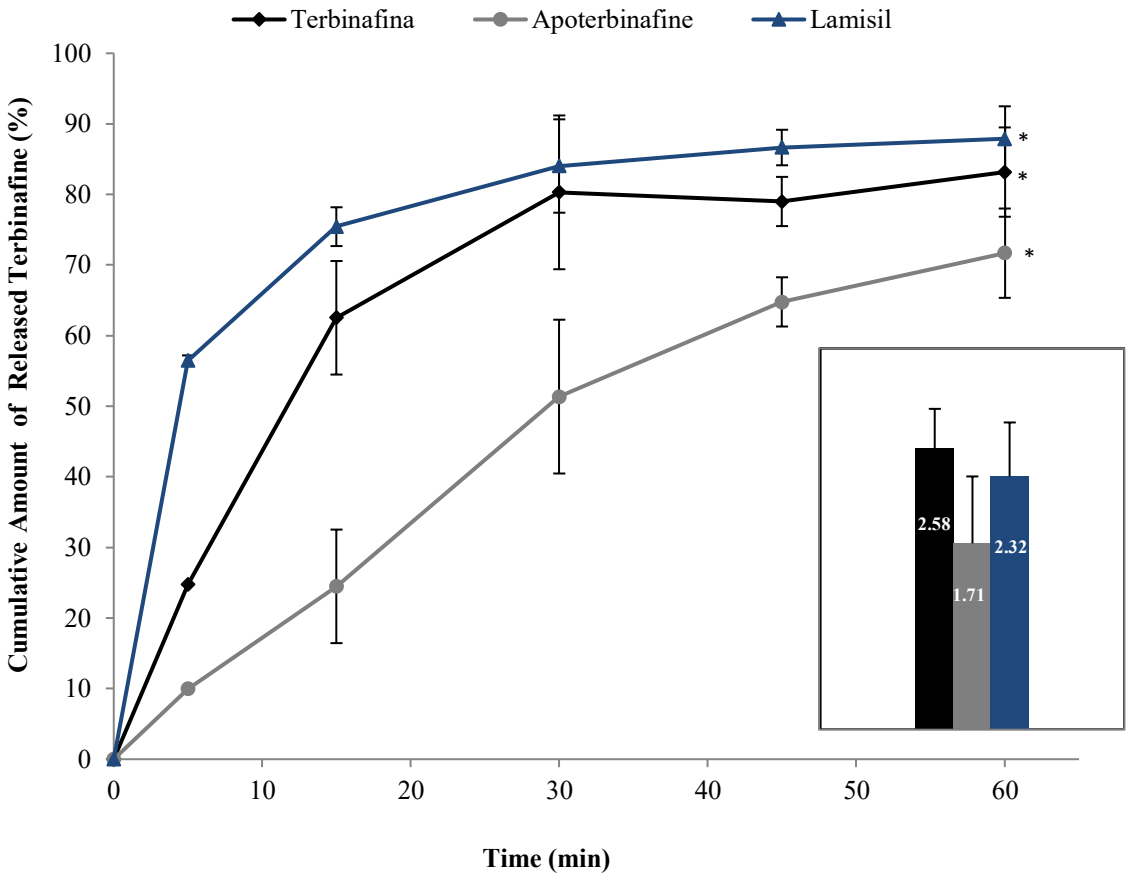

Figure 9.2. Cumulative percentage of dissolved terbinafine from the commercial products into Modified USP Apparatus II. The line graph represents the dissolution vessel profile and the columns represent the % of the drug with respect to the total dose in the lymphatic vicinity (dialysis membrane containing the artificial chylomicrons) after 60 minutes. Data represent the mean values and bars represent the stansard error (n = 4-6). * Denotes statistically significant from other groups $p < 0.05$.

9.4 Discussion:

Following oral administration, immediate-release dosage forms have to disintegrate to liberate drugs that dissolve in the physiological fluid before moving across the GIT (529, 530). While most drugs travel from the GIT into the systemic circulation via portal blood,

others might take a different route to the systemic circulation through intestinal lymphatic voyage via chylomicrons (56, 264). The latter mainly have log P > 5 and solubility in long chain triglycerides > 50 mg/g, however other molecular descriptors may also play a role (350). These drugs get packaged into chylomicrons which are taken up by the lymphatics rather than blood capillaries once they get exocytosized from the enterocytes (51, 273).

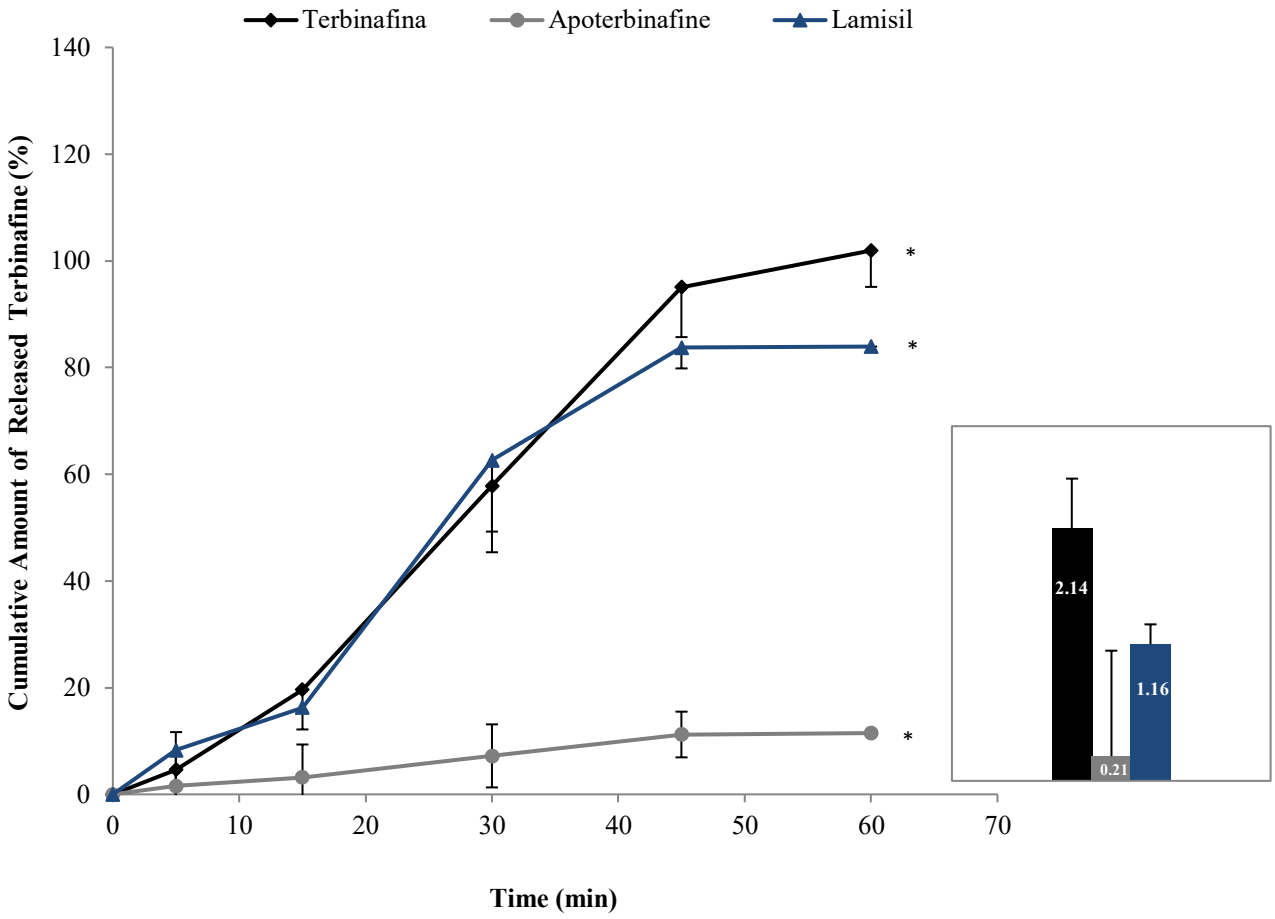

Figure 9.3. Cumulative percentage of dissolved terbinafine from the commercial products into Modified USP Apparatus IV. The line graph represents the dissolution vessel profile and the columns represent the % of the drug with respect to the total dose in the lymphatic vicinity (dialysis membrane containing the artificial chylomicrons) after 60 minutes. Data represent the mean values and bars represent the stansard error (n=4-6). * Denotes statistically significant from other groups $p < 0.05$.

Dissolution testing of oral dosage forms quantifies the release of the active pharmaceutical ingredient (API) in a specified dissolution media that might mimic the physiological environment in which the same process would happen *in-vivo* (531). For drugs not subjected to first-pass effect or other physiological phenomenon and whose permeability is not limited, dissolution testing performance can be an indicative method of the *in-vivo* drug bioavailability in plasma (532). However, not all drugs reach the systemic circulation via the portal vein. For those xenobiotics a more representative dissolution model should be considered; one that considers both blood and lymphatic pathways through which candidate APIs may reach the general circulation.

In the proposed models for the measurement of dissolution of lymphotropic drugs, artificial chylomicrons (264, 350) were added to the dissolution media in the vessel of modified USP Apparatus II and to the media in the collection vessel of modified USP Apparatus IV to facilitate the drug uptake into a lymphatic-like environment and hence account for the proportion of the lymphatic uptake of the dissolved drug.

Terbinafine was the selected model drug in this study. It has been documented to go through intestinal lymphatics (384). The molecular descriptors of terbinafine are in **Table 9.1**. It comes in various oral solid dosage forms including tablets and granules (533). Three commercial product of 250 mg terbinafine hydrochloride tablets were sampled and utilized in this work (Terbinafina, Apo-terbinafine and Lamisil).

Terbinafine hydrochloride is listed officially in the United States Pharmacopoeia, British Pharmacopoeia, and European Pharmacopoeia (534). For collecting preliminary data, a standard USP Apparatus II was employed with different media, namely standard

simulated gastric fluid (SGF, pH = 1.2), modified simulated gastric fluid (modified SGF, pH = 1.9), and phosphate buffer (pH = 6.8). Standard simulated gastric fluid has been reported as a dissolution medium for terbinafine tablets and other dosage forms in the literature (529). Preliminary findings (data not shown) indicated that the cumulative percent dissolved of terbinafine from the different products in SGF was quite low. The highest amount of the drug detected in the media was about 15%. Nevertheless, the performance of the tablets in terms of dissolution rate was increased in the modified SGF, and was ultimately utilized instead of the standard SGF. Results in phosphate buffer results showed close to zero drug release over time.

Table 9.1. Molecular descriptors of terbinafine.

Drug	MW (g/mol)	MV (cm^3)	pKa	LogP	HBD	HBA	MP (°C)	PSA ($A^{\circ 2}$)	Density (g/cm^3)	Structure
Terbinafine	291.4	289.1± 3.0	7.12	5.9	0	1	205	3 *	1.0 ± 0.1 *	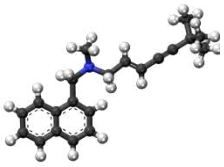

Abbreviations: molecular weight (MW), molar volume (MV), number of H-bond donors (HBD), number of H-bond acceptors (HBA), melting point (MP), and polar surface area (PSA). All data were obtained from PubChem, and ChemSpider databases *. (last accessed on 30 May 2024). Structure is available under CC BY-SA 4.0 DEED licence from https://pubchem.ncbi.nlm.nih.gov/compound/1549008.

Being a basic drug whose solubility is pH-dependent with maximum solubility at acidic pH, modified SGF yielded understandably better results than the basic phosphate buffer. As seen from the solubility graph of terbinafine (**Figure 9.4**), the drug solubility in both pHs of the standard and modified SGFs (1.2 and 1.9, respectively) remains the same. However, the superior performance of the modified SGF than the standard SGF might be attributed to the excipients utilized in the different products as will be discussed later.

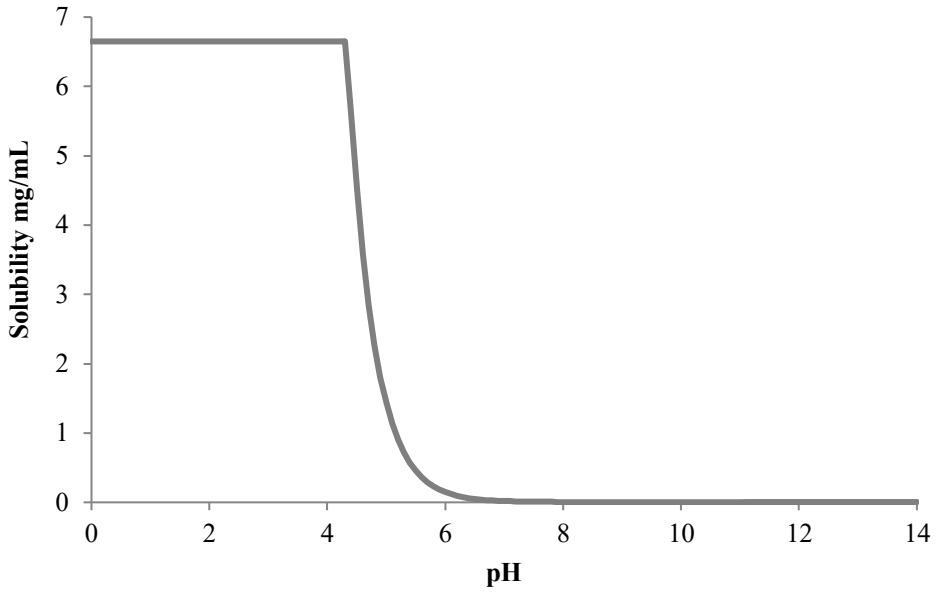

Figure 9.4. Solubility graph of terbinafine hydrochloride in different pHs. Data was predicted by ADMET predictor (version 10.4 (Simulations Plus Inc., Lancaster, CA, USA).

Results obtained from modified Apparatus II could be justified by the excipients used in the different products. While all three products are pharmaceutically equivalent according to the FDA definitions, differences in the formulation, specifically in the excipients used are evident (**Table 9.2**). Terbinafina and Lamisil have identical formulations, while the percent ratio of the excipients in the formulation and processing variables are not known. In contrast, excipients utilized in Apo-terbinafine are different. Sodium starch glycolate was used as the disintegrant in Terbinafina and Lamisil, while croscarmellose sodium was used in Apo-terbinafine. Sodium starch glycolate is known to be highly effective in promoting a more rapid tablet disintegration and dissolution, while croscarmellose sodium may be less effective in this regard, likely due to functional differences between the two disintegrants. Specifically, sodium starch glycolate has a higher swelling and wicking capacity, meaning it can absorb additional water and distribute

it more evenly throughout the tablet, leading to more uniform disintegration. It also has greater compressibility, allowing it to be used in higher concentrations without compromising tablet hardness or friability, ultimately enhancing tablet disintegration and dissolution (535, 536).

Although the hydrophobicity of hydroxypropyl cellulose and hydroxypropylmethyl cellulose is different (537). Yet, that did not affect the performance of their formulations (Terbinafina and Lamisil, respectively). However, for Apo-terbinafine, the usage of methylcellulose in Apo-terbinafine could have impacted the drug release. Methylcellulose is a water-soluble polymer that can form a gel-like matrix in the presence of water (538). The presence of this gel can decrease tablet porosity, water diffusivity, and increase the time it takes for the tablet to disintegrate, all of which can result in a slower drug release rate from the tablet. This property is utilized in controlled release formulations (12, 539). The hydration of methyl cellulose is lower compared to both hydroxypropyl methyl cellulose (540) and hydroxypropyl cellulose (537). The adhesive property of methyl cellulose, which could potentially block tablet pores, may explain the prolonged disintegration time observed in Apo-terbinafine tablets compared to Lamisil and Terbinafina.

Moreover, the manufacturing process of these products could also have affected their dissolution performance (541). Terbinafina and Lamisil may have been manufactured under conditions that result in a more porous or more rapidly dissolving tablet. For example, the less compression force used during production could impact the tablets and impart superior dissolution performance compared with Apo-terbinafine. Other factors could be granulation or direct compression, however, this information is proprietary (451).

In an attempt to simulate the changing conditions inside the gastrointestinal tract, modified USP Apparatus IV was utilized (542). A dynamic dissolution protocol with two different media was applied: one that mimicked the environment of the stomach (modified SGF), followed by one that simulated the environment of the intestines (phosphate buffer with a pH of 6.8). In experiments, when switching to the intestinal-like media, a dialysis bag containing artificial chylomicrons media was added to the collection vessel to account for the intestinal lymphatic uptake of the dissolved drug.

Table 9.2. Excipients used in the different terbinafine hydrochloride products (Terbinafina, Laboratorio; Apo-terbinafine, Apotex; and Lamisil, Novartis).

Product	**Terbinafina***	**Lamisil****	**Apo-terbinafine*****
Excipients	Hydroxypropylcellulose	Hydroxypropyl methylcellulose	Methylcellulose
	Microcrystalline cellulose	Microcrystalline cellulose	Colloidal anhydrous silica
	Colloidal silicon dioxide	Colloidal silicon dioxide	Croscarmellose sodium
	Sodium starch glycolate	Sodium starch glycolate	Magnesium stearate
	Magnesium stearate	Magnesium stearate	

Data were obtained from:

*https://www.laboratoriochile.cl/producto/terbinafina-250-mg/

**https://www.accessdata.fda.gov/drugsatfda_docs/label/2012/020539s021lbl.pdf

***https://www.nps.org.au/medicine-finder/apo-terbinafine-tablets

The observed differences in release when the modified USP Apparatus IV was used were attributed to the rate of disintegration and dissolution of the different products. For Terbinafina and Lamisil, a faster disintegration and dissolution resulted in higher drug release, whereas Apo-terbinafine exhibited low release due to its slow disintegration and subsequent dissolution, which may be attributed to its excipients or tableting processes as previously discussed.

It is noteworthy to mention that the solution in the collection vessel turned turbid at completion of the experiments. The solubility of the drug and the pH change between the stomach and intestine may explain this displayed phenomenon of precipitation. A dissolved basic drug entering a basic intestinal environment may cause first a supersaturated solution followed by precipitation out of solution (543). However, due to sink conditions and drug absorption from the intestinal lumen, the drug redissolves and is subsequently absorbed (544, 545). In this experiment set-up, the presence of phosphate buffer in the collection vessel, combined with simulated gastric fluid, altered the pH of the local media. As the solubility of terbinafine is pH-dependent, and when the pH of the media is suboptimal, the drug can precipitate out of the solution, as observed in this case.

To ensure the ability of the model to distinguish lymphotropic drugs accurately, a comparative analysis with the biphasic method (530) was conducted. Interestingly, the accumulation in the octanol phase in the biphasic model showed almost identical behaviour for both a lymphotropic drug (rifampicin) and a non-lymphotropic drug (Ibuprofen (530)). However, in the model proposed in this paper, the uptake into lymphatic compartment varied among different lymphotropic drugs (terbinafine and rifampicin), despite the fact that the aqueous solubility of rifampicin was comparable to one of the terbinafine products (Supplementary Materials).

Nonetheless, refinements in the proposed experimental models can be tailored according to the specific goals of the study. For the second model, it is important to consider the more alkaline pH conditions in the collection vessel, which can present solubility challenges, especially for drugs with basic properties, as observed in our tested compounds. To address this concern, one potential strategy is to introduce surfactants into

the dissolution media, which can enhance drug solubility under alkaline conditions. Additionally, continuous sampling from the lymphatic compartment could be explored as a refinement. This approach would allow for the simultaneous monitoring of drug uptake profiles into the lymphatic vicinity along with the aqueous dissolution profile. That can help gain deeper insights into the dynamics of drug absorption and distribution, particularly in the context of lymphatic uptake.

Overall, the evolution of dissolution testing and USP apparatus represents an on-going commitment to enhancing the quality assessment of pharmaceutical products. The innovative models introduced herein have the potential to expand this evolution by focusing on the often-underestimated lymphatic absorption pathway facilitated by chylomicrons and the increasingly recognized use of hydrophobic xenobiotics in formulations. These models offer greater discriminatory power in dissolution testing, allowing for precise evaluations in complex contexts. Additionally, they open doors to post-approval changes, enabling pharmaceutical companies to adapt to evolving regulatory requirements and emerging scientific insights with precision and efficacy.

9.5 Conclusion:

Lymphotropic candidate formulations are specifically designed to facilitate uptake via the intestinal lymphatic system as an alternative absorption route to the enteric-portal pathway. However, conventional dissolution tests assess drug release in aqueous media solely for quality and performance assurance, without contemplating the absorption pathway, be it portal or lymphatic. This study showed that it may be possible to develop lymphatic-focused dissolution models to assess formulations and factors potentially

affecting chylomicron uptake. With the challenges encountered in solubilizing hydrophobic drugs and the increased focus on lipid based formulations of xenobiotics, it is prudent that dissolution testing and development are also developed and refined in an attempt to more accurately assess increase possible lymphatic uptake, and variables such as excipients and manufacturing that may impact formulation performance. Given the rising complexity of pharmaceutical products and further refining and developing performance testing methods must also be reconceptualised and refined accordingly where possible.

Supplementary Materials:

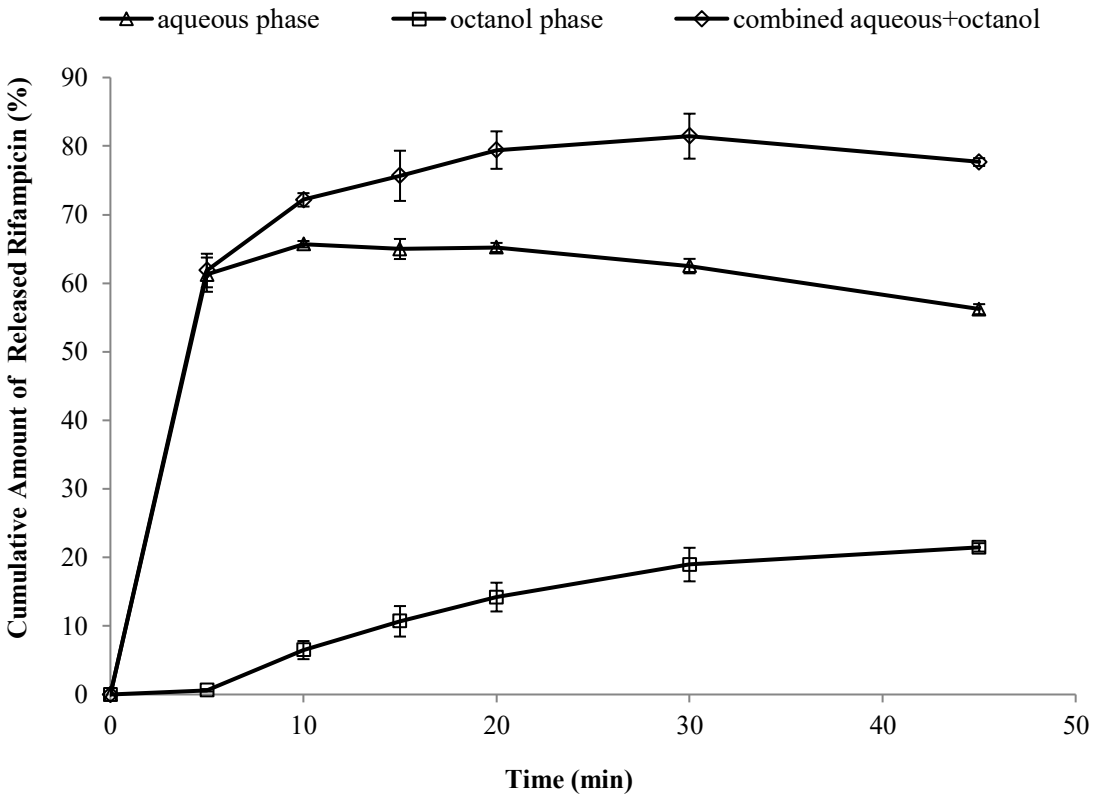

Figure 9.5. Dissolution profile and organic phase partition of Rofact capsules (300 mg) into 200 mL of 0.1 N HCl and 100 mL octanol, respectively. Error bars represent the standard deviation (n=3).

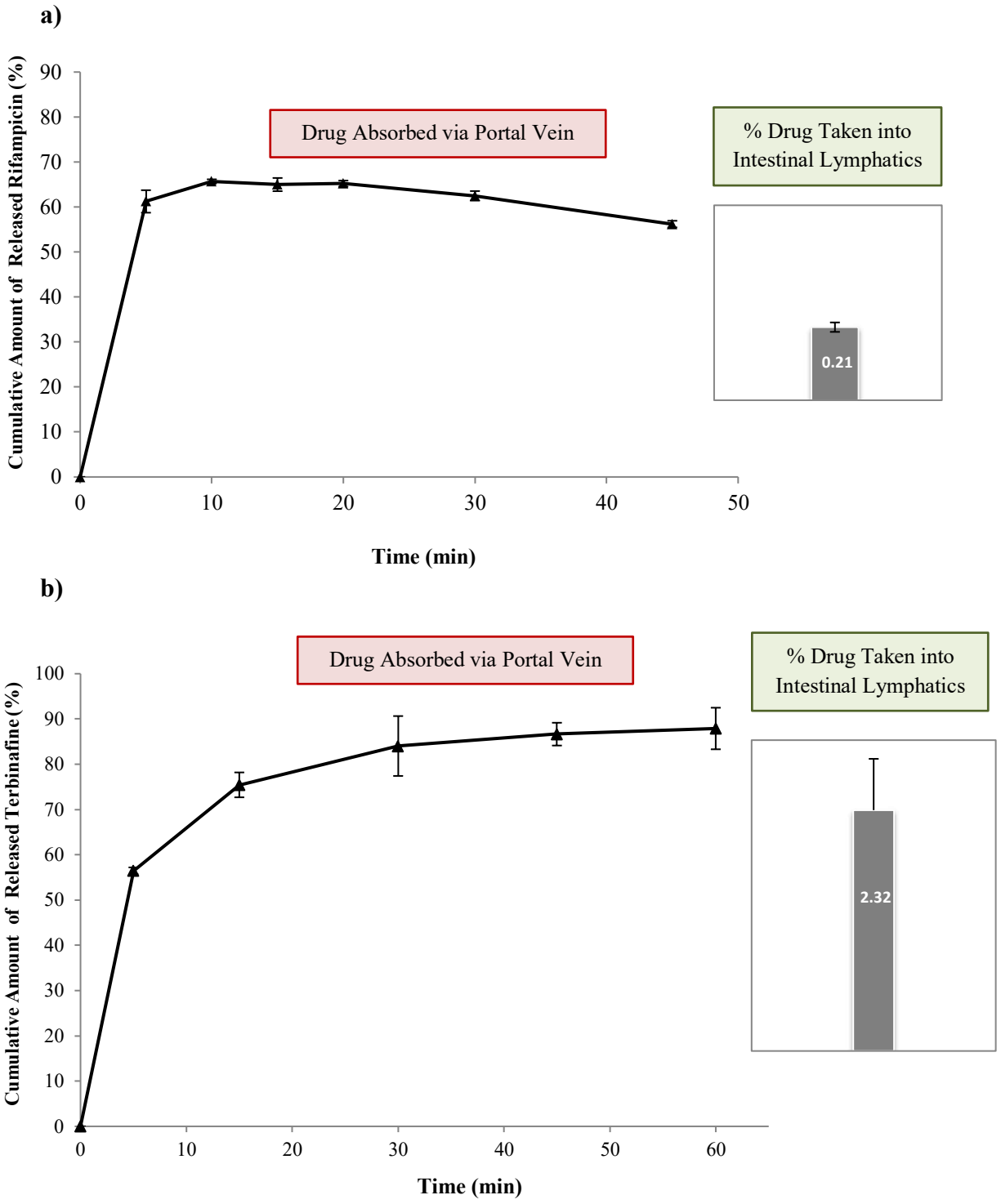

Figure 9.6. Dissolution profile and lymphatic uptake of a) Rofact capsules (rifampicin) and b) Lamisil tablets (terbinafine) into the aqueous media (vessel, blue line) and 5 mL Intralipid® (lymphatic vicinity, green column), respectively. Error bars represent the standard deviation (n=3) and the standard error of the mean (n=4-6) for a) and b), respectively.

CHAPTER TEN

Modelling Intestinal Lymphatic Uptake of Halofantrine Post-prandially: Advancements and Implications in Physiologically Based Pharmacokinetic Modelling

A version of this chapter has been submitted to be published in:

J Pharm Pharmcol. 2024

10.1 Introduction:

After absorption, dietary fats and lipophilic vitamins traverse intestinal enterocytes and are packaged into excretory enterocyte lipoproteins, known as chylomicrons. These chylomicrons primarily transport the absorbed fats and lipophilic xenobiotics into the bloodstream via the lymphatic network (51, 53, 56). Particularly for drug molecules, especially lipophilic ones (with a log P > 5), hitchhiking on chylomicrons enables them to bypass first-pass liver metabolism, thus potentially enhancing their bioavailability. Additionally, these extracellular lipoprotein particles shows great promise for drugs targeting the lymphatic system, offering potential for enhancing therapeutic efficacy while minimizing off-target toxicity (51, 54, 56, 182, 234).

Despite the significance and unique characteristics of the intestinal lymphatic absorption pathway, the field of *in-silico* modeling for lymphatic oral absorption remains relatively underexplored (54, 184). To our knowledge, only one model has been reported, aiming to establish a quantitative relationship between molecular structure and the lymphatic transfer of lipophilic compounds co-administered with a long-chain triglyceride vehicle. Molecular descriptors were computed using the VolSurf computer program, and a structure–property relationship was established through partial least squares analysis (PLS). The predictive power of the PLS model was found to surpass that of the frequently used method correlating log P values (LogKow) with lymphatic transfer (235).

In the context of mechanistic *in-silico* modeling, physiological-based pharmacokinetic (PBPK) modeling has emerged as a promising approach to assess drug exposure in virtual populations and to obtain mechanistic insight into drug characteristics

(546-549). PBPK models provide simulated concentration versus time profiles of a drug and its metabolite(s) in plasma or an organ of interest and simultaneously allow for estimation of a variety of PK parameters (550). This modeling approach provides a mechanistic understanding of drug behavior by integrating physiological parameters, allowing for personalized predictions of drug pharmacokinetics and the assessment of interindividual variability (551). It enables the prediction of first in-human dose selection and optimization of dosing regimens (552, 553), drug interactions involving enzymes, transporters, and multiple interaction mechanisms (554, 555), evaluation of drug disposition and safety in special populations (556), and other application (549, 550, 554). This approach is both commonly and increasingly being accepted by regulatory agencies as a valuable tool in drug development and new drug and formulation approvals (546, 557, 558).

Intestinal lymphatic uptake still remains a relatively overlooked aspect in drug development and clinical pharmacokinetics using PBPK modeling, despite the significant implications for drug absorption, especially with the growing use of lipid-based formulations such as solid-lipid nanoparticles and other formulations aimed at enhancing systemic absorption via this additional pathway. This study aims to address this gap by developing a PBPK model that incorporates intestinal lymphatic transport for absorption prediction, using halofantrine as a model drug for lymphotropism. Halofantrine is an antimalarial treatment that demonstrates unique absorption characteristics, related to its erratic absorption (559). To ensure consistent absorption and improved bioavailability of halofantrine, it is recommended to be administered with a fatty meal, leveraging its lipophilic nature to facilitate additional absorption through the intestinal lymphatics (469,

560). Therefore, modeling the intestinal lymphatic uptake of halofantrine is crucial in accurately elucidating and characterizing its disposition, efficacy, and safety.

10.2 Materials and Methods:

The input parameters used in the pharmacokinetic and the physiologically-based pharmacokinetic models (PK, and PBPK, respectively) were obtained via ADMET predictor 10.4 (AP 10.4, Simulations Plus, Lancaster, CA, USA) or from published and reported *in-vitro* values. All input model parameters are listed in **Table 10.1**. The data for absorption, distribution, metabolism, and elimination of halofantrine in both fasted and fed states, has been previously reported by Miton *et al.* (60), and was modeled and constructed using GastroPlus™ 9.8.3 (Simulation Plus, Inc., Lancaster, US). The Advanced Compartmental Absorption and Transit (ACAT™) model and PBPK Plus™ was utilized, alongside the drug metabolism module. Halofantrine pharmacokinetic parameters were determined utilizing the PKPlus tool within GastroPlus™ software. For the PBPK modeling, human organ weights, volume, and blood perfusion rates were derived from the Population Estimate of Age-Related (PEAR™) physiology module within GastroPlus™. Tissue plasma partition coefficients (Kp) were predicted using the default *in-silico* Lukacova Kp method (561). Metabolic clearance was estimated from *in-vitro* K_m and V_{max} values of CYP3A4 sourced from literature (562).

The PK model was derived from a selected IV profile construct using data in Krishna *et al.* (563), where a 1 mg/kg IV infusion of halofantrine was administered over one hour to nine adults (primarily male). These individuals had a mean age of 21 years and an average weight of 52 kg.

The modeled oral halofantrine pharmacokinetic profiles in both fasting and fed states were reported by Milton *et al.* (60). In their study, six healthy males were administered a 250-mg tablet of halofantrine hydrochloride after an overnight fast. These same subjects underwent a washout period of at least 6 weeks before receiving the same dose in the same tablet form, after consuming a standardized fatty meal consisting of 60 g of fat (including sausage, scrambled egg, fried potato, and one pint, 568 mL, of whole pasteurized milk). The pharmacokinetic profiles obtained included mean values reported for all individuals with an average weight of 68 kg and a mean age of 28 years in both the fasting and fed states.

Table 10.1. Input parameters for the different properties of halofantrine used in developed PK and PBPK models obtained via ADMET predictor 10.4 (AP 10.4, Simulations Plus, Lancaster, CA, USA) or from published reports.

Property	Value	Reference
Molecular weight (g/mol)	500.44	AP 10.4
pKa	8.18	(564)
	5.58	(565)
Log P	7.58	AP 10.4
Aqueous Solubility (mg/mL)	0.0001 (pH =1.2)	(566)
	0.00024 (pH =7.4)	
Solubility in Fasting State Simulated Gastric Fluid (FaSSIF, mg/mL)	0.00552 (pH=6)	(565)
Solubility in Fed State Simulated Gastric Fluid (FeSSIF, mg/mL)	2.311 (pH =6)	(565)
Solubility factor	105000	AP 10.4
Permeability (cm/s. $10E^4$)	1.44	AP 10.4
Percent unbound in plasma (%)	0.7*	(567)
Blood/plasma concentration ratio	1.5	(567),(568)
***In-vitro* CYP3A4 K_m halofantrine (µM)**	48	(562)
***In-vitro* CYP3A4 V_{max} halofantrine (pmol min^{-1} mg^{-1} protein)**	215	(562)

* F_{uent} = 2% to account for lysosomal trapping

10.3 Results:

10.3.1 PK Modeling of Halofantrine:

Several differences were noted in the halofantrine pharmacokinetic profiles in both fasting and fed states (**Figure 10.1**). One important distinction between the two states was the decreased pre-systemic loss due to the first-pass effect in the fed state (9.9%) compared to the fasting state (77.2%). This is demonstrated through the absorption of halofantrine, as indicated by maximum plasma concentration (C_{max}) and area under the curve up to time (t) (AUC_{0-t}) (569), being higher in the fed state (**Table 10.2**).

10.3.2 PBPK Modeling of Halofantrine:

Two PBPK models were developed for halofantrine for the fasting and the fed states, respectively. The fasting state profile closely matched the reported data in terms of C_{max} and AUC_{0-t} for the drug, as illustrated in the **Figure 10.2** and summarized in **Table 10.3**. For the fed state, the final profile is depicted in **Figure 10.3**. Values of the different parameters in comparison to the observed data are in **Table 10.3.**

Table 10.2. PK model parameters for simulated and observed (60) fasting and fed states of halofantrine.

PK Parameter	Fasting-state		Fed-state	
	Observed value ± s.d. (n = 6)	Predicted value	Observed value ± s.d. (n = 6)	Predicted value
$C_{max\ (\mu g/L)}$	184.0 ± 115.0	181.5	1218.0 ± 464.0	1106.6
$T_{max\ (h)}$	6.0 ± 1.3	5.8	3.3 ± 1.5	4.1
$AUC_{0-t\ (\mu g.L^{-1}.h)}$	3.9 ± 2.6	3.9	11.3 ± 3.5	11.9

s.d. represents the standard deviation.

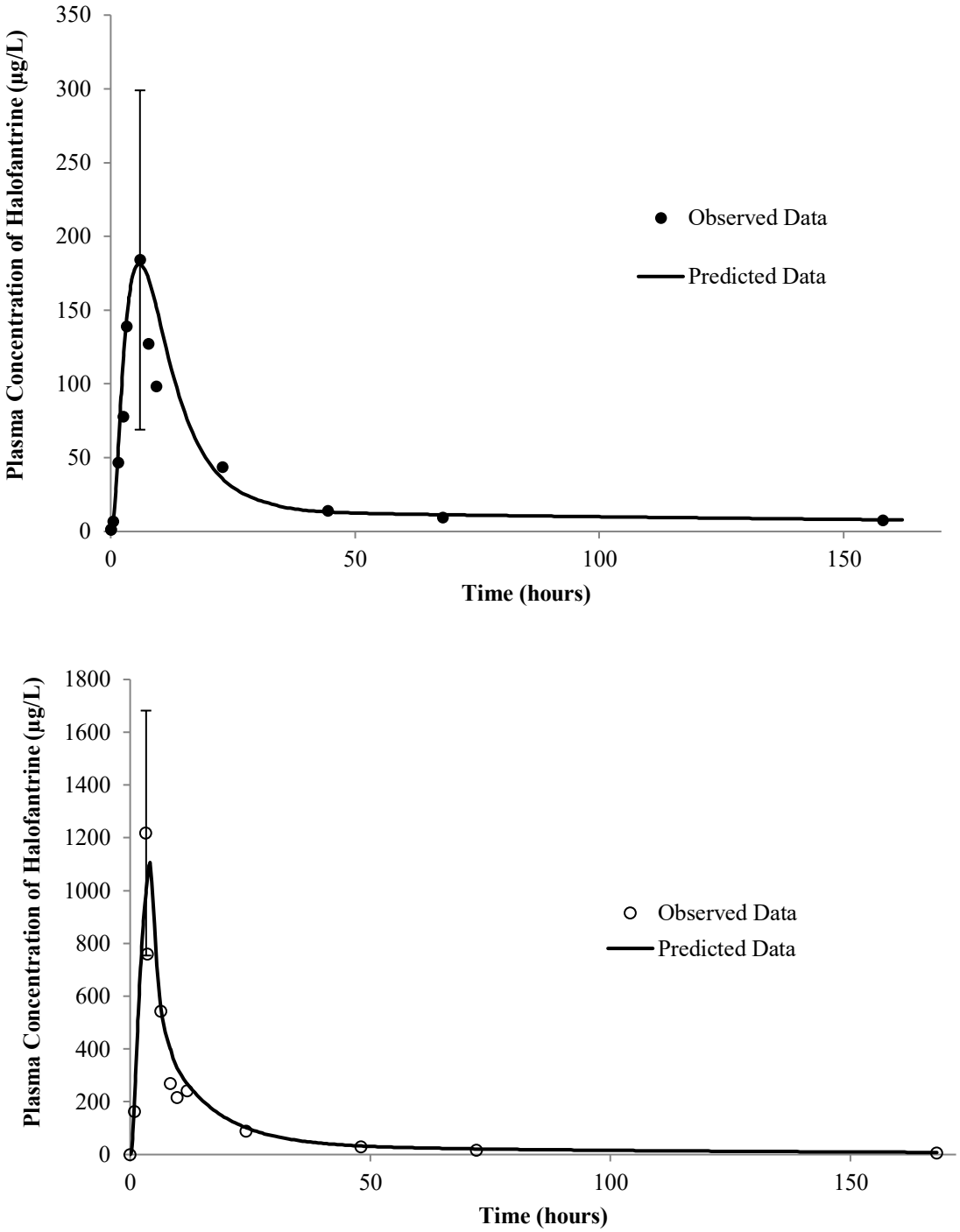

Figure 10.1. Pharmacokinetic (PK) model of simulated and observed (60) profiles of halofantrine in the fasting (top) and fed (bottom) States. Observed data represent the mean values for 6 subjects and the error bars represent the standard deviation of the observed highest plasma concentration (C_{max}).

Table 10.3. PBPK model parameters for simulated and observed (60) fasting and fed states of halofantrine.

Parameter	Fasting-state		Fed-state	
	Observed value ± s.d. (n = 6)	Predicted value	Observed value ± s.d. (n = 6)	Predicted value
$C_{max\ (\mu g/L)}$	184.0 ± 115.0	189.7	1218.0 ± 464.0	764.9
$T_{max\ (h)}$	6.0 ± 1.3	3.9	3.3 ± 1.5	3.3
$AUC_{0\text{-}t\ (\mu g.L^{-1}.h)}$	3.9 ± 2.6	4.5	11.3 ± 3.5	12.3

s.d. represents the standard deviation.

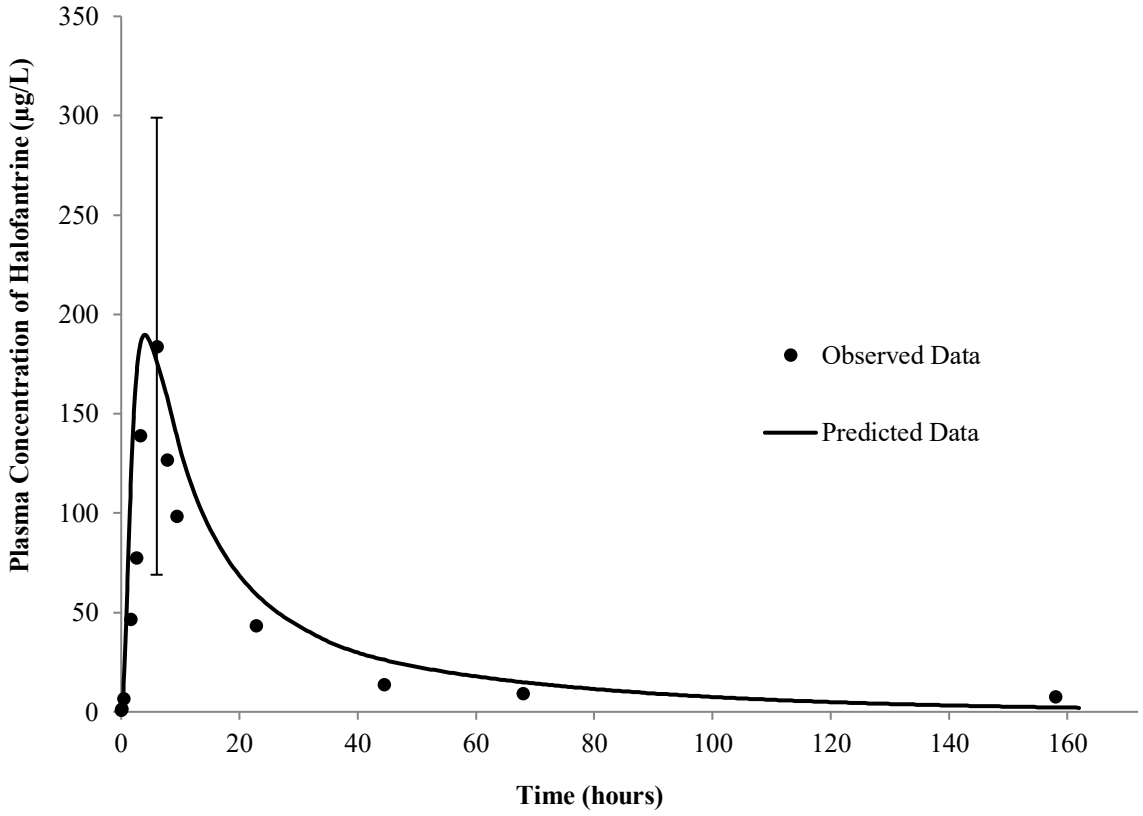

Figure 10.2. Physiologically Based Pharmacokinetic (PBPK) model of simulated and observed (60) profiles of halofantrine in the fasting state. Observed data represent the mean values for 6 subjects and the error bars represent the standard deviation of the observed highest plasma concentration (C_{max}).

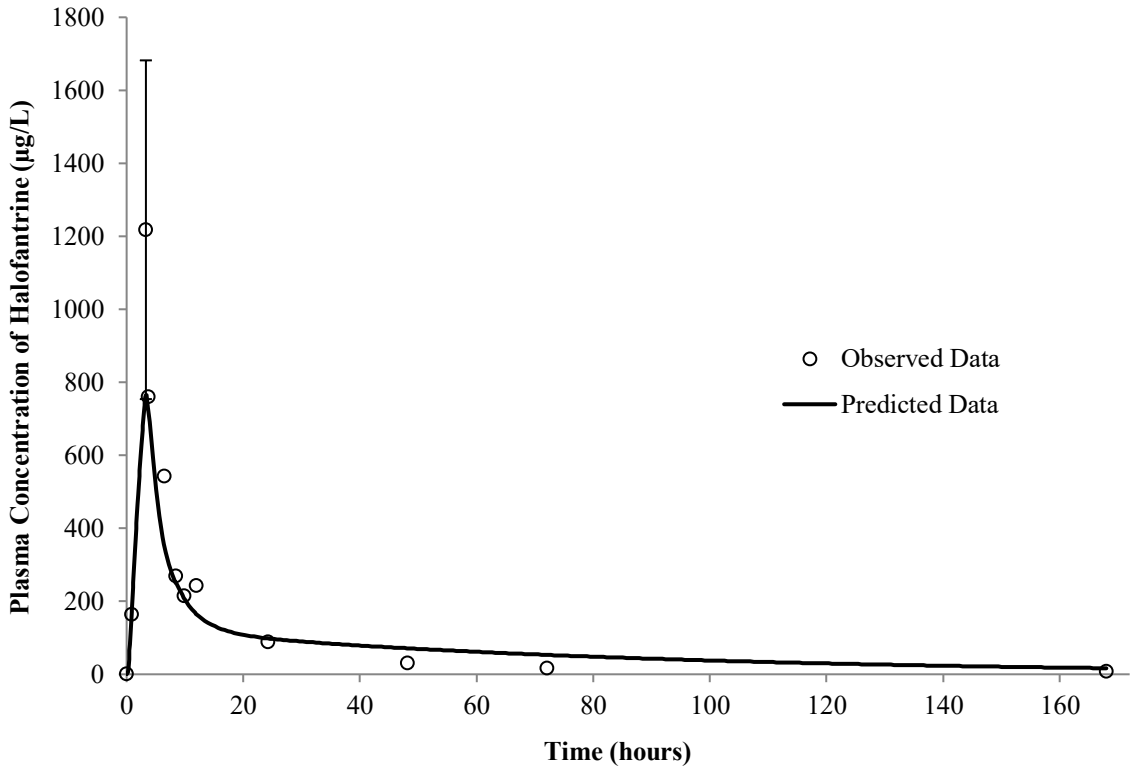

Figure 10.3. Physiologically Based Pharmacokinetic (PBPK) model of simulated and observed (60) profiles of halofantrine in the fed state. Observed data represent the mean values for 6 subjects and the error bars represent the standard deviation of the observed highest plasma concentration (C_{max}).

10.4 Discussion:

Gastroplus™ uses an advanced compartmental and transit (ACAT) model to predict absorption, distribution, metabolism, and excretion properties of drugs. In this model, the gastrointestinal tract is divided into nine compartments from the stomach to the ascending colon and accounts for the different physicochemical factors of the drug, along with the mechanistic descriptions of the underlying biophysical and biochemical processes to predict the intestinal drug absorption and *in-vivo* drug behaviour (570-572).

This work aimed at using Gastroplus™ to develop a PBPK model to investigate the behaviour of halofantrine after oral administration in the fasting and the fed-state, where in the latter significant contribution of intestinal lymphatic uptake is likely enhanced.

For the PBPK generation, determining the pharmacokinetic parameters through appropriate PK models is the first step to provide insights into the observed drug plasma profiles (573) which can be used to further develop and define the PBPK model and to help direct the building of a PBPK model based on the determined pharmacokinetic parameters.

10.4.1 PK Modeling of Halofantrine:

To obtain an accurate and descriptive PK model, an intravenous (IV) dose profile is essential to utilize in conjunction with the oral plasma profile. Intravenous administration usually provides complete bioavailability and drug delivery into the bloodstream, allowing the isolation of the absorption phase, which can be used to establish a baseline pharmacokinetic profile and model pharmacokinetic parameters such as total body clearance, volume of distribution, and elimination half-life without the possibility of contamination by unabsorbed drug (574). Additionally, it will act as a reference when calculating the oral bioavailability by comparing the oral profile to the intravenous profile from Krishna *et al.* (563, 575, 576).

For the halofantrine profiles in both states (fasting and fed), identical input parameters for the drug were utilized, as outlined in **Table 10.1**. However, the fasting-state physiology of the human body was employed for modeling the fasting-state profile, while the fed state (characterized by high fat and high calorie intake) was chosen for the fed-state profile. Additionally, the fed-state profile incorporated a shift to zero-order gastric

emptying kinetics where the gastric emptying time is calculated based on a linear correlation to the caloric content of the meal. Moreover, the bile salt concentrations in the intestinal compartments are calculated based on the percentage of fat in the meal (577).

Appreciably greater extent of halofantrine evaded the first-pass extraction by the liver when administered in the fed state. This enhanced absorption of halofantrine is likely facilitated by the absorption through the intestinal lymphatic pathway, which anatomically bypasses the liver, reducing first-pass effects and leading to higher systemic drug exposure (467, 469).

The theoretical effect of food on extraction ratio of a high extraction ratio (E) drug suggests that in the fed state, the reduced first-pass effect results in a higher proportion of the drug reaching systemic circulation compared to the fasting state and a lower extraction ratio would be evident. This phenomenon where a high E drug such as halofantrine in fasted conditions is changed to a low E drug under fed conditions can lead to an increased $C_{max,}$ and AUC, indicating enhanced oral drug bioavailability (F) in the fed state due to reduced hepatic extraction and thus more drug available for lymphatic absorption. An increase in drug AUC with increases in fraction absorbed lymphatically is highly pronounced with a high E drug (>10-fold), along with significant increases in C_{max} and AUC (284).

Another significant consideration noticed between the halofantrine fasting and fed states profiles is the number of compartments necessary to accurately model each profile. While a two-compartment model adequately represented the fasting-state condition, applying the two-compartment model to the fed-state profile failed to precisely capture its

disposition characteristics, as evidenced by two crucial goodness-of-fit criteria—the Akaike Information Criterion (AIC) and Schwarz Criterion (SC) (578, 579). For the fed-state profile, the AIC and SC values for the two-compartment model were -24.954 and -17.643, respectively. In contrast, the three-compartment model exhibited a markedly improved fit, with an AIC of -60.348 and an SC value of -50.947, both more than two-fold lower (Supplementary Materials). Therefore, the three-compartment model was selected.

In pharmacokinetic modeling, a two-compartment model typically represents drug distribution between the central compartment (blood) and a peripheral compartment (tissue). This model assumes that drug distribution throughout the body can be adequately described by these two compartments. However, in some cases, particularly when considering complex absorption processes or additional tissue compartments, a two-compartment model may not fully capture the behavior of drugs. In cases where there are significant delays in absorption, extensive tissue distribution, multiple metabolic pathways, lymphatic or lysosomal trapping, in addition to other scenarios, a more comprehensive approach with additional compartments may offer a more comprehensive understanding of the pharmacokinetic behavior of drugs. The decision to use a multi-compartment model depends on the specific characteristics of the drug being studied and the objectives of the analysis. However, introducing a third compartment in this scenario enables a more nuanced representation of the distribution and elimination kinetics of the drug under different conditions (580, 581).

In the case of the fed-state profile of halofantrine, the addition of a third compartment was proposed to better describe its disposition characteristics when taken with a fatty meal. This third compartment may help us identify the importance of an

additional input pathway of absorption and disposition is particularly evident in the fed state that may be related to the intestinal lymphatic system. Compartmental PK modeling in this software (PK Plus) is built so that the drug once crossing the basolateral intestinal barrier, it proceeds to the portal vein and subsequently enters the liver. Upon evading first-pass metabolism, the drug gains access to the systemic circulation, allowing distribution to peripheral compartments (**Figure 10.4**). Thus, the third compartment can be related theoretically to the undetermined mechanistic distribution or the uptake through the lymphatics which is involved in its absorption postprandially. Yet, the lymphatic absorption pathway is not incorporated directly into the software but accounted for indirectly in the ACAT model with the bile salt concentrations after a fatty meal and the solubility of the drug in the FeSSIF condition (577). Therefore, the third compartment was linked to a process that would be captured by the software building and it is related to disposition of the drug after reaching the general circulation which is the lysosomal trapping. Halofantrine being a weak basic lipophilic drug is reported to be trapped inside cellular lysosomes (lysosomotropic) (41, 582). This additional tissue compartment accounts for the third compartment within the fed-state profile.

Capturing lysosomal trapping in the fed-state profile rather than the fasting state profile may be attributed to the higher drug concentration reaching the general circulation and tissues, including lysosomes, when in the fed state compared to the fasting state. In the fasting state, the goodness of fit of the three-compartment model exhibited significant decline compared to the two-compartment model. Adjusting the unbound fraction in the enterocyte (Fu_{ent}) in the fasting state facilitated the lysosomally-trapped portion of halofantrine, leading to the development of a more representative PK model.

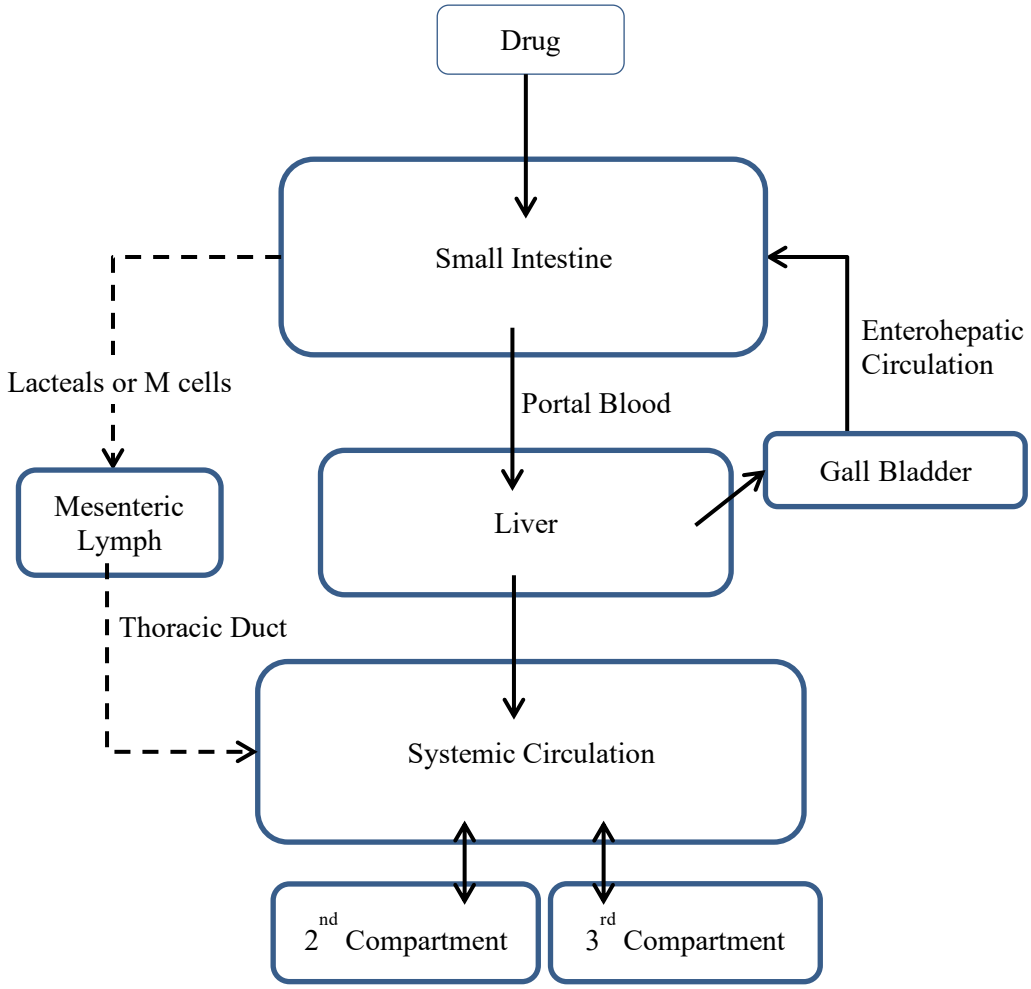

Figure 10.4. Diagram depicts the absorption pathway adopted in the *in-silico* models for orally administered drugs, utilizing continuous arrows to signify the route from the intestine through the portal vein to the liver and subsequently to the general circulation. Additionally, the overlooked absorption pathway is illustrated with dotted arrows, indicating that drugs can travel through the mesenteric lymph to enter the general circulation.

10.4.2 PBPK Modeling of Halofantrine:

The genesis here is a PBPK model for the fasting-state profile of halofantrine using physicochemical properties derived from the values presented in **Table 10.1** and the profiles documented by Milton *et al.* (60).

Given the low solubility and high permeability of halofantrine (biopharmaceutical classification system, BCS, Class II drug) (583), the distribution of the drug was determined to be perfusion-rate limited. With the perfusion-limited distribution, the accumulation rate of the drug in tissues is constrained by the blood flow rate within the tissue (perfusion rate) (584). Instantaneous partitioning is assumed, where the tissue's specific partition coefficient (Kp) is employed to determine drug partitioning between plasma and the entire tissue at each time interval. As a result, the drug concentration in the tissue is calculated as the product of the tissue Kp and the instantaneous drug concentration in the plasma during the relevant time period (585).

Renal clearance was set to (glomerular filtration rate * unbound drug fraction (GFR * Fu)) to account for the portion cleared through the kidneys. As halofantrine is primarily metabolized by the liver, chiefly through CYP 3A4 (586, 587), the K_m and V_{max} of this enzyme were incorporated, based on literature data (562).

The initial profile of the fasting-state, shaped by these inputs, aligned with the observed data but indicated a greater clearance phase than observed. Optimization of the metabolism constant and maximum velocity of enzyme reaction (K_m and V_{max}, respectively), values for CYP 3A4 resulted in the profile presented in **Figure 10.2**.

In a physiologically based model, changing the physiology to the fed-state would often predict the fed-state plasma profile especially for low extraction ratio drugs (588, 589). Thus after uploading the observed fed-state profile, and adjusting the physiological conditions to reflect the fed state (characterized by high fat and high calories) zero-order emptying option was selected for as previously mentioned. However, in this scenario a

change in the fed-state physiology is involved but an additional absorption route with pharmacokinetic implication related to the first-pass effect is suggested. As the intestinal lymphatic uptake cannot yet be directly simulated here, and taking into account that halofantrine is a high E drug, then reducing the first-pass percentage as shown with the PK modeling would be a suitable approach to adjust the PBPK model in the fed-state to reflect the increase in the drug absorption caused by reduced hepatic extraction and intestinal lymphatic uptake. Firstly, the linear clearance obtained from the non-compartment model of the concentration-time profile used was employed to develop the model in the fed-state. However, the observed C_{max} value was 2.6 times higher than the predicted one.

By altering the pKa of halofantrine to 5.6, the predicted profile approached closer to the observed profile and fell within the statistically observed values. Subsequent optimization of K_m and V_{max} was performed to eventually result in the profile depicted in **Figure 10.3**. The explanation for more accurate modeling when pKa was altered can be attributed to the administered dosage form which was the hydrochloride salt, which undergoes conversion to the free base to enhance its association with lipid digestion products. This transformation facilitates packaging into chylomicrons formed by enterocytes, enabling transportation through the intestinal lymphatic route. This process bypasses the first-pass liver extraction and clearance, leading to increased fraction absorbed. Halofantrine, being a tertiary aliphatic amine, is expected to have a high pKa. The calculated pKa was found to be 8.16 (564) as used in all previously described models. However, in a representative fed-state media (pH = 6), it was documented in the literature that halofantrine has a pKa of 5.58 ± 0.07 (565). Molecular modeling calculations suggested that the decrease in pKa might result from the folding of the side chain, bringing

the tertiary amine closer to the benzylic hydroxyl group. This spatial arrangement forms an intramolecular hydrogen bond, reducing the basicity of the amine in halofantrine (**Figure 10.5**). The shift in pKa from 8.16 to 5.58 brought about significant implications for the solubilization and absorption of halofantrine. This change increased the solubilization ratio by 16-fold, favoring its unionized form. Consequently, it enhanced its association with lipid digestion products, facilitating its absorption with approximately 80% predicted to occur primarily in the duodenum and jejunum (pH=5.4-6, according to the ACAT Model). These segments have a higher density of villi (274), where lymphatic capillaries (lacteals) are located (53) which will facilitate the traverse of halofantrine through the intestinal pathway into the general circulation.

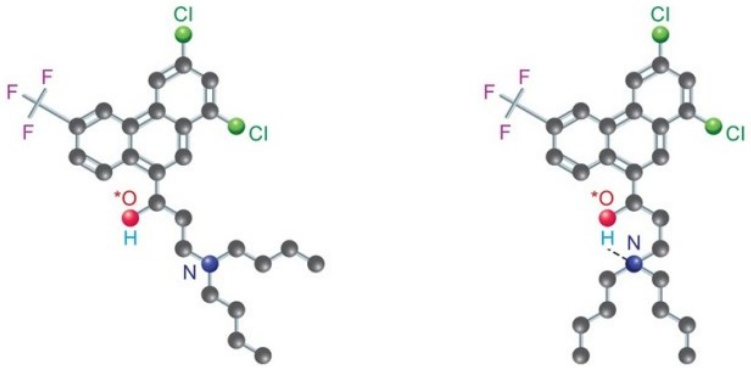

Figure 10.5. Illustration showing the side chain folding, drawing the tertiary amine nearer to the benzylic hydroxyl group (*). This spatial configuration creates an intramolecular hydrogen bond, consequently lowering the basicity of amine in halofantrine and changing the PKa from 8.16 for the left molecular configuration to 5.58 for the right molecular configuration.

As demonstrated, developing a PBPK model to reflect the intestinal lymphatic uptake is not a straightforward process, at least using the existing algorithms in Gastroplus^{TM}. For high E drugs, the most prominent and likely effect would be related to

changes in pre-systemic metabolism -as seen with the example used here- then adjusting the enzyme kinetics might help reflect additional intestinal lymphatic uptake. However, for medium and low E drugs, where adjusting the metabolism profile might not be as efficient in reflecting drugs lymphatic uptake, empirical adjustment of the different properties of individual gut compartments might also be an option. Important considerations from this could be the significance of updating the ACAT model to accommodate the intestinal lymphatic uptake route to further characterize the model and dual absorption processes of drugs reaching the general circulation through the intestinal lymphatics. By including such updates in the model, pharmaceutical scientists could more optimally simulate the absorption kinetics of lymphotropics and rationally account for the impact of food or formulation on their pharmacokinetics. Additionally, integrating the relevant equations and functions is crucial to accurately address the impact of this route on the metabolism and disposition of potential drugs and the increasingly prevalent lipid formulations utilized for hydrophobic drug delivery.

10.4 Conclusion:

This study presents an initial investigation into the *in-silico* modeling of intestinal lymphatic uptake using halofantrine as a case study. Despite the importance of the intestinal lymphatic absorption pathway, this area of research remains relatively underexplored. Theoretical considerations regarding the impact of food on the extraction ratio of high extraction ratio (E) drugs, such as halofantrine, offer avenues to modulate PBPK models for such drugs when administered in formulations targeting lymphatics or alongside food-effects that can enhance intestinal lymphatic uptake. However, it is crucial to integrate experimental data into pharmacokinetic modeling approaches for precise

predictions, as demonstrated by the variation in halofantrine pKa under post-prandial intestinal conditions. Additionally, alternative measures may be considered for medium and low E drugs. Nonetheless, all these methods are indirect, underscoring the necessity for developing alternative and direct modeling options for this critical route. Overall, this study contributes to advancing our understanding of intestinal lymphatic uptake using existing models. It also emphasizes the need to refine these models to make direct and better predictions of the intestinal lymphatic uptake, which will be reflected in improving drug development strategies, and ultimately enhancing therapeutic outcomes for patient.

Supplementary Materials:

Table 10.4. Goodness-of-fit criteria parameters for compartmental pharmacokinetic models of halofantrine in fasting and fed states.

Parameter	Fasting-state			Fed-state		
	One-Compartment Model	Two-Compartment Model	Three-Compartment Model	One-Compartment Model	Two-Compartment Model	Three-Compartment Model
AIC	-0.064	-18.297	-14.298	5.109	-24.954	-60.348
SC	5.613	-10.348	-4.078	10.332	-17.643	-50.947

AIC = Akaike Information Criterion, SC = Schwarz Criterion

SECTION FOUR: GENERAL DISCUSSION, CONCLUSION, AND FUTURE DIRECTIONS

CHAPTER ELEVEN

General Discussion

11.1 General Discussion:

11.1.1 Sub-cellular Sequestration of Orally Administered Drugs through Lysosomal Trapping:

Enterocyte lysosomal trapping represents a critical checkpoint for some orally administered drugs, which can directly affect their onset of action, distribution, half-life, and other pharmacokinetic parameters (24, 33). In the early 1970s, the Nobel laureate Christian de Duve who discovered lysosomes described the theoretical basis for lysosomal trapping. Recently, drugs undergoing this process (lysosomotropics) have been investigated for repurposing as potential treatments for COVID-19 (coronavirus disease 2019). Numerous studies have revisited known lysosomotropics to identify promising candidates for this indication (71, 590, 591). This is not unprecedented, as lysosomotropics have previously garnered attention for their potential in treating other viral infections (91) and as a novel strategy for targeting cancer (43). They are also of interest due to their involvement in drug-drug interactions (37), their role in drug resistance, particularly in anticancer treatments (95), and their association with inducing phospholipidosis and disrupting other normal cellular functions (34, 113).

In spite of the recognized significance of lysosomal trapping in enterocytes and other cells, and lysosomotropics in pharmaceutical and biomedical sciences, there is currently no universally accepted simulated or lysosomal fluid utilized within the pharmaceutical industry or endorsed by the United States Pharmacopeia. Existing fluids, such as artificial lysosomal fluid (122) and phagolysosomal fluid (123), are categorized under simulated lung fluids (126). They do not reflect lysosomal conditions but rather

represent conditions associated with cellular phagocytosis and inside phagolysosomes, respectively.

Therefore, in Chapter 2, following the introduction, our research focused on developing a simulated lysosomal fluid (SLYF) to standardize and enhance the *in-vitro* assessment of lysosomal trapping of drugs. The newly developed SLYF was designed to replicate the essential components and physiological conditions of lysosomes. To evaluate its effectiveness, the composition of the prepared fluid was compared with that of a commercially available artificial lysosomal fluid. The results indicated that SLYF more accurately reflected physiological ionic conditions than the commercial fluid (Chapter 2, table 2.7). SLYF demonstrated superiority compared to lysosomal fluids reported in the literature as well (**Table 11.1**). The *in-vitro* lysosomal trapping of dextromethorphan and racemic chloroquine was also evaluated using SLYF. The model successfully predicted lysosomal trapping for both drugs, with chloroquine demonstrating higher lysosomal accumulation than dextromethorphan, aligning with *in-vivo* expectations.

Table 11.1. Comparison of key ions for lysosomal function across the developed simulated lysosomal fluid (SLYF), and the literature reported ones (artificial lysosomal fluid, and phagolysosomal fluid).

Ions	Amount in the prepared lysosomal fluid (SLYF, mM) (29)	Amount in the artificial lysosomal fluid (mM) (122, 124-126)	Amount in the phagolysosomal fluid (mM) (123, 126)	Optimum concentration for lysosomal homeostasis (mM) (69)
Na+	59.08 ± 2.0 √	160.14 X	113.81 √	20-140
K+	3.09 ± 0.06 √	_	19.99 √	2-50
Ca2+	0.46 ± 0.02 √	0.87 X	0.2 X	~0.5
Cl-	59.1 ± 5.0 √	109.88 X	227.62 X	< 80

Standardization of SLYF would enable consistent and reproducible testing conditions across different laboratories and studies, which is crucial for comparing results and validating findings. Furthermore, utilizing a standardized SLYF can facilitate the early identification of drugs with lysosomal targeting properties, streamlining the drug development process by identifying lysosomotropic drug candidates early on. Conducting *in-vitro* experiments with SLYF can reduce the initial reliance on more complex and costly *in-vitro* and *in-vivo* studies during the early stages of drug development, saving both time and resources. Additionally, it can help identify drugs with previously unrecognized lysosomal targeting potential, supporting drug repurposing efforts for new therapeutic indications. The SLYF can be adapted for a wide range of pharmaceutical and biomedical research applications.

11.1.2 Post-cellular Uptake of Orally Administered Drugs (Intestinal Lymphatic Uptake via Chylomicrons):

Another important and sometimes overlooked consideration for orally administered drugs is their uptake through the intestinal lymphatics. The term "lymphatics" was coined in the seventeenth century, although recognition of the entire system dates back to the 4th century B.C.E (141). Despite its crucial role, the lymphatic system is underappreciated –at times- in pharmaceutical research. In **Chapter 3**, we aimed to enhance our understanding of lymphatic physiology and leverage this knowledge in pharmaceutical sciences. This chapter provided a comprehensive review of the lymphatic system and its significance in health and disease, particularly emphasizing its potential applications in the pharmaceutical field (56).

With a complex structural organization, the lymphatic system serves three main physiological roles: maintaining fluid balance, facilitating immune response, and absorbing dietary lipids (51). These functions are simultaneously active only in the intestinal region, as it is the sole area where ingested fats are absorbed. Central to this process are the lacteals, specialized lymphatic capillaries located in the intestinal villi. Lacteals absorb chylomicrons (lipid-protein complexes) formed in the enterocytes and transport them through the mesenteric lymphatic vessels to the cisterna chyli, and subsequently to the thoracic duct, which empties into the bloodstream (53). This pathway initially bypasses the liver, avoiding hepatic first-pass metabolism, allowing drugs to achieve higher bioavailability and improved pharmacokinetic profiles. This approach is particularly valuable for lipophilic drugs and those subject to significant hepatic metabolism (234, 273). Additionally, it enhances therapeutic outcomes for drugs targeting lymph-related conditions such as cancer, infections, and inflammatory diseases, as evidenced by several case studies demonstrating the efficacy of lymphatic-targeted drug delivery (56).

To further advocate for additional research aimed at optimizing lymphatic drug delivery especially via chylomicrons, **Chapter 4** elucidated the interactions between these enterocyte-formed lipoproteins and other lipoproteins within the lymphatic system. It also underscored an overview of lipoprotein biology in the lymphatic system and its implications for health and disease. Additionally, it highlighted the roles of various lipoprotein classes and their intricate interplay with the lymphatic system, providing insights into the pathophysiology of diseases such as atherosclerosis, diabetes, and obesity (178).

To investigate the intestinal lymphatic uptake, researchers have employed the mesenteric lymph duct cannulation model in rats. This approach allows for direct sampling of the mesenteric lymph node, providing a streamlined method for quantifying drugs entering the systemic circulation through the intestinal lymphatics. However, the procedure is invasive and involves complex surgical steps that can affect lymph flow and pressure, complicating sequential sampling (54, 283).

A more widely adopted technique that circumvents the limitations of the previously mentioned method is the lymph-blocking approach also in rodents. This method aims to inhibit the production and/or release of chylomicrons from enterocytes. A comprehensive compilation of various agents used in this approach, including Pluronic® L-81, puromycin, vinca alkaloids, colchicine, and cycloheximide, can be found in **Chapter 5**. This chapter provides a thorough analysis of diverse models, listing and evaluating existing studies while highlighting the gaps in current research regarding these models (592).

Urinary drug excretion has been proposed as a potential non-invasive method to investigate intestinal lymphatic uptake and renal excretion of drugs. The elimination rate of drugs through urine is directly proportional to their concentration in the bloodstream, facilitating the assessment of bioavailability. By comparing the amount of unchanged drug excreted with and without a blocking agent, the bioavailability of drugs and the extent of lymphatic transport can be estimated. However, this method is limited to drugs excreted unchanged in urine and can be influenced by factors such as hydration, renal function, and urinary pH. Additionally, it requires time-consuming sample collection, and variations in urinary flow rate and drug degradation can affect results. Inter-subject differences in renal

function introduce variability, and frequent urine collection may still pose practical, research, and clinical concerns (592).

The need for simpler and cost-effective representative models to study intestinal lymphatic uptake has been emphasized. While *in-vivo* models provide the most accurate evaluation, they pose technical challenges that require advanced surgical expertise and raise ethical concerns regarding human application (184). An alternative approach involves the use of *in-vitro* models. However, to the best of our knowledge, no representative *in-vitro* model currently exists for investigating the intestinal lymphatic uptake of drugs via chylomicrons.

To develop an *in-vitro* model for studying intestinal lymphatic uptake, the initial focus was on creating simulated lymphatic fluids (**Chapter 6**). This was driven by the lack of standardized simulated lymphatic fluid, despite its recognized importance in biopharmaceutical and dissolution studies. Consequently, two versions of simulated lymphatic fluid were developed: a general version and an intestinal version. The intestinal lymphatic fluid differs primarily by containing absorbed dietary fats in the form of chylomicrons, giving it a white color, in contrast to the clear general lymphatic fluid from other body parts (142).

Lymphatic fluid or lymph is known to contain salts, proteins, cells (primarily lymphocytes), and other components filtered from plasma into the extracellular matrix. Given that lymphatic fluid is primarily derived from the extracellular matrix (136), the ionic composition of the simulated fluids was based on that of interstitial fluid (120). Albumin, a key protein that affects drug binding and pharmacokinetics (452), constituting

about 60% of lymph protein (438), was added to the simulated fluids at concentrations reported for both general and intestinal lymphatic fluids. Additionally, artificial chylomicrons were incorporated into the intestinal lymphatic fluid to better mimic the natural composition. Findings indicated that the prepared simulated fluids more accurately resembled biological lymphatic fluid than the commercial option, particularly concerning key physicochemical variables such as pH and chemical content (ions and proteins) (264). This makes them more suitable for *in-vitro* pharmaceutical studies.

In **Chapter 7**, for developing the non-cellular *in-vitro* model, chylomicron media was utilized instead of the entire simulated lymphatic fluid. This approach was chosen because the drug-chylomicron association is a reliable indicator for assessing intestinal lymphatic uptake (52). Using natural chylomicrons can be impractical for routine use and costly due to complex technical requirements, so artificial chylomicrons were employed. These artificial chylomicrons, commercially available as the total parenteral nutrition product Intralipid® (Fresenius Kabi Canada Ltd, Toronto), mimic the size and composition of natural chylomicrons (455). They contain the same long-chain fatty acids that can form the core of natural chylomicrons (455), with 90% of natural chylomicrons composed of triglycerides of such acids (490).

The model emulates the *in-vivo* process and consists of a donor compartment that resembles the intestinal lumen, where the drug solution is placed. Additionally, there is a receiver compartment containing an artificial chylomicron medium, simulating the environment within enterocytes. These two compartments are separated by an octanol-immersed membrane, representing the lipophilic cell membrane of enterocytes. The extent

of drug incorporation into the artificial chylomicrons in this model reflects the *in-vitro* uptake portion.

Different drugs with varying lymphotropic affinities were tested, and the results indicated a correlation between their *in-vitro* lymphatic uptake and their *in-vivo* performance (350). This relationship was influenced by different molecular descriptors affecting intestinal lymphatic uptake through chylomicrons (52). To challenge the model, Pluronic® L-81, an inhibitor capable of functioning *in-vitro* (254), was used and it effectively inhibited the *in-vitro* uptake at a concentration of 1%. Upon analyzing TEM images and the size of the artificial chylomicrons with and without Pluronic® L-81, it was hypothesized that Pluronic® L-81 acts by enveloping the artificial chylomicrons, resulting in larger sizes proportional to the amount of Pluronic® L-81 used (350). This encapsulation likely prevents the tested drugs from entering the chylomicrons, suggesting a new mechanism in addition to those previously reported (334, 339, 348). This finding adds to the existing understanding of how Pluronic® L-81 inhibits chylomicron-mediated intestinal lymphatic transport of drugs. Furthermore, the enhancement of uptake was tested using peanut oil, which contains the same fatty acids as those forming the artificial chylomicrons (488). Peanut oil improved uptake, as observed through TEM, by being emulsified into the lipidic core of the artificial chylomicrons. This emulsification created a larger "carrier" area for the lymphotropic drugs to enter (350).

In **Chapter 8**, more agents were evaluated using an *in-vitro* model for their enhancement action of intestinal lymphatic uptake, focusing particularly on olive, sesame, and coconut oils due to their distinct percentages and chain lengths of fatty acids, which are known to influence *in-vivo* lymphatic uptake via chylomicrons (501, 505, 507). The

findings aligned with *in-vivo* observations that the enhancement of lymphatic uptake was associated with the percentage of long-chain fatty acids present in olive, sesame, and peanut oils (277). Interestingly, coconut oil, which is rich in medium-chain fatty acids, demonstrated the most effective performance. This superior performance was attributed to the better solubility of medium-chain fatty acids in the chylomicron media used in the *in-vitro* model. It was noted that while the model could distinguish between oils containing long-chain fatty acids, it could not effectively differentiate between long-chain and medium-chain fatty acids (62).

Following the results obtained with Pluronic® L-81 and the proposed mechanism in the previous chapter, zeta potential was considered as another biophysical factor that could influence drug-chylomicron association and consequently, intestinal lymphatic uptake. To investigate this, racemic chloroquine ($C_{18}H_{26}ClN_3$) and sodium lauryl sulfate ($C_{12}H_{25}NaO_4S$) were used, having been tested to affect the zeta potential of artificial chylomicrons in opposite ways. Chloroquine decreased the zeta potential of the artificial chylomicrons and inhibited *in-vitro* uptake, whereas sodium lauryl sulfate increased the zeta potential and enhanced the uptake (62). This prompted further questions about whether similar effects would be observed *in-vivo*, as there were no existing reports linking these agents to the lymphatic uptake of potential lymphotropics. Additionally, the various mechanisms underlying the incorporation of drugs into chylomicrons remain to be elucidated.

A practical application of the model was demonstrated in developing a formulation for cannflavin A, incorporating a known synthetic enhancer of lymphatic uptake (Labrafil®

M 2125 CS). Upon testing, the *in-vitro* uptake of cannflavin A was significantly better when combined with Labrafil® M 2125 CS compared to when it was tested without it (62).

In Chapter 5 it was shown that general bioavailability equation does not account for all pathways through which orally administered drugs enter the systemic circulation. While most drugs pass from the GIT into the systemic circulation via the portal blood, some may take alternative routes, such as the intestinal lymphatic system and possibly through chylomicrons. This assumption that all drugs are absorbed through the portal blood underlies known dissolution testing methods as well (527). Therefore, for lymphotropics a more representative dissolution model should be used—one that considers both blood and lymphatic pathways through which active pharmaceutical ingredients (APIs) may enter the general circulation.

In **Chapter 9**, the release profiles of three commercial products of the lymphotropic drug, terbinafine, were evaluated using modified USP Apparatus II and IV. These modified apparatuses featured an artificial chylomicron-containing compartment within the dissolution vessel, providing a lipid dissolution sink specifically for lymphotropic drugs. Distinct release patterns were noted in both aqueous and lymphatic media, with the modified USP IV apparatus demonstrating greater variation in aqueous release profiles. This setup more accurately represented physiological conditions, incorporating both simulated gastric and intestinal environments (593).

To verify the ability of the developed model to accurately distinguish lymphotropic drugs, a comparative analysis was performed using the biphasic method (530). Interestingly, in the biphasic model, both a lymphotropic drug and a non-lymphotropic

drug exhibited almost identical behavior in the octanol phase (530). However, in the model proposed in this chapter, the uptake into the lymphatic compartment varied among different lymphotropic drugs, even though the aqueous solubility of these lymphotropics was similar (Figure 9.6).

Another alternative that avoids the complexity of *in-vivo* models is the use of *in-silico* models. However, for studying intestinal lymphatic uptake, this approach remains largely unexplored. To our knowledge, only one *in-silico* model has been developed to quantify the relationship between molecular structure and lymphatic transfer of lipophilic compounds using long-chain triglyceride vehicles. This model employed the VolSurf program and partial least squares (PLS) analysis (235). With physiologically based pharmacokinetic (PBPK) models increasingly being used in regulatory submissions, **Chapter 10** addresses this gap by constructing a PBPK model using GastroPlus™ software 9.8.3 (Simulation Plus, Inc., Lancaster, US) and data from published literature to simulate the lymphatic uptake of halofantrine after a fatty meal (60).

One report was found for a PBPK model including intestinal lymphatic uptake using the Multi-layer gut wall Advanced Dissolution, Absorption and Metabolism (M-ADAM) framework in Simcyp software (V19 Release 1, Simcyp, Sheffield, UK), which simulates drug absorption across different sections of the gastrointestinal tract. Parameters such as capillary permeability, lymph flow rate, and the lymphatic reflection coefficient were adjusted to represent the transport of halofantrine through the lymphatic system after a meal. Additionally, micelle-to-buffer partitioning and solubility data were included to mimic the interaction of the drug with bile micelles, which aided in its movement into the lymph, allowing the model to capture lymphatic absorption (594).

Interestingly, in the PBPK model developed in Chapter 10, the modeling strategy was differnet and the interplay between lysosomal trapping and lymphatic uptake primarily in the fed-state was evident. The presence of a third compartment in the pharmacokinetic (PK) model in the fed-state, absent in the fasting-state model, underscored the significant role of lysosomal trapping alongside enhanced lymphatic uptake. The lymphatic absorption pathway resulted in higher drug bioavailability and distinct pharmacokinetic profiles under post-prandial conditions. However, it is not directly incorporated into the GastroPlus™; it was accounted for indirectly in the PBPK model through adjustments of metabolism kinetics of halofantrine under fed conditions. These findings highlighted the need to update existing algorithms and built-in models to include the intestinal lymphatic uptake route. Such updates would enable the development of validated PBPK models that more accurately simulate lymphotropic drug absorption kinetics. This improvement would enhance drug development, support regulatory approval, provide mechanistic insights, reduce animal testing, and facilitate applications to special populations among other potential advantages (595).

CHAPTER TWELVE

Conclusion and Future Directions

12.1 Conclusion:

This thesis enhances our understanding of lysosomal trapping and intestinal lymphatic uptake via chylomicrons, two important phenomena in oral drug delivery. It introduced the SLYF fluid, a new laboratory-prepared lysosomal fluid, which surpassed existing commercial options in replicating lysosomal conditions. Additionally, a new simulated lymphatic fluid was developed, which more accurately mimiced biological fluids than existing commercial versions. The research also identified limitations in current models and agents used for quantifying intestinal lymphatic uptake, along with the development of more accurate *in-vitro* and dissolution models for investigating the intestinal lymphatic uptake through chylomicrons. These models demonstrated their potential for use to optimize drug formulations by evaluating excipients, oils, and other factors that affect lymphatic uptake, offering practical applications for drug delivery systems targeting intestinal lymphatics. Furthermore, the study highlighted the necessity of refining *in-silico* models to include lymphatic uptake for more accurate predictions of drug behaviour, facilitating future drug development and regulatory approval.

For the lysosomal trapping part, a lysosomal fluid, termed SLYF fluid, was developed incorporating the essential components necessary for lysosomal homeostasis. The superiority of SLYF fluid over existing commercial fluids, in terms of composition and physiological attributes, was demonstrated in a basic model for capturing lysosomal sequestration. This indicates that SLYF fluid could effectively fill the current gap for a standardized lysosomal fluid applicable to various pharmaceutical and biomedical applications.

Reviewing existing reports on intestinal uptake, particularly through chylomicrons, helped identify gaps in knowledge and applications that could facilitate developing optimized lymphatic-targeted drug delivery formulations and systems. A new and detailed pharmacokinetic equation for bioavailability incorporating this pathway was formulated. Moreover, the current limitations of the agents frequently used in *in-vivo* models for studying the lymphatic route of chylomicrons, including PL-81, puromycin, vinca alkaloids, colchicine, and cycloheximide, were identified. In addition, a non-invasive method utilizing urinary excretion of drug data was proposed, with its advantages and limitations highlighted.

For the *in-vitro* studies related to intestinal lymphatic uptake, the developed simulated general and intestinal lymphatic fluids were found to more closely resemble biological fluid than the commercially available artificial lymphatic fluid. These findings represent a step towards addressing the current need for a standardized simulated lymphatic fluid in pharmaceutical research.

Additionally, the developed *in-vitro* model offered a promising platform for evaluating the lymphatic uptake of drugs and their potential for targeted drug delivery. It was demonstrated that the model can be utilized to explore the impact of excipients on enhancing or inhibiting intestinal lymphatic uptake, thereby aiding in formulation development. Also, the model could potentially investigate the effects of fat-containing meals that may stimulate lymphatic uptake. The model successfully differentiated between drugs with varying lymphotropic affinities, correlating these differences to potential *in-vivo* behavior based on the molecular descriptors of the tested drugs. Furthermore, the model was utilized to enhance uptake using oils recognized as natural enhancers of the

chylomicron pathway for lymphatic uptake. This is relevant to the food effect and its impact on the pharmacokinetics and pharmacodynamics of potential lymphotropics. The obtained results revealed the ability of the model to distinguish between oils containing long-chain fatty acids. However, it did not differentiate between these long-chain-rich oils and medium-chain-rich oil in terms of lymphatic uptake. Pluronic® L-81, another known agent, exhibited an inhibitory effect in the model, likely through a novel biophysical mechanism involving the coating of Intralipid® particles. Moreover, the data indicated that zeta potential influences intestinal lymphatic uptake, resulting in corresponding increases and decreases in uptake within the *in-vitro* model based on the agent used. This novel finding necessitates further *in-vitro* and *in-vivo* investigations.

In a practical application, the utility of the model was demonstrated by investigating and confirming the enhanced intestinal uptake of a tested formulation containing a known synthetic enhancer for intestinal lymphatic uptake. This finding highlighted the potential of the model to develop more effective drug delivery systems targeting the intestinal lymphatics.

The increasing focus on lipid-based formulations has highlighted an imminent need for more refined performance testing methods. To address this, lymph-focused first-generation dissolution models were developed to assess formulations and identify factors that may influence chylomicron uptake. These new models considered the lymphatic absorption pathway, which was overlooked in all current existing USP dissolution tests. They also demonstrated superiority to the biphasic dissolution test in assessing lipid solubility related to lymphatic uptake via chylomicrons. This development represented an

important step towards more representative performance testing for lymph-targeted formulations.

For the various benefits offered by *in-silico* models, particularly Physiologically Based Pharmacokinetic (PBPK) modelling, a case study of halofantrine was used to advance our understanding of intestinal lymphatic uptake. Being lysosomotropic, the development of the model linked both lysosomal trapping and lymphatic uptake of halofantrine to their potential effects on different pharmacokinetic parameters. More importantly, it emphasized the need to refine existing simulation algorithms and *in-silico* absorption models to include intestinal lymphatic uptake. This inclusion would allow for more accurate predictions of drug behaviour and a better mechanistic understanding of lymphotropic drugs or formulations, ultimately aiding in enhanced formulation development and facilitate regulatory submission.

12.2 Future Directions:

12.2.1 Sub-cellular Sequestration of Orally Administered Drugs through Lysosomal Trapping:

Preliminary data from the fluid and the basic model for lysosomal trapping of drugs have demonstrated its pharmaceutical utility (**Chapter 2**). By refining the model to reflect physiological temperature and validating it through correlating *in-vitro* performance with *in-vivo* results for a larger group of lysosomotropic drugs, this experimental design approach can be further extended to investigate drug sequestration in other subcellular compartments, such as mitochondria, endosomes, and others.

12.2.2 Post-cellular Uptake of Orally Administered Drugs (Intestinal Lymphatic Uptake via Chylomicrons):

Documented reports highlighted the need for future research to elucidate the detailed mechanisms of the entry and transport of drugs through the intestinal lymphatic system. Moreover, additional studies related to *in-vivo* chylomicron blockage models could be explored. While many vinca alkaloids have been reported to affect triglyceride profiles and potentially block chylomicrons, only vincristine and vinblastine have been tested for this purpose. Therefore, other vinca alkaloids that have been reported to disrupt triglyceride absorption could be investigated as potential chylomicron blockers. Furthermore, additional research is needed to determine the effective and toxic doses of colchicine to gain a better understanding of its clinical impact on blocking the chylomicron pathway in humans.

The developed *in-vitro* model for studying lymphatic uptake via chylomicrons represents a foundational step towards creating a physiologically-based predictive tool for estimating drug interactions with chylomicrons and their subsequent lymphatic transport. Enhancing the model by incorporating microsomes would help simulate the pre-systemic metabolic loss occurring at the enterocyte stage of drug absorption. Moreover, integrating lipolysis into the current framework could account for the portion of the drug that is digested and absorbed by enterocytes, thereby further improving the accuracy of the model and its physiological relevance.

The developed lymph-focused dissolution models have demonstrated potential in evaluating lymphatic uptake via chylomicrons, an area previously unexplored. However, these models can be further refined; for instance, incorporating surfactants could help

maintain drug solubility in the alkaline conditions of the modified apparatus IV, which simulates both gastric and intestinal environments and thus presents solubility challenges for alkaline drugs in the second stage. Also, continuous sampling from the lymphatic compartment could be explored to enable simultaneous monitoring of drug uptake profiles into the lymphatic region alongside the aqueous dissolution profile. This approach would provide insights into the dynamics of drug absorption into both portal and lymphatic pathways.

For all models, establishing a correlation with *in-vivo* lymphatic uptake through a mathematical framework would aid in achieving the ultimate goal of *in-vitro-in-vivo* correlation. This correlation would provide a predictive capability that would reduce the reliance on animal studies, thereby addressing animal ethics concerns and cutting down on the time and resources required for preclinical testing. Furthermore, having a validated mathematical model that reliably predicts *in-vivo* behavior could streamline regulatory submissions, providing strong supportive data and potentially accelerating the approval process for new therapies. This approach will hopefully enhance scientific understanding and also foster innovation in drug development.

Bibliography

1. Alqahtani MS, Kazi M, Alsenaidy MA, Ahmad MZ. Advances in oral drug delivery. Frontiers in Pharmacology. 2021;12:618411.

2. Lou J, Duan H, Qin Q, Teng Z, Gan F, Zhou X, et al. Advances in oral drug delivery systems: Challenges and opportunities. Pharmaceutics. 2023;15(2):484.

3. Homayun B, Lin X, Choi H-J. Challenges and recent progress in oral drug delivery systems for biopharmaceuticals. Pharmaceutics. 2019;11(3):129.

4. Abuhelwa AY, Williams DB, Upton RN, Foster DJR. Food, gastrointestinal pH, and models of oral drug absorption. European Journal of Pharmaceutics and Biopharmaceutics. 2017;112:234-48.

5. Hogben CAM, Tocco DJ, Brodie BB, Schanker LS. On the mechanism of intestinal absorption of drugs. Journal of Pharmacology and Experimental Therapeutics. 1959;125(4):275-82.

6. Caspary WF. Physiology and pathophysiology of intestinal absorption. The American Journal of Clinical Nutrition. 1992;55(1):299S-308S.

7. Reid EW. IV. On intestinal absorption, especially on the absorption of serum, peptone, and glucose. Philosophical Transactions of the Royal Society of London Series B, Containing Papers of a Biological Character. 1900;192(178-184):211-97.

8. Zhu L, Lu L, Wang S, Wu J, Shi J, Yan T, et al. Oral absorption basics: Pathways and physicochemical and biological factors affecting absorption. Developing Solid Oral Dosage Forms: Elsevier; 2017. p. 297-329.

9. Mudie DM, Amidon GL, Amidon GE. Physiological parameters for oral delivery and *in-vitro* testing. Molecular Pharmaceutics. 2010;7(5):1388-405.

10. Chillistone S, Hardman JG. Factors affecting drug absorption and distribution. Anaesthesia & Intensive Care Medicine. 2017;18(7):335-9.

11. Pusztai A. Transport of proteins through the membranes of the adult gastrointestinal tract—a potential for drug delivery? Advanced Drug Delivery Reviews. 1989;3(2):215-28.

12. Aulton ME, Taylor KMG. Aulton's Pharmaceutics E-Book: The Design and Manufacture of Medicines: Elsevier Health Sciences; 2017.

13. Lennernäs H. Intestinal permeability and its relevance for absorption and elimination. Xenobiotica. 2007;37(10-11):1015-51.

14. Sugano K, Kansy M, Artursson P, Avdeef A, Bendels S, Di L, et al. Coexistence of passive and carrier-mediated processes in drug transport. Nature Reviews Drug Discovery. 2010;9(8):597-614.

15. Yalkowsky SH. Perspective on improving passive human intestinal absorption. Journal of Pharmaceutical Sciences. 2012;101(9):3047-50.

16. Foroozandeh P, Jusoh SAM, Shamsuddin S. Passive drug delivery, mechanisms of uptake, and intracellular trafficking. Organelle and Molecular Targeting: CRC Press; 2021. p. 129-52.

17. Mandal A, Agrahari V, Khurana V, Pal D, Mitra AK. Transporter effects on cell permeability in drug delivery. Expert Opinion on Drug Delivery. 2017;14(3):385-401.

18. Wanamaker R, Grimm I. Encyclopedia of Gastroenterology. Gastroenterology. 2004;127(4):1274-5.

19. Peterson LW, Artis D. Intestinal epithelial cells: Regulators of barrier function and immune homeostasis. Nature Reviews Immunology. 2014;14(3):141-53.

20. Okumura R, Takeda K. Roles of intestinal epithelial cells in the maintenance of gut homeostasis. Experimental & Molecular Medicine. 2017;49(5):e338-e.

21. Kong S, Zhang YH, Zhang W. Regulation of intestinal epithelial cells properties and functions by amino acids. BioMed Research International. 2018;2018(1):2819154.

22. Gavhane YN, Yadav AV. Loss of orally administered drugs in GI tract. Saudi Pharmaceutical Journal. 2012;20(4):331-44.

23. Martinez MN, Amidon GL. A mechanistic approach to understanding the factors affecting drug absorption: A review of fundamentals. The Journal of Clinical Pharmacology. 2002;42(6):620-43.

24. Bednarczyk D, Sanghvi MV. The impact of assay recovery on the apparent permeability, a function of lysosomal trapping. Xenobiotica. 2020;50(7):753-60.

25. Kazmi F, Hensley T, Pope C, Funk RS, Loewen GJ, Buckley DB, et al. Lysosomal sequestration (trapping) of lipophilic amine (cationic amphiphilic) drugs in immortalized human hepatocytes (Fa2N-4 cells). Drug Metabolism and Disposition. 2013;41(4):897-905.

26. Bonam SR, Wang F, Muller S. Lysosomes as a therapeutic target. Nature reviews Drug discovery. 2019;18(12):923-948.

27. Baltazar GC, Guha S, Lu W, Lim J, Boesze-Battaglia K, Laties AM, et al. Acidic nanoparticles are trafficked to lysosomes and restore an acidic lysosomal pH and degradative function to compromised ARPE-19 cells. PloS One. 2012;7(12):e49635.

28. Trapp S, Rosania GR, Horobin RW, Kornhuber J. Quantitative modeling of selective lysosomal targeting for drug design. European Biophysics Journal. 2008;37:1317-28.

29. Yousef M, Le TS, Zuo J, Park C, Chacra NB, Davies NM, et al. Sub-cellular sequestration of alkaline drugs in lysosomes: New insights for pharmaceutical development of lysosomal fluid. Research in Pharmaceutical Sciences. 2023;18(1):1-15.

30. Fu D, Zhou J, Zhu WS, Manley PW, Wang YK, Hood T, et al. Imaging the intracellular distribution of tyrosine kinase inhibitors in living cells with

quantitative hyperspectral stimulated Raman scattering. Nature Chemistry. 2014;6(7):614-22.

31. Peng B, Lloyd P, Schran H. Clinical pharmacokinetics of imatinib. Clinical Pharmacokinetics. 2005;44:879-94.

32. Hayeshi R, Masimirembwa C, Mukanganyama S, Ungell ALB. Lysosomal trapping of amodiaquine: Impact on transport across intestinal epithelia models. Biopharmaceutics & Drug Disposition. 2008;29(6):324-34.

33. Bolger MB, Macwan JS, Sarfraz M, Almukainzi M, Löbenberg R. The irrelevance of *in-vitro* dissolution in setting product specifications for drugs like dextromethorphan that are subject to lysosomal trapping. Journal of Pharmaceutical Sciences. 2019;108(1):268-78.

34. Funk RS, Krise JP. Cationic amphiphilic drugs cause a marked expansion of apparent lysosomal volume: Implications for an intracellular distribution-based drug interaction. Molecular Pharmaceutics. 2012;9(5):1384-95.

35. Assmus F, Houston JB, Galetin A. Incorporation of lysosomal sequestration in the mechanistic model for prediction of tissue distribution of basic drugs. European Journal of Pharmaceutical Sciences. 2017;109:419-30.

36. Daniel WA, Wojcikowski J. The role of lysosomes in the cellular distribution of thioridazine and potential drug interactions. Toxicology and Applied Pharmacology. 1999;158(2):115-24.

37. Logan R, Funk RS, Axcell E, Krise JP. Drug-drug interactions involving lysosomes: Mechanisms and potential clinical implications. Expert Opinion on Drug Metabolism & Toxicology. 2012;8(8):943-58.

38. Homewood CA, Warhurst DC, Peters W, Baggaley VC. Lysosomes, pH and the anti-malarial action of chloroquine. Nature. 1972;235(5332):50-2.

39. Zhai X, El Hiani Y. Getting lost in the cell–lysosomal entrapment of chemotherapeutics. Cancers. 2020;12(12):3669.

40. Daniel WA. Mechanisms of cellular distribution of psychotropic drugs. Significance for drug action and interactions. Progress in Neuro-Psychopharmacology and Biological Psychiatry. 2003;27(1):65-73.

41. Logan R, Kong A, Krise JP. Evaluating the roles of autophagy and lysosomal trafficking defects in intracellular distribution-based drug-drug interactions involving lysosomes. Journal of Pharmaceutical Sciences. 2013;102(11):4173-80.

42. Kornhuber J, Retz W, Riederer P. Slow accumulation of psychotropic substances in the human brain. Relationship to therapeutic latency of neuroleptic and antidepressant drugs? Journal of Neural Transmission-Supplements only. 1995(46):315-24.

43. Kaufmann AM, Krise JP. Lysosomal sequestration of amine-containing drugs: analysis and therapeutic implications. Journal of Pharmaceutical Sciences. 2007;96(4):729-46.

44. Breiden B, Sandhoff K. Emerging mechanisms of drug-induced phospholipidosis. Biological Chemistry. 2019;401(1):31-46.

45. Anderson N, Borlak J. Drug-induced phospholipidosis. FEBS letters. 2006;580(23):5533-40.

46. Pessayre D, Fromenty B, Berson A, Robin M-A, Lettéron P, Moreau R, et al. Central role of mitochondria in drug-induced liver injury. Drug Metabolism Reviews. 2012;44(1):34-87.

47. Gong Y, Duvvuri M, Krise JP. Separate roles for the Golgi apparatus and lysosomes in the sequestration of drugs in the multidrug-resistant human leukemic cell line HL-60. Journal of Biological Chemistry. 2003;278(50):50234-9.

48. Lee CM, Tannock IF. Inhibition of endosomal sequestration of basic anticancer drugs: influence on cytotoxicity and tissue penetration. British Journal of Cancer. 2006;94(6):863-9.

49. Hussain MM. A proposed model for the assembly of chylomicrons. Atherosclerosis. 2000;148(1):1-15.

50. Williams CM, Bateman PA, Jackson KG, Yaqoob P. Dietary fatty acids and chylomicron synthesis and secretion. Biochemical Society Transactions. 2004;32(1):55-8.

51. Trevaskis NL, Kaminskas LM, Porter CJH. From sewer to saviour—targeting the lymphatic system to promote drug exposure and activity. Nature Reviews Drug Discovery. 2015;14(11):781-803.

52. Lu Y, Qiu Y, Qi J, Feng M, Ju D, Wu W. Biomimetic reassembled chylomicrons as novel association model for the prediction of lymphatic transportation of highly lipophilic drugs via the oral route. International Journal of Pharmaceutics. 2015;483(1-2):69-76.

53. Cifarelli V, Eichmann A. The intestinal lymphatic system: functions and metabolic implications. Cellular and Molecular Gastroenterology and Hepatology. 2019;7(3):503-13.

54. Zhang Z, Lu Y, Qi J, Wu W. An update on oral drug delivery via intestinal lymphatic transport. Acta Pharmaceutica Sinica B. 2021.

55. Managuli RS, Raut SY, Reddy MS, Mutalik S. Targeting the intestinal lymphatic system: A versatile path for enhanced oral bioavailability of drugs. Expert Opinion on Drug Delivery. 2018;15(8):787-804.

56. Yousef M, Silva D, Chacra NB, Davies N, Löbenberg R. The lymphatic system: A sometimes-forgotten compartment in pharmaceutical sciences. Journal of Pharmacy & Pharmaceutical Sciences. 2021;24:533-47.

57. Wang D, Jiang Q, Dong Z, Meng T, Hu F, Wang J, et al. Nanocarriers transport across the gastrointestinal barriers: the contribution to oral bioavailability via blood circulation and lymphatic pathway. Advanced Drug Delivery Reviews. 2023;203:115130.

58. Feeney OM, Gracia G, Brundel DHS, Trevaskis NL, Cao E, Kaminskas LM, et al. Lymph-directed immunotherapy–Harnessing endogenous lymphatic distribution

pathways for enhanced therapeutic outcomes in cancer. Advanced Drug Delivery Reviews. 2020;160:115-35.

59. Elz AS, Trevaskis NL, Porter CJH, Bowen JM, Prestidge CA. Smart design approaches for orally administered lipophilic prodrugs to promote lymphatic transport. Journal of Controlled Release. 2022;341:676-701.

60. Milton KA, Edwards G, Ward SA, Orme ML, Breckenridge AM. Pharmacokinetics of halofantrine in man: Effects of food and dose size. British Journal of Clinical Pharmacology. 1989;28(1):71-7.

61. Yao M, McClements DJ, Zhao F, Craig RW, Xiao H. Controlling the gastrointestinal fate of nutraceutical and pharmaceutical-enriched lipid nanoparticles: From mixed micelles to chylomicrons. NanoImpact. 2017;5:13-21.

62. Yousef M, O'Croinin C, Le TS, Park C, Zuo J, Bou Chacra N, et al. *In-vitro* predictive model for intestinal lymphatic uptake: Exploration of additional enhancers and inhibitors. Pharmaceutics. 2024;16(6):768.

63. Fung CH, Woo HE, Asch SM, editors. Controversies and legal issues of prescribing and dispensing medications using the Internet, 2004: Elsevier.

64. Shackleford DM, Faassen WAF, Houwing N, Lass H, Edwards GA, Porter CJH, et al. Contribution of lymphatically transported testosterone undecanoate to the systemic exposure of testosterone after oral administration of two andriol formulations in conscious lymph duct-cannulated dogs. Journal of Pharmacology and Experimental Therapeutics. 2003;306(3):925-33.

65. Lee JB, Zgair A, Malec J, Kim TH, Kim MG, Ali J, et al. Lipophilic activated ester prodrug approach for drug delivery to the intestinal lymphatic system. Journal of Controlled Release. 2018;286:10-9.

66. Yoshida T, Kojima H, Sako K, Kondo H. Drug delivery to the intestinal lymph by oral formulations. Pharmaceutical Development and Technology. 2022;27(2):175-89.

67. Pandya P, Giram P, Bhole RP, Chang H-I, Raut SY. Nanocarriers based oral lymphatic drug targeting: Strategic bioavailability enhancement approaches. Journal of Drug Delivery Science and Technology. 2021;64:102585.

68. Miao YB, Lin YJ, Chen KH, Luo PK, Chuang SH, Yu YT, et al. Engineering nano- and microparticles as oral delivery vehicles to promote intestinal lymphatic drug transport. Advanced Materials. 2021;33(51):2104139.

69. Bernier-Latmani J, Petrova TV. Intestinal lymphatic vasculature: Structure, mechanisms and functions. Nature Reviews Gastroenterology & Hepatology. 2017;14(9):510.

70. Schmitt MV, Lienau P, Fricker G, Reichel A. Quantitation of lysosomal trapping of basic lipophilic compounds using *in-vitro* assays and in silico predictions based on the determination of the full pH profile of the endolysosomal system in rat hepatocytes. Drug Metabolism and Disposition. 2019;47(1):49-57.

71. Norinder U, Tuck A, Norgren K, Kos VM. Existing highly accumulating lysosomotropic drugs with potential for repurposing to target COVID-19. Biomedicine & Pharmacotherapy. 2020;130:110582.

72. Lane TR, Dyall J, Mercer L, Goodin C, Foil DH, Zhou H, et al. Repurposing Pyramax®, quinacrine and tilorone as treatments for Ebola virus disease. Antiviral Research. 2020;182:104908.

73. Hu M, Carraway Iii KL. Repurposing cationic amphiphilic drugs and derivatives to engage lysosomal cell death in cancer treatment. Frontiers in Oncology. 2020;10:605361.

74. Trapp S, Horobin RW. A predictive model for the selective accumulation of chemicals in tumor cells. European Biophysics Journal. 2005;34:959-66.

75. Macintyre AC, Cutler DJ. The potential role of lysosomes in tissue distribution of weak bases. Biopharmaceutics & Drug Disposition. 1988;9(6):513-26.

76. Radisavljevic Z. Lysosome activates AKT inducing cancer and metastasis. Journal of Cellular Biochemistry. 2019;120(8):12123-7.

77. Saftig P, Klumperman J. Lysosome biogenesis and lysosomal membrane proteins: trafficking meets function. Nature Reviews Molecular Cell Biology. 2009;10(9):623-35.

78. Govindaraj J, Govindaraj K, Padmavathy K, Jayesh R, Mathangi VU. Review On lysosomal enzymes. European Journal of Molecular and Clinical Medicin. 2020;7(8):1688-92.

79. Christensen KA, Myers JT, Swanson JA. pH-dependent regulation of lysosomal calcium in macrophages. Journal of Cell Science. 2002;115(3):599-607.

80. DiCiccio JE, Steinberg BE. Lysosomal pH and analysis of the counter ion pathways that support acidification. Journal of General Physiology. 2011;137(4):385-90.

81. De Duve C, De Barsy T, Poole B, Tulkens P. Lysosomotropic agents. Biochemical Pharmacology. 1974;23(18):2495-531.

82. Ndolo RA, Luan Y, Duan S, Forrest ML, Krise JP. Lysosomotropic properties of weakly basic anticancer agents promote cancer cell selectivity *in-vitro*. PloS One. 2012;7(11):e49366.

83. Marceau F, Bawolak M-T, Lodge R, Bouthillier J, Gagné-Henley A, René C, et al. Cation trapping by cellular acidic compartments: Beyond the concept of lysosomotropic drugs. Toxicology and Applied Pharmacology. 2012;259(1):1-12.

84. Daniel WA, Wöjcikowski J. Contribution of lysosomal trapping to the total tissue uptake of psychotropic drugs. Pharmacology & Toxicology. 1997;80(2):62-8.

85. Daniel WA, Bickel MH, Honegger UE. The contribution of lysosomal trapping in the uptake of desipramine and chloroquine by different tissues. Pharmacology & Toxicology. 1995;77(6):402-6.

86. Fong KY, Wright DW. Hemozoin and antimalarial drug discovery. Future Medicinal Chemistry. 2013;5:1437–1450.

87. Kornhuber J, Reichel M, Tripal P, Groemer TW, Henkel AW, Mühle C, et al. The role of ceramide in major depressive disorder. European Archives of Psychiatry and Clinical Neuroscience. 2009;259:199-204.

88. Beckmann N, Sharma D, Gulbins E, Becker KA, Edelmann B. Inhibition of acid sphingomyelinase by tricyclic antidepressants and analogons. Frontiers in Physiology. 2014;5:331.

89. Llanos S, Megias D, Blanco-Aparicio C, Hernández-Encinas E, Rovira M, Pietrocola F, et al. Lysosomal trapping of palbociclib and its functional implications. Oncogene. 2019;38(20):3886-902.

90. Dhillon S. Palbociclib: First global approval. Drugs. 2015;75:543-51.

91. Salata C, Calistri A, Parolin C, Baritussio A, Palù G. Antiviral activity of cationic amphiphilic drugs. Expert Review of Anti-infective Therapy. 2017;15(5):483-92.

92. Naghipour S, Ghodousi M, Rahsepar S, Elyasi S. Repurposing of well-known medications as antivirals: Hydroxychloroquine and chloroquine–from HIV-1 infection to COVID-19. Expert Review of Anti-infective Therapy. 2020;18(11):1119-33.

93. Vaugeois J-M. Psychotropics drugs with cationic amphiphilic properties may afford some protection against SARS-CoV-2: a mechanistic hypothesis. Psychiatry Research. 2020;291:113220.

94. Zhitomirsky B, Assaraf YG. Lysosomes as mediators of drug resistance in cancer. Drug Resistance Updates. 2016;24:23-33.

95. Halaby R. Influence of lysosomal sequestration on multidrug resistance in cancer cells. Cancer Drug Resistance. 2019;2(1):31.

96. Azijli K, Gotink KJ, Verheul HMW. The potential role of lysosomal sequestration in sunitinib resistance of renal cell cancer. Journal of Kidney Cancer and VHL. 2015;2(4):195.

97. Sacramento CQ, Fintelman-Rodrigues N, Dias SSG, Temerozo JR, Da Silva AdPD, da Silva CS, et al. Unlike chloroquine, mefloquine inhibits SARS-CoV-2 infection in physiologically relevant cells and does not induce viral variants. BioRxiv. 2021:2021-07.

98. DeWald LE, Johnson JC, Gerhardt DM, Torzewski LM, Postnikova E, Honko AN, et al. *In-vivo* activity of amodiaquine against Ebola virus infection. Scientific Reports. 2019;9(1):20199.

99. Vela JM. Repurposing sigma-1 receptor ligands for COVID-19 therapy? Frontiers in Pharmacology. 2020;11:582310.

100. Nobile B, Durand M, Olié E, Guillaume S, Molès J-P, Haffen E, et al. The anti-inflammatory effect of the tricyclic antidepressant clomipramine and its high penetration in the brain might be useful to prevent the psychiatric consequences of SARS-CoV-2 infection. Frontiers in Pharmacology. 2021;12:615695.

101. Schafer A, Xiong R, Cooper L, Nowar R, Lee H, Li Y, et al. Evidence for distinct mechanisms of small molecule inhibitors of filovirus entry. PLoS Pathogens. 2021;17(2):e1009312.

102. Gunesch AP, Zapatero-Belinchón FJ, Pinkert L, Steinmann E, Manns MP, Schneider G, et al. Filovirus antiviral activity of cationic amphiphilic drugs is associated with lipophilicity and ability to induce phospholipidosis. Antimicrobial Agents and Chemotherapy. 2020;64(8):10-1128.

103. Oliver ME, Hinks TSC. Azithromycin in viral infections. Reviews in Medical Virology. 2021;31(2):e2163.

104. Bogush TA, Polezhaev BB, Mamichev IA, Bogush EA, Polotsky BE, Tjulandin SA, et al. Tamoxifen never ceases to amaze: New findings on non-estrogen receptor molecular targets and mediated effects. Cancer Investigation. 2018;36(4):211-20.

105. Johansen LM, Brannan JM, Delos SE, Shoemaker CJ, Stossel A, Lear C, et al. FDA-approved selective estrogen receptor modulators inhibit Ebola virus infection. Science Translational Medicine. 2013;5(190):190ra79-ra79.

106. Allegretti M, Cesta MC, Zippoli M, Beccari A, Talarico C, Mantelli F, et al. Repurposing the estrogen receptor modulator raloxifene to treat SARS-CoV-2 infection. Cell Death & Differentiation. 2022;29(1):156-66.

107. Mũller-Hõcker J, Schmid H, Weiss M, Dendorfer U, Braun GS. Chloroquine-induced phospholipidosis of the kidney mimicking Fabry's disease: Case report and review of the literature. Human Pathology. 2003;34(3):285-9.

108. Fischer H, Atzpodien E-A, Csato M, Doessegger L, Lenz B, Schmitt G, et al. I*n-silico* assay for assessing phospholipidosis potential of small druglike molecules:

Training, validation, and refinement using several data sets. Journal of Medicinal Chemistry. 2012;55(1):126-39.

109. Sawada H, Takami K, Asahi S. A toxicogenomic approach to drug-induced phospholipidosis: Analysis of its induction mechanism and establishment of a novel *in-vitro* screening system. Toxicological Sciences. 2005;83(2):282-92.

110. Vitovic P, Alakoskela J-M, Kinnunen PKJ. Assessment of drug− lipid complex formation by a high-throughput langmuir-balance and correlation to phospholipidosis. Journal of Medicinal Chemistry. 2008;51(6):1842-8.

111. Hanumegowda UM, Wenke G, Regueiro-Ren A, Yordanova R, Corradi JP, Adams SP. Phospholipidosis as a function of basicity, lipophilicity, and volume of distribution of compounds. Chemical Research in Toxicology. 2010;23(4):749-55.

112. Bauch C, Bevan S, Woodhouse H, Dilworth C, Walker P. Predicting *in-vivo* phospholipidosis-inducing potential of drugs by a combined high content screening and *in-silico* modelling approach. Toxicology in Vitro. 2015;29(3):621-30.

113. Shayman JA, Abe A. Drug induced phospholipidosis: An acquired lysosomal storage disorder. Biochimica et Biophysica Acta (BBA)-Molecular and Cell Biology of Lipids. 2013;1831(3):602-11.

114. Kazmi F, Funk R, Pope C, Czerwinski M, Yerino P, Bolliger P, et al. A robust method to identify compounds that undergo intracellular lysosomal sequestration. Drug Metabolism Reviews. 2011;43:136-7.

115. Ufuk A, Assmus F, Francis L, Plumb J, Damian V, Gertz M, et al. *In-vitro* and i*n-silico* tools to assess extent of cellular uptake and lysosomal sequestration of respiratory drugs in human alveolar macrophages. Molecular Pharmaceutics. 2017;14(4):1033-46.

116. Easwaranathan A, Inci B, Ulrich S, Brunken L, Nikiforova V, Norinder U, et al. Quantification of intracellular accumulation and retention of lysosomotropic macrocyclic compounds by high-throughput imaging of lysosomal changes. Journal of Pharmaceutical Sciences. 2019;108(1):652-60.

117. Garcia DS, Sjödin M, Hellstrandh M, Norinder U, Nikiforova V, Lindberg J, et al. Cellular accumulation and lipid binding of perfluorinated alkylated substances (PFASs)–A comparison with lysosomotropic drugs. Chemico-Biological Interactions. 2018;281:1-10.

118. Ashoor R, Yafawi R, Jessen B, Lu S. The contribution of lysosomotropism to autophagy perturbation. PloS One. 2013;8(11):e82481.

119. Ufuk A, Somers G, Houston JB, Galetin A. *In-vitr*o assessment of uptake and lysosomal sequestration of respiratory drugs in alveolar macrophage cell line NR8383. Pharmaceutical Research. 2015;32:3937-51.

120. Marques MRC, Loebenberg R, Almukainzi M. Simulated biological fluids with possible application in dissolution testing. Dissolution Technologies. 2011;18(3):15-28.

121. Innes E, Yiu HHP, McLean P, Brown W, Boyles M. Simulated biological fluids–a systematic review of their biological relevance and use in relation to inhalation toxicology of particles and fibres. Critical Reviews in Toxicology. 2021;51(3):217-48.

122. Pelfrêne A, Cave MR, Wragg J, Douay F. *In-vitro* investigations of human bioaccessibility from reference materials using simulated lung fluids. International Journal of Environmental Research and Public Health. 2017;14(2):112.

123. Stefaniak AB, Guilmette RA, Day GA, Hoover MD, Breysse PN, Scripsick RC. Characterization of phagolysosomal simulant fluid for study of beryllium aerosol particle dissolution. Toxicology in Vitro. 2005;19(1):123-34.

124. Colombo C, Monhemius AJ, Plant JA. Platinum, palladium and rhodium release from vehicle exhaust catalysts and road dust exposed to simulated lung fluids. Ecotoxicology and Environmental Safety. 2008;71(3):722-30.

125. Midander K, Pan J, Wallinder IO, Leygraf C. Metal release from stainless steel particles *in-vitro* —influence of particle size. Journal of Environmental Monitoring. 2007;9(1):74-81.

126. Kastury F, Smith E, Karna RR, Scheckel KG, Juhasz AL. Methodological factors influencing inhalation bioaccessibility of metal (loid) s in $PM_{2.5}$ using simulated lung fluid. Environmental Pollution. 2018;241:930-7.

127. Kubo Y, Yamada M, Konakawa S, Akanuma S-i, Hosoya K-i. Uptake study in lysosome-enriched fraction: Critical involvement of lysosomal trapping in

quinacrine uptake but not fluorescence-labeled verapamil transport at blood-retinal Barrier. Pharmaceutics. 2020;12(8):747.

128. Xu H, Ren D. Lysosomal physiology. Annual Review of Physiology. 2015;77:57-80.

129. de Souza JB, de Souza J, de Castro LML, Siqueira MF, Savedra RML, Silva-Barcellos NM. Evaluation of the losartan solubility in the biowaiver context by shake-flask method and intrinsic dissolution. Pharmaceutical development and technology. 2019;24(3):283-92.

130. Trapp S, Rosania GR, Horobin RW, Kornhuber J. Quantitative modeling of selective lysosomal targeting for drug design. European Biophysics Journal. 2008;37(8):1317.

131. Bezzina JP, Ogden MD, Moon EM, Soldenhoff KL. REE behavior and sorption on weak acid resins from buffered media. Journal of Industrial and Engineering Chemistry. 2018;59:440-55.

132. Davidson AG, Mkoji LMM. The simultaneous assay of triprolidine, pseudoephedrine and dextromethorphan in combined preparations by derivative-difference spectrophotometry. Journal of Pharmaceutical and Biomedical Analysis. 1988;6(5):449-60.

133. Gao Z, Yu L, Clark S, Trehy M, Moore T, Westenberger B, et al. Dissolution Testing for bioavailability of over-the-counter (OTC) drugs—a technical note. AAPS PharmSciTech. 2015;16(5):1227-33.

134. Mostafa HF, Ibrahim MA, Sakr A. Development and optimization of dextromethorphan hydrobromide oral disintegrating tablets: Effect of formulation and process variables. Pharmaceutical Development and Technology. 2013;18(2):454-63.

135. Hansen KC, D'Alessandro A, Clement CC, Santambrogio L. Lymph formation, composition and circulation: A proteomics perspective. International Immunology. 2015;27(5):219-27.

136. Moore Jr JE, Bertram CD. Lymphatic system flows. Annual Review of Fluid Mechanics. 2018;50:459-82.

137. Breslin JW, Yang Y, Scallan JP, Sweat RS, Adderley SP, Murfee WL. Lymphatic vessel network structure and physiology. Comprehensive Physiology. 2011;9(1):207-99.

138. Khan AA, Mudassir J, Mohtar N, Darwis Y. Advanced drug delivery to the lymphatic system: lipid-based nanoformulations. International Journal of Nanomedicine. 2013;8:2733.

139. Choi I, Lee S, Hong Y-K. The new era of the lymphatic system: No longer secondary to the blood vascular system. Cold Spring Harbor Perspectives in Medicine. 2012;2(4):a006445.

140. Suy R, Thomis S, Fourneau I. The discovery of the lymphatics in the seventeenth century. Part III: the dethroning of the liver. Acta Chirurgica Belgica. 2016;116(6):390-7.

141. Suy R, Thomis S, Fourneau I. The discovery of lymphatic system in the seventeenth century. Part I: the early history. Acta Chirurgica Belgica. 2016;116(4):260-6.

142. Suy R, Thomis S, Fourneau I. The discovery of the lymphatic system in the seventeenth century. Part II: the discovery of Chyle vessels. Acta Chirurgica Belgica. 2016;116(5):329-35.

143. Natale G, Bocci G, Ribatti D. Scholars and scientists in the history of the lymphatic system. Journal of Anatomy. 2017;231(3):417-29.

144. Gracia G, Cao E, Feeney OM, Johnston APR, Porter CJH, Trevaskis NL. High-density lipoprotein composition influences lymphatic transport after subcutaneous administration. Molecular Pharmaceutics. 2020;17(8):2938-51.

145. Ijpma FFA, van Gulik TM. "Anatomy Lesson of Frederik Ruysch" of 1670: A tribute to Ruysch's contributions to lymphatic anatomy. World Journal of Surgery. 2013;37(8):1996-2001.

146. Di Matteo B, Tarabella V, Filardo G, Viganò A, Tomba P, Kon E, et al. Art in science: Giovanni Paolo Mascagni and the art of anatomy. Clinical Orthopaedics and Related Research. 2015;473(3):783-8.

147. Aukland K. Arnold Heller and the lymph pump. Acta Physiologica Scandinavica. 2005;185(3):171-80.

148. Louveau A, Smirnov I, Keyes TJ, Eccles JD, Rouhani SJ, Peske JD, et al. Structural and functional features of central nervous system lymphatic vessels. Nature. 2015;523(7560):337-41.

149. Ohtani O, Ohtani Y. Organization and developmental aspects of lymphatic vessels. Archives of Histology and Cytology. 2008;71(1):1-22.

150. Zoltzer H. Initial lymphatics-morphology and function of the endothelial cells. Lymphology. 2003;36(1):7-25.

151. Baluk P, Fuxe J, Hashizume H, Romano T, Lashnits E, Butz S, et al. Functionally specialized junctions between endothelial cells of lymphatic vessels. Journal of Experimental Medicine. 2007;204(10):2349-62.

152. Swartz MA. The physiology of the lymphatic system. Advanced Drug Delivery Reviews. 2001;50(1-2):3-20.

153. Murfee WL, Rappleye JW, Ceballos M, Schmid-Schönbein GW. Discontinuous expression of endothelial cell adhesion molecules along initial lymphatic vessels in mesentery: The primary valve structure. Lymphatic Research and Biology. 2007;5(2):81-90.

154. Leak LV, Burke JF. Fine structure of the lymphatic capillary and the adjoining connective tissue area. American Journal of Anatomy. 1966;118(3):785-809.

155. Leak LV, Burke JF. Ultrastructural studies on the lymphatic anchoring filaments. The Journal of Cell Biology. 1968;36(1):129-49.

156. Gerli R, Solito R, Weber E, Agliano M. Specific adhesion molecules bind anchoring filaments and endothelial cells in human skin initial lymphatics. Lymphology. 2000;33(4):148-57.

157. Wick N, Haluza D, Gurnhofer E, Raab I, Kasimir M-T, Prinz M, et al. Lymphatic precollectors contain a novel, specialized subpopulation of podoplaninlow, CCL27-expressing lymphatic endothelial cells. The American Journal of Pathology. 2008;173(4):1202-9.

158. Zöltzer H. Morphology and physiology of lymphatic endothelial cells. Encyclopedia of the Microvasculature, Biology and Pathology. 2006;83:535-44.

159. Margaris KN, Black RA. Modelling the lymphatic system: Challenges and opportunities. Journal of the Royal Society Interface. 2012;9(69):601-12.

160. Ohhashi T, Fukushima S, Azuma T. Vasa vasorum within the media of bovine mesenteric lymphatics. Proceedings of the Society for Experimental Biology and Medicine. 1977;154(4):582-6.

161. Pan WR, Le Roux CM, Levy SM, Briggs CA. The morphology of the human lymphatic vessels in the head and neck. Clinical Anatomy. 2010;23(6):654-61.

162. Tortora GJ, Derrickson BH. Principles of anatomy and physiology: John Wiley & Sons; 2018.

163. Hsu MC, Itkin M. Lymphatic anatomy. Techniques in Vascular and Interventional Radiology. 2016;19(4):247-54.

164. Ilahi M, Ilahi TB. Anatomy, thorax, thoracic duct. StatPearls [Internet]: StatPearls Publishing LLC; 2018. Available from: https://www.ncbi.nlm.nih.gov/books/NBK513227/

165. Brotons ML, Bolca C, Fréchette É, Deslauriers J. Anatomy and physiology of the thoracic lymphatic system. Thoracic Surgery Clinics. 2012;22(2):139-53.

166. Hematti H, Mehran RJ. Anatomy of the thoracic duct. Thoracic Surgery Clinics. 2011;21(2):229-38.

167. Rehfeld A, Nylander M, Karnov K. The Immune System and the Lymphatic Organs. Compendium of Histology: Springer; 2017. p. 379-409.

168. Cesta MF. Normal structure, function, and histology of mucosa-associated lymphoid tissue. Toxicologic Pathology. 2006;34(5):599-608.

169. Verbrugghe P, Kujala P, Waelput W, Peters PJ, Cuvelier CA. Clusterin in human gut-associated lymphoid tissue, tonsils, and adenoids: Localization to M cells and follicular dendritic cells. Histochemistry and Cell Biology. 2008;129(3):311-20.

170. Skandalakis JE, Skandalakis LJ, Skandalakis PN. Anatomy of the lymphatics. Surgical Oncology Clinics of North America. 2007;16(1):1-16.

171. Ohtani O, Ohtani Y. Structure and function of rat lymph nodes. Archives of Histology and Cytology. 2008;71(2):69-76.

172. Willard-Mack CL. Normal structure, function, and histology of lymph nodes. Toxicologic Pathology. 2006;34(5):409-24.

173. Mempel TR, Henrickson SE, Von Andrian UH. T-cell priming by dendritic cells in lymph nodes occurs in three distinct phases. Nature. 2004;427(6970):154-9.

174. Muraoka D, Harada N, Hayashi T, Tahara Y, Momose F, Sawada S-i, et al. Nanogel-based immunologically stealth vaccine targets macrophages in the medulla of lymph node and induces potent antitumor immunity. ACS Nano. 2014;8(9):9209-18.

175. Bui T, Bordoni B. Anatomy, Abdomen and Pelvis, Inguinal Lymph Node. StatPearls [Internet]: StatPearls Publishing LLC; 2020. Available from: https://www.ncbi.nlm.nih.gov/books/NBK557639/

176. Zhang F, Zarkada G, Han J, Li J, Dubrac A, Ola R, et al. Lacteal junction zippering protects against diet-induced obesity. Science. 2018;361(6402):599-603.

177. Hokkanen K, Tirronen A, Ylä-Herttuala S. Intestinal lymphatic vessels and their role in chylomicron absorption and lipid homeostasis. Current Opinion in Lipidology. 2019;30(5):370-6.

178. Yousef M, Chacra NB, Davies NM, Löbenberg R. Lipoproteins within the lymphatic system: Insights into health, disease, and therapeutic implications. Applied Chemical Engineering. 2023;6(2):2202.

179. Suh SH, Choe K, Hong SP, Jeong Sh, Mäkinen T, Kim KS, et al. Gut microbiota regulates lacteal integrity by inducing VEGF-C in intestinal villus macrophages. EMBO Reports. 2019;20(4):e46927.

180. Simons M, Gordon E, Claesson-Welsh L. Mechanisms and regulation of endothelial VEGF receptor signalling. Nature Reviews Molecular Cell Biology. 2016;17(10):611.

181. Kobayashi N, Takahashi D, Takano S, Kimura S, Hase K. The roles of Peyer's patches and microfold cells in the gut immune system: Relevance to autoimmune diseases. Frontiers in Immunology. 2019;10:2345.

182. Ms P, Naha A, Shetty D, Nayak UY. Lymphatic drug transport and associated drug delivery technologies: A comprehensive review. Current Pharmaceutical Design. 2021;27(17):1992-98.

183. Schudel A, Francis DM, Thomas SN. Material design for lymph node drug delivery. Nature Reviews Materials. 2019;4(6):415-28.

184. Chaturvedi S, Garg A, Verma A. Nano lipid based carriers for lymphatic voyage of anti-cancer drugs: An insight into the *in-vitro*, *ex-viv*o, *in-situ* and *in-vivo* study models. Journal of Drug Delivery Science and Technology. 2020:101899.

185. Stachura J, Wachowska M, Kilarski WW, Güç E, Golab J, Muchowicz A. The dual role of tumor lymphatic vessels in dissemination of metastases and immune response development. Oncoimmunology. 2016;5(7):e1182278.

186. Ma Q, Dieterich LC, Detmar M. Multiple roles of lymphatic vessels in tumor progression. Current Opinion in Immunology. 2018;53:7-12.

187. Cote B, Rao D, Alany RG, Kwon GS, Alani AWG. Lymphatic changes in cancer and drug delivery to the lymphatics in solid tumors. Advanced Drug Delivery Reviews. 2019;144:16-34.

188. Laakkonen P, Porkka K, Hoffman JA, Ruoslahti E. A tumor-homing peptide with a targeting specificity related to lymphatic vessels. Nature Medicine. 2002;8(7):751-5.

189. Timur SS, Yöyen-Ermiş D, Esendağlı G, Yonat S, Horzum U, Esendağlı G, et al. Efficacy of a novel LyP-1-containing self-microemulsifying drug delivery system (SMEDDS) for active targeting to breast cancer. European Journal of Pharmaceutics and Biopharmaceutics. 2019;136:138-46.

190. Ling R, Li Y, Yao Q, Chen T, Zhu D, Jun Y, et al. Lymphatic chemotherapy induces apoptosis in lymph node metastases in a rabbit breast carcinoma model. Journal of Drug Targeting. 2005;13(2):137-42.

191. Alrushaid S, Sayre CL, Yáñez JA, Forrest ML, Senadheera SN, Burczynski FJ, et al. Pharmacokinetic and toxicodynamic characterization of a novel doxorubicin derivative. Pharmaceutics. 2017;9(3):35.

192. Singla AK, Garg A, Aggarwal D. Paclitaxel and its formulations. International Journal of Pharmaceutics. 2002;235(1-2):179-92.

193. Videira M, Almeida AJ, Fabra À. Preclinical evaluation of a pulmonary delivered paclitaxel-loaded lipid nanocarrier antitumor effect. Nanomedicine. 2012;8(7):1208-15.

194. Reddy LH, Sharma RK, Chuttani K, Mishra AK, Murthy RSR. Influence of administration route on tumor uptake and biodistribution of etoposide loaded solid

lipid nanoparticles in Dalton's lymphoma tumor bearing mice. Journal of Controlled Release. 2005;105(3):185-98.

195. Paliwal R, Rai S, Vaidya B, Khatri K, Goyal AK, Mishra N, et al. Effect of lipid core material on characteristics of solid lipid nanoparticles designed for oral lymphatic delivery. Nanomedicine. 2009;5(2):184-91.

196. Zara GP, Bargoni A, Cavalli R, Fundarò A, Vighetto D, Gasco MR. Pharmacokinetics and tissue distribution of idarubicin-loaded solid lipid nanoparticles after duodenal administration to rats. Journal of Pharmaceutical Sciences. 2002;91(5):1324-33.

197. Lawson KA, Anderson K, Snyder RM, Simmons-Menchaca M, Atkinson J, Sun L-Z, et al. Novel vitamin E analogue and 9-nitro-camptothecin administered as liposome aerosols decrease syngeneic mouse mammary tumor burden and inhibit metastasis. Cancer Chemotherapy and Pharmacology. 2004;54(5):421-31.

198. Xie Y, Aillon KL, Cai S, Christian JM, Davies NM, Berkland CJ, et al. Pulmonary delivery of cisplatin–hyaluronan conjugates via endotracheal instillation for the treatment of lung cancer. International Journal of Pharmaceutics. 2010;392(1-2):156-63.

199. Cai S, Xie Y, Davies NM, Cohen MS, Forrest ML. Carrier-based intralymphatic cisplatin chemotherapy for the treatment of metastatic squamous cell carcinoma of the head & neck. Therapeutic Delivery. 2010;1(2):237-45.

200. Schwager S, Detmar M. Inflammation and lymphatic function. Frontiers in Immunology. 2019;10:308.

201. Smedby KE, Ponzoni M. The aetiology of B-cell lymphoid malignancies with a focus on chronic inflammation and infections. Journal of Internal Medicine. 2017;282(5):360-70.

202. Mezu-Ndubuisi OJ, Maheshwari A. The role of integrins in inflammation and angiogenesis. Pediatric research. 2021;89(7):1619-26.

203. Lane RS, Femel J, Breazeale AP, Loo CP, Thibault G, Kaempf A, et al. IFNγ-activated dermal lymphatic vessels inhibit cytotoxic T cells in melanoma and inflamed skin. Journal of Experimental Medicine. 2018;215(12):3057-74.

204. Teijeira A, Hunter MC, Russo E, Proulx ST, Frei T, Debes GF, et al. T cell migration from inflamed skin to draining lymph nodes requires intralymphatic crawling supported by ICAM-1/LFA-1 interactions. Cell Reports. 2017;18(4):857-65.

205. Ge Y, Li Y, Gong J, Zhu W. Mesenteric organ lymphatics and inflammatory bowel disease. Annals of Anatomy-Anatomischer Anzeiger. 2018;218:199-204.

206. Bouta EM, Bell RD, Rahimi H, Xing L, Wood RW, Bingham CO, et al. Targeting lymphatic function as a novel therapeutic intervention for rheumatoid arthritis. Nature Reviews Rheumatology. 2018;14(2):94-106.

207. Aldrich MB, Velasquez FC, Kwon S, Azhdarinia A, Pinkston K, Harvey BR, et al. Lymphatic delivery of etanercept via nanotopography improves response to collagen-induced arthritis. Arthritis Research & Therapy. 2017;19(1):1-13.

208. Shinriki S, Jono H, Ueda M, Ota K, Ota T, Sueyoshi T, et al. Interleukin-6 signalling regulates vascular endothelial growth factor-C synthesis and lymphangiogenesis in human oral squamous cell carcinoma. The Journal of Pathology. 2011;225(1):142-50.

209. Polzer K, Baeten D, Soleiman A, Distler J, Gerlag DM, Tak PP, et al. Tumour necrosis factor blockade increases lymphangiogenesis in murine and human arthritic joints. Annals of the Rheumatic Diseases. 2008;67(11):1610-6.

210. Escobedo N, Oliver G. The lymphatic vasculature: Its role in adipose metabolism and obesity. Cell Metabolism. 2017;26(4):598-609.

211. Rehal S, Kataru RP, Hespe GE, Baik JE, Park HJ, Ly C, et al. Regulation of lymphatic function and injury by nitrosative stress in obese mice. Molecular Metabolism. 2020;42:101081.

212. Chachaj A, Puła B, Chabowski M, Grzegrzółka J, Szahidewicz-Krupska E, Karczewski M, et al. Role of the lymphatic system in the pathogenesis of hypertension in humans. Lymphatic Research and Biology. 2018;16(2):140-6.

213. Csányi G, Singla B. Arterial lymphatics in atherosclerosis: Old questions, new insights, and remaining challenges. Journal of Clinical Medicine. 2019;8(4):495.

214. Zheng Z, Ren K, Peng X, Zhu X, Yi G. Lymphatic vessels: A potential approach to the treatment of atherosclerosis? Lymphatic Research and Biology. 2018;16(6):498-506.

215. Nayak Y, Avadhani K, Mutalik S, Y Nayak U. Lymphatic delivery of anti-HIV drug nanoparticles. Recent Patents on Nanotechnology. 2016;10(2):116-27.

216. Qin C, Chu Y, Feng W, Fromont C, He S, Ali J, et al. Targeted delivery of lopinavir to HIV reservoirs in the mesenteric lymphatic system by lipophilic ester prodrug approach. Journal of Controlled Release. 2020.

217. Williams JB, Hüppner A, Mulrooney-Cousins PM, Michalak TI. Differential expression of woodchuck toll-like receptors 1–10 in distinct forms of infection and stages of hepatitis in experimental hepatitis B virus infection. Frontiers in Microbiology. 2018;9:3007.

218. Uzzan M, Corcos O, Martin JC, Treton X, Bouhnik Y. Why is SARS-CoV-2 infection more severe in obese men? The gut lymphatics–Lung axis hypothesis. Medical Hypotheses. 2020;144:110023.

219. Sathekge M, Maes A, Kgomo M, Van de Wiele C. Fluorodeoxyglucose uptake by lymph nodes of HIV patients is inversely related to CD4 cell count. Nuclear Medicine Communications. 2010;31(2):137-40.

220. Kinman L, Brodie SJ, Tsai CC, Bui T, Larsen K, Schmidt A, et al. Lipid–drug association enhanced HIV-1 protease inhibitor indinavir localization in lymphoid

tissues and viral load reduction: A proof of concept study in HIV-2287-infected macaques. Journal of Acquired Immune Deficiency Syndromes. 2003;34(4):387-97.

221. Holm R, Porter CJH, Edwards GA, Müllertz A, Kristensen HG, Charman WN. Examination of oral absorption and lymphatic transport of halofantrine in a triple-cannulated canine model after administration in self-microemulsifying drug delivery systems (SMEDDS) containing structured triglycerides. European Journal of Pharmaceutical Sciences. 2003;20(1):91-7.

222. Beg S, Swain S, Singh HP, Patra CN, Rao MEB. Development, optimization, and characterization of solid self-nanoemulsifying drug delivery systems of valsartan using porous carriers. AAPS PharmsSciTech. 2012;13(4):1416-27.

223. Thakkar H, Nangesh J, Parmar M, Patel D. Formulation and characterization of lipid-based drug delivery system of raloxifene-microemulsion and self-microemulsifying drug delivery system. Journal of Pharmacy and Bioallied Sciences. 2011;3(3):442.

224. Sheue Nee Ling S, Magosso E, Abdul Karim Khan N, Hay Yuen K, Anne Barker S. Enhanced oral bioavailability and intestinal lymphatic transport of a hydrophilic drug using liposomes. Drug Development and Industrial Pharmacy. 2006;32(3):335-45.

225. Cavalli R, Zara GP, Caputo O, Bargoni A, Fundarò A, Gasco MR. Transmucosal transport of tobramycin incorporated in SLN after duodenal administration to rats. Part I—A pharmacokinetic study. Pharmacological Research. 2000;42(6):541-5.

226. Venkateswarlu V, Manjunath K. Preparation, characterization and *in-vitro* release kinetics of clozapine solid lipid nanoparticles. Journal of Controlled Release. 2004;95(3):627-38.

227. Sanjula B, Shah FM, Javed A, Alka A. Effect of poloxamer 188 on lymphatic uptake of carvedilol-loaded solid lipid nanoparticles for bioavailability enhancement. Journal of Drug Targeting. 2009;17(3):249-56.

228. Chalikwar SS, Belgamwar VS, Talele VR, Surana SJ, Patil MU. Formulation and evaluation of nimodipine-loaded solid lipid nanoparticles delivered via lymphatic transport system. Colloids and Surfaces B: Biointerfaces. 2012;97:109-16.

229. Yang KY, Du Hyeong Hwang AMY, Kim DW, Shin Y-J, Bae O-N, Kim Y, II, et al. Silymarin-loaded solid nanoparticles provide excellent hepatic protection: Physicochemical characterization and *in-vivo* evaluation. International Journal of Nanomedicine. 2013;8:3333.

230. Jain CP, Vyas SP, Dixit VK. Niosomal system for delivery of rifampicin to lymphatics. Indian Journal of Pharmaceutical Sciences. 2006;68(5): 575-78.

231. Zhuang C-Y, Li N, Wang M, Zhang X-N, Pan W-S, Peng J-J, et al. Preparation and characterization of vinpocetine loaded nanostructured lipid carriers (NLC) for improved oral bioavailability. International Journal of Pharmaceutics. 2010;394(1-2):179-85.

232. Jain RK. Barriers to drug delivery in solid tumors. Scientific American. 1994;271(1):58-65.

233. Harvey AJ, Kaestner SA, Sutter DE, Harvey NG, Mikszta JA, Pettis RJ. Microneedle-based intradermal delivery enables rapid lymphatic uptake and distribution of protein drugs. Pharmaceutical Research. 2011;28(1):107-16.

234. Yáñez JA, Wang SWJ, Knemeyer IW, Wirth MA, Alton KB. Intestinal lymphatic transport for drug delivery. Advanced Drug Delivery Reviews. 2011;63(10-11):923-42.

235. Holm R, Hoest J. Successful *in-silico* predicting of intestinal lymphatic transfer. International Journal of Pharmaceutics. 2004;272(1-2):189-93.

236. Porter CJH. Drug delivery to the lymphatic system. Critical Reviews in Therapeutic Drug Carrier Systems. 1997;14(4):333-94.

237. Clogston JD, Patri AK. Zeta potential measurement. Characterization of nanoparticles intended for drug delivery: Springer; 2011. p. 63-70.

238. Oussoren C, Zuidema J, Crommelin DJA, Storm G. Lymphatic uptake and biodistribution of liposomes after subcutaneous injection.: II. Influence of liposomal size, lipid composition and lipid dose. Biochimica et Biophysica Acta (BBA)-Biomembranes. 1997;1328(2):261-72.

239. Hawley AE, Davis SS, Illum L. Targeting of colloids to lymph nodes: influence of lymphatic physiology and colloidal characteristics. Advanced Drug Delivery Reviews. 1995;17(1):129-48.

240. Charman WNA, Stella VJ. Estimating the maximal potential for intestinal lymphatic transport of lipophilic drug molecules. International Journal of Pharmaceutics. 1986;34(1-2):175-8.

241. Brouillette CG, Anantharamaiah GM, Engler JA, Borhani DW. Structural models of human apolipoprotein AI: a critical analysis and review. Biochimica et Biophysica Acta (BBA)-Molecular and Cell Biology of Lipids. 2001;1531(1-2):4-46.

242. Afonso CB, Spickett CM. Lipoproteins as targets and markers of lipoxidation. Redox Biology. 2019;23:101066.

243. Morrisett JD, Jackson RL, Gotto Jr AM. Lipoproteins: Sructure and function. Annual Review of Biochemistry. 1975;44(1):183-207.

244. Feingold KR, Grunfeld C. Introduction to lipids and lipoproteins. Endotext [Internet]: MDText.com, Inc.; 2024. Available from: https://www.ncbi.nlm.nih.gov/books/NBK305896/

245. Smith LC, Pownall HJ, Gotto Jr AM. The plasma lipoproteins: Structure and metabolism. Annual Review of Biochemistry. 1978;47(1):751-77.

246. O'Brien PJ, Alborn WE, Sloan JH, Ulmer M, Boodhoo A, Knierman MD, et al. The novel apolipoprotein A5 is present in human serum, is associated with VLDL, HDL, and chylomicrons, and circulates at very low concentrations compared with other apolipoproteins. Clinical Chemistry. 2005;51(2):351-9.

247. Pirillo A, Catapano AL. Lipoprotein remnants: To be or not to be. European Heart Journal. 2021;42(47):4844-6.

248. Chaudhary S, Garg T, Murthy RSR, Rath G, Goyal AK. Recent approaches of lipid-based delivery system for lymphatic targeting via oral route. Journal of Drug Targeting. 2014;22(10):871-82.

249. Masulli M, Patti L, Riccardi G, Vaccaro O, Annuzzi G, Ebbesson SOE, et al. Relation among lipoprotein subfractions and carotid atherosclerosis in Alaskan Eskimos (from the GOCADAN Study). The American Journal of Cardiology. 2009;104(11):1516-21.

250. Rigotti A. Absorption, transport, and tissue delivery of vitamin E. Molecular Aspects of Medicine. 2007;28(5-6):423-36.

251. Liu X, Suo R, Xiong S-L, Zhang Q-H, Yi G-H. HDL drug carriers for targeted therapy. Clinica Chimica Acta. 2013;415:94-100.

252. Ikonen E. Cellular cholesterol trafficking and compartmentalization. Nature reviews Molecular Cell Biology. 2008;9(2):125-38.

253. Bell FP. The effect of fat-soluble xenobiotics on intestinal lipid, apoprotein, and lipoprotein synthesis and secretion. Fat Absorption: Volume II. 2018; pp.167-188.

254. Dahan A, Hoffman A. Evaluation of a chylomicron flow blocking approach to investigate the intestinal lymphatic transport of lipophilic drugs. European Journal of Pharmaceutical Sciences. 2005;24(4):381-8.

255. Bisgaier CL, Glickman RM. Intestinal synthesis, secretion, and transport of lipoproteins. Annual Review of Physiology. 1983;45(1):625-36.

256. Ko C-W, Qu J, Black DD, Tso P. Regulation of intestinal lipid metabolism: current concepts and relevance to disease. Nature Reviews Gastroenterology & Hepatology. 2020;17(3):169-83.

257. Xiao C, Stahel P, Lewis GF. Regulation of chylomicron secretion: focus on post-assembly mechanisms. Cellular and Molecular Gastroenterology and Hepatology. 2019;7(3):487-501.

258. Bickerton AST, Roberts R, Fielding BA, Hodson L, Blaak EE, Wagenmakers AJM, et al. Preferential uptake of dietary fatty acids in adipose tissue and muscle in the postprandial period. Diabetes. 2007;56(1):168-76.

259. Voshol PJ, Rensen PCN, van Dijk KW, Romijn JA, Havekes LM. Effect of plasma triglyceride metabolism on lipid storage in adipose tissue: studies using genetically engineered mouse models. Biochimica et Biophysica Acta (BBA)-Molecular and Cell Biology of Lipids. 2009;1791(6):479-85.

260. Cooper AD. Hepatic uptake of chylomicron remnants. Journal of Lipid Research. 1997;38(11):2173-92.

261. Zannis VI, Chroni A, Kypreos KE, Kan H-Y, Cesar TB, Zanni EE, et al. Probing the pathways of chylomicron and HDL metabolism using adenovirus-mediated gene transfer. Current Opinion in Lipidology. 2004;15(2):151-66.

262. Linton MF, Yancey PG, Davies SS, Jerome WG, Linton EF, Song WL, et al. The role of lipids and lipoproteins in atherosclerosis. Endotext [Internet]: MDText.com, Inc.; 2019. Available from: https://www.ncbi.nlm.nih.gov/books/NBK343489/.

263. Williams KJ. Molecular processes that handle—and mishandle—dietary lipids. The Journal of Clinical Investigation. 2008;118(10):3247-59.

264. Yousef M, Park C, Le TS, Chacra NB, Davies NM, Löbenberg R. Simulated lymphatic fluid for *in-vitro* assessment in pharmaceutical development. 2022;29:86-93.

265. Solari E, Marcozzi C, Bartolini B, Viola M, Negrini D, Moriondo A. Acute exposure of collecting lymphatic vessels to low-density lipoproteins increases both contraction frequency and lymph flow: An *in-vivo* mechanical insight. Lymphatic Research and Biology. 2020;18(2):146-55.

266. Huang L-H, Elvington A, Randolph GJ. The role of the lymphatic system in cholesterol transport. Frontiers in Pharmacology. 2015;6:182.

267. Vuorio T, Nurmi H, Moulton K, Kurkipuro J, Robciuc MR, Öhman M, et al. Lymphatic vessel insufficiency in hypercholesterolemic mice alters lipoprotein levels and promotes atherogenesis. Arteriosclerosis, Thrombosis, and Vascular Biology. 2014;34(6):1162-70.

268. Rafieian-Kopaei M, Setorki M, Doudi M, Baradaran A, Nasri H. Atherosclerosis: process, indicators, risk factors and new hopes. International Journal of Preventive Medicine. 2014;5(8):927.

269. Gracia G, Cao E, Johnston APR, Porter CJH, Trevaskis NL. Organ-specific lymphatics play distinct roles in regulating HDL trafficking and composition.

American Journal of Physiology-Gastrointestinal and Liver Physiology. 2020;318(4):G725-35.

270. Chakraborty S, Zawieja S, Wang W, Zawieja DC, Muthuchamy M. Lymphatic system: A vital link between metabolic syndrome and inflammation. Annals of the New York Academy of Sciences. 2010;1207:E94-102.

271. Pandita D, Ahuja A, Lather V, Benjamin B, Dutta T, Velpandian T, et al. Development of lipid-based nanoparticles for enhancing the oral bioavailability of paclitaxel. AAPS PharmSciTech. 2011;12:712-22.

272. Maisel K, McClain CA, Bogseth A, Thomas SN. Nanotechnologies for physiology-informed drug delivery to the lymphatic system. Annual Review of Biomedical Engineering. 2023;25:233-56.

273. Porter CJH, Charman WN. Intestinal lymphatic drug transport: An update. Advanced Drug Delivery Reviews. 2001;50(1-2):61-80.

274. DeSesso JM, Jacobson CF. Anatomical and physiological parameters affecting gastrointestinal absorption in humans and rats. Food and Chemical Toxicology. 2001;39(3):209-28.

275. Kroeker CG. Cardiovascular system: Anatomy and physiology. Cardiovascular Mechanics. 2018;2(5):1.

276. Fedi A, Vitale C, Ponschin G, Ayehunie S, Fato M, Scaglione S. *In-vitro* models replicating the human intestinal epithelium for absorption and metabolism studies: A systematic review. Journal of Controlled Release. 2021;335:247-68.

277. Feng W, Qin C, Abdelrazig S, Bai Z, Raji M, Darwish R, et al. Vegetable oils composition affects the intestinal lymphatic transport and systemic bioavailability of co-administered lipophilic drug cannabidiol. International Journal of Pharmaceutics. 2022;624:121947.

278. Trevaskis NL, Charman WN, Porter CJH. Lipid-based delivery systems and intestinal lymphatic drug transport: A mechanistic update. Advanced Drug Delivery Reviews. 2008;60(6):702-16.

279. Markovic M, Ben-Shabat S, Aponick A, Zimmermann EM, Dahan A. Lipids and lipid-processing pathways in drug delivery and therapeutics. International Journal of Molecular Sciences. 2020;21(9):3248.

280. Feeney OM, Crum MF, McEvoy CL, Trevaskis NL, Williams HD, Pouton CW, et al. 50 years of oral lipid-based formulations: Provenance, progress and future perspectives. Advanced Drug Delivery Reviews. 2016;101:167-94.

281. Kim H, Kim Y, Lee J. Liposomal formulations for enhanced lymphatic drug delivery. Asian Journal of Pharmaceutical Sciences. 2013;8(2):96-103.

282. Gershkovich P, Hoffman A. Uptake of lipophilic drugs by plasma derived isolated chylomicrons: linear correlation with intestinal lymphatic bioavailability. European Journal of Pharmaceutical Sciences. 2005;26(5):394-404.

283. Trevaskis NL, Hu L, Caliph SM, Han S, Porter CJH. The mesenteric lymph duct cannulated rat model: Application to the assessment of intestinal lymphatic drug transport. (Journal of Visualized Experiments). 2015(97):e52389.

284. Brocks DR, Davies NM. Lymphatic drug absorption via the enterocytes: Pharmacokinetic simulation, modeling, and considerations for optimal drug development. Journal of Pharmacy & Pharmaceutical Sciences. 2018;21(1s):254s-70s.

285. Iwanaga K, Kushibiki T, Miyazaki M, Kakemi M. Disposition of lipid-based formulation in the intestinal tract affects the absorption of poorly water-soluble drugs. Biological and Pharmaceutical Bulletin. 2006;29(3):508-12.

286. Dahan A, Hoffman A. Use of a dynamic *in-vitro* lipolysis model to rationalize oral formulation development for poor water soluble drugs: Correlation with *in-vivo* data and the relationship to intra-enterocyte processes in rats. Pharmaceutical Research. 2006;23:2165-74.

287. Tang T-T, Hu X-B, Liao D-H, Liu X-Y, Xiang D-X. Mechanisms of microemulsion enhancing the oral bioavailability of puerarin: comparison between oil-in-water and water-in-oil microemulsions using the single-pass intestinal perfusion method and a chylomicron flow blocking approach. International Journal of Nanomedicine. 2013;8:4415-26.

288. Sun D, Wei X, Xue X, Fang Z, Ren M, Lou H, et al. Enhanced oral absorption and therapeutic effect of acetylpuerarin based on D-α-tocopheryl polyethylene glycol 1000 succinate nanoemulsions. International Journal of Nanomedicine. 2014;9:3413-23.

289. Arzani G, Haeri A, Daeihamed M, Bakhtiari-Kaboutaraki H, Dadashzadeh S. Niosomal carriers enhance oral bioavailability of carvedilol: Effects of bile salt-

enriched vesicles and carrier surface charge. International Journal of Nanomedicine. 2015;10:4797-813.

290. Garg B, Katare OP, Beg S, Lohan S, Singh B. Systematic development of solid self-nanoemulsifying oily formulations (S-SNEOFs) for enhancing the oral bioavailability and intestinal lymphatic uptake of lopinavir. Colloids and Surfaces B: Biointerfaces. 2016;141:611-22.

291. Wang T, Shen L, Zhang Z, Li H, Huang R, Zhang Y, et al. A novel core-shell lipid nanoparticle for improving oral administration of water soluble chemotherapeutic agents: inhibited intestinal hydrolysis and enhanced lymphatic absorption. Drug Delivery. 2017;24(1):1565-73.

292. Liao H, Gao Y, Lian C, Zhang Y, Wang B, Yang Y, et al. Oral absorption and lymphatic transport of baicalein following drug–phospholipid complex incorporation in self-microemulsifying drug delivery systems. International Journal of Nanomedicine. 2019;14:7291-306.

293. Patel MH, Mundada VP, Sawant KK. Novel drug delivery approach via self-microemulsifying drug delivery system for enhancing oral bioavailability of asenapine maleate: Optimization, characterization, cell uptake, and *in-vivo* pharmacokinetic studies. AAPS PharmSciTech. 2019;20(2):44.

294. Patel MH, Sawant KK. Self microemulsifying drug delivery system of lurasidone hydrochloride for enhanced oral bioavailability by lymphatic targeting: *In-vitro*, Caco-2 cell line and *in-vivo* evaluation. European Journal of Pharmaceutical Sciences. 2019;138:105027.

295. Ravi PR, Vats R. Comparative pharmacokinetic evaluation of lopinavir and lopinavir-loaded solid lipid nanoparticles in hepatic impaired rat model. Journal of Pharmacy and Pharmacology. 2017;69(7):823-33.

296. de Souza A, Scarim CB, Cotrim PC, Barbosa, Junior F, Rocha BA, et al. Hydroxymethylnitrofurazone lymphatic uptake with nanostructured lipid carrier after oral administration in rats. Nanomedicine (Lond). 2024;19(4):293-301.

297. Rizk SA, Elsheikh MA, R Elnaggar YS, Abdallah OY. Novel bioemulsomes for baicalin oral lymphatic targeting: Development, optimization and pharmacokinetics. Nanomedicine. 2021;16(22):1983-98.

298. Zheng B, Pan F, Shi M, He C, He B, Wang R, et al. 2-Monoacylglycerol mimetic liposomes to promote intestinal lymphatic transport for improving oral bioavailability of dihydroartemisinin. International Journal of Nanomedicine. 2024;19:5273-95.

299. Valicherla GR, Dave KM, Syed AA, Riyazuddin M, Gupta AP, Singh A, et al. Formulation optimization of Docetaxel loaded self-emulsifying drug delivery system to enhance bioavailability and anti-tumor activity. Scientific Reports. 2016;6(1):26895.

300. Meher JG, Dixit S, Singh Y, Pawar VK, Konwar R, Saklani R, et al. Paclitaxel-loaded colloidal silica and TPGS-based solid self-emulsifying system interferes Akt/mTOR pathway in MDA-MB-231 and demonstrates anti-tumor effect in syngeneic mammary tumors. AAPS PharmSciTech. 2020;21(8):313.

301. Gao F, Zhang Z, Bu H, Huang Y, Gao Z, Shen J, et al. Nanoemulsion improves the oral absorption of candesartan cilexetil in rats: performance and mechanism. Journal of Controlled Release. 2011;149(2):168-74.

302. Jitta SR, Salwa, Bhaskaran NA, Marques SM, Kumar L, Cheruku SP, et al. Enhanced tissue distribution of ritonavir-loaded nanostructured lipid carriers—recommending its dose reduction. Drug Delivery and Translational Research. 2021;14(1):116-130.

303. Shrivastava S, Gidwani B, Kaur CD. Development of mebendazole loaded nanostructured lipid carriers for lymphatic targeting: Optimization, characterization, *in-vitro* and *in-vivo* evaluation. Particulate Science and Technology. 2021;39(3):380-90.

304. Fuentes P, Bernabeu E, Bertera F, Garces M, Oppezzo J, Zubillaga M, et al. Dual strategy to improve the oral bioavailability of efavirenz employing nanomicelles and curcumin as a bio-enhancer. International Journal of Pharmaceutics. 2024;651:123734.

305. Bao X, Qian K, Yao P. Insulin-and cholic acid-loaded zein/casein–dextran nanoparticles enhance the oral absorption and hypoglycemic effect of insulin. Journal of Materials Chemistry B. 2021;9(31):6234-45.

306. Ryšánek P, Grus T, Lukáč P, Kozlik P, Křížek T, Pozniak J, et al. Validity of cycloheximide chylomicron flow blocking method for the evaluation of lymphatic transport of drugs. British Journal of Pharmacology. 2021;178(23):4663-74.

307. Lind ML, Jacobsen J, Holm R, Müllertz A. Intestinal lymphatic transport of halofantrine in rats assessed using a chylomicron flow blocking approach: The influence of polysorbate 60 and 80. European Journal of Pharmaceutical Sciences. 2008;35(3):211-8.

308. Sun M, Zhai X, Xue K, Hu L, Yang X, Li G, et al. Intestinal absorption and intestinal lymphatic transport of sirolimus from self-microemulsifying drug delivery systems assessed using the single-pass intestinal perfusion (SPIP) technique and a chylomicron flow blocking approach: Linear correlation with oral bioavailabilities in rats. European Journal of Pharmaceutical Sciences. 2011;43(3):132-40.

309. Mishra A, Vuddanda PR, Singh S. Intestinal lymphatic delivery of praziquantel by solid lipid nanoparticles: formulation design, *in-vitro* and *in-vivo* studies. Journal of Nanotechnology. 2014.

310. El-Laithy HM, Basalious EB, El-Hoseiny BM, Adel MM. Novel self-nanoemulsifying self-nanosuspension (SNESNS) for enhancing oral bioavailability of diacerein: Simultaneous portal blood absorption and lymphatic delivery. International Journal of Pharmaceutics. 2015;490(1-2):146-54.

311. Makwana V, Jain R, Patel K, Nivsarkar M, Joshi A. Solid lipid nanoparticles (SLN) of Efavirenz as lymph targeting drug delivery system: Elucidation of mechanism of uptake using chylomicron flow blocking approach. International Journal of Pharmaceutics. 2015;495(1):439-46.

312. Bhalekar MR, Upadhaya PG, Madgulkar AR, Kshirsagar SJ, Dube A, Bartakke US. *In-vivo* bioavailability and lymphatic uptake evaluation of lipid nanoparticulates of darunavir. Drug Delivery. 2016;23(7):2581-6.

313. Xing Q, Song J, You X, Xu D, Wang K, Song J, et al. Microemulsions containing long-chain oil ethyl oleate improve the oral bioavailability of piroxicam by increasing drug solubility and lymphatic transportation simultaneously. International Journal of Pharmaceutics. 2016;511(2):709-18.

314. Li F, Hu R, Wang B, Gui Y, Cheng G, Gao S, et al. Self-microemulsifying drug delivery system for improving the bioavailability of huperzine A by lymphatic uptake. Acta pharmaceutica sinica B. 2017;7(3):353-60.

315. Qiao J, Ji D, Sun S, Zhang G, Liu X, Sun B, et al. Oral bioavailability and lymphatic transport of pueraria flavone-loaded self-emulsifying drug-delivery systems containing sodium taurocholate in rats. Pharmaceutics. 2018;10(3):147.

316. Wu L, Bi Y, Wu H. Formulation optimization and the absorption mechanisms of nanoemulsion in improving baicalin oral exposure. Drug Development and Industrial Pharmacy. 2018;44(2):266-75.

317. Xu Q, Zhou A, Wu H, Bi Y. Development and *in-vivo* evaluation of baicalin-loaded W/O nanoemulsion for lymphatic absorption. Pharmaceutical Development and Technology. 2019;24(9):1155-63.

318. Mundada VP, Patel MH, Mundada PK, Sawant KK. Enhanced bioavailability and antihypertensive activity of nisoldipine loaded nanoemulsion: Optimization,

cytotoxicity and uptake across Caco-2 cell line, pharmacokinetic and pharmacodynamic studies. Drug Development and Industrial Pharmacy. 2020;46(3):376-87.

319. Rangaraj N, Pailla SR, Shah S, Prajapati S, Sampathi S. QbD aided development of ibrutinib-loaded nanostructured lipid carriers aimed for lymphatic targeting: Evaluation using chylomicron flow blocking approach. Drug Delivery and Translational Research. 2020;10:1476-94.

320. Ye J-Y, Chen Z-Y, Huang C-L, Huang B, Zheng Y-R, Zhang Y-F, et al. A non-lipolysis nanoemulsion improved oral bioavailability by reducing the first-pass metabolism of raloxifene, and related absorption mechanisms being studied. International Journal of Nanomedicine. 2020;15:6503-18.

321. Elsheikh MA, Rizk SA, Elnaggar YSR, Abdallah OY. Nanoemulsomes for enhanced oral bioavailability of the anticancer phytochemical andrographolide: characterization and pharmacokinetics. AAPS PharmSciTech. 2021;22:1-12.

322. Patel P, Patel M. Enhanced oral bioavailability of nintedanib esylate with nanostructured lipid carriers by lymphatic targeting: *In-vitro*, cell line and *in-vivo* evaluation. European Journal of Pharmaceutical Sciences. 2021;159:105715.

323. Gausuzzaman SAL, Saha M, Dip SJ, Alam S, Kumar A, Das H, et al. A QbD approach to design and to optimize the self-emulsifying resveratrol–phospholipid complex to enhance drug bioavailability through lymphatic transport. Polymers. 2022;14(15):3220.

324. Goo YT, Sa C-K, Kim MS, Sin GH, Kim CH, Kim HK, et al. Enhanced dissolution and bioavailability of revaprazan using self-nanoemulsifying drug delivery system. Pharmaceutical Development and Technology. 2022;27(4):414-24.

325. Gurumukhi VC, Bari SB. Quality by design (QbD)–based fabrication of atazanavir-loaded nanostructured lipid carriers for lymph targeting: bioavailability enhancement using chylomicron flow block model and toxicity studies. Drug Delivery and Translational Research. 2022;12(5):1230-52.

326. Harisa GI, Sherif AY, Alanazi FK, Ali EA, Omran GA, Nasr FA, et al. TPGS decorated NLC shift gefitinib from portal absorption into lymphatic delivery: Intracellular trafficking, biodistribution and bioavailability studies. Colloids and Surfaces B: Biointerfaces. 2023;223:113148.

327. Muheem A, Wasim M, Aldosari E, Baboota S, Ali J. Fabrication of TPGS decorated Etravirine loaded lipidic nanocarriers as a neoteric oral bioavailability enhancer for lymphatic targeting. Discover Nano. 2024;19(1):5.

328. Fu Q, Sun J, Ai X, Zhang P, Li M, Wang Y, et al. Nimodipine nanocrystals for oral bioavailability improvement: Role of mesenteric lymph transport in the oral absorption. International Journal of Pharmaceutics. 2013;448(1):290-7.

329. Li H, Lu S, Luo M, Li X, Liu S, Zhang T. A matrix dispersion based on phospholipid complex system: Preparation, lymphatic transport, and pharmacokinetics. Drug Development and Industrial Pharmacy. 2020;46(4):557-65.

330. Lin L, Chen Q, Dai Y, Xia Y. Self-Nanoemulsifying Drug Delivery System for Enhanced Bioavailability of Madecassic Acid: *In-vitro* and *in-vivo* Evaluation. International Journal of Nanomedicine. 2023;18:2345-58.

331. Liu Y, Guerrero DQ, Lechuga-Ballesteros D, Tan M, Ahmad F, Aleiwi B, et al. Lipid-based self-microemulsion of niclosamide achieved enhanced oral delivery and anti-tumor efficacy in orthotopic patient-derived xenograft of hepatocellular carcinoma in mice. International Journal of Nanomedicine. 2024;19:2639-53.

332. Al Nebaihi HM, Davies NM, Brocks DR. Pharmacokinetics of cycloheximide in rats and evaluation of its effect as a blocker of intestinal lymph formation. European Journal of Pharmaceutics and Biopharmaceutics. 2023;193:89-95.

333. Desmarchelier C, Borel P, Lairon D, Maraninchi M, Valéro R. Effect of nutrient and micronutrient intake on chylomicron production and postprandial lipemia. Nutrients. 2019;11(6):1299.

334. Fatma S, Yakubov R, Anwar K, Hussain MM. Pluronic L81 enhances triacylglycerol accumulation in the cytosol and inhibits chylomicron secretion. Journal of Lipid Research. 2006;47(11):2422-32.

335. Krupka TM, Solorio L, Wilson RE, Wu H, Azar N, Exner AA. Formulation and characterization of echogenic lipid− pluronic nanobubbles. Molecular Pharmaceutics. 2010;7(1):49-59.

336. Tso P, Balint JA, Bishop MB, Rodgers JB. Acute inhibition of intestinal lipid transport by Pluronic L-81 in the rat. American Journal of Physiology-Gastrointestinal and Liver Physiology. 1981;241(6):G487-G97.

337. Bochenek WJ, Rodgers JB. Effect of polyol detergents on cholesterol and triglyceride absorption: Hypolipidemic action of chronic administration of hydrophobic detergent. Biochimica et Biophysica Acta (BBA)-Lipids and Lipid Metabolism. 1977;489(3):503-6.

338. Tso P, Balint JA, Rodgers JB. Effect of hydrophobic surfactant (Pluronic L-81) on lymphatic lipid transport in the rat. American Journal of Physiology-Gastrointestinal and Liver Physiology. 1980;239(5):G348-G53.

339. Tso P, Gollamudi SR. Pluronic L-81: a potent inhibitor of the transport of intestinal chylomicrons. American Journal of Physiology-Gastrointestinal and Liver Physiology. 1984;247(1):G32-G6.

340. Nutting D, Hall J, Barrowman JA, Tso P. Further studies on the mechanism of inhibition of intestinal chylomicron transport by Pluronic L-81. Biochimica et Biophysica Acta (BBA)-Lipids and Lipid Metabolism. 1989;1004(3):357-62.

341. Hayashi H, Nutting DF, Fujimoto K, Cardelli JA, Black D, Tso P. Transport of lipid and apolipoproteins AI and A-IV in intestinal lymph of the rat. Journal of Lipid Research. 1990;31(9):1613-25.

342. Black DD. Effect of intestinal chylomicron secretory blockade on apolipoprotein synthesis in the newborn piglet. Biochemical Journal. 1992;283(1):81-5.

343. Pidlich J, Renner F, Ellinger A, Huttinger M, Pavelka M, Gangl A. Effect of pluronic L-81 on intestinal lipoprotein secretion in the rat. Digestive Diseases and Sciences. 1996;41(7):1445-51.

344. Wollin A, Wang X, Tso P. Nutrients regulate diamine oxidase release from intestinal mucosa. American Journal of Physiology-Regulatory, Integrative and Comparative Physiology. 1998;275(4):R969-R75.

345. Nauli AM, Zheng S, Yang Q, Li R, Jandacek R, Tso P. Intestinal alkaline phosphatase release is not associated with chylomicron formation. American Journal of Physiology-Gastrointestinal and Liver Physiology. 2003;284(4):G583-G7.

346. Schweigert FJ, Trüpschuch A, Hantschel C. Modulation of absorption of beta-carotene and tissue accumulation of beta-carotene and vitamin A by different surfactants in rats. Annals of Nutrition and Metabolism. 2002;46(5):200-4.

347. Han S, Hu L, Quach T, Simpson JS, Trevaskis NL, Porter CJH. Constitutive triglyceride turnover into the mesenteric lymph is unable to support efficient lymphatic transport of a biomimetic triglyceride prodrug. Journal of Pharmaceutical Sciences. 2016;105(2):786-96.

348. Morita S-y, Kawabe M, Nakano M, Handa T. Pluronic L81 affects the lipid particle sizes and apolipoprotein B conformation. Chemistry and Physics of Lipids. 2003;126(1):39-48.

349. Craig RM, Atkinson Jr AJ. D-xylose testing: A review. Gastroenterology. 1988;95(1):223-31.

350. Yousef M, Park C, Henostroza M, Bou Chacra N, Davies NM, Löbenberg R. Development of a novel *in-vitro* model to study lymphatic uptake of drugs via artificial chylomicrons. Pharmaceutics. 2023;15(11):2532.

351. Young CW, Robinson PF, Sacktor B. Inhibition of the synthesis of protein in intact animals by acetoxycycloheximide and a metabolic derangement concomitant with this blockade. Biochemical Pharmacology. 1963;12(8):855-65.

352. Sabesin SM, Isselbacher KJ. Protein synthesis inhibition: mechanism for the production of impaired fat absorption. Science. 1965;147(3662):1149-51.

353. Redgrave TG, Zilversmit DB. Does puromycin block release of chylomicrons from the intestine? American Journal of Physiology-Legacy Content. 1969;217(2):336-40.

354. Kayden HJ, Medick M. The absorption and metabolism of short and long chain fatty acids in puromycin-treated rats. Biochimica et Biophysica Acta (BBA)-Lipids and Lipid Metabolism. 1969;176(1):37-43.

355. Spring DJ, Chen-Liu LW, Chatterton JE, Elovson J, Schumaker VN. Lipoprotein assembly. Apolipoprotein B size determines lipoprotein core circumference. Journal of Biological Chemistry. 1992;267(21):14839-45.

356. Schumaker VN, Phillips ML, Chatterton JE. Apolipoprotein B and low-density lipoprotein structure: implications for biosynthesis of triglyceride-rich lipoproteins. Advances in Protein Chemistry. 1994;45:205-48.

357. Vahouny GV, Ito M, Blendermann EM, Gallo LL, Treadwell CR. Puromycin inhibition of cholesterol absorption in the rat. Journal of Lipid Research. 1977;18(6):745-52.

358. Miura S, Asakura H, Morishita T, Nagata H, Miyairi M, Tsuchiya M. Studies on the difference of lymphatic absorption between saturated and unsaturated long chain fatty acids in rats particularly in reference with the effect of puromycin and colchicine. The Keio Journal of Medicine. 1979;28(3):121-30.

359. Dasgeb B, Kornreich D, McGuinn K, Okon L, Brownell I, Sackett DL. Colchicine: An ancient drug with novel applications. British Journal of Dermatology. 2018;178(2):350-6.

360. Sternberg SS, Ferguson Jr FC, Theodore PS. Colchicine. III. Pathology and hematology in cats and rats. Cancer. 1954;7(3):607-16.

361. Rosenbloom SJ, Ferguson Jr FC. Fatty change in organs of the rat treated with colchicine. Toxicology and Applied Pharmacology. 1968;13(1):50-61.

362. Wiesenfeld PL, Garthoff LH, Sobotka TJ, Suagee JK, Barton CN. Acute oral toxicity of colchicine in rats: effects of gender, vehicle matrix and pre-exposure to lipopolysaccharide. Journal of Applied Toxicology. 2007;27(5):421-33.

363. Stein O, Sanger L, Stein Y. Colchicine-induced inhibition of lipoprotein and protein secretion into the serum and lack of interference with secretion of biliary phospholipids and cholesterol by rat liver *in-vivo*. The Journal of Cell Biology. 1974;62(1):90-103.

364. Arreaza-Plaza CA, Bosch V, Otayek MA. Lepid transport across the intestinal epithelial cell: Effect of colchicine. Biochimica et Biophysica Acta (BBA)-Lipids and Lipid Metabolism. 1976;431(2):297-302.

365. Glickman RM, Perrotto JL, Kirsch K. Intestinal lipoprotein formation: Effect of cholchicine. Gastroenterology. 1976;70(3):347-52.

366. Miura S, Asakura H, Miyairi M, Morishita T, Nagata H, Tsuchiya M. Effect of colchicine on intestinal alkaline phosphatase activity during linoleic acid absorption in rats. Digestion. 1982;23(4):224-31.

367. Pavelka M, Gangl A. Effects of colchicine on the intestinal transport of endogenous lipid: ultrastructural, biochemical, and radiochemical studies in fasting rats. Gastroenterology. 1983;84(3):544-55.

368. Liu H-X, Adachi I, Horikoshi I, Ueno M. Mechanism of promotion of lymphatic drug absorption by milk fat globule membrane. International Journal of Pharmaceutics. 1995;118(1):55-64.

369. Chen Y-J, Huang S-M, Liu C-Y, Yeh P-H, Tsai T-H. Hepatobiliary excretion and enterohepatic circulation of colchicine in rats. International Journal of Pharmaceutics. 2008;350(1-2):230-9.

370. Al Nebaihi HM, Le TS, Davies NM, Brocks DR. Liquid chromatography tandem mass spectrometric analytical method for study of colchicine in rats given low doses. Processes. 2021;9(11):2007.

371. Al Nebaihi HM, Davies NM, Brocks DR. Evaluation of the pharmacokinetics, chylomicron inhibition, and toxicity of colchicine in rats given low doses. European Journal of Pharmaceutics and Biopharmaceutics. 2024;202:114392.

372. Martino E, Casamassima G, Castiglione S, Cellupica E, Pantalone S, Papagni F, et al. Vinca alkaloids and analogues as anti-cancer agents: Looking back, peering ahead. Bioorganic & Medicinal Chemistry Letters. 2018;28(17):2816-26.

373. Kremmer T, Holczinger L, Somfai-Relle S. Serum lipid-lowering effect of vinca alkaloids. Biochemical Pharmacology. 1979;28(2):227-30.

374. Sethi VS, Lewis JC, Clair RWS. Vincristine and vinblastine lower plasma cholesterol concentrations in rhesus monkeys. Biochimica et Biophysica Acta (BBA)-Lipids and Lipid Metabolism. 1983;752(3):482-7.

375. Verbin RS, Goldblatt PJ, Farber E. The biochemical pathology of inhibition of protein synthesis *in-vivo*. The effects of cycloheximide on hepatic parenchymal cell ultrastructure. Laboratory Investigation. 1969;20(6):529-36.

376. Verbin RS, Longnecker DS, Liang H, Farber E. Some observations on the acute histopathologic effects of cycloheximide *in-vivo*. The American Journal of Pathology. 1971;62(1):111.

377. Glickman RM, Kirsch K, Isselbacher KJ. Fat absorption during inhibition of protein synthesis: studies of lymph chylomicrons. The Journal of Clinical Investigation. 1972;51(2):356-63.

378. Glickman RM, Kirsch K. Lymph chylomicron formation during the inhibition of protein synthesis. Studies of chylomicron apoproteins. The Journal of Clinical Investigation. 1973;52(11):2910-20.

379. Glickman RM, Kilgore A, Khorana J. Chylomicron apoprotein localization within rat intestinal epithelium: studies of normal and impaired lipid absorption. Journal of Lipid Research. 1978;19(2):260-8.

380. Bernard A, Carlier H. Intestinal Lymphatic Absorption of Labelled Oleic Acid in the Normal Rat and Rat Treated with Actidione-cycloheximide or Acetoxycycloheximide. Comptes Rendus des Seances de L'academie des sciences. Serie III, Sciences De La Vie. 1981;292(1):97-100.

381. Sitrin MD, Pollack KL, Bolt MJ, Rosenberg IH. Comparison of vitamin D and 25-hydroxyvitamin D absorption in the rat. American Journal of Physiology-Gastrointestinal and Liver Physiology. 1982;242(4):G326-G32.

382. Sitrin MD, Pollack KL, Bolt MJ. Intestinal absorption of 1, 25-dihydroxyvitamin D3 in the rat. American Journal of Physiology-Gastrointestinal and Liver Physiology. 1985;248(6):G718-G25.

383. Attili-Qadri S, Karra N, Nemirovski A, Schwob O, Talmon Y, Nassar T, et al. Oral delivery system prolongs blood circulation of docetaxel nanocapsules via lymphatic

absorption. Proceedings of the National Academy of Sciences. 2013;110(43):17498-503.

384. Baheti A, Srivastava S, Sahoo D, Lowalekar R, Prasad Panda B, Kumar Padhi B, et al. Development and pharmacokinetic evaluation of industrially viable self-microemulsifying drug delivery systems (SMEDDS) for terbinafine. Current Drug Delivery. 2016;13(1):65-75.

385. Elsheikh MA, Elnaggar YSR, Otify DY, Abdallah OY. Bioactive-chylomicrons for oral lymphatic targeting of berberine chloride: Novel flow-blockage assay in tissue-based and caco-2 cell line models. Pharmaceutical Research. 2018;35:1-15.

386. Singh D, Tiwary AK, Bedi N. Role of porous carriers in the biopharmaceutical performance of solid SMEDDS of canagliflozin. Recent Patents on Drug Delivery & Formulation. 2018;12(3):179-98.

387. Lin PY, Chen KH, Miao YB, Chen HL, Lin KJ, Chen CT, et al. Phase-changeable nanoemulsions for oral delivery of a therapeutic peptide: toward targeting the pancreas for antidiabetic treatments using lymphatic transport. Advanced Functional Materials. 2019;29(13):1809015.

388. Agarwal S, HariKumar SL, Negi P, Upadhyay N, Garg R. Quetiapine fumarate loaded nanostructured lipid carrier for enhancing oral bioavailability: design, development and pharmacokinetic assessment. Current Drug Delivery. 2021;18(2):184-98.

389. Emzhik M, Haeri A, Javidi J, Abdollahizad E, Qaribnejad A, Rezaee E, et al. Bile salt integrated cerasomes: A potential nanocarrier for enhancement of the oral bioavailability of idarubicin hydrochloride. International Journal of Pharmaceutics. 2024;662:124518.

390. Wexler P, Anderson BD. Encyclopedia of toxicology: Academic Press; 2005.

391. Miyata S, Saku N, Akiyama S, Javaregowda PK, Ite K, Takashima N, et al. Puromycin-based purification of cells with high expression of the cytochrome P450 CYP3A4 gene from a patient with drug-induced liver injury (DILI). Stem Cell Research & Therapy. 2022;13(1):6.

392. Au W-S, Lu L-W, Tam S, Ko OKH, Chow BKC, He M-L, et al. Pluronic L-81 ameliorates diabetic symptoms in db/db mice through transcriptional regulation of microsomal triglyceride transfer protein. World Journal of Gastroenterology. 2009;15(24):2987.

393. Senthilkumar M, Dash S, Vigneshwari R, Paulraj E. Aceclofenac-loaded pluronic F108/L81 mixed polymeric micelles: Effect of HLB on solubilization. Designed Monomers and Polymers. 2022;25(1):1-11.

394. Batrakova EV, Han H-Y, Alakhov VY, Miller DW, Kabanov AV. Effects of pluronic block copolymers on drug absorption in Caco-2 cell monolayers. Pharmaceutical Research. 1998;15:850-5.

395. McEwan T, Robinson PC. A systematic review of the infectious complications of colchicine and the use of colchicine to treat infections: Elsevier; 2021.

396. Schlesinger N, Firestein BL, Brunetti L. Colchicine in COVID-19: An old drug, new use. Current Pharmacology Reports. 2020;6(4):137-45.

397. Taher MA, Nyeem MAB, Billah MM, Ahammed MM. Vinca alkaloid-the second most used alkaloid for cancer treatment-A review. International Journal of Physiology, Nutrition, and Physical Education. 2017;2:723-7.

398. Griffin JP, D'Arcy PF. A manual of adverse drug interactions: Elsevier; 1997.

399. Zhou X-J, Rahmani R. Preclinical and clinical pharmacology of vinca alkaloids. Drugs. 1992;44:1-16.

400. Moudi M, Go R, Yien CYS, Nazre M. Vinca alkaloids. International Journal of Preventive Medicine. 2013;4(11):1231.

401. Hansten PD, Tan MS, Horn JR, Gomez-Lumbreras A, Villa-Zapata L, Boyce RD, et al. Colchicine drug interaction errors and misunderstandings: Recommendations for improved evidence-based management. Drug Safety. 2023;46(3):223-42.

402. Terkeltaub RA, editor Colchicine update: 20082009: Elsevier.

403. Oh KT, Bronich TK, Kabanov AV. Micellar formulations for drug delivery based on mixtures of hydrophobic and hydrophilic Pluronic® block copolymers. Journal of Controlled Release. 2004;94(2-3):411-22.

404. Lee C-T, Huang Y-W, Yang C-H, Huang K-S. Drug delivery systems and combination therapy by using vinca alkaloids. Current Topics in Medicinal Chemistry. 2015;15(15):1491-500.

405. Aschenbrenner DS. First extended-release injectable drug therapy for HIV. The American Journal of Nursing. 2021;121(5):24-5.

406. Slobodnick A, Shah B, Pillinger MH, Krasnokutsky S. Colchicine: Old and new. The American Journal of Medicine. 2015;128(5):461-70.

407. Food and Drug A. Guidance for industry: Estimating the maximum safe starting dose in initial clinical trials for therapeutics in adult healthy volunteers. Center for Drug Evaluation and Research. 2005;7(0.001).

408. Finkelstein Y, Aks SE, Hutson JR, Juurlink DN, Nguyen P, Dubnov-Raz G, et al. Colchicine poisoning: The dark side of an ancient drug. Clinical Toxicology. 2010;48(5):407-14.

409. Niel E, Scherrmann J-M. Colchicine today. Joint Bone Spine. 2006;73(6):672-8.

410. Gebert A, Rothkötter H-J, Pabst R. M cells in Peyer's patches of the intestine. International Review of Cytology. 1996;167:91-159.

411. Brayden DJ, Jepson MA, Baird AW. Keynote review: Intestinal Peyer's patch M cells and oral vaccine targeting. Drug Discovery Today. 2005;10(17):1145-57.

412. Patel RP, Shah P, Barve K, Patel N, Gandhi J. Peyer’s patch: Targeted drug delivery for therapeutics benefits. Novel Drug Delivery Technologies: Innovative Strategies for Drug Re-positioning. 2019:121-49.

413. He H, Xie Y, Lv Y, Qi J, Dong X, Zhao W, et al. Bioimaging of intact polycaprolactone nanoparticles using aggregation-caused quenching probes: Size-

dependent translocation via oral delivery. Advanced Healthcare Materials. 2018;7(22):1800711.

414. Bachhav SS, Dighe VD, Devarajan PV. Exploring Peyer's patch uptake as a strategy for targeted lung delivery of polymeric rifampicin nanoparticles. Molecular Pharmaceutics. 2018;15(10):4434-45.

415. Shi L-L, Xie H, Lu J, Cao Y, Liu J-Y, Zhang X-X, et al. Positively charged surface-modified solid lipid nanoparticles promote the intestinal transport of docetaxel through multifunctional mechanisms in rats. Molecular Pharmaceutics. 2016;13(8):2667-76.

416. Channarong S, Chaicumpa W, Sinchaipanid N, Mitrevej A. Development and evaluation of chitosan-coated liposomes for oral DNA vaccine: The improvement of Peyer's patch targeting using a polyplex-loaded liposomes. AAPS PharmSciTech. 2011;12(1):192-200.

417. Ensign LM, Cone R, Hanes J. Oral drug delivery with polymeric nanoparticles: The gastrointestinal mucus barriers. Advanced Drug Delivery Reviews. 2012;64(6):557-70.

418. Schleh C, Semmler-Behnke M, Lipka J, Wenk A, Hirn S, Schäffler M, et al. Size and surface charge of gold nanoparticles determine absorption across intestinal barriers and accumulation in secondary target organs after oral administration. Nanotoxicology. 2012;6(1):36-46.

419. Li D, Zhuang J, He H, Jiang S, Banerjee A, Lu Y, et al. Influence of particle geometry on gastrointestinal transit and absorption following oral administration. ACS Applied Materials & Interfaces. 2017;9(49):42492-502.

420. Rivera-Gil P, Jimenez De Aberasturi D, Wulf V, Pelaz B, Del Pino P, Zhao Y, et al. The challenge to relate the physicochemical properties of colloidal nanoparticles to their cytotoxicity. Accounts of Chemical Research. 2013;46(3):743-9.

421. Taft DR. Drug excretion. Pharmacology: Elsevier; 2009. p. 175-99.

422. Thompson GA, Toothaker RD. Urinary excretion: Does it accurately reflect relative differences in bioavailability/systemic exposure when renal clearance is nonlinear? Pharmaceutical Research. 2004;21(5):781-4.

423. Serra CHdR, Chang KH, Dezani TM, Porta V, Storpirtis S. Dissolution efficiency and bioequivalence study using urine data from healthy volunteers: A comparison between two tablet formulations of cephalexin. Brazilian Journal of Pharmaceutical Sciences. 2015;51:383-92.

424. Otoom S, Hasan M, Najib N. Comparative bioavailability of two cefadroxil products using serum and urine data in healthy human volunteers. Clinical and Experimental Pharmacology and Physiology. 2004;31(7):433-7.

425. Cawello W, Bökens H, Nickel B, Andreas JO, Halabi A. Tolerability, pharmacokinetics, and bioequivalence of the tablet and syrup formulations of lacosamide in plasma, saliva, and urine: Saliva as a surrogate of pharmacokinetics in the central compartment. Epilepsia. 2013;54(1):81-8.

426. Levick JR, Michel CC. Microvascular fluid exchange and the revised Starling principle. Cardiovascular Research. 2010;87(2):198-210.

427. Santambrogio L. Immunology of the lymphatic system: Springer; 2013.

428. Trevaskis NL, Lee G, Escott A, Phang KL, Hong J, Cao E, et al. Intestinal lymph flow, and lipid and drug transport scale allometrically from pre-clinical species to humans. Frontiers in Physiology. 2020;11:458.

429. Dharmarajan AM, Bruce NW, McArdle HJ. Comparison of flow rates and composition of ovarian lymph and blood in the day-16 pregnant rat. Reproduction. 1986;77(1):169-76.

430. Dixon JB, Greiner ST, Gashev AA, Cote GL, Moore Jr JE, Zawieja DC. Lymph flow, shear stress, and lymphocyte velocity in rat mesenteric prenodal lymphatics. Microcirculation. 2006;13(7):597-610.

431. Renkin EM. Some consequences of capillary permeability to macromolecules: Starling's hypothesis reconsidered. American Journal of Physiology-Heart and Circulatory Physiology. 1986;250(5):H706-H10.

432. Adair TH, Guyton AC. Modification of lymph by lymph nodes. II. Effect of increased lymph node venous blood pressure. American Journal of Physiology-Heart and Circulatory Physiology. 1983;245(4):H616-H22.

433. Adair TH, Guyton AC. Modification of lymph by lymph nodes. III. Effect of increased lymph hydrostatic pressure. American Journal of Physiology-Heart and Circulatory Physiology. 1985;249(4):H777-H82.

434. Heim JW. On the chemical composition of lymph from subcutaneous vessels. American Journal of Physiology-Legacy Content. 1933;103(3):553-8.

435. Staples LD, Fleet IR, Heap RB. Anatomy of the utero-ovarian lymphatic network and the composition of afferent lymph in relation to the establishment of pregnancy in the sheep and goat. Reproduction. 1982;64(2):409-20.

436. Morris B, Sass MB. The formation of lymph in the ovary. Proceedings of the Royal Society of London Series B Biological Sciences. 1966;164(997):577-91.

437. Ikomi F, Kawai Y, Ohhashi T. Recent advance in lymph dynamic analysis in lymphatics and lymph nodes. Annals of Vascular Diseases. 2012:ra-12.

438. Rutili G, Arfors KE. Protein concentration in interstitial and lymphatic fluids from the subcutaneous tissue. Acta Physiologica Scandinavica. 1977;99(1):1-8.

439. Wang Y, Lang L, Huang P, Wang Z, Jacobson O, Kiesewetter DO, et al. *In-vivo* albumin labeling and lymphatic imaging. Proceedings of the National Academy of Sciences. 2015;112(1):208-13.

440. Chi J, Xie Q, Jia J, Liu X, Sun J, Chen J, et al. Prognostic value of albumin/globulin ratio in survival and lymph node metastasis in patients with cancer: A systematic review and meta-analysis. Journal of Cancer. 2018;9(13):2341.

441. Lucas CE, Denis R, Ledgerwood AM, Grabow D. The effects of Hespan on serum and lymphatic albumin, globulin, and coagulant protein. Annals of Surgery. 1988;207(4):416.

442. Fang J-F, Shih L-Y, Yuan K-C, Fang K-Y, Hwang T-L, Hsieh S-Y. Proteomic analysis of post-hemorrhagic shock mesenteric lymph. Shock. 2010;34(3):291-8.

443. Dzieciatkowska M, Wohlauer MV, Moore EE, Damle S, Peltz E, Campsen J, et al. Proteomic analysis of human mesenteric lymph. Shock. 2011;35(4):331-8.

444. Dzieciatkowska M, D'Alessandro A, Moore EE, Wohlauer M, Banerjee A, Silliman CC, et al. Lymph is not a plasma ultrafiltrate: A proteomic analysis of injured patients. Shock. 2014;42(6):485-98.

445. Meng Z, Veenstra TD. Proteomic analysis of serum, plasma, and lymph for the identification of biomarkers. Proteomics Clinical Applications. 2007;1(8):747-57.

446. Randolph GJ, Miller NE. Lymphatic transport of high-density lipoproteins and chylomicrons. The Journal of Clinical Investigation. 2014;124(3):929-35.

447. Santambrogio L. The lymphatic fluid. International Review of Cell and Molecular Biology. 2018;337:111-33.

448. Engeset A, Hager B, Nesheim A, Kolbenstvedt A. Studies on human peripheral lymph. Lymphology. 2017;6(1):1-5.

449. Ahn H, Park J-H. Liposomal delivery systems for intestinal lymphatic drug transport. Biomaterials Research. 2016;20(1):36.

450. Galia E, Nicolaides E, Hörter D, Löbenberg R, Reppas C, Dressman JB. Evaluation of various dissolution media for predicting *in-vivo* performance of class I and II drugs. Pharmaceutical Research. 1998;15(5):698-705.

451. Silva DA, Al-Gousous J, Davies NM, Chacra NB, Webster GK, Lipka E, et al. Simulated, biorelevant, clinically relevant or physiologically relevant dissolution media: The hidden role of bicarbonate buffer. European Journal of Pharmaceutics and Biopharmaceutics. 2019;142:8-19.

452. Sleep D. Albumin and its application in drug delivery. Expert Opinion on Drug Delivery. 2015;12(5):793-812.

453. Hamill JM. Observations on human chyle. The Journal of Physiology. 1906;35(1-2):151-62.

454. Bragdon JH. On the composition of chyle chylomicrons. The Journal of Laboratory and Clinical Medicine. 1958;52(4):564-70.

455. Dureau P, Charbit B, Nicolas N, Benhamou D, Mazoit J-X. Effect of Intralipid® on the dose of ropivacaine or levobupivacaine tolerated by volunteers: A clinical and pharmacokinetic study. Anesthesiology. 2016;125(3):474-83.

456. Férézou J, Gulik A, Domingo N, Milliat F, Dedieu J-C, Dunel-Erb S, et al. Intralipid 10%: Physicochemical characterization. Nutrition. 2001;17(11-12):930-3.

457. Oscarsson J, Hurt-Camejo E. Omega-3 fatty acids eicosapentaenoic acid and docosahexaenoic acid and their mechanisms of action on apolipoprotein B-containing lipoproteins in humans: A review. Lipids in Health and Disease. 2017;16(1):1-13.

458. Bergofsky EH, Jacobson JH, Fishman AP. The use of lymph for the measurement of gas tensions in interstitial fluid and tissues. The Journal of Clinical Investigation. 1962;41(11):1971-80.

459. Gao Y, Zuo J, Bou-Chacra N, Pinto TdJA, Clas S-D, Walker RB, et al. *In-vitro* release kinetics of antituberculosis drugs from nanoparticles assessed using a modified dissolution apparatus. BioMed Research International. 2013;2013:136590.

460. Charman WN, Porter CJH. Lipophilic prodrugs designed for intestinal lymphatic transport. Advanced Drug Delivery Reviews. 1996;19(2):149-69.

461. Muchow M, Maincent P, Müller RH, Keck CM. Testosterone undecanoate–increase of oral bioavailability by nanostructured lipid carriers (NLC). Journal of Pharmaceutical Technology and Drug Research. 2013;2(1):1-10.

462. Noguchi T, Charman WNA, Stella VJ. Lymphatic appearance of DDT in thoracic or mesenteric lymph duct cannulated rats. International Journal of Pharmaceutics. 1985;24(2-3):185-92.

463. Redgrave TG. Inhibition of protein synthesis and absorption of lipid into thoracic duct lymph of rats. Proceedings of the Society for Experimental Biology and Medicine. 1969;130(3):776-80.

464. Gibb M, Pradhan SH, Mulenos MR, Lujan H, Liu J, Ede JD, et al. Characterization of a human *in-vitro* intestinal model for the hazard assessment of nanomaterials used in cancer immunotherapy. Applied Sciences. 2021;11(5):2113.

465. Dahan A, Hoffman A. Rationalizing the selection of oral lipid based drug delivery systems by an *in-vitro* dynamic lipolysis model for improved oral bioavailability of poorly water soluble drugs. Journal of Controlled Release. 2008;129(1):1-10.

466. Lepore M, Delfino I. Intralipid-based phantoms for the development of new optical diagnostic techniques. The Open Biotechnology Journal. 2019;13(1).

467. Khoo SM, Edwards GA, Porter CJH, Charman WN. A conscious dog model for assessing the absorption, enterocyte-based metabolism, and intestinal lymphatic transport of halofantrine. Journal of Pharmaceutical Sciences. 2001;90(10):1599-607.

468. Khoo S-M, Shackleford DM, Porter CJH, Edwards GA, Charman WN. Intestinal lymphatic transport of halofantrine occurs after oral administration of a unit-dose lipid-based formulation to fasted dogs. Pharmaceutical Research. 2003;20:1460-5.

469. Caliph SM, Charman WN, Porter CJH. Effect of short-, medium-, and long-chain fatty acid-based vehicles on the absolute oral bioavailability and intestinal lymphatic transport of halofantrine and assessment of mass balance in lymph-cannulated and non-cannulated rats. Journal of Pharmaceutical Sciences. 2000;89(8):1073-84.

470. Murota K, Cermak R, Terao J, Wolffram S. Influence of fatty acid patterns on the intestinal absorption pathway of quercetin in thoracic lymph duct-cannulated rats. British Journal of Nutrition. 2013;109(12):2147-53.

471. Gardouh A, Gamal Al, Gad S. Formulation and pharmacokinetic evaluation of rifampicin solid lipid nanoparticles. Journal of Research in Pharmacy. 2020; 24(4): 539-551.

472. Olivas-Aguirre M, Torres-López L, Pottosin I, Dobrovinskaya O. Phenolic compounds cannabidiol, curcumin and quercetin cause mitochondrial dysfunction and suppress acute lymphoblastic leukemia cells. International Journal of Molecular Sciences. 2020;22(1):204.

473. Holm R, Porter CJH, Müllertz A, Kristensen HG, Charman WN. Structured triglyceride vehicles for oral delivery of halofantrine: Examination of intestinal lymphatic transport and bioavailability in conscious rats. Pharmaceutical Research. 2002;19:1354-61.

474. Aliyu S. Viral, fungal, protozoal and helminthic infections. Clinical Pharmacology: Elsevier; 2012. p. 213-39.

475. Chen IL, Tsai Y-J, Huang C-M, Tsai T-H. Lymphatic absorption of quercetin and rutin in rat and their pharmacokinetics in systemic plasma. Journal of Agricultural and Food Chemistry. 2010;58(1):546-51.

476. Lesser S, Cermak R, Wolffram S. Bioavailability of quercetin in pigs is influenced by the dietary fat content. The Journal of Nutrition. 2004;134(6):1508-11.

477. Zgair A, Wong JCM, Lee JB, Mistry J, Sivak O, Wasan KM, et al. Dietary fats and pharmaceutical lipid excipients increase systemic exposure to orally administered

cannabis and cannabis-based medicines. American Journal of Translational Research. 2016;8(8):3448.

478. Franco V, Gershkovich P, Perucca E, Bialer M. The interplay between liver first-pass effect and lymphatic absorption of cannabidiol and its implications for cannabidiol oral formulations. Clinical Pharmacokinetics. 2020;59(12):1493-500.

479. Zgair A, Lee JB, Wong JCM, Taha DA, Aram J, Di Virgilio D, et al. Oral administration of cannabis with lipids leads to high levels of cannabinoids in the intestinal lymphatic system and prominent immunomodulation. Scientific Reports. 2017;7(1):14542.

480. Abu-Sawwa R, Scutt B, Park Y. Emerging use of epidiolex (cannabidiol) in epilepsy. The Journal of Pediatric Pharmacology and Therapeutics. 2020;25(6):485-99.

481. Singh S, Mariappan TT, Shankar R, Sarda N, Singh B. A critical review of the probable reasons for the poor variable bioavailability of rifampicin from anti-tubercular fixed-dose combination (FDC) products, and the likely solutions to the problem. International Journal of Pharmaceutics. 2001;228(1-2):5-17.

482. Sosnik A, Carcaboso ÁM, Glisoni RJ, Moretton MA, Chiappetta DA. New old challenges in tuberculosis: potentially effective nanotechnologies in drug delivery. Advanced Drug Delivery Reviews. 2010;62(4-5):547-59.

483. Chokshi NV, Khatri HN, Patel MM. Formulation, optimization, and characterization of rifampicin-loaded solid lipid nanoparticles for the treatment of tuberculosis. Drug Development and Industrial Pharmacy. 2018;44(12):1975-89.

484. Glatzle Jr, Kalogeris TJ, Zittel TT, Guerrini S, Tso P, Raybould HE. Chylomicron components mediate intestinal lipid-induced inhibition of gastric motor function. American Journal of Physiology-Gastrointestinal and Liver Physiology. 2002;282(1):G86-G91.

485. Winstanley PA, Orme ML. The effects of food on drug bioavailability. British Journal of Clinical Pharmacology. 1989;28(6):621.

486. Karmen A, Whyte M, Goodman DS. Fatty acid esterification and chylomicron formation during fat absorption: 1. Triglycerides and cholesterol esters. Journal of Lipid Research. 1963;4(3):312-21.

487. Gershkovich P, Qadri B, Yacovan A, Amselem S, Hoffman A. Different impacts of intestinal lymphatic transport on the oral bioavailability of structurally similar synthetic lipophilic cannabinoids: Dexanabinol and PRS-211,220. European Journal of Pharmaceutical Sciences. 2007;31(5):298-305.

488. Shad MA, Pervez H, Zafar ZI, Nawaz H, Khan H. Physicochemical properties, fatty acid profile and antioxidant activity of peanut oil. Pakistan Journal of Botany. 2012;44(1):435-40.

489. Clemente TE, Cahoon EB. Soybean oil: Genetic approaches for modification of functionality and total content. Plant physiology. 2009;151(3):1030-40.

490. Wang TY, Liu M, Portincasa P, Wang DQH. New insights into the molecular mechanism of intestinal fatty acid absorption. European Journal of Clinical Investigation. 2013;43(11):1203-23.

491. Grifoni L, Vanti G, Bilia AR. Nanostructured lipid carriers loaded with cannabidiol enhance its bioaccessibility to the small intestine. Nutraceuticals. 2023;3(2):210-21.

492. Ndifor AM. Drug metabolism in malaria parasites and its possible role in drug resistance: The University of Liverpool (United Kingdom); 1992.

493. Rowe RC, Sheskey PJ, Owen SC. Handbook of pharmaceutical excipients: Pharmaceutical Press London; 2006.

494. O'Croinin C, Le TS, Doschak M, Löbenberg R, Davies NM. A validated method for detection of cannflavins in hemp extracts. Journal of Pharmaceutical and Biomedical Analysis. 2023;235:115631.

495. Demignot S, Beilstein F, Morel E. Triglyceride-rich lipoproteins and cytosolic lipid droplets in enterocytes: Key players in intestinal physiology and metabolic disorders. Biochimie. 2014;96:48-55.

496. Miao YB, Xu T, Gong Y, Chen A, Zou L, Jiang T, Shi Y. Cracking the intestinal lymphatic system window utilizing oral delivery vehicles for precise therapy. Journal of Nanobiotechnology. 2023;21(1):263.

497. Jeong SJ, Song WY, Park CW, Kim DW. Recent approaches to investigate drug delivery systems through the lymphatic pathway using oral lipid-based formulations. Journal of Pharmaceutical Investigation. 2024;54(2):131-44.

498. You YQN, Ling PR, Qu JZ, Bistrian BR. Effects of medium-chain triglycerides, long-chain triglycerides, or 2-monododecanoin on fatty acid composition in the portal vein, intestinal lymph, and systemic circulation in rats. Journal of Parenteral and Enteral Nutrition. 2008;32(2):169-75.

499. Mu H, Høy CE. Effects of different medium-chain fatty acids on intestinal absorption of structured triacylglycerols. Lipids. 2000;35(1):83-9.

500. Swift LL, Hill JO, Peters JC, Greene HL. Medium-chain fatty acids: evidence for incorporation into chylomicron triglycerides in humans. The American Journal of Clinical Nutrition. 1990;52(5):834-6.

501. Boateng L, Ansong R, Owusu W, Steiner-Asiedu M. Coconut oil and palm oil's role in nutrition, health and national development: A review. Ghana Medical Journal. 2016;50(3):189-96.

502. Ruppin DC, Middleton WRJ. Clinical use of medium chain triglycerides. Drugs. 1980;20(3):216-24.

503. Phan CT, Tso P. Intestinal lipid absorption and transport. Frontiers in Bioscience. 2001;6(5):D299-D319.

504. Prajapati HN, Patel DP, Patel NG, Dalrymple DD, Serajuddin ATM. Effect of difference in fatty acid chain lengths of medium-chain lipids on lipid-surfactant-water phase diagrams and drug solubility. Journal of Excipients and Food Chemicals. 2011;2(3):73-88.

505. Boskou D, Blekas G, Tsimidou M. Phenolic compounds in olive oil and olives. Current Topics in Nutraceutical Research. 2005;3(2):125-36.

506. Pathak N, Rai AK, Kumari R, Bhat KV. Value addition in sesame: A perspective on bioactive components for enhancing utility and profitability. Pharmacognosy Reviews. 2014;8(16):147.

507. Wrigley CW, Corke H, Seetharaman K, Faubion J. Encyclopedia of food grains: Academic Press; 2015.

508. Feng W, Qin C, Cipolla E, Lee JB, Zgair A, Chu Y, et al. Inclusion of medium-chain triglyceride in lipid-based formulation of cannabidiol facilitates micellar solubilization *in-vitro*, but *in-vivo* performance remains superior with pure sesame oil vehicle. Pharmaceutics. 2021;13(9):1349.

509. Porter CJH, Kaukonen AM, Boyd BJ, Edwards GA, Charman WN. Susceptibility to lipase-mediated digestion reduces the oral bioavailability of danazol after administration as a medium-chain lipid-based microemulsion formulation. Pharmaceutical Research. 2004;21:1405-12.

510. Field FJ, Albright E, Mathur SN. Regulation of triglyceride-rich lipoprotein secretion by fatty acids in CaCo-2 cells. Journal of Lipid Research. 1988;29(11):1427-37.

511. Fox NJ, Stachowiak GW. Vegetable oil-based lubricants—a review of oxidation. Tribology International. 2007;40(7):1035-46.

512. Kaukonen AM, Boyd BJ, Porter CJH, Charman WN. Drug solubilization behavior during *in-vitro* digestion of simple triglyceride lipid solution formulations. Pharmaceutical Research. 2004;21:245-53.

513. Daily JP, Minuti A, Khan N. Diagnosis, treatment, and prevention of malaria in the US: a review. JAMA. 2022;328(5):460-71.

514. Browning DJ. Pharmacology of chloroquine and hydroxychloroquine. Hydroxychloroquine and Chloroquine Retinopathy. 2014:35-63.

515. Farn RJ. Chemistry and technology of surfactants. Wiley Online Library; 2006.

516. Briseid G, Briseid K, Kirkevold K. Increased intestinal absorption in the rat caused by sodium lauryl sulphate, and its possible relation to the cAMP system. Naunyn-Schmiedeberg's Archives of Pharmacology. 1976;292:137-44.

517. United States Pharmacopeia and National Formulary USP 41- NF 36: The United States Pharmacopeial Convention; 2018.

518. Nelson E. Solution rate of theophylline salts and effects from oral administration. Journal of the American Pharmaceutical Association. 1957;46(10):607-14.

519. US Department of Health and Human Services, Food and Drug Administration, Center for Drug Evaluation and Research. Office of Generic Drugs/Office of Generic Drugs Policy. Approved Drug Products With Therapeutic Equivalence Evaluations. https://www.fda.gov/media/71474/download?attachment. 2024. Accessed 24 Mar 2024.

520. Grady H, Elder D, Webster GK, Mao Y, Lin Y, Flanagan T, et al. Industry's view on using quality control, biorelevant, and clinically relevant dissolution tests for pharmaceutical development, registration, and commercialization. Journal of Pharmaceutical Sciences. 2018;107(1):34-41.

521. Uddin R, Saffoon N, Sutradhar KB. Dissolution and dissolution apparatus: A review. International Journal of Current Biomedical and Pharmaceutical Research. 2011;1(4):201-7.

522. Azarmi S, Roa W, Löbenberg R. Current perspectives in dissolution testing of conventional and novel dosage forms. International Journal of Pharmaceutics. 2007;328(1):12-21.

523. United States Pharmacopeia. <711> Dissolution. United States Pharmacopeia and National Formulary USP 43- NF 38: The United States Pharmacopeial Convention; 2023.

524. United States Pharmacopeia. <724> Drug Release. United States Pharmacopeia and National Formulary USP 43- NF 38: The United States Pharmacopeial Convention; 2020.

525. Vimalson DC. Techniques to enhance solubility of hydrophobic drugs: An overview. Asian Journal of Pharmaceutics (AJP). 2016;10(2).

526. Vishwakarma N, Jain A, Sharma R, Mody N, Vyas S, Vyas SP. Lipid-based nanocarriers for lymphatic transportation. AAPS PharmSciTech. 2019;20(2):83.

527. Dissolution Methods Database. US Department of Health and Human Services, Food and Drug Administration, Center for Drug Evaluation and Research. Office of Pharmaceutical Quality/Office of New Drug Products Division of Biopharmaceutics. 2022. https://www.accessdata.fda.gov/scripts/cder/dissolution/dsp_SearchResults.cfm. Accessed 20 Apr 2024.

528. Zhang Y, Huo M, Zhou J, Zou A, Li W, Yao C, et al. DDSolver:An add-in program for modeling and comparison of drug dissolution profiles. The AAPS journal. 2010;12:263-71.

529. Devadasu VR, Deb PK, Maheshwari R, Sharma P, Tekade RK. Physicochemical, pharmaceutical, and biological considerations in GIT absorption of drugs. Dosage Form Design Considerations: Elsevier; 2018. p. 149-78.

530. Silva DA, Melo KJC, Davies NM, Bou-Chacra N, Ferraz HG, Löbenberg R. A BCS-based biowaiver approach using biphasic dissolution test. Dissolution Technologies. 2021;28(4):40-8.

531. Dressman JB, Amidon GL, Reppas C, Shah VP. Dissolution testing as a prognostic tool for oral drug absorption: Immediate release dosage forms. Pharmaceutical Research. 1998;15:11-22.

532. Li S, He H, Parthiban LJ, Yin H, Serajuddin ATM. IV-IVC considerations in the development of immediate-release oral dosage form. Journal of Pharmaceutical Sciences. 2005;94(7):1396-417.

533. Kuminek G, Rauber GS, Riekes MK, de Campos CEM, Monti GA, Bortoluzzi AJ, et al. Single crystal structure, solid state characterization and dissolution rate of terbinafine hydrochloride. Journal of Pharmaceutical and Biomedical Analysis. 2013;78:105-11.

534. Kanakapura B, Penmatsa VK. Analytical methods for determination of terbinafine hydrochloride in pharmaceuticals and biological materials. Journal of Pharmaceutical Analysis. 2016;6(3):137-49.

535. Shafiq-un-Nabi S, Shakeel F, Talegaonkar S, Ali J, Baboota S, Ahuja A, et al. Formulation development and optimization using nanoemulsion technique: A technical note. AAPS PharmSciTech. 2007;8:E12-E7.

536. Berardi A, Janssen PHM. Technical insight into potential functional-related characteristics (FRCs) of sodium starch glycolate, croscarmellose sodium and crospovidone. Journal of Drug Delivery Science and Technology. 2022;70:103261.

537. Brady J, Dürig T, Lee PI, Li JX. Polymer properties and characterization. Developing solid oral dosage forms: Elsevier; 2017. p. 181-223.

538. Hu Z, Patten T, Pelton R, Cranston ED. Synergistic stabilization of emulsions and emulsion gels with water-soluble polymers and cellulose nanocrystals. ACS Sustainable Chemistry & Engineering. 2015;3(5):1023-31.

539. Cheng Y, Qin H, Acevedo NC, Shi X. Development of methylcellulose-based sustained-release dosage by semisolid extrusion additive manufacturing in drug

delivery system. Journal of Biomedical Materials Research Part B: Applied Biomaterials. 2021;109(2):257-68.

540. Ford JL. Thermal analysis of hydroxypropylmethylcellulose and methylcellulose: powders, gels and matrix tablets. International Journal of Pharmaceutics. 1999;179(2):209-28.

541. Arshad MS, Zafar S, Yousef B, Alyassin Y, Ali R, AlAsiri A, et al. A review of emerging technologies enabling improved solid oral dosage form manufacturing and processing. Advanced Drug Delivery Reviews. 2021;178:113840.

542. Singh I, Aboul-Enein HY. Advantages of USP apparatus IV (flow-through cell apparatus) in dissolution studies. Journal of the Iranian Chemical Society. 2006;3:220-2.

543. Okumu A, DiMaso M, Löbenberg R. Computer simulations using GastroPlus™ to justify a biowaiver for etoricoxib solid oral drug products. European Journal of Pharmaceutics and Biopharmaceutics. 2009;72(1):91-8.

544. de la Cruz-Moreno MP, Montejo C, Aguilar-Ros A, Dewe W, Beck B, Stappaerts J, et al. Exploring drug solubility in fasted human intestinal fluid aspirates: Impact of inter-individual variability, sampling site and dilution. International Journal of Pharmaceutics. 2017;528(1-2):471-84.

545. Sugita K, Takata N, Yonemochi E. Dose-dependent solubility–permeability interplay for poorly soluble drugs under non-sink conditions. Pharmaceutics. 2021;13(3):323.

546. Lin W, Chen Y, Unadkat JD, Zhang X, Wu D, Heimbach T. Applications, challenges, and outlook for PBPK modeling and simulation: a regulatory, industrial and academic perspective. Pharmaceutical Research. 2022;39(8):1701-31.

547. Krstevska A, Đuriš J, Ibrić S, Cvijić S. In-depth analysis of physiologically based pharmacokinetic (PBPK) modeling utilization in different application fields using text mining tools. Pharmaceutics. 2022;15(1):107.

548. El-Khateeb E, Burkhill S, Murby S, Amirat H, Rostami-Hodjegan A, Ahmad A. Physiological-based pharmacokinetic modeling trends in pharmaceutical drug development over the last 20-years; in-depth analysis of applications, organizations, and platforms. Biopharmaceutics & Drug Disposition. 2021;42(4):107-17.

549. Sager JE, Yu J, Ragueneau-Majlessi I, Isoherranen N. Physiologically based pharmacokinetic (PBPK) modeling and simulation approaches: A systematic review of published models, applications, and model verification. Drug Metabolism and Disposition. 2015;43(11):1823-37.

550. Peters SA. Physiologically based pharmacokinetic (PBPK) modeling and simulations: principles, methods, and applications in the pharmaceutical industry: John Wiley & Sons; 2021.

551. Perry C, Davis G, Conner TM, Zhang T. Utilization of physiologically based pharmacokinetic modeling in clinical pharmacology and therapeutics: An overview. Current Pharmacology Reports. 2020;6:71-84.

552. Jones HM, Gardner IB, Watson KJ. Modelling and PBPK simulation in drug discovery. The AAPS journal. 2009;11:155-66.

553. Miller NA, Reddy MB, Heikkinen AT, Lukacova V, Parrott N. Physiologically based pharmacokinetic modelling for first-in-human predictions: an updated model building strategy illustrated with challenging industry case studies. Clinical Pharmacokinetics. 2019;58:727-46.

554. Zhuang X, Lu C. PBPK modeling and simulation in drug research and development. Acta Pharmaceutica Sinica B. 2016;6(5):430-40.

555. Min JS, Bae SK. Prediction of drug–drug interaction potential using physiologically based pharmacokinetic modeling. Archives of Pharmacal Research. 2017;40:1356-79.

556. Chu X, Prasad B, Neuhoff S, Yoshida K, Leeder JS, Mukherjee D, et al. Clinical implications of altered drug transporter abundance/function and PBPK modeling in specific populations: an ITC perspective. Clinical Pharmacology & Therapeutics. 2022;112(3):501-26.

557. Jamei M. Recent advances in development and application of physiologically-based pharmacokinetic (PBPK) models: A transition from academic curiosity to regulatory acceptance. Current Pharmacology Reports. 2016;2:161-9.

558. Luzon E, Blake K, Cole S, Nordmark A, Versantvoort C, Berglund EG. Physiologically based pharmacokinetic modeling in regulatory decision-making at

the European Medicines Agency. Clinical Pharmacology & Therapeutics. 2017;102(1):98-105.

559. Giao PT, de Vries PJ. Pharmacokinetic interactions of antimalarial agents. Clinical Pharmacokinetics. 2001;40:343-73.

560. Karbwang J, Bangchang KN. Clinical pharmacokinetics of halofantrine. Clinical Pharmacokinetics. 1994;27:104-19.

561. Lukacova V, Parrott N, Lave T, Fraczkiewicz G, Bolger M, Woltosz W. General approach to calculation of tissue:plasma partition coefficients for physiologically based pharmacokinetic (PBPK) modeling, in: AAPS National Annual Meeting and Exposition; 2008; Atlanta, GA.

562. Baune B, Flinois JP, Furlan V, Gimenez F, Taburet AM, Becquemont L, et al. Halofantrine metabolism in microsomes in man: major role of CYP 3A4 and CYP 3A5. Journal of Pharmacy and Pharmacology. 1999;51(4):419-26.

563. Krishna S, Ter Kuile F, Supanaranond W, Pukrittayakamee S, Teja-Isavadharm P, Kyle D, et al. Pharmacokinetics, efficacy and toxicity of parenteral halofantrine in uncomplicated malaria. British Journal of Clinical Pharmacology. 1993;36(6):585-91.

564. Babalola CP, Adegoke AO, Ogunjinmi MA, Osimosu MO. Determination of physicochemical properties of halofantrine. African Journal of Medicine and Medical Sciences. 2003;32(4):357-9.

565. Khoo S-M, Prankerd RJ, Edwards GA, Porter CJH, Charman WN. A physicochemical basis for the extensive intestinal lymphatic transport of a poorly lipid soluble antimalarial, halofantrine hydrochloride, after postprandial administration to dogs. Journal of Pharmaceutical Sciences. 2002;91(3):647-59.

566. Onyeji CO, Omoruyi SI, Oladimeji FA. Dissolution properties and characterization of halofantrine-2-hydroxypropyl-β-cyclodextrin binary systems. Pharmazie. 2007;62(11):858-63.

567. Chackalamannil S, Rotella D, Ward S. Comprehensive medicinal chemistry III: Elsevier; 2017.

568. Klein K, Aarons L, Ter Kuile FO, Nosten F, White NJ, Edstein MD, et al. Population pharmacokinetics of halofantrine in healthy volunteers and patients with symptomatic falciparum malaria. Journal of Pharmacy and Pharmacology. 2012;64(11):1603-13.

569. Rosenbaum SE. Basic pharmacokinetics and pharmacodynamics: An integrated textbook and computer simulations: John Wiley & Sons; 2016.

570. Gobeau N, Stringer R, De Buck S, Tuntland T, Faller B. Evaluation of the GastroPlus™ advanced compartmental and transit (acat) model in early discovery. Pharmaceutical Research. 2016;33:2126-39.

571. Willmann S, Lippert J, Schmitt W. From physicochemistry to absorption and distribution: predictive mechanistic modelling and computational tools. Expert Opinion on Drug Metabolism & Toxicology. 2005;1(1):159-68.

572. Aljutayli A, Marsot A, Nekka F. An update on population pharmacokinetic analyses of vancomycin, part I: In adults. Clinical Pharmacokinetics. 2020;59:671-98.

573. Heller AA, Lockwood SY, Janes TM, Spence DM. Technologies for measuring pharmacokinetic profiles. Annual Review of Analytical Chemistry. 2018;11:79-100.

574. Yáñez JA, Remsberg CM, Sayre CL, Forrest ML, Davies NM. Flip-flop pharmacokinetics–delivering a reversal of disposition: challenges and opportunities during drug development. Therapeutic Delivery. 2011;2(5):643-72.

575. Wu D, Sanghavi M, Kollipara S, Ahmed T, Saini AK, Heimbach T. Physiologically based pharmacokinetics modeling in biopharmaceutics: Case studies for establishing the bioequivalence safe space for innovator and generic drugs. Pharmaceutical Research. 2023;40(2):337-57.

576. Chryssafidis P, Tsekouras AA, Macheras P. Revising pharmacokinetics of oral drug absorption: II bioavailability-bioequivalence considerations. Pharmaceutical Research. 2021;38:1345-56.

577. Belubbi T, Bassani D, Stillhart C, Parrott N. Physiologically Based Biopharmaceutics modeling of food effect for basmisanil: A retrospective case study of the utility for formulation bridging. Pharmaceutics. 2023;15(1):191.

578. Imbimbo BP, Martinelli P, Rocchetti M, Ferrari G, Bassotti G, Imbimbo E. Efficiency of different criteria for selecting pharmacokinetic multiexponential equations. Biopharmaceutics & Drug Disposition. 1991;12(2):139-47.

579. Ludden TM, Beal SL, Sheiner LB. Comparison of the Akaike Information Criterion, the Schwarz criterion and the F test as guides to model selection. Journal of Pharmacokinetics and Biopharmaceutics. 1994;22(5):431-45.

580. Holz M, Fahr A. Compartment modeling. Advanced Drug Delivery Reviews. 2001;48(2-3):249-64.

581. Chen B, Abuassba AOM. Compartmental Models with Application to Pharmacokinetics. Procedia Computer Science. 2021;187:60-70.

582. Pisonero-Vaquero S, Medina DL. Lysosomotropic drugs: Pharmacological tools to study lysosomal function. Current Drug Metabolism. 2017;18(12):1147-58.

583. Charman SA, Andreu A, Barker H, Blundell S, Campbell A, Campbell M, et al. An *in-vitro* toolbox to accelerate anti-malarial drug discovery and development. Malaria Journal. 2020;19:1-27.

584. Espié P, Tytgat D, Sargentini-Maier M-L, Poggesi I, Watelet J-B. Physiologically based pharmacokinetics (PBPK). Drug Metabolism Reviews. 2009;41(3):391-407.

585. De Sutter P-J, De Cock P, Johnson TN, Musther H, Gasthuys E, Vermeulen A. Predictive performance of physiologically based pharmacokinetic modelling of beta-lactam antibiotic concentrations in adipose, bone, and muscle tissues. Drug Metabolism and Disposition. 2023;51(4):499-508.

586. El-Din SHS, Sabra A-NA-A, Hammam OA, El-Lakkany NM. Effect of ketoconazole, a cytochrome p450 inhibitor, on the efficacy of quinine and

halofantrine against schistosoma mansoni in mice. The Korean Journal of Parasitology. 2013;51(2):165.

587. Charbit B, Becquemont L, Lepère B, Peytavin G, Funck-Brentano C. Pharmacokinetic and pharmacodynamic interaction between grapefruit juice and halofantrine. Clinical Pharmacology & Therapeutics. 2002;72(5):514-23.

588. Parrott N, Lukacova V, Fraczkiewicz G, Bolger MB. Predicting pharmacokinetics of drugs using physiologically based modeling—application to food effects. The AAPS Journal. 2009;11:45-53.

589. Pepin XJH, Huckle JE, Alluri RV, Basu S, Dodd S, Parrott N, et al. Understanding mechanisms of food effect and developing reliable PBPK models using a middle-out approach. The AAPS Journal. 2021;23:1-14.

590. Derendorf H. Excessive lysosomal ion-trapping of hydroxychloroquine and azithromycin. International Journal of Antimicrobial Agents. 2020;55(6):106007.

591. Homolak J, Kodvanj I. Widely available lysosome targeting agents should be considered as potential therapy for COVID-19. International Journal of Antimicrobial Agents. 2020;56(2):106044.

592. Yousef M, Bou-Chacra N, Löbenberg R, Davies NM. Understanding lymphatic drug delivery through chylomicron blockade: A retrospective and prospective analysis. Journal of Pharmacological and Toxicological Methods. 2024;129:107548.

593. Yousef M, Park C, Chacra NB, Davies NM, Löbenberg R. Novel first-generation dissolution models to investigate the release and uptake of oral lymphotropic drug products. AAPS PharmSciTech. 2024;25(6):187.

594. Dolton MJ, Chiang PC, Chen Y. Mechanistic oral absorption modeling of halofantrine: Exploring the role of intestinal lymphatic transport. Journal of Pharmaceutical Sciences. 2021;110(3):1427-30.

595. Wu D, Li M. Current state and challenges of physiologically based biopharmaceutics modeling (PBBM) in oral drug product development. Pharmaceutical Research. 2023;40(2):321-36.

Appendix 1

Development of an *In-silico* Model to Study Lymphatic Uptake of Drugs Following Oral Administration via Chylomicrons

Background:

The lymphatic system comprises different components (tissues, organs, and vessels) distributed throughout the body. It is involved in all immunological processes in addition to its main role in balancing body fluids and conveying absorbed fat and lipophilic molecules from the gastrointestinal tract to the general circulation (A1.1). It is now associated with more diseases than ever thought, ranging from cancer, inflammatory and metabolic conditions to infections including viral ones like the COVID-19 (A1.2). Additionally, delivering drugs through the lymphatic system, particularly intestinal lymphatics- offers many advantages. They include enhanced therapeutic efficacy, increased drug exposure, and selective targeting to localized and metastatic conditions (cancer) among others (A1.3, A1.4).

Many studies aimed at developing lipid-based nanoparticles as promising candidates for lymphatic delivery (A1.2, A1.5). To assess their performance, various models have been established. Generally, the *in-vivo* models are the best, but in our case, they involve irreversible invasive surgical procedures that cannot be performed on humans. Several *in-vitro* models have also been developed (A1.5). One in-vitro model that was found to be significantly correlated to the in-vivo lymphatic voyage after oral administration depends on the extent of drugs association with the chylomicrons (A1.6). The only *in-silico* model using the same approach relied on correlating the molecular descriptors to the lymphatic uptake of drugs (A1.7).

With the stated correlation between the in-vitro drug-chylomicron association and the extent of the in-vivo lymphatic uptake, the aim was set at developing a structure-based

model to appropriately forecast the in-vivo outcome of the oral formulations targeting lymphatics.

To achieve that, two things have to be done: 1) to simulate the chylomicrons and 2) to study the association of different lymphotropic drugs with the simulated chylomicrons and compare the results with the reported in-vitro and in-vivo data to validate the virtual model. The focus was set on simulating the chylomicron and specifically on the part constituting the majority of its structure; the triglyceride part of the core (**Figure 1**). Thus, the objective was determined to simulate that part of the chylomicrons via molecular dynamic simulations.

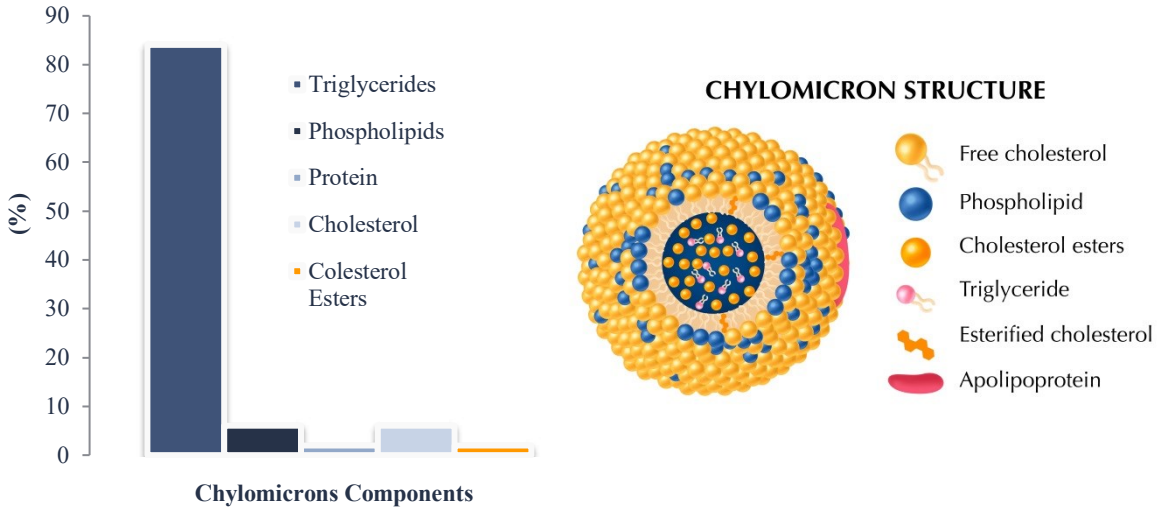

Figure 1. Illustration showing chylomicron structure (right) and the percentage of its different components (left). Triglycerides forms more than 80% of the total composition.

Methodology:

Tripalmitin ($C_{51}H_{98}O_6$) was selected to represent the triglyceride core of the chylomicrons; as it is one of the common triglycerides encountered in diet and with chylomicrons (A1.8). It is a saturated molecule having three palmitoyl chains connected to a glycerol backbone. A schematic figure of the tripalmitin is shown **in Figure 2.** The steps

for conducting the tripalmitin simulation can be classified into as pre-simulation, simulation and post-simulation stages (**Figure 3**) and will be detailed next.

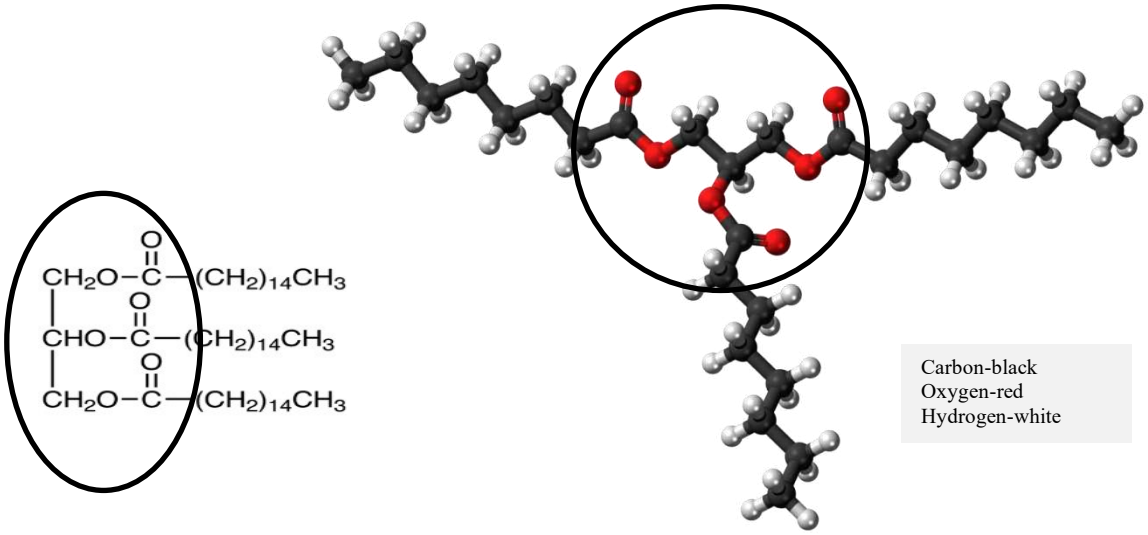

Figure 2. Schematic representation of tripalmitin ($C_{51}H_{98}O_6$), showing the glycerol backbone with the three palmitoyl moieties .The black circles denotes the hydrophilic part (head), while the uncricles part represents the hydrophobic part of the structure (tails). Image is available under Creative Commons CC0 1.0 Universal Public Domain Dedication

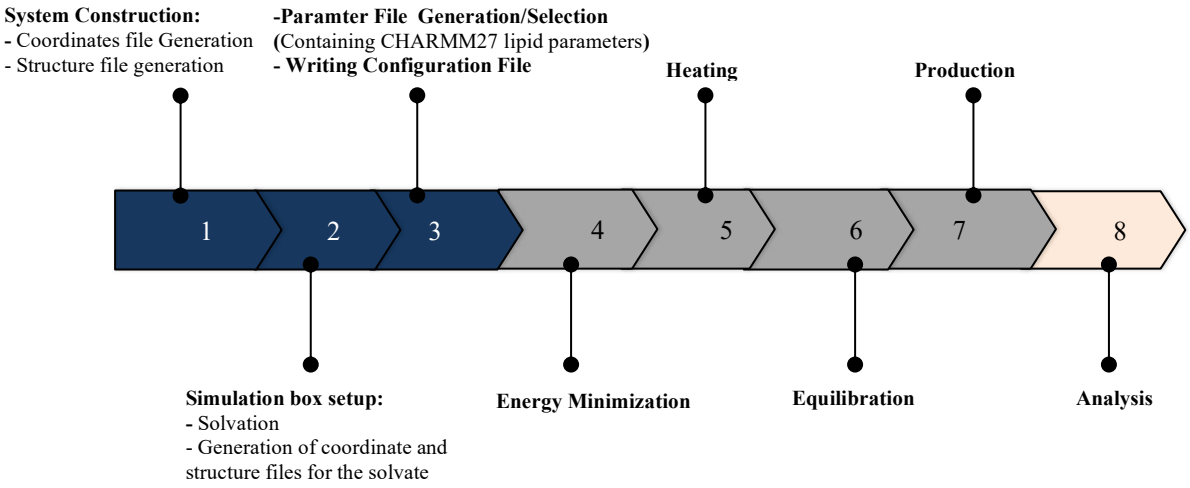

Figure 3. Scheme showing the different steps followed to complete the project. They can fall into pre-simulation (1-3), simulation (4-7) and post-simulation (8) steps.

I. Pre-simulation stage:

The input files formatted as protein data bank (PDB) and protein structure file (PSF) were generated through the charmm-gui membrane builder tool (A1.9-A1.11). The monolayer builder was selected to add 40 residues on the upper leaflet and the same number in the lower leaflet, to have a molecule with a total number of 80 tripalmitin residues (**Figure 4**). The produced system dimensions were based on the number of lipid molecules added in each leaflet. The files were visualized using visual molecular dynamic software (VMD 1.9.4) and were checked for any possible errors (A1.12). Next, the tripalmitin system was solvated using VMD. Water was used as a solvent and the simulation box was set to be added in a 20Å in each direction from the atom with the largest coordinate in that direction. The coordinate and structure files were also generated for the solvate to be used in the simulation.

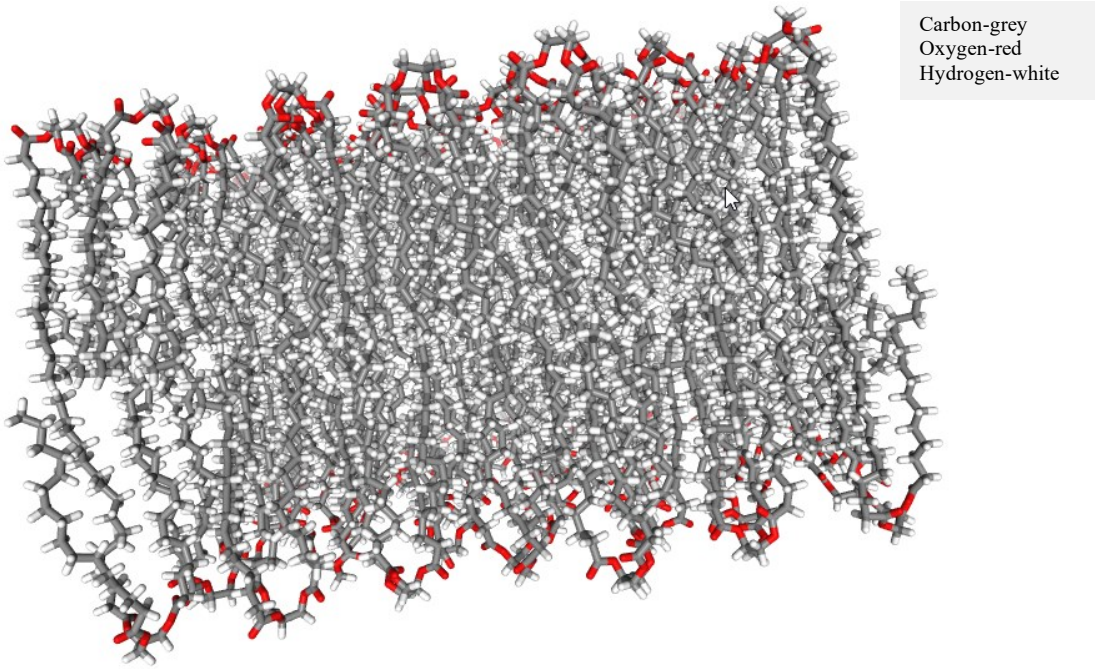

Figure 4. Visualization of the system built by charmm-gui membrane builder tool to be used in the simulation. It contains 40 residues of tripalmitin in each leaflet.

The used parameter file defines the following force fields; CHARMM22 for proteins and CHARMM27 for lipids. Other parameters defining the connectivity between the atoms including, bonds length, angles, dihedrals and improper dihedrals are all included (A1.13, A1.14). The partial charges on atoms are defined in the psf file while, the Van der Waals interactions are represented by Lennard-Jones potential, whose parameters are detailed in the parameter file for the different atoms (A1.15).

II. Simulation stage:

The simulation was run through NAMD 2.14 on Compute Canada platform (A1.16). The simulation was run in four steps; energy minimization, heating, equilibration, and production. Periodic boundary conditions were applied with a cut-off of 10 Å, as the Particle Mesh Ewald (PME) was used for the for full-system periodic electrostatics. The group-based pressure was selected to control the periodic cell fluctuations. In the minimization step, the temperature was set to 310 K. The initial coordinates were taken from the provided PDB file and the velocities were randomly initiated from a Boltzmann distribution. The integration time step was set at 2fs; as the length of bonds involving hydrogen atoms was fixed. Non-bonded forces must be calculated at least every 2fs, which was the case here, and the electrostatics forces were measured every other step. NPT ensemble was used and Langevin dynamics was employed to bring the system to the set temperature. For the pressure, the Langevin dynamics were applied to the Nosé-Hoover Langevin piston that was coupled to a heat bath to control the pressure at the required target. Constraints were applied on the head atoms with a harmonic constraint force constant of 20 N/m set in the beta column of new PDB file of the solvate in the box. The minimization was done over 100,000 steps (0.2 ns)

For the heating step, all was kept the same; however the start was form the last coordinates in the minimization step. Heating was done through rescaling through 100 iterations with 250 steps at each time. The constraints were also kept the same at this step. Yet, in the equilibration step, the constraints were gradually decreased and the run was over 5000 iterations with 1000 steps in each. Finally, starting form the final equilibration coordinates, the production step was run for 1000,000 steps without any applied constraints.

III. Post-simulation Stage:

The results of the different simulation runs were visualized and analyzed using VMD and the relevant data was acquired and is depicted in the discussion section.

Results and discussion:

Chylomicrons represent the class of lipoproteins that did not get the same attention as the other lipoproteins when it comes to molecular dynamic simulations. The focus has always been on the high-density lipoproteins and the low-density lipoproteins (HDL and LDL, respectively) due to their association with major health risks such as cardiovascular diseases (A1.17). Despite being a class of lipoproteins, chylomicrons are unique in the structural compositions that differ greatly from the HDL and LDL moieties. They are mainly composed of triglycerides (more than 80%) as shown earlier, while the LDL and the HDL only contain about 10% and 5%, respectively of the triglycerides in their cores (A1.18, A1.19). Moreover, coarse-grained simulations have been widely used to study these lipoproteins in order to overcome the timescale issues of the atomistic models (A1.20,

A1.21). Such models group the atoms with similar properties into a bead to compute the different properties from a simplified representation of the studied systems (A1.22-A1.24).

For all of what was mentioned, this project aimed at modeling the chylomicrons with atomic resolution in an explicit solvent to best represent the actual system. The goal is to use the simulated model for predicting the lymphatic uptake of drugs which is to best of our knowledge has not been applied before through a similar approach. For this part though, only the triglyceride core will be simulated.

Even for the part being simulated at this stage, the triglycerides- most of the available models were in the absence of solvents and utilized coarse-grained simulations and united atom (UA) force field (A1.8, A1.20). These approaches were utilized to study mainly liquid–solid transition involving the crystallization and the melting processes of triglycerides to obtain the crystal structure of triglycerides using a quenching process (A1.8) and to study how the length of aliphatic chains and the number and location of unsaturated bonds would affect the physical properties of the triglycerides (A1.25).

The triglyceride system chosen to be simulated was generated by the charmm-gui membrane builder as shown in **Figure 4**. The intended goal is to have a stable system by the end of the simulation; therefore the focus in the discussion will be on the energy part of the system as it is the indicator of the system stability. The approach taken to reach the proposed goal relied on the basics of the molecular dynamic simulations. The energy minimization step was executed to enable the system to find an arrangement which is more energetically stable than the starting conformation (A1.26). During this step, the atoms forming the tripalmitin heads were fixed to make simulation more computationally efficient

without sacrificing its accuracy. It was run for 0.2 ns, over a 100,000 steps. As the energy minimization algorithm usually stops once the first stable set of coordinates (local minimum) is reached (A1.27), it was observed that in our system no major changes in energy occurred after the first 8000 steps (0.016 ns). The potential energy of the whole system was decreased from 28391713 to -308788.8484 Kcal/mol as seen in **Figure 5**.

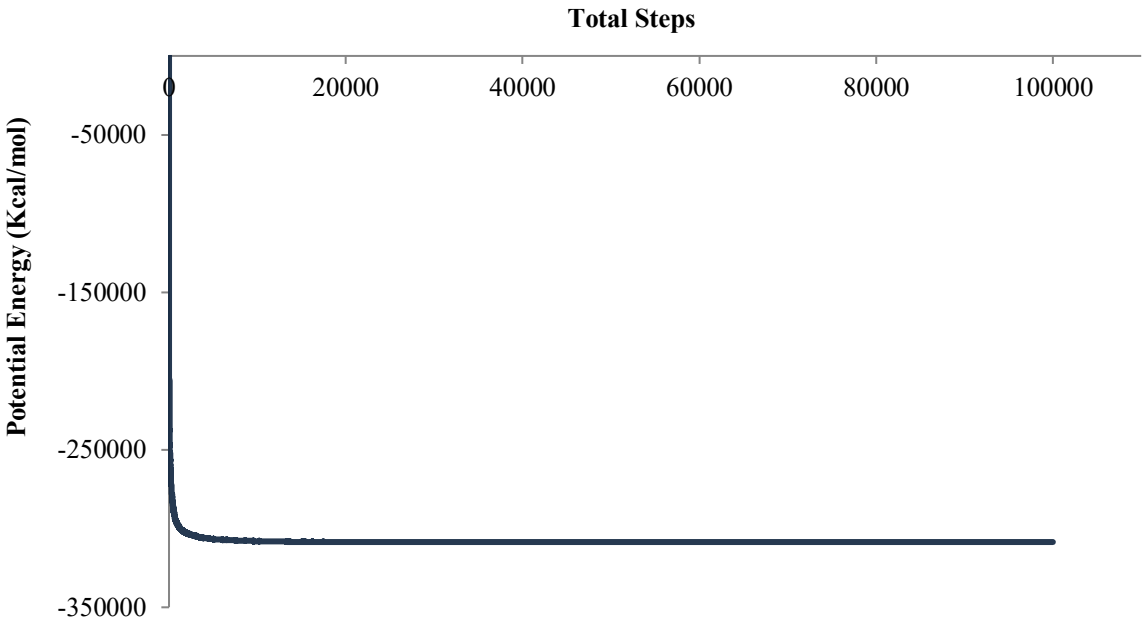

Figure 5. Graph displaying the reduction of the potential energy in the energy minimization step of the simulation. The potential energy of the whole system was decreased from 28391713 to -308788.8484 Kcal/mol in the first 8000 steps.

Next was heating that was run for 0.05 ns. It was essential to help the system escape the local minimum and overcome the energy barrier to access the surrounding conformational space, looking for the most stable arrangement (global minimum) (A1.28). Here again, the constraints were kept as they were. As the temperature was increasing, so was the kinetic energy of the system (kinetic energy = 0.5 mass / velocity ^2) (A1.29). On the contrary, the potential energy was decreasing, while the total energy which is the result of the addition of two was in between as depicted in **Figure 6.**

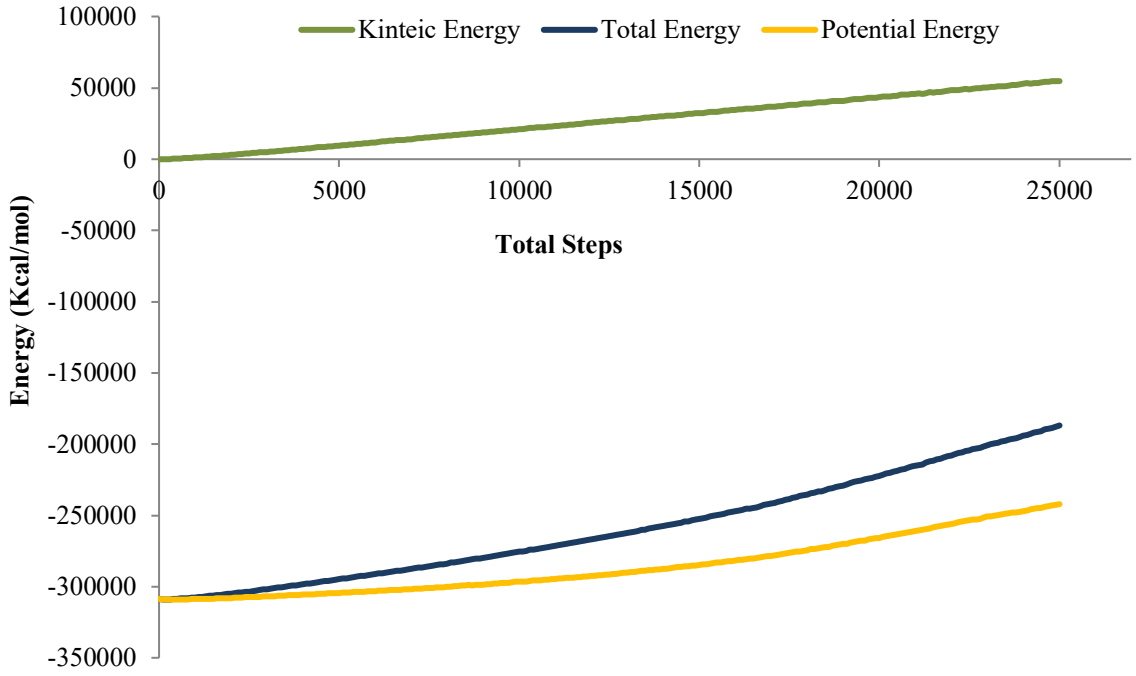

Figure 6. Chart showing the different energies during the heating step. The kinetic energy (green) was increasing while the potential (yellow) was decreasing as the system was escaping a local minimum.

In the equilibration step the run was for 0.1 ns. In that step, the system was brought close to its equilibrium states to assure that the proper conditions for the initiation of a simulation at the given thermodynamic parameters. The constraints were alleviated gradually. It was observed that all energies equilibrate for long enough to proceed to the next step as shown in **Figure 7**. Other thermodynamic energies were also checked to confirm the equilibration (A1.30). Temperature and pressure were found to flocculate within a narrow window as observed in (data not shown).

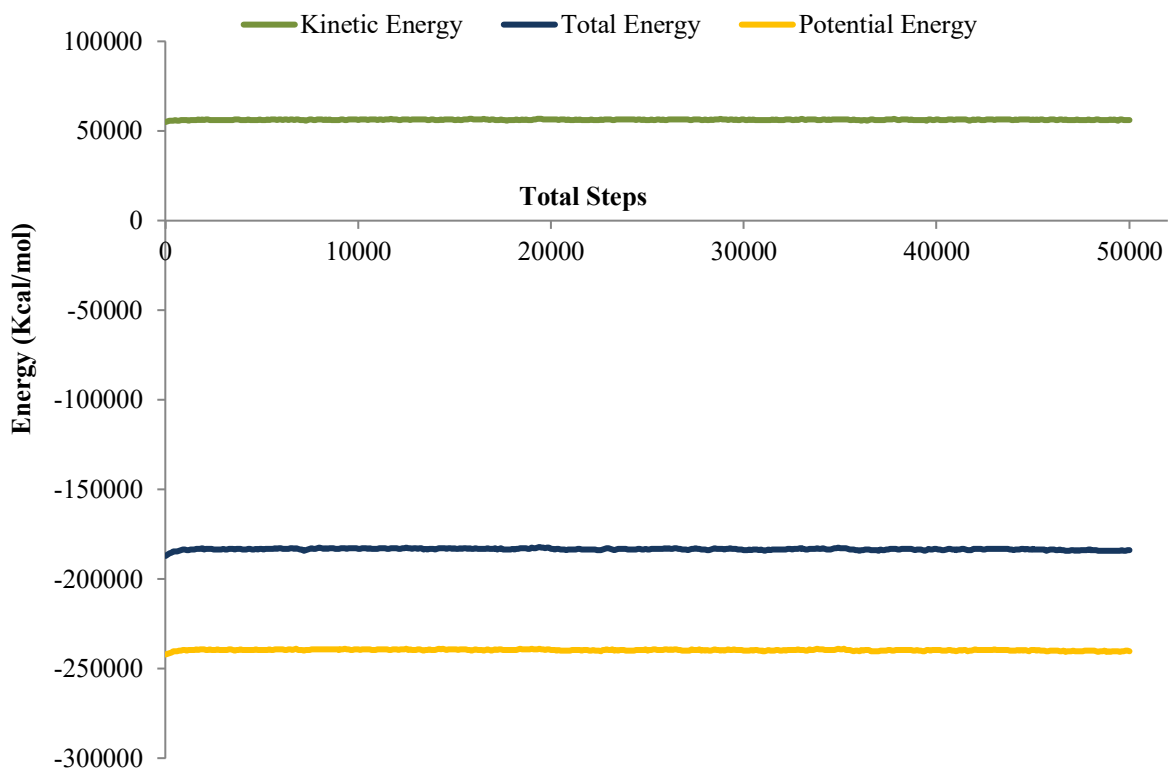

Figure 7. Illustration of the equilibration of the kinetic (green), potential (yellow) and total (blue) energies during the equilibration step.

The final step was the production that lasted for 2ns, over which the energies were at equilibrium (**Figure 8**). However with a closer look at the root mean square deviation (RMSD), which is an indication of the structural difference in the system (A1.31)- it was noticed that, at the beginning the production the RMSD values were increasing (**Figure 9**). Nevertheless, towards the end of the simulation, the fluctuation started to decrease. In the last 500 steps, the RMSD value was less than 1.4 A indicating that the system might be approaching the arrangement of the most stable set of coordinates. A definitive conclusion requires running the simulation for a long time, 1 ps or more might be sufficient to achieve that.

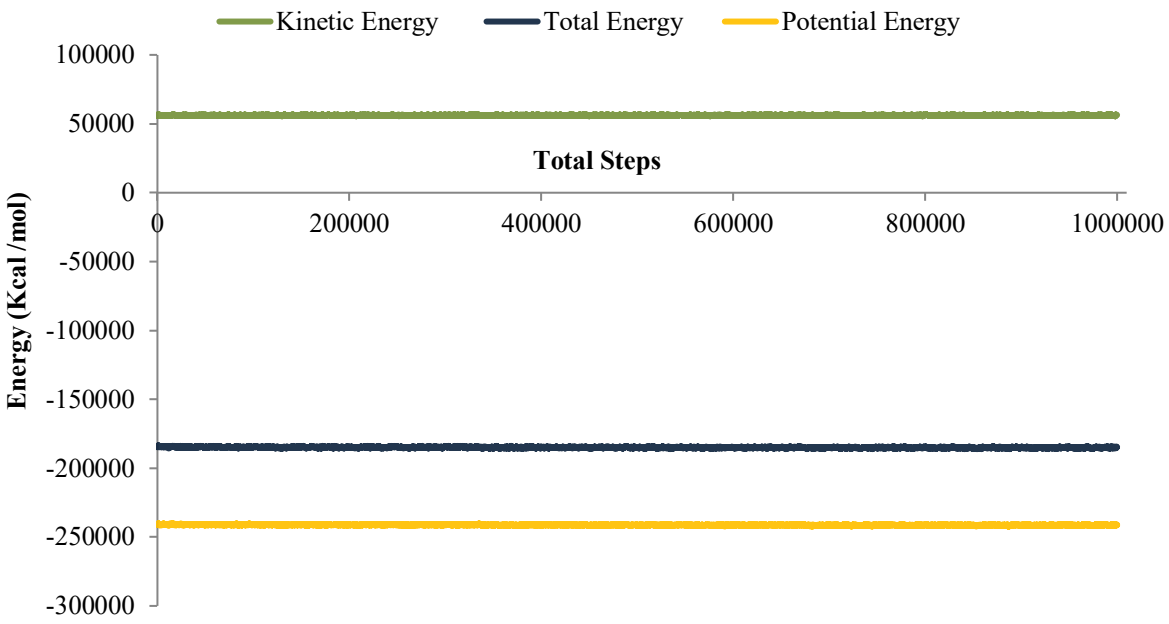

Figure 8. Chart illustarting the equilibration of the kinetic (green), potential (yellow) and total (blue) energies during the production step.

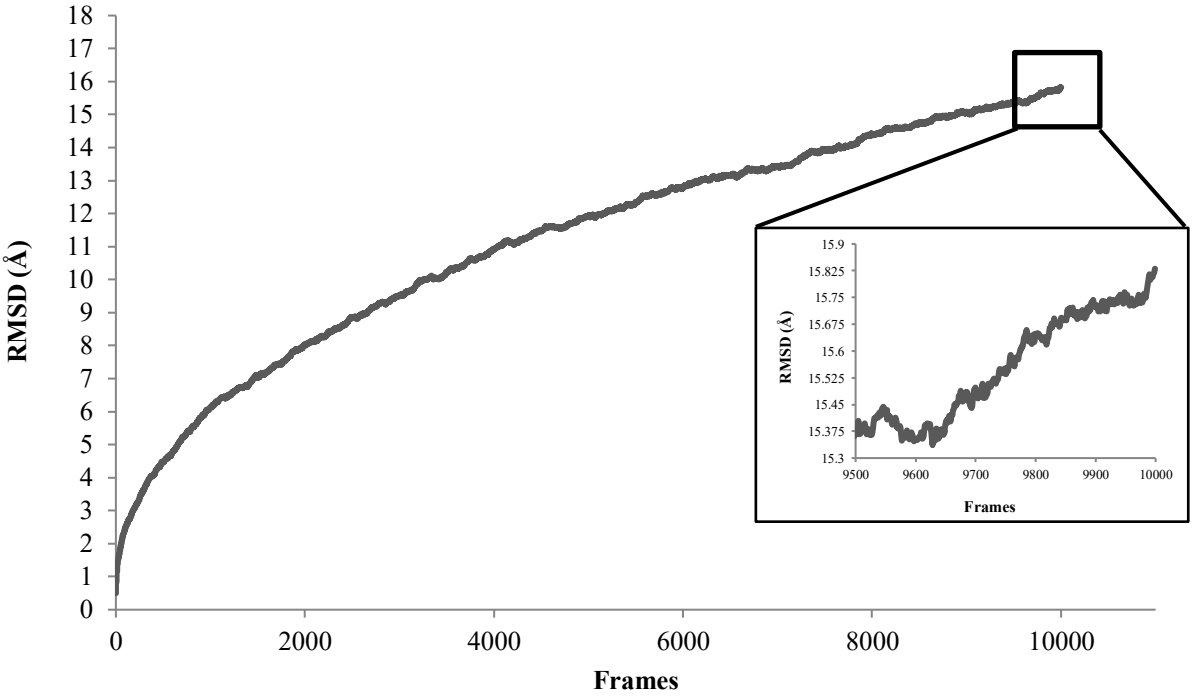

Figure 9. Graph depicting the root mean square deviation (RMSD) during the production step. At the beginning the production the RMSD values were increasing, however in the last 500 steps, the fluctuation in the RMSD value was within less than 1 Å indicating that the system might be approaching the arrangement of the most stable set of coordinates.

It is worth mentioning that, comparing the system throughout the simulation time, it was observed that the hydrophilic heads started to group in contact with the water surface while the hydrophobic tails started to cluster in the middle (video is attached to this link*). Moreover, the different conformations of the tripalmitin were seen during the simulation, the trident, tuning fork and chair (**Figure 10**) (A1.8). Characterizing the proportioned these confirmations later after the end of the simulation will help determine the polymorph of the tripalmitin produced in the simulation. That can be added to the analysis that will be done when a longer production time is applied.

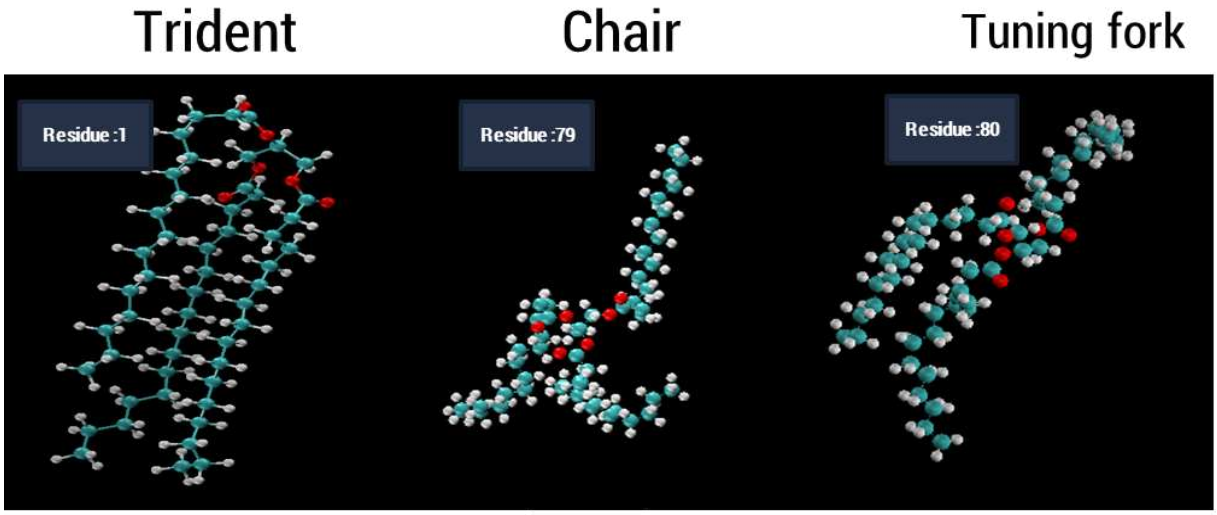

Figure 10. Illustration of the different tripalmitin conformations (trident, chair and tuning fork) seen during the simulation which were reported in literature (A1.8).

Conclusion:

Chylomicron-drug association can serve in predicting the *in-vivo* lymphatic uptake of drugs. The aim was modeling the triglyceride part of the chylomicrons core which represents more than 80% of their structure. Tripalmitin was chosen to achieve that and the modeled system was simulated until equilibration was attained. However, a longer

*Link: https://drive.google.com/file/d/1ngOnjQB3Axqram1XL2eFmGsfiPNkqZNZ/view?usp=sharing

production time is required to ensure the stability and reproducibility of the simulated system. This initial step can be followed by simulating the remaining parts of the chylomicron (both core and surface) and testing the association of selected lymphotropic drugs with the developed *in-silico* chylomicrons. Then, validating the model by comparing the association results with *in-vivo* data would create a robust model.

References:

A1.1. Yousef M, Park C, Le TS, Chacra NB, Davies NM, Löbenberg R. Simulated lymphatic fluid for in-vitro assessment in pharmaceutical development. Dissolution Technology. 2022;29:86-93.

A1.2. Yousef M, Silva D, Chacra NB, Davies N, Löbenberg R. The lymphatic system: A sometimes-forgotten compartment in pharmaceutical sciences. Journal of Pharmacy & Pharmaceutical Sciences. 2021;24:533-47.

A1.3. Cifarelli, V. and A. Eichmann, The intestinal lymphatic system: functions and metabolic implications. Cellular and Molecular Gastroenterology and Hepatology. 2019;7(3):503-513.

A1.4. Zhang Z, Lu Y, Qi J, Wu W. An update on oral drug delivery via intestinal lymphatic transport. Acta Pharmaceutica Sinica B. 2021;11(8):2449-68.

A1.5. Punjabi MS, Naha A, Shetty D, Nayak UY. Lymphatic Drug Transport and Associated Drug Delivery Technologies: A Comprehensive Review. Current Pharmaceutical Design. 2021;27(17):1992-8.

A1.6. Gershkovich, P. and A. Hoffman, Uptake of lipophilic drugs by plasma derived isolated chylomicrons: linear correlation with intestinal lymphatic bioavailability. European Journal of Pharmaceutical Sciences. 2005;26(5):394-404.

A1.7. Gershkovich P, Fanous J, Qadri B, Yacovan A, Amselem S, Hoffman A. The role of molecular physicochemical properties and apolipoproteins in association of

drugs with triglyceride-rich lipoproteins: in-silico prediction of uptake by chylomicrons. Journal of Pharmacy and Pharmacology. 2009;61(1):31-9.

A1.8. Hall A, Repakova J, Vattulainen I. Modeling of the triglyceride-rich core in lipoprotein particles. The Journal of Physical Chemistry B. 2008;112(44):13772-82.

A1.9. Jo S, Kim T, Iyer VG, Im W. CHARMM-GUI: a web-based graphical user interface for CHARMM. Journal of Computational Chemistry. 2008;29(11):1859-65.

A1.10. Wu EL, Cheng X, Jo S, Rui H, Song KC, Dávila-Contreras EM, et al. CHARMM-GUI membrane builder toward realistic biological membrane simulations. Wiley Online Library; 2014.

A1.11. Jo S, Kim T, Im W. Automated builder and database of protein/membrane complexes for molecular dynamics simulations. PloS one. 2007;2(9):e880.

A1.12. Humphrey W, Dalke A, Schulten K. VMD: visual molecular dynamics. Journal of Molecular Graphics. 1996;14(1):33-8.

A1.13. Schlenkrich M, Brickmann J, MacKerell AD, Karplus M. An empirical potential energy function for phospholipids: criteria for parameter optimization and applications. Biological Membranes: Springer; 1996. p. 31-81.

A1.14. Feller SE, Yin D, Pastor RW, MacKerell Jr AD. Molecular dynamics simulation of unsaturated lipid bilayers at low hydration: parameterization and comparison with diffraction studies. Biophysical Journal. 1997;73(5):2269-79.

A1.15. Phillips J, Isgro T, Sotomayor M, Villa E. NAMD TUTORIAL. 2003.

A1.16. Phillips JC, Hardy DJ, Maia JDC, Stone JE, Ribeiro JV, Bernardi RC, et al. Scalable molecular dynamics on CPU and GPU architectures with NAMD. The Journal of Chemical Physics. 2020;153(4):044130.

A1.17. Barter P, Gotto AM, LaRosa JC, Maroni J, Szarek M, Grundy SM, et al. HDL cholesterol, very low levels of LDL cholesterol, and cardiovascular events. New England Journal of Medicine. 2007;357(13):1301-10.

A1.18. Rosenson RS, Davidson MH, Hirsh BJ, Kathiresan S, Gaudet D. Genetics and causality of triglyceride-rich lipoproteins in atherosclerotic cardiovascular disease. Journal of the American College of Cardiology. 2014;64(23):2525-40.

A1.19. Tada H, Takamura M, Kawashiri M-a. Genomics of hypertriglyceridemia. Advances in Clinical Chemistry. 2020;97:141-69.

A1.20. Pizzirusso A, Brasiello A, De Nicola A, Marangoni AG, Milano G. Coarse-grained modelling of triglyceride crystallisation: A molecular insight into tripalmitin tristearin binary mixtures by molecular dynamics simulations. Journal of Physics D: Applied Physics. 2015;48(49):494004.

A1.21. Hammad MA, Akram HM, Raza MS. Atomistic Molecular Dynamics Simulations of Trioleoylglycerol–Phospholipid Membrane Systems. bioRxiv. 2020

A1.22. Damirchi B, Rouhollahi A, Sohrabi S, Nemati Mehr SM, editors. Modeling and Stability Analysis of Truncated High Density Lipoprotein (HDL) System Using

Martini Coarse Grain Technique 2013: American Society of Mechanical Engineers.

A1.23. Shih AY, Freddolino PL, Arkhipov A, Schulten K. Assembly of lipoprotein particles revealed by coarse-grained molecular dynamics simulations. Journal of Structural Biology. 2007;157(3):579-92.

A1.24. Pan L, Segrest JP. Computational studies of plasma lipoprotein lipids. Biochimica et Biophysica Acta (BBA)-Biomembranes. 2016;1858(10):2401-20.

A1.25. Hsu W-D, Violi A. Order− disorder phase transformation of triacylglycerols: Effect of the structure of the aliphatic chains. The Journal of Physical Chemistry B. 2009;113(4):887-93.

A1.26. Adcock SA, McCammon JA. Molecular dynamics: survey of methods for simulating the activity of proteins. Chemical Reviews. 2006;106(5):1589-615.

A1.27. Roy K, Kar S, Das RN. Understanding the basics of QSAR for applications in pharmaceutical sciences and risk assessment: Academic press; 2015.

A1.28. Pietrucci F. Strategies for the exploration of free energy landscapes: Unity in diversity and challenges ahead. Reviews in Physics. 2017;2:32-45.

A1.29. Leng Y, Jiang S. Spanning time scales in dynamic simulations of atomic-scale friction. Tribology Letters. 2001;11(2):111-5.

A1.30. Smith LJ, Daura X, van Gunsteren WF. Assessing equilibration and convergence in biomolecular simulations. Proteins: Structure, Function, and Bioinformatics. 2002;48(3):487-96.

A1.31. Knapp B, Frantal S, Cibena M, Schreiner W, Bauer P. Is an intuitive convergence definition of molecular dynamics simulations solely based on the root mean square deviation possible? Journal of Computational Biology. 2011;18(8):997-1005.

.

Appendix 2

Development of Flubendazole Nano-structured Lipid Carriers (FLU-NLCs) Utilizing Precirol® ATO 5, Gelucire®50/13, Maisine® CC, and Lipoid®

Introduction:

Flubendazole (FLU), chemically known as 5-(4-fluorobenzoyl)-1H-benzimidazole-2-yl-carbamic acid methyl ester, is a benzimidazole derivative (**Figure 1**). This compound was first approved in 1980 to target the gastrointestinal nematode infections for both human and animal treatment (A2.1).

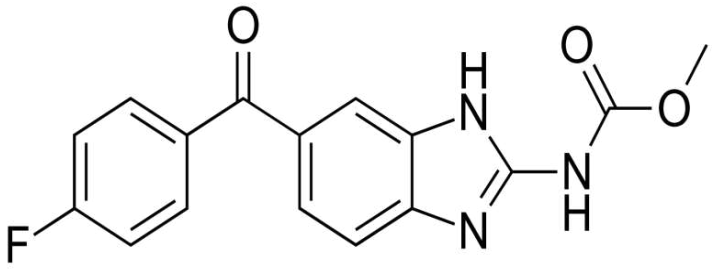

Figure 1. Structure of flubendazole (PubChem CID: 35802).

FLU imparts its anthelmintic action by altering microtubule structure, hindering tubulin polymerization, disrupting microtubule function, and impeding the microtubule-mediated transport of secretory vesicles in the absorptive tissues of helminthes (A2.2, A2.3). In recent years, it has been reported to exhibit anti-tumor activity in various types of cancers, including melanoma (A2.4), neuroblastoma (A2.5), lung cancer (A2.6), colorectal cancer (A2.7), squamous cell carcinoma (A2.8), breast cancer (A2.9), and others (A2.10-A2.12). The antitumor effect of FLU has been associated with its ability to inhibit the tumor cell cycle, proliferation, and growth (A2.11). Ongoing research continues to explore the different mechanisms in greater detail.

FLU is classified under the Biopharmaceutics Classification System (BCS) as a Class II drug, which is characterized low aqueous solubility (0.005 mg/mL @ 25 ºC) and high permeability (log P = 3) (A2.13). This classification accounts for the limited oral

bioavailability of FLU; even with an oral dose of 2 g in humans, the maximum plasma concentration of FLU remained below 5 ng/mL (A2.11).

To improve bioavailability, flubendazole has been reformulated into an amorphous solid dispersion (ASD) oral preparation (A2.14), nanocrystals (A2.15), nanoemulsions (A2.16), PEGylated nanoparticles (A2.17), as well as other nano-based systems (A2.18, A2.19). To the best of our knowledge, there are no documented reports of FLU being formulated into nanostructured lipid carriers (NLCs).

NLCs consist of a lipid phase, an aqueous phase, and surfactant(s). The lipid phase is a blend of solid and liquid lipids (oils) that are generally recognized as safe (GRAS) (A2.20). This combination creates an imperfect lattice structure, which provides high drug entrapment efficiency and minimizes the risk of drug expulsion, making NLCs an improvement over solid lipid nanoparticles (SLNs) (A2.20, A2.21). Moreover, NLCs share the advantages of other nano-based systems including biocompatibility and safety, protection of the drug from enzymatic degradation, suitability for large-scale manufacturing, and controlled drug release (A2.20).

In addition to the previously mentioned advantages of NLCs, they offer further benefits related to being lipid-based formulations. These formulations can enhance bioavailability by stimulating enterocytes to form chylomicrons, which are then absorbed into the intestinal lymphatics rather than the portal blood (A2.22). This process helps evade first-pass metabolism, thereby increasing bioavailability (A2.23). Furthermore, intestinal lymphatic uptake can offer therapeutic advantages for drugs that treat diseases originating or spreading through the lymphatic system (A2.23). Flubendazole is such a drug, with both

anthelmintic and specific anti-leishmanial properties, and has demonstrated antitumor activity (A2.8). Leishmaniasis spreads by infecting immune cells that travel through the lymphatic system. In its visceral form, the disease affects internal organs, leading to complications like persistent lymphadenopathy (enlarged lymph nodes) and lymphedema (swelling due to lymphatic obstruction) (A2.24). Additionally, cancers often spread through the lymphatics, which have wider vessels, lower pressure gradients, and higher permeability (A2.23).

The development of NLCs entails a complex, multistage production process with numerous formulation variables (A2.20), makes it challenging to manage these variables through multiple experiments. Therefore, a systematic approach such as the Quality by Design (QbD) is advantageous. QbD helps in recognizing and understanding critical quality attributes (CQAs). These CQAs are the vital properties and characteristics that must be controlled within specified limits to ensure that the final product achieves the intended quality, safety, and efficacy, consistent with the Quality Target Product Profile (QTPP) (A2.25).

The objective was to develop nanostructured lipid carriers for flubendazole using a QbD-based approach, specifically targeting delivery through the intestinal lymphatics via the chylomicron pathway.

Materials and Methods:

Materials:

The various solid lipids used in this study were generously provided by IOI Oleo Chemical (Germany) and Gattefossé (France). **Table 1** details their chemical compositions

as specified in the technical documents. Lipoid® S100 (phosphatidyl choline from soybean) was kindly donated by Lipoid GmBH (Brazil). Dimethyl sulfoxide (DMSO) was procured from Sigma Aldrich (Darmstadt, Germany), and ultrapure water was obtained from the Milli-Q® Plus (Gradient 10 system, Millipore®, USA).

Methods:

Selection of lipids:

For the selection of solid lipids, the lipids listed in **Table 1** were tested by adding a specific amount of flubendazole to known weight of the lipid, which was heated to 10 degrees above its melting point. Only clear mixtures were considered to indicate successful drug solubilisation. For the liquid lipids, prior work by Yukuyama *et al.* (A2.16) identified the suitable liquid lipid options for the FLU-NLCs.

Table 1. List of tested solid lipids for developing the nanostructured lipid carriers of flubendazole (FLU-NLCs).

Solid Lipids	Chemical Composition
Compritol® 888 ATO**	Mono-, di- and triglycerides of behenic acid (C22)
Precirol® ATO 5**	Glyceryl palmito-stearate (C16-C18)
Softisan® 154*	Hydrogenated Palm Oil
Dynasan® 116*	Tripalmitin (C16)
Dynasan® 118*	Glyceryl Tristearate (C18)
Dynasan® P 60 F*,#	Palmitic (C16)/stearic (C18)triglycerides
Witepsol® E85*	Hard fat
IMWITOR® 900 K*	Glycerol Monostearate (C18, 40-55%)
Gelucire® 50/13**	Stearoyl (C18) macrogol-32 glycerides
Gelucire® 44/14**	Lauroyl (C12) macrogol-32 glycerides

***** These lipids were kindly donated by IOI Oleo Chemical (Germany), ****** These lipids were kindly donated by Gattefossé (France), # Dynasan P 60 F is no longer being produced.

Preparation of nanostructured lipid carriers of flubendazole (FLU-NLCs):

Formulations totaling 50.0 g were prepared, incorporating the chosen liquid lipid (Maisine® CC), along with the selected solid lipids (Precirol® ATO 5, Gelucire® 50/13), and Lipoid® S 100. Initially, the oil and aqueous phases were heated to 80-85°C using an RTC basic IKA® magnetic stirrer at 300 rpm until complete dissolution was achieved. Subsequently, the oil phase was dispersed into the aqueous phase and homogenized using a mechanical homogenizer at 8000 rpm (Ultraturrax, IKA from Sigma-Aldrich® (Merck KGaA, Darmstadt, Germany)) for 5 min. The resulting coarse emulsion underwent further processing through a high-pressure homogenizer, specifically the Nano DeBEE® (BEE International, Inc. USA), employing five consecutive cycles at 600 bar.

Optimization of the prepared nanostructured lipid carriers of flubendazole (FLU-NLCs):

To generate a mathematical model to study the effects of the independent variables on the produced NLCs, central composite design (CCD) was used. The average particle size (z-average, nm) was selected as the dependent or the response variable. Based on the preliminary experiments, the independent variables were identified to be the ratio of Precirol® ATO 5 to Gelucire® 50/13 **(A)**, the percentage of Lipoid® S 100 (w/w) **(B)**, the amount of flubendazole in the formulation (mg/g lipid) **(C)**. Also, the levels of these input variables were determined to be as listed in **Table 2**. With this design, a total of 20 runs were designed using Minitab® 22.1 (State College, PA, USA).

Table 2. The Input variables with their upper and lower levels incorporated in the central composite design for developing nanostructured lipid of flubendazole (FLU-NLCs).

	Independent Variable	Levels	
		Lower Level (-1)	Upper Level (+1)
A	Precirol® ATO 5 : Gelucire® 50/13	0.4	2.5
B	% Lipoid® S 100 (w/w)	1	1.5
C	Amount of Flubendazole (mg/ g lipid)	1	3

Measurement of particle size, polydispersity index (PDI) and potential zeta:

The z-average of the NLCs was measured through dynamic light scattering technique (DLS) via Ultra Malvern Ultra Zeta Sizer (Malvern, UK) at an angle of 173° and 25 °C. This device employs a 10 mW, 632.08 nm HeNe laser, an adaptive correlation algorithm, and an avalanche photodiode (APD) detector. The samples were diluted with ultrapure water with each being run 3 times in quintuplicate. The obtained particle sizes along with the polydispersity index (PDI) were noted as mean ± standard deviation (s.d.).

Zeta potential was measured using the same instrument via the electrophoretic light scattering technique (ELS). To do so, ultrapure water with a conductivity adjusted to 50 μS.cm−1 was prepared by adding NaCl 0.2 % (w/v) and used to dilute the samples before measurement (n=5). Obtained values were quoted as mean ± s.d.

Assessment of Entrapment Efficiency (EE) and Drug Loading (DL):

To determine the entrapment efficiency (EE) and the drug loading (DL), FLU-NLCs were centrifuged in 0.5 mL-Amicon® Ultra Centrifugal Filter units (Sigma-Aldrich®, Merck KGaA, Darmstadt, Germany) with a molecular weight cut-off of 10 KDa. Centrifugation was done at 25 ºC, 10,000g for 30 min in Eppendorf® Centrifuge 5427R

(Sigma-Aldrich®, Merck KGaA, Darmstadt, Germany). The resultant filtrate was diluted and using equations 1 and 2, the entrapment efficiency and the drug loading were calculated, respectively.

$$\text{EE (\%)} = \frac{Amount\ of\ Flubedazole\ in\ the\ Formulation - Flubendazole\ Amount\ in\ the\ Filterate}{Amount\ of\ Flubendazole\ in\ the\ Formulation} \times 100 \quad \text{(Eq.1)}$$

$$\text{DL (\%)} = \frac{Amount\ of\ Flubedazole\ in\ the\ Formulation - Flubendazole\ Amount\ in\ the\ Filterate}{Total\ Amount\ of\ Lipids\ in\ the\ Formulation\ (mg)} \times 100 \quad \text{(Eq.2)}$$

Drug concentration analysis – Sample preparation and calibration curve:

A stock solution of FLU was prepared by dissolving 0.0025 g of FLU in 25 mL of DMSO in a volumetric flask, resulting in a concentration of 100 µg/mL. Working standard solutions were then prepared through serial dilutions of the stock solution with DMSO. A calibration curve (R^2 = 0.994) for flubendazole was constructed using Evolution™ 201 UV-visible spectrophotometer (Thermo Fisher Scientific Inc., MA, USA) at a wavelength of 310. The resultant equation was as follows:

Absorbance = 96.526 (Flubendazole conc. mg/mL) + 0.0244 (Eq.3)

Results and Discussion:

Selection of formulation components: Solid and liquid lipids and surfactants:

For the selection of solid lipids, the results obtained with different lipids are presented in **Table 3**. Due to the discontinuation of the best option, Dynasan® P 60 F, the second-best lipids were considered. Gelucires emerged as the second-best choice, known for their widespread application in formulations to improve solubility, dissolution, and bioavailability of drugs (A2.26). However, Gelucires, primarily being surfactants composed polyethylene glycol (PEG) esters, a small glyceride fraction, and free PEG

(A2.26, A2.27), require other solid lipids to form the core of nanostructured lipid carriers (NLCs). Preliminary studies confirmed that Gelucires would produce heterogeneously distributed NLCs (PDI > 0.3).

Gelucire® 50/13, is mainly used for the preparation of solid dispersions to improve the aqueous solubility of hydrophobic drugs (A2.26). It was selected due to its content of long-chain fatty acids which are known to be incorporated into chylomicrons, thereby facilitating lymphatic uptake (A2.28). The preliminary studies also revealed that NLCs prepared with Gelucire® 50/13 fell within the desired size range, which will be discussed in detail later. Specifically, these NLCs had sizes of 151.70 ± 1.36 nm when compared with those prepared using Gelucire® 44/14 that had a size of and 245.00 ± 1.64 nm. Gelucire® 50/13 has a hydrophilic-lipophilic balance (HLB) value of 11-13 and a melting point of 50 °C (A2.26, A2.29). Its incorporation into NLCs have been reported to enhance the drug loading of hydrophobic drugs, especially those with poor affinity for solid lipids, and stabilize the resultant NLCs (A2.30).

Precirol® ATO 5 was identified as the best solid lipid for incorporation to form the NLC core, considering its composition of esters of long-chain fatty acids (A2.31). It has a melting point (50-60 °C) and HLB of 2 (A2.31) that make it suitable for improving the bioavailability of many drugs incorporated into NLCs (A2.32) and through the intestinal lymphatics (A2.33).

For the liquid lipids, Maisine CC® demonstrated the highest solubilization capacity, measured at 0.34 mg/g, as reported by Yukuyama *et al.* (A2.16) and presented in **Table 4**. Interestingly, Maisine CC®, a glyceryl monolinoleate, is particularly advantageous for

lymphatic targeting due to its long-chain fatty acid content. This compound has been incorporated into formulations due to these beneficial properties (A2.34, A2.35).

Table 3. Results of flubendazole solubilisation in the tetsed solid lipids for developing the nanostructured lipid carriers of flubendazole (FLU-NLCs).

Solid Lipids	Flubendazole Solubilisation @ 1 mg / g lipid	Flubendazole Solubilisation @ 0.5 mg / g lipid
Compritol® 888 ATO**	NO	NO
Precirol® ATO 5**	NO	YES
Softisan ® 154*	NO	NO
Dynasan® 116*	NO	NO
Dynasan® 118*	NO	NO
Dynasan® P 60 F*#	YES	YES
Witepsol® E85*	NO	_
IMWITOR® 900 K*	NO	_
Gelucire® 50/13**	YES	YES
Gelucire ® 44/14**	YES	YES

Table 4. List of tested liquid lipids considered for developing nanostructured lipid carriers of flubendazole (FLU-NLCs) adopted from Yukuyama *et al.* (A2.16).

Liquid Lipids	Flubendazole Solubilisation @ 1 mg / g lipid
Maisine CC®	0.34
Labrafac Lip. WC1349®	0.21
Miglyol 812®	0.16
Captex 8000®	0.17
Captex 300®	0.13
Captex 355®	0.13

However, both the solid and liquid forms tested showed low FLU solubilization (< 1 mg/g). Consequently, Lipoid® S 100 was investigated for its potential to solubilize flubendazole. The use of the phosphatidylcholine product (Lipoid® S 100) achieved three

key outcomes: it increased the amount of solubilized flubendazole by nearly 15 times (15 mg/g), acted as a surfactant, and facilitated targeted delivery to the lymphatics via chylomicrons. In the gastrointestinal tract, phosphatidylcholine was reported to be incorporated into chylomicrons upon reaching the enterocytes. It specifically assembles with apolipoprotein B (apoB-48) in the endoplasmic reticulum to merge into the triglyceride-rich core of chylomicrons (A2.36).

FLU-NLCs Development and Optimization:

Based on the recommendations of International Council for Harmonisation of Technical Requirements for Pharmaceuticals for Human Use (ICH) Q8 guidelines, experimental judgment, and previous reports, a QbD-based approach was used for developing and optimizing FLU-NLCs. The QTPP for these NLCs included nano-structured particles with a z-average of 80.00-200.00 nm, a PDI < 0.30, and physical stability at 4°C ± 2°C over 3 months.

CCD was chosen to model both linear and quadratic effects in the studied FLU-NLCs. CCD is known for its robustness in experimental design and optimization. By incorporating both factorial and axial points, along with center points, CCD enables accurate estimation of interaction effects and curvature in the response surface. This ensures a comprehensive understanding of the behavior of the studied system (A2.37, A2.38).

Using the chosen components and selected variables, the experimental formulations based on the CCD were prepared. **Table 5** provides detailed information on these formulations and the results obtained, including the selected response (z-average) as well as

two other physicochemical parameters (zeta potential and PDI). Measured particle size peaks of the produced formulations are shown in **Figure 2**.

Table 5. Formulations (F1-F20) of the central composite design (experimental matrix) used to study and optimize the nanostructured lipid of flubendazole (FLU-NLCs).

	Precirol® ATO 5 (%w/w)	Gelucire® 50/13 (%w/w)	Maisine® CC (%w/w)	Lipoid® S100 (%w/w)	Purified Water (%w/w)	Flubendazole Amount (mg/g lipid)	z-average (nm ± s.d.)	PDI ± s.d.	Zeta Potential (mV ± s.d.)
F1	5.91	4.09	1.00	1.25	88.75	3.00	209.08 ± 2.27	0.19 ± 0.02	-16.26 ± 0.81
F2	5.91	4.09	1.00	1.00	89.00	2.00	166.60 ± 1.68	0.14 ± 0.02	-15.33 ± 0.53
F3	5.91	4.09	1.00	1.50	88.50	2.00	235.10 ± 2.59	0.17 ± 0.02	-19.29 ± 1.01
F4	5.91	4.09	1.00	1.25	88.75	2.00	311.90 ± 2.84	0.23 ± 0.01	-17.74 ± 0.95
F5	5.91	4.09	1.00	1.25	88.75	2.00	275.60 ± 2.25	0.19 ± 0.02	-16.40 ± 0.20
F6	2.87	7.13	1.00	1.25	88.75	2.00	58.40 ± 0.41	0.14 ± 0.02	-8.19 ± 1.79
F7	7.13	2.87	1.00	1.50	88.50	3.00	226.40 ± 1.56	0.25 ± 0.01	-16.80 ± 0.60
F8	2.87	7.13	1.00	1.00	89.00	1.00	99.26 ± 0.82	0.11 ± 0.01	-11.98 ± 0.54
F9	2.87	7.13	1.00	1.00	89.00	3.00	314.60 ± 10.94	0.49 ± 0.08	-15.50 ± 0.87
F10	2.87	7.13	1.00	1.50	88.50	1.00	582.80 ± 22.91	0.41 ± 0.10	-14.78 ± 0.95
F11	2.87	7.13	1.00	1.50	88.50	3.00	91.86 ± 0.81	0.12 ± 0.03	-7.30 ± 0.67
F12	5.91	4.09	1.00	1.25	88.75	2.00	237.30 ± 4.11	0.20 ± 0.01	-16.67 ± 0.47
F13	5.91	4.09	1.00	1.25	88.75	2.00	312.30 ± 3.82	0.21 ± 0.01	-20.06 ± 0.74
F14	7.13	2.87	1.00	1.00	89.00	3.00	249.10 ± 2.04	0.25 ± 0.02	-17.38 ± 0.84
F15	7.13	2.87	1.00	1.25	88.75	2.00	457.70 ± 32.83	0.85 ± 0.09	-31.40 ± 1.27
F16	7.13	2.87	1.00	1.50	88.50	1.00	219.90 ± 1.33	0.25 ± 0.01	-18.12 ± 1.02
F17	7.13	2.87	1.00	1.00	89.00	1.00	205.00 ± 1.63	0.25 ± 0.02	-20.22 ± 0.32
F18	5.91	4.09	1.00	1.25	88.75	1.00	359.10 ± 6.00	0.25 ± 0.01	-18.50 ± 0.75
F19	5.91	4.09	1.00	1.25	88.75	2.00	849.70 ± 129.00	0.21 ± 0.11	-16.17 ± 1.59
F20	5.91	4.09	1.00	1.25	88.75	2.00	635.00 ± 61.35	0.20 ± 0.08	-26.68 ± 1.04

The values for formulations 9, 10, 15, 19, and 20 were excluded from the statistical model due to high standard deviations.

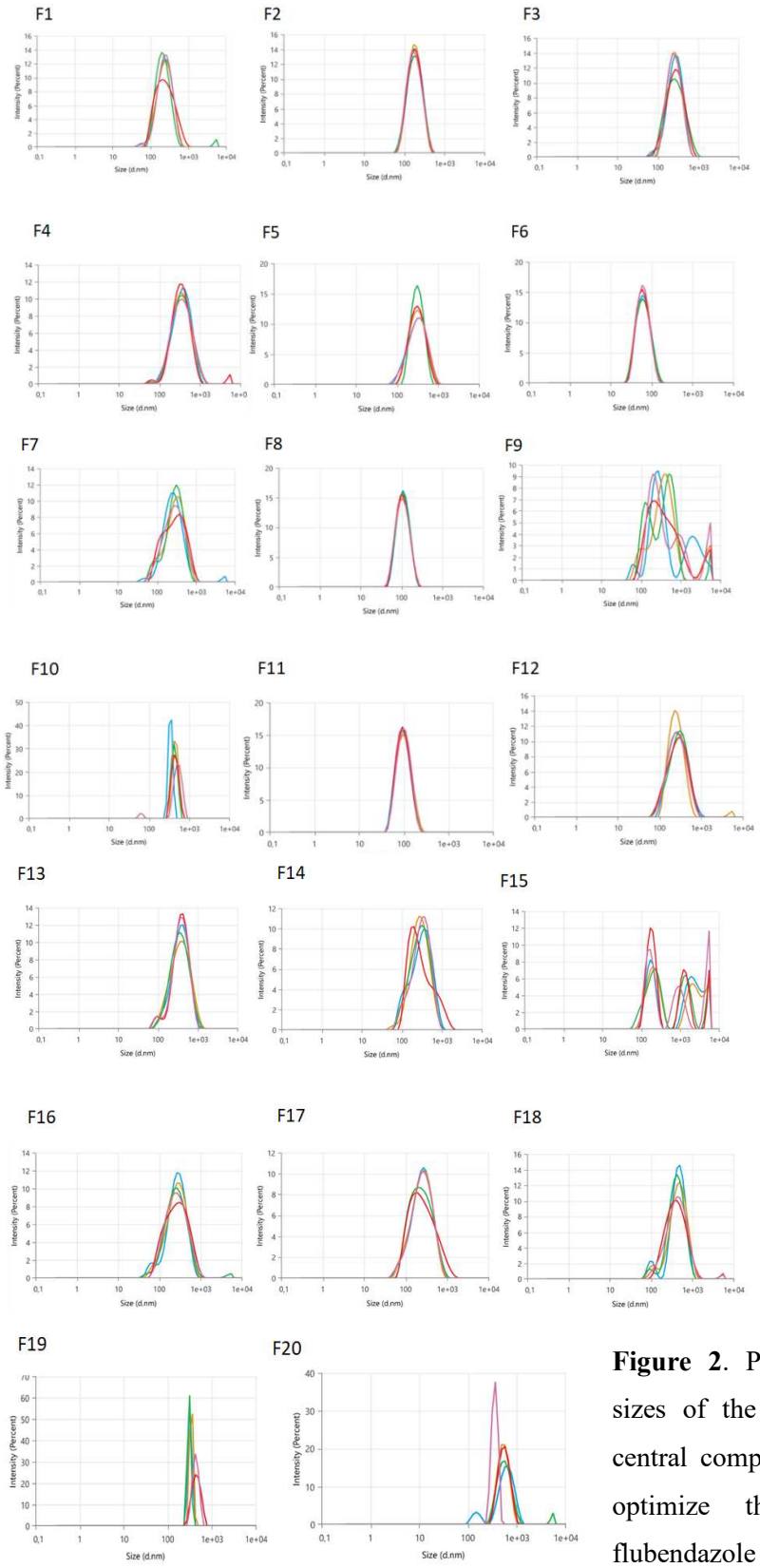

Figure 2. Peaks of the measured particle sizes of the produced formulations of the central composite design used to study and optimize the nanostructured lipid of flubendazole (FLU-NLCs).

Upon analyzing the obtained results, a second order (quadratic) polynomial model was obtained. The p-value for the lack of fit (0.469) was greater than the significance level ($\alpha = 0.05$), indicating that the model fitted the data well and there was a strong functional relationship between the independent variables and the response variable. The analysis of variance (ANOVA) of the model is depicted in **Table 6**. A strong relationship between the model and the response variable (z-average) was demonstrated by a coefficient of determination (R^2) of 95.67%. Additionally, the adjusted coefficient of determination (R^2(adj)), which accounts for the number of predictors relative to the number of data points, indicated an excellent model fit (R^2(adj) = 93.94%). Moreover, the predicted coefficient of determination (R^2(pred)) of the model demonstrated its sufficient capability to make accurate predictions for new observations (R^2(pred) = 88.82%).

Table 6. Analysis of variance of the size quadratic model of the nano-structured lipid carriers of flubendazole (FLU-NLCs).

Source	DF	Adj SS	Adj MS	F-Value	P-Value
Model	4	92764	23191.0	55.29	0.000
Linear	3	73179	24393.1	58.15	0.000
Precirol® ATO 5: Gelucire®50/13	1	44800	44800.3	106.81	0.000
Lipoid % m/m	1	10658	10658.2	25.41	0.001
Flubendazole Amount (mg/g lipid)	1	23933	23932.8	57.06	0.000
Square	1	38033	38033.3	90.67	0.000
Lipoid % m/m*Lipoid % m/m	1	38033	38033.3	90.67	0.000
Error	10	4195	419.5		
Lack-of-Fit	7	3121	445.8	1.25	0.469
Pure Error	3	1074	358.0		
Total	14	96959			
Model Summary					
R^2	95.67				
R^2(adj)	93.94%				
R^2(pred)	88.82%				

DF: Degrees of freedom, Adj SS: Adjusted sum of squares for a term, Adj MS: Adjusted mean squares, R^2: Coefficient of determination, R^2 (adj): Adjusted coefficient of determination, R^2 (pred): Predicted coefficient of determination.

The normal probability plot of residuals indicated homoscedasticity and a normal distribution of the residuals. The residuals versus fits plot displayed points randomly distributed around zero, confirming that the residuals are randomly distributed and exhibit constant variance. Additionally, the residuals versus order plot showed no discernible pattern, suggesting that the residuals were independent (**Figure 3**).

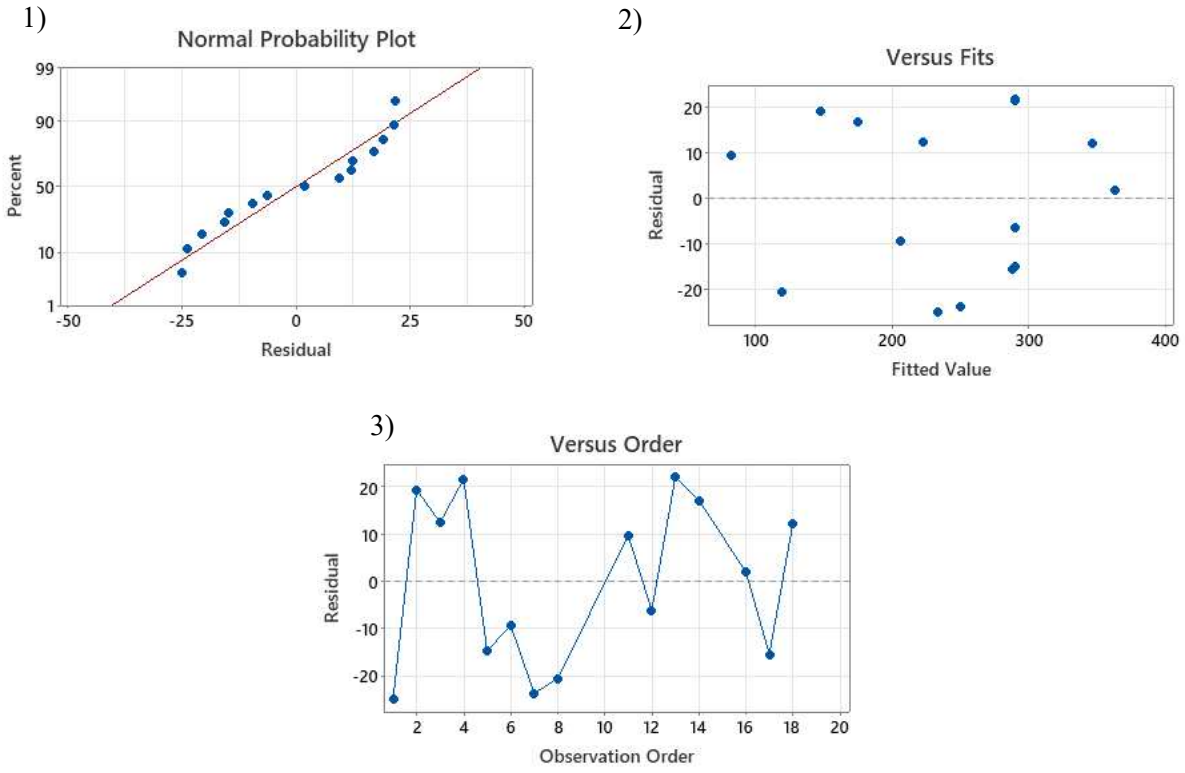

Figure 3. Normal probability plot (1), residuals versus fits plot (2), and residuals versus order plot (3) of the obtained quadratic model of nanostructured lipid carriers of flubendazole (FLU-NLCs).

The statistically significant factors ($p < 0.05$) were identified as the ratio of Precirol® ATO 5 to Gelucire® 50/13 (A), the percentage of Lipoid® S 100 (w/w) (B) and its quadratic term, and the amount of flubendazole in the formulation (mg/g lipid) (C). The p-values were 0.00 for all factors except for the quadratic term of the percentage of Lipoid® S 100 (w/w) (BB), which had a p-value of 0.001.

According to the regression equation of the model (Eq. 4), increasing the amount of Precirol® ATO 5 and the percentage of Lipoid® S 100 would result in an increase in particle size. Conversely, increasing the amount of the drug in the formulation would lead

to a decrease in particle size. Additionally, Lipoid® S 100 exhibits a quadratic effect, where the particle size decreases up to a certain point before increasing again. The same effects can be seen in the counter plots (**Figure 4**).

Z-average (nm) = -2536 + 79.95 Precirol® ATO 5: Gelucire®50/13 + 4367 Lipoid® S 100 % w/w - 56.49 Flubendazole Amount (mg/g lipid) - 1687 Lipoid % w/w*Lipoid % m/m (Eq. 4)

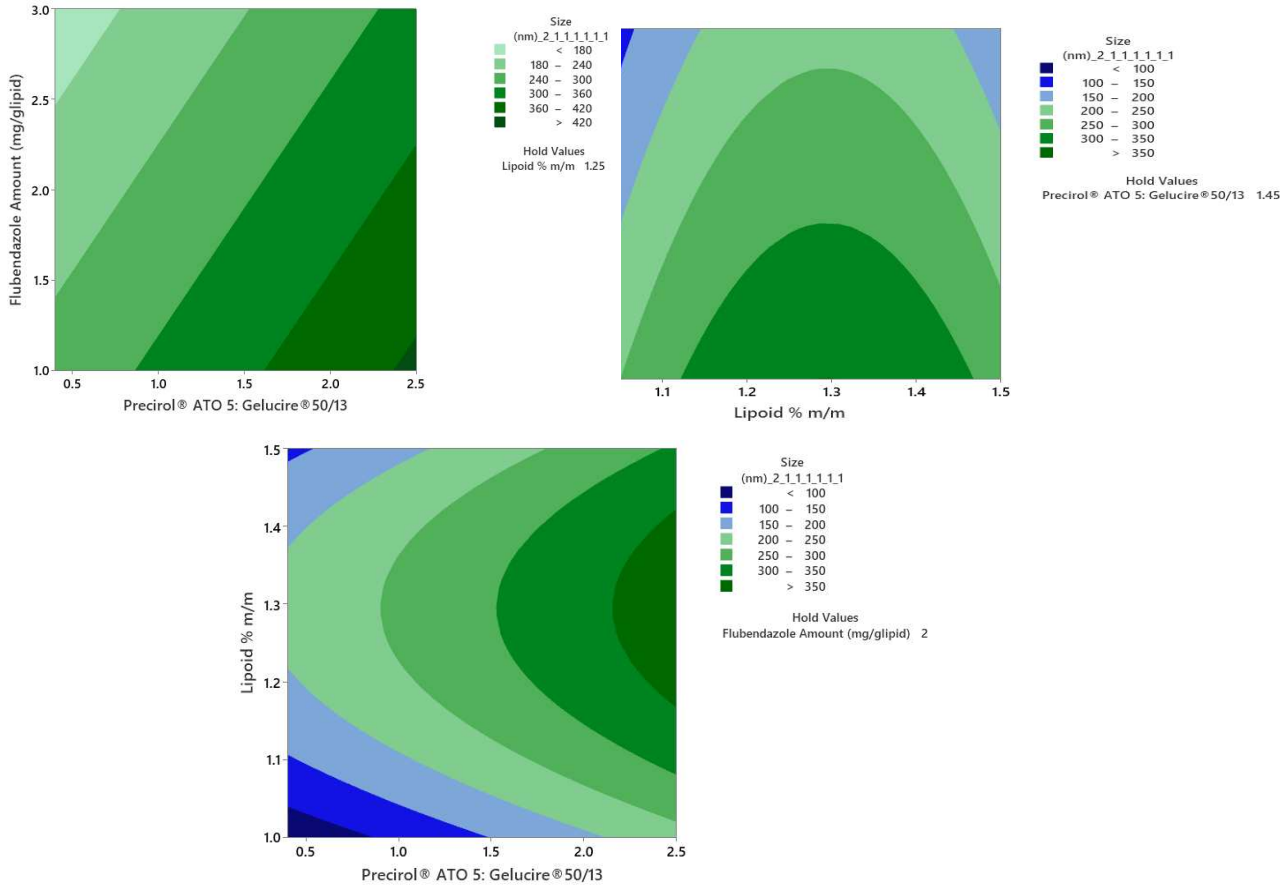

Figure 4. Contour plots showing the effects of the selected variables (Precirol® ATO 5: Gelucire®50/13, Lipoid® S 100 % w/w (or m/m), and Flubendazole Amount (mg/g lipid)) on the z-average (nm) of the nanostructured lipid carriers of flubendazole (FLU-NLCs).

From the obtained model, increasing the amount of Precirol® ATO 5, or conversely decreasing the amount of Gelucire® 50/13, results in an increase in the particle size of the NLCs. As previously mentioned Gelucire® 50/13 acts as a stabilizer (A2.26, A2.30); thus, reducing its concentration in the formulation leads to larger NLC particles. Additionally,

both lipids exhibit polymorphic forms, influencing their interaction and the resulting NLC matrix structure (A2.33). It has been reported that heating Precirol® ATO 5 at 85°C alters its polymorphic nature. Precirol® ATO 5 exists in a single β-polymorphic form prior to heat exposure but transforms into a mixture of α- and β-polymorphic forms following heat exposure (A2.39). Polymorphism is linked to gelation, as encountered in at least one of the experimental matrix formulations. As solid lipids transition to another polymorphic form, insufficient surfactant is available to fully cover the lipid phase, promoting particle aggregation through hydrophobic attraction. (A2.40). In this scenario, the transformation of the main core lipid, Precirol® ATO 5, may result in inadequate surfactant coverage, particularly as the amount of Precirol® increases. Additionally, it has been reported that incorporating Gelucire® 50/13 with Precirol® ATO 5 causes an interaction that suppresses the polymorphic transitions of both components at specific ratios (A2.30, A2.33). This interaction is potentially evidenced by some of the formulations obtained in the design.

Additionally, the model indicates that increasing the percentage of Lipoid® S 100 results in an increase in particle size. Typically, surfactants support emulsifying the lipid phase within the aqueous phase, stabilizing the particles, and preventing aggregation up to a certain concentration. Beyond this concentration, the opposite effect occurs (A2.41). The specified range for the used stabilizer (Lipoid® S 100) potentially encompasses both scenarios, which is evidenced by the quadratic term in the model referring to this phenomenon.

The reduction in particle size with increasing concentrations of flubendazole was likely due to its influence on lipid packing. Flubendazole may have interacted with the core-forming lipids, leading to tighter lipid packing, which results in smaller particle sizes.

Alternatively, it could have inhibited the crystallization of the core-forming lipids, promoting a more disordered (amorphous) lipid structure, which also contributes to size reduction. To confirm this, further analysis of the formed NLCs using appropriate methods is required.

In developing the model, it is important to note that more than 25% of the data were either excluded or adjusted. To assess the effectiveness of the model in describing the developed FLU-NLCs, the predicted values of the formulations within the design space have to be compared with the observed values. If the predicted and observed values did not align, this would suggest that the model is inadequate and that additional factors should be considered for improved accuracy. These factors likely pertain to process parameters, as formulations with identical compositions (central points) produced different responses.

For validation purposes, a z-average value of 120 nm, within a range of 100-140 nm was selected. This target value was given a weight of 1, highlighting its importance. The drug amount was maximized at 3 mg/g lipid, while other input variables were kept consistent with the original design. With a desirability score of 1, five formulations were proposed, each with different ratios of solid lipids and 100% w/w Lipoid® S 100. All proposed formulations were of 120 nm, as shown in **Table 7** and **Figure 5**. Getting comparable observed results would guarantee the model robustness.

Among the CCD formulations, F11 was identified as the one meeting the desired QTPP and containing the highest drug concentration. Consequently, F11 was selected for evaluating entrapment efficiency, which was found to be 99.05%, with a drug loading of 0.29%. The stability of F11 was monitored by measuring the size, PDI, and zeta potential

values weekly over a period of 28 days. Size and PDI served as the primary indicators of the stability of F11 (**Table 8**).

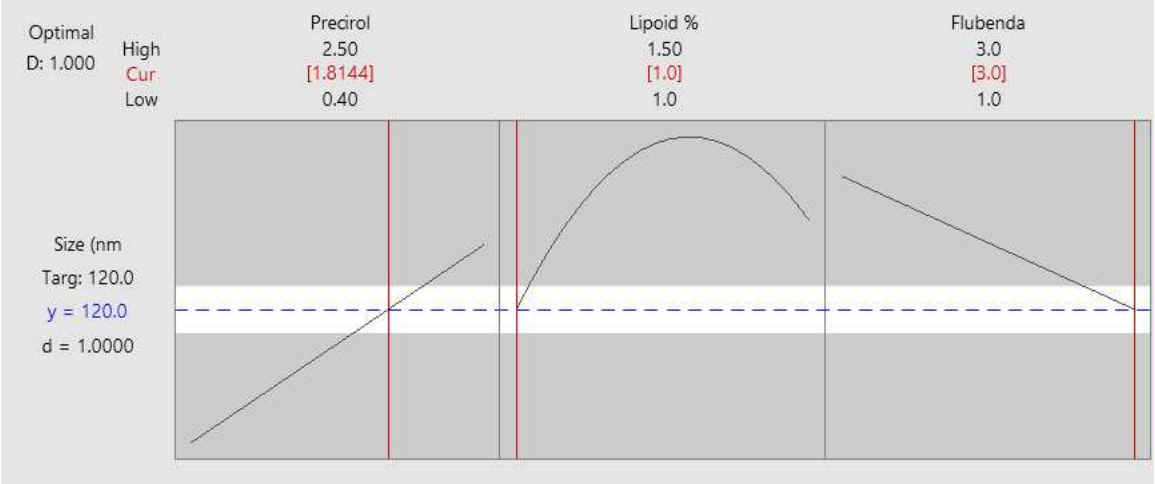

Figure 5. Optimization plot showing the values of the selected variables (Precirol® ATO 5: Gelucire®50/13 (Precirol), Lipoid® S 100 % w/w (Lipoid %), and Flubendazole Amount (mg/g lipid) (Flubenda)) which would result in the target response (size, nm) of the developed nanostructured lipid carriers of flubendazole (FLU-NLCs) with a desirability of 1.

Table 7. Values of Precirol® ATO 5: Gelucire®50/13 and Lipoid® S 100 % w/w (Lipoid %) which would result in the target response (z-average, nm) of the developed nanostructured lipid carriers of flubendazole (FLU-NLCs) that have 3 mg/g lipid of flubendazole.

	Precirol® ATO 5: Gelucire®50/13	**Lipoid ® S 100 % w/w**	**FlubendazoleAmount (mg/g lipid)**	**Size (nm)_Fit**	**Composite Desirability**
1	1.81440	1.00000	3.00	120.00	1.00
2	0.87138	1.50000	3.00	120.00	1.00
3	0.55059	1.13057	3.00	120.00	1.00
4	0.44688	1.44311	3.00	120.00	1.00
5	0.45105	1.14564	3.00	120.00	1.00

Table 8. Stability of the best produced formulation (F11) for 28 days at 4ºC indicated by its size and PDI.

Days	Size (nm ± s.d.)	PDI ± s.d.
7 Days	91.86 ± 0.81	0.12 ± 0.03
14 Days	91.02 ± 0.75	0.13 ± 0.05
21 days	91.55 ± 1.05	0.10 ± 0.01
28 days	92.26 ± 0.82	0.12 ± 0.02

Conclusion:

Nanostructured lipid carriers of flubendazole (FLU-NLCs) were successfully produced using Precirol® ATO 5, Gelucire®50/13, Maisine® CC, and Lipoid®, achieving the desired attributes to be potentially taken up by the intestinal lymphatics via chylomicrons. These carriers demonstrated stability for a one-month period. To further refine the process, testing the developed statistical model will help identify the optimization space within the design space. This will facilitate the selection of formulation variables necessary to achieve the desired quality target product profile for the FLU-NLCs before progressing further to *in-vitro* and *in-vivo* tests.

References:

A2.1. Geary TG, Mackenzie CD, Silber SA. Flubendazole as a macrofilaricide: History and background. PLoS Neglected Tropical Diseases. 2019;13(1):e0006436.

A2.2. Lacey E. Mode of action of benzimidazoles. Parasitology Today. 1990;6(4):112-115.

A2.3. Spagnuolo PA, Hu J, Hurren R, Wang X, Gronda M, Sukhai MA, et al. The antihelmintic flubendazole inhibits microtubule function through a mechanism distinct from Vinca alkaloids and displays preclinical activity in leukemia and myeloma. Blood, The Journal of the American Society of Hematology. 2010;115(23):4824-33.

A2.4. Li Y, Acharya G, Elahy M, Xin H, Khachigian LM. The anthelmintic flubendazole blocks human melanoma growth and metastasis and suppresses programmed cell death protein-1 and myeloid-derived suppressor cell accumulation. Cancer Letters. 2019;459:268-76.

A2.5. Michaelis M, Agha B, Rothweiler F, Löschmann N, Voges Y, Mittelbronn M, et al. Identification of flubendazole as potential anti-neuroblastoma compound in a large cell line screen. Scientific Reports. 2015;5(1):8202.

A2.6. Xie X, Cai X, Tang Y, Jiang C, Zhou F, Yang L, et al. Flubendazole elicits antitumor effects by inhibiting STAT3 and Activating autophagy in non-small cell lung cancer. Frontiers in Cell and Developmental Biology. 2021;9:680600.

A2.7. Hanušová V, Skálová L, Králová V, Matoušková P. The effect of flubendazole on adhesion and migration in SW480 and SW620 colon cancer cells. Anti-Cancer Agents in Medicinal Chemistry. 2018;18(6):837-46.

A2.8. Tao J, Zhao H, Xie X, Luo M, Gao Z, Sun H, et al. The anthelmintic drug flubendazole induces cell apoptosis and inhibits NF-κB signaling in esophageal squamous cell carcinoma. Oncotargets and Therapy. 2019:471-8.

A2.9. Zhang L, Guo M, Li J, Zheng Y, Zhang S, Xie T, et al. Systems biology-based discovery of a potential Atg4B agonist (Flubendazole) that induces autophagy in breast cancer. Molecular BioSystems. 2015;11(11):2860-6.

A2.10. Khachigian LM. Emerging insights on functions of the anthelmintic flubendazole as a repurposed anticancer agent. Cancer Letters. 2021;522:57-62.

A2.11. Chen C, Ding Y, Liu H, Sun M, Wang H, Wu D. Flubendazole plays an important anti-tumor role in different types of cancers. International Journal of Molecular Sciences. 2022;23(1):519.

A2.12. Zhou X, Zou L, Chen W, Yang T, Luo J, Wu K, et al. Flubendazole, FDA-approved anthelmintic, elicits valid antitumor effects by targeting P53 and promoting ferroptosis in castration-resistant prostate cancer. Pharmacological Research. 2021;164:105305.

A2.13. Vialpando M, Smulders S, Bone S, Jager C, Vodak D, Van Speybroeck M, et al. Evaluation of three amorphous drug delivery technologies to improve the oral

absorption of flubendazole. Journal of Pharmaceutical Sciences. 2016;105(9):2782-93.

A2.14. Bezzon VDN, Ferreira FF, Smith P, Benmore CJ, Byrn SR, de Araujo GLB. Amorphous dispersions of flubendazole in hydroxypropyl methylcellulose: Formulation stability assisted by pair distribution function analysis. International Journal of Pharmaceutics. 2021;600:120500.

A2.15. de Souza Gonçalves D, Yukuyama MN, Miyagi MYS, Silva TJV, Lameu C, Bou-Chacra NA, et al. Revisiting flubendazole through nanocrystal technology: statistical design, characterization and its potential inhibitory effect on xenografted lung tumor progression in mice. Journal of Cluster Science. 2023;34(1):261-72.

A2.16. Yukuyama MN, Ishida K, de Araujo GLB, de Castro Spadari C, de Souza A, Löbenberg R, et al. Rational design of oral flubendazole-loaded nanoemulsion for brain delivery in cryptococcosis. Colloids and Surfaces A: Physicochemical and Engineering Aspects. 2021;630:127631.

A2.17. Farhadi M, Haniloo A, Rostamizadeh K, Faghihzadeh S. Efficiency of flubendazole-loaded mPEG-PCL nanoparticles: A promising formulation against the protoscoleces and cysts of Echinococcus granulosus. Acta Tropica. 2018;187:190-200.

A2.18. Vigh T, Démuth B, Balogh A, Galata DL, Van Assche I, Mackie C, et al. Oral bioavailability enhancement of flubendazole by developing nanofibrous solid dosage forms. Drug Development and Industrial Pharmacy. 2017;43(7):1126-33.

A2.19. Devanesan S, Jayamala M, AlSalhi MS, Umamaheshwari S, Ranjitsingh AJA. Antimicrobial and anticancer properties of Carica papaya leaves derived di-methyl flubendazole mediated silver nanoparticles. Journal of Infection and Public Health. 2021;14(5):577-87.

A2.20. Elmowafy M, Al-Sanea MM. Nanostructured lipid carriers (NLCs) as drug delivery platform: Advances in formulation and delivery strategies. Saudi Pharmaceutical Journal. 2021;29(9):999-1012.

A2.21. Gordillo-Galeano A, Mora-Huertas CE. Solid lipid nanoparticles and nanostructured lipid carriers: A review emphasizing on particle structure and drug release. European Journal of Pharmaceutics and Biopharmaceutics. 2018;133:285-308.

A2.22. Chaudhary S, Garg T, Murthy RSR, Rath G, Goyal AK. Development, optimization and evaluation of long chain nanolipid carrier for hepatic delivery of silymarin through lymphatic transport pathway. International Journal of Pharmaceutics. 2015;485(1-2):108-21.

A2.23. Yousef M, Silva D, Chacra NB, Davies N, Löbenberg R. The lymphatic system: a sometimes-forgotten compartment in pharmaceutical sciences. Journal of Pharmacy & Pharmaceutical Sciences. 2021;24:533-47.

A2.24. Kumar A. Leishmania and leishmaniasis. Springer Science & Business Media, 2013.

A2.25. Lee S-H, Kim J-K, Jee J-P, Jang D-J, Park Y-J, Kim J-E. Quality by Design (QbD) application for the pharmaceutical development process. Journal of Pharmaceutical Investigation. 2022;52(6):649-82.

A2.26. Panigrahi KC, Patra CN, Jena GK, Ghose D, Jena J, Panda SK, et al. Gelucire: A versatile polymer for modified release drug delivery system. Future Journal of Pharmaceutical Sciences. 2018;4(1):102-8.

A2.27. Jadhav N, Gubbi S, Kadam H. Gelucires: Pharmaceutical applications. Latest Reviews. 2008;6(4).

A2.28. Yousef M, O'Croinin C, Le TS, Park C, Zuo J, Bou Chacra N, et al. *In-Vitro* predictive model for intestinal lymphatic uptake: Exploration of additional enhancers and inhibitors. Pharmaceutics. 2024;16(6):768.

A2.29. Panda TK, Das D, Panigrahi L. Formulation development of solid dispersions of bosentan using Gelucire 50/13 and Poloxamer 188. Journal of Applied Pharmaceutical Science. 2016;6(9):027-33.

A2.30. Date AA, Vador N, Jagtap A, Nagarsenker MS. Lipid nanocarriers (GeluPearl) containing amphiphilic lipid Gelucire 50/13 as a novel stabilizer: fabrication, characterization and evaluation for oral drug delivery. Nanotechnology. 2011;22(27):275102.

A2.31. Hamdani J, Moës AJ, Amighi K. Physical and thermal characterisation of Precirol® and Compritol® as lipophilic glycerides used for the preparation of

controlled-release matrix pellets. International Journal of Pharmaceutics. 2003;260(1):47-57.

A2.32. Beloqui A, del Pozo-Rodríguez A, Isla A, Rodríguez-Gascón A, Solinís MÁ. Nanostructured lipid carriers as oral delivery systems for poorly soluble drugs. Journal of Drug Delivery Science and Technology. 2017;42:144-54.

A2.33. de Souza A, Yukuyama MN, Barbosa EJ, Monteiro LM, Faloppa ACB, Calixto LA, et al. A new medium-throughput screening design approach for the development of hydroxymethylnitrofurazone (NFOH) nanostructured lipid carrier for treating leishmaniasis. Colloids and Surfaces B: Biointerfaces. 2020;193:111097.

A2.34. Holm R, Porter CJH, Edwards GA, Müllertz A, Kristensen HG, Charman WN. Examination of oral absorption and lymphatic transport of halofantrine in a triple-cannulated canine model after administration in self-microemulsifying drug delivery systems (SMEDDS) containing structured triglycerides. European Journal of Pharmaceutical Sciences. 2003;20(1):91-7.

A2.35. El-Laithy HM, Basalious EB, El-Hoseiny BM, Adel MM. Novel self-nanoemulsifying self-nanosuspension (SNESNS) for enhancing oral bioavailability of diacerein: Simultaneous portal blood absorption and lymphatic delivery. International Journal of Pharmaceutics. 2015;490(1-2):146-54.

A2.36. Murota K. Digestion and absorption of dietary glycerophospholipids in the small intestine: Their significance as carrier molecules of choline and n-3

polyunsaturated fatty acids. Biocatalysis and Agricultural Biotechnology. 2020;26:101633.

A2.37. Rakić T, Kasagić-Vujanović I, Jovanović M, Jančić-Stojanović B, Ivanović D. Comparison of full factorial design, central composite design, and box-behnken design in chromatographic method development for the determination of fluconazole and its impurities. Analytical Letters. 2014;47(8):1334-47.

A2.38. Bhattacharya S. Central composite design for response surface methodology and its application in pharmacy. Response surface methodology in engineering science: IntechOpen; 2021.

A2.39. Kasongo WA, Pardeike J, Müller RH, Walker RB. Selection and characterization of suitable lipid excipients for use in the manufacture of didanosine-loaded solid lipid nanoparticles and nanostructured lipid carriers. Journal of pharmaceutical sciences. 2011;100(12):5185-96.

A2.40. Helgason T, Awad TS, Kristbergsson K, McClements DJ, Weiss J. Influence of polymorphic transformations on gelation of tripalmitin solid lipid nanoparticle suspensions. Journal of the American Oil Chemists' Society. 2008;85:501-11.

A2.41. McClements DJ, Jafari SM. Improving emulsion formation, stability and performance using mixed emulsifiers: A review. Advances in Colloid and Interface Science. 2018 ;251:55-79.

Appendix 3

Upholding or Breaking the Law of Superposition in Pharmacokinetics: An Overview

A version of this appendix is published in:

Biomedicines. 2024;12(8),1843. DOI: 10.3390/biomedicines12081843

1. Introduction:

Although there are some drugs that can be taken acutely as a single dose such as anti-migraine drugs (1-4) or hypnotics (5-8) for a limited period of time, the vast majority of drugs such as antibiotics (9-12), anti-diabetics (13-15) and blood pressure medication (16-18) are designed to be repeatedly administered orally. Chronic disease states often require a multiple dose regimen to enable accumulation of drug and attain steady-state concentrations (19-21). The Law of Superposition or sometimes referred to as the Principle of Superposition enables the pharmacokinetics understanding of a drug after a single dose to be accurately predicted at steady-state conditions after repeated dosing or potentially vice versa (22, 23). While some scientists particularly in the pharmaceutical industry may have training during Pharmacy education in pharmacokinetics, others have a varied biomedical background and are less versed in the underlying pharmacokinetic theorems. In the 21st century drug development there are a myriad of pharmacokinetic technology programs and simulation software that will enable investigators to take and input single-dose pharmacokinetic concentration time data and predict steady-state concentrations after a specific dose regimen. Modeling programs offer the advantages of large data handling capacities and execution speed; however, the conceptual and mathematical limitations to this modeling and interpretation of the results must be clearly understood and delineated.

The Law of Superposition is a fundamental aspect of pharmacokinetics and it is often dealt within a cursory manner in textbooks. Few articles have tried to deal with a conceptual understanding of superposition in a practical pharmacokinetic manner to demonstrate the application of the principle (19, 22-32). In this article, we first present a review of the principle of superposition and then discuss its application to multiple dosing.

Finally, we apply this principle through simulations to an understanding where the Law of Superposition does not hold and illustrate the non-linearity in processes that can in fact overturn this law.

1.1. Law of Superposition:

Pharmacokinetically, the body can be considered to be a construct function that in mathematical terms converts the input (dose rate) into output or response (plasma concentration of drug) as a function of time (32-34). A linear system is characterized by input-output relationships that are completely defined by one or more linear equations, exhibiting properties of homogeneity and additivity. Linear systems applications to the field of pharmacokinetics were explored by Cutler (24, 25) where the differential equations involved define a function. The most important feature of a linear system is that it is additive and obeys the law of superposition, where the output of a linear system equals the sum of the outputs of separately applied inputs (23). The application of a linear model is contingent upon the condition that the concentrations involved are within a range where saturation effects are absent, indicating a limited scope of inputs (34, 35). For a specific inputs range, the linearity of the system can be experimentally tested to either reject or disprove the null hypothesis.

Simply put, the Law of Superposition is a mathematical concept that enables pharmaceutical scientists to predict concentration-time data (36, 37). It has, however, an underlying assumption that the preceding dose of a drug and its pharmacokinetics does not alter or affect in any way subsequent doses of a drug and the expressed pharmacokinetic profile (38-40). In practice, the plasma concentration time data after the first, second, or n^{th} dose will be superimposed by the plasma concentration reached after the $(n - 1)^{th}$ dose (39).

For practical purposes the area under the plasma concentration time curve after a single dose is equal to the area under the plasma concentration time curve after multiple doses when steady-state concentrations are attained (39) (**Figure 1**).

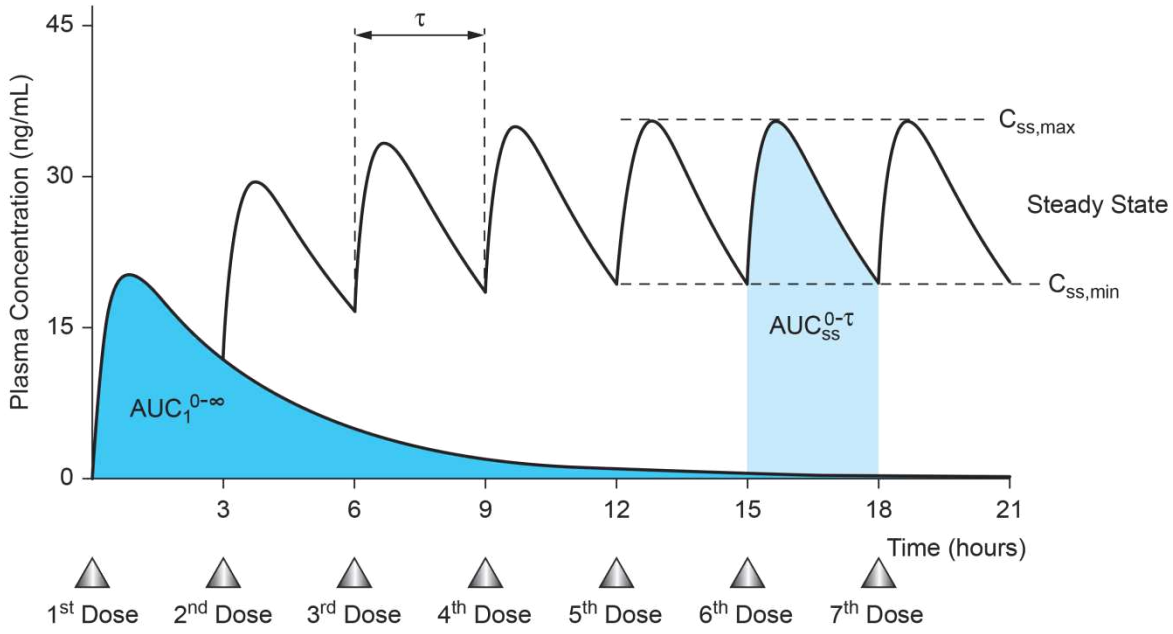

Figure 1. Concentration time profile after a single dose and multiple dosing when reaching steady state.

The Law of Superposition allows the pharmacokineticist to project the plasma drug concentration–time curve of a drug after multiple consecutive doses based on the plasma drug concentration–time curve obtained after a single dose (39, 40). This is important in clinical setting to have the patient exposed to the target drug concentration without excessive fluctuation and drug accumulation outside of the therapeutic window (37). Following a single dose, the extent of overall drug exposure over time can be quantified by estimating the area under the concentration-time curve from zero to infinity ($AUC_{0-\infty}$). During multiple dosing, the area under the concentration-time curve over a steady-state dosing interval ($AUC_{0-\tau}$) serves as a measure of overall drug exposure. When the clearance

(CL)—the aggregate of all elimination processes—remains constant (i.e., it does not change with increasing drug concentrations), the $AUC_{0-\tau}$ at steady state will be equivalent to the $AUC_{0-\infty}$ following a single-dose administration (39, 41).

In the analysis of AUC data in pharmacokinetics, the Law of Superposition provides a simple test for detecting the presence of non-linear processes that do obey the law, i.e., processes which are first-order (34). Practically, a greater than or less than response in area under the drug concentration-time curve (AUC) with repeated doses is the expressed result of involvement of zero-order processes (39). An AUC equivalence presumes that the dose administered as a single dose matches the dose given in a multiple-dose. This is useful for determining pharmacokinetic parameters (23, 27, 42). For example, after a single IV bolus dose, the total body clearance (CL) can be computed using equation 1.

$$\boldsymbol{CL = \frac{Dose}{AUC_{0-\infty}}} \qquad \textbf{(equation 1)}$$

AUC equivalence enables the estimation of clearance under steady-state conditions using the same equation but using $AUC_{0-\tau}$ instead of $AUC_{0-\infty}$. The latter clearance estimate is often referred to as steady state clearance (CL_{ss}). In the case of a single oral dose, AUC is calculated taking into consideration the bioavailability (F) of the drug when using CL_{total} (**equation 2**) or taking into consideration the fraction unbound in blood (fu) when using intrinsic clearance (CLint) (22) (**equation 3**).

$$\boldsymbol{AUC = \frac{F \times Dose}{CL_{total}}} \qquad \textbf{(equation 2)}$$

$$\boldsymbol{AUC = \frac{F \times Dose}{fu \times CLint}} \qquad \textbf{(equation 3)}$$

It becomes readily apparent in **Figure 2** that in multiple dosing the concentrations oscillate at steady state between minimum concentration at steady state (C_{SSmin}) and maximum concentration at steady state (C_{SSmax}) and that an average steady state concentration $C_{av,SS}$ can be calculated (19).

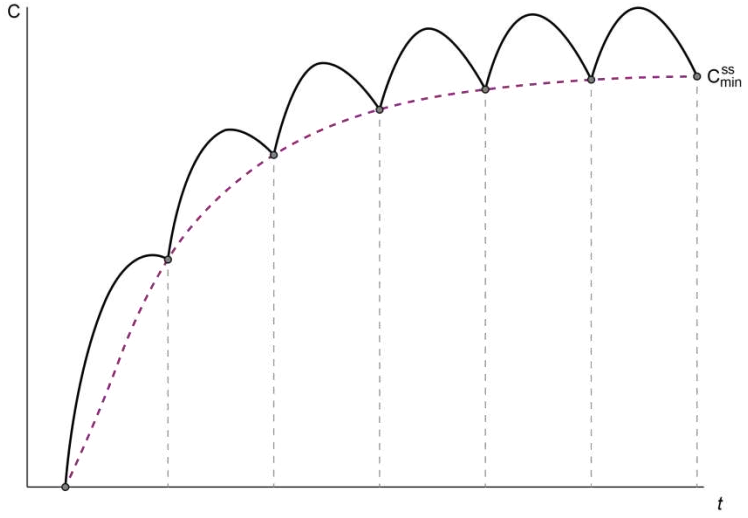

Figure 2. Concentration time profile of an ideal scenario after a multiple dose regimen administered at the same time interval and reaching steady state. Modified from Wang *et al.* (19) with permission.

The drug clearance can be determined by dividing the dose by either of the afore-mentioned two AUC values, or by dividing the dosing rate by the average steady-state concentration ($C_{av,SS}$). The $C_{av,SS}$ is calculated by dividing either of the two AUC values by the dosing interval (Tau, T) (27). Thus, the average steady-state plasma level ($C_{p,ss}$) can by calculated by **equation 4**.

$$\boldsymbol{C_{p,ss} = \frac{AUC_{0-\infty}}{T}} \qquad \textbf{(equation 4)}$$

Superposition is based on mathematical equations describing linear processes (34, 35). Both experimental data and drug development results can uphold or refute the

mathematical relationship (43). Pharmaceutical development that relies solely on equations or theoretical superposition can be misleading or incorrect. There are observational limits to when superposition occurs and when it may deviate from linearity. Ab initio superposition involves multiple untested assumptions that might not hold for a particular drug in a particular disease state, as discussed in further detail below. Modeling approaches required for predictive analytics, including superposition, can utilize simple inductive reasoning and are only sometimes correlative with observational findings (30). Further, a causally-based understanding of drugs is achieved through deductive reasoning and the application of the scientific method.

The Law of Superposition would predict that for a drug the AUC after a single dose is equal to the AUC at steady state. Therefore, equation 5 would hold true.

$$\frac{AUC_{Single\ Dose}}{AUC_{SS}} = 1 \qquad \textbf{(equation 5)}$$

This is independent of a compartmental model and is simply a function of linearity. Furthermore, the CL (after IV administration) or CL/F (after oral administration) following a single dose will equal the clearance values at steady state. In the case of oral administration, the bioavailability remains constant between a single dose and steady state. The AUC at steady state (AUC_{SS}) can be defined as in equation 6.

$$AUC_{SS} = \lim_{n\to\infty} \int_{t_n}^{t_{n+1}} C_n\,(t)dt \qquad \textbf{(equation 6)}$$

Non-linearity can cause that the AUC_{SS} to differ from the $AUC_{Single\ Dose}$ (32, 43), this will be later discussed in the section Breaking the Law of Superposition. Most drugs will

exhibit some deviation from the ideal accumulation as described (37). Nevertheless, comprehending the principle of superposition permits reasonable predictions of the pharmacokinetic behavior of drugs under repeat-dose conditions for a broad range of compounds. This understanding proves especially beneficial when transitioning from single-dose studies to repeat-dose studies during the initial stages of drug development. Additionally, this knowledge facilitates the design of repeat-dose regimens that achieve the desired drug concentrations efficiently and reliably within a clinically acceptable timeframe. When determining multiple-dose regimens, it is crucial to assess whether successive doses will impact the effects of previous doses. The principle of superposition assumes that earlier doses do not influence the pharmacokinetics of later doses. As a result, the blood levels following the second, third, or nth dose will overlay those achieved after the $(n - 1)^{th}$ dose (39). In addition, the $AUC_{0-\infty}$ following single-dose administration is equal to the steady-state area between doses (**Figure 1**). The disposition processes after an oral dose are absorption, distribution, metabolism and excretion (ADME). Therefore, the superposition principle is applicable when the ADME processes exhibit linear or first-order kinetics. With this approach, concentrations after multiple doses can be determined by summing the concentrations from each dose (24, 25, 42). Furthermore, doubling the dose will result in proportional doubling of the concentrations at each time. However, this principle does not apply when any of the disposition processes are non-linear (24, 25, 34).

Mathematically a single-dose concentration-time curve $C(t)$ is a function over time denoted as a function over time $f(t)$ (42). Multiple dosing occurs when the administered doses remain constant over the time, where the drug is administered at fixed time intervals (tau) (**Figure 3**). The concentration at time t after n doses is equal to the sum of the

concentration at *t* after *n - 1* doses and the single-dose concentration at *t* - t_n (from the last dose) (22). Therefore, the contribution of the last dose can be superimposed to that of the first *n - 1* doses (22). The concentration-time curve C*n(t)* is described in equations 7 and 8.

$$\boldsymbol{C_n(t) = C_{n-1}(t) + f(t - t_n)} \qquad \textbf{(equation 7)}$$

$$\boldsymbol{C_n(t) = \sum_{i=1}^{n} f(t - t_i)} \qquad \textbf{(equation 8)}$$

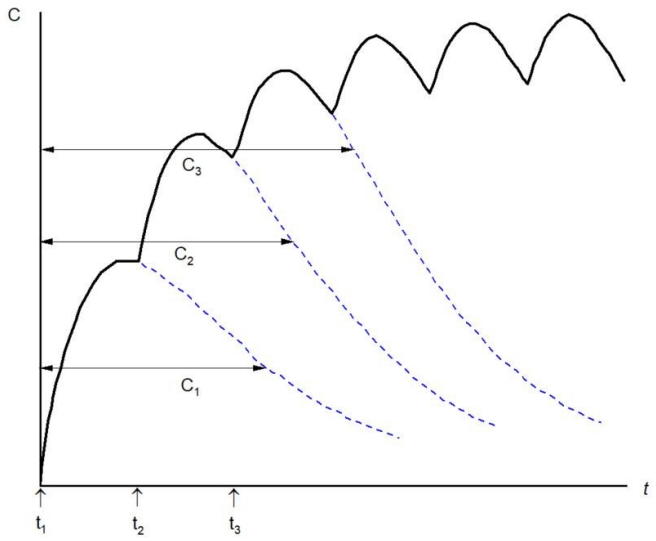

Figure 3. Representation of a concentration time profile after six sequential doses ad-ministered at the same time interval to steady-state. Modified from Wang *et al.* (19) with permission.

2. Modeling A Hypothetical Drug "Canadamycin":

2.1 Pharmacokinetics After a Single Intravenous Dose:

For practical purposes we named our hypothetical drug as Canadamycin, which was to be administered via intravenous (IV) route at a dose of 100 mg. It has a volume of distribution of 5 L, a half-life of 4 hours, and dosing interval (tau) of 8 hours. Therefore, it is a typical three times daily dosing (TID). The C_0 was estimated to be 20 mg/L (µg/mL) after dividing the dose by the volume of distribution (100 mg / 5 L).

A direct intravenous bolus injection into a vein results in nearly an instantaneous achievement of C_0, followed by a first-order reduction in the concentration. This route is frequently employed for drugs administered in hospitals clinic or emergency settings, where a quick onset of action is critical. Pharmacokinetics textbooks typically utilize this approach to elucidate key concepts associated with drug accumulation(37, 39). Regardless of the administration route, as the number of doses progressively increases during a therapeutic drug regimen, drug concentrations within the dosing intervals (tau) will eventually stabilize, forming a plateau (42). This phenomenon consistently occurs under the Law of Superposition when conditions exhibit constant total clearance. At this plateau, the rate of drug administration matches the rate of drug elimination. When this equilibrium is achieved, plasma concentrations are considered to be at a steady state (42).

After a single IV bolus dose administration the concentrations of drug will begin to decline and will be removed (cleared) and eliminated by the body. The concentrations will decrease over time in terms of half-life (the time required for concentration to decline by 50%). Canadamycin has a half-life of 4 hours meaning that eight hours post-dose we would observe a concentration of 5 mg/L, a concentration of 1.25 mg/L at 16 hours post-dose, a concentration of 0.3124 mg/L at 24 hours post-dose, etc. (Table 1). If no further doses are administered, the concentration will continue to decline by an additional 50% every 4 hours. In this scenario, each subsequent dose is given before the previous dose is fully cleared from the body. As a result, the concentration at the beginning of the next dose is the sum of the drug amount remaining in the body (C_{min}, denoted as $C\tau$ above), plus the C_{max} from a single IV bolus dose (or C_0). This cumulative effect of drug concentrations from

previous doses and additional doses is the principle of superposition, which implies that each dose will additively influence overall concentrations.

Table 1. Concentration of Canadamycin (a hypothetical drug) in mg/L before each subsequent multiple dose to be administered.

Dose	Canadamycin (mg/L)	Start Multiple	Trough End (r)	Time (h)	Concentration lost during dosage interval
1	20.00	20.00	5.0	8	15.00
2	5.00	25.00	6.25	16	18.75
3	1.25	26.25	6.56	24	19.69
4	0.3125	26.56	6.64	32	19.92
5	0.078125	26.64	6.66	40	19.98
6	0.01953125	26.66	6.67	48	19.99
7	0.004882812	26.67	6.67	54	20.00

Drug accumulation has a limit because, as plasma concentration increases, the amount of drug eliminated (1-r) during the dosing interval also grows. This is due to the fact that the elimination rate is directly proportional to the drug amount in the body, multiplied by the rate constant for first-order elimination (21, 42). As seen above, accumulation will occur if dosing interval is less than 6 half-lives. Accumulation is inversely proportional to the fraction of the dose lost in an interval. The accumulation factor is equal to 1 over the fraction of the dose lost in a dosing interval = 1/(1-fraction remaining) (21, 42). If a drug is given once every half-life, in the case of Canadamycin every 4 hours, the accumulation of the dose is 2 [1/(1-0.5)]. If Canadamycin is

administered every 8 hours (or 2 half-lives), the accumulation factor is 1.33 [1/(1-0.25)] since there would be a 25% of the drug remaining.

When a drug is administered at a fixed dose and a regular interval, as in multiple-dose regimens, the amount of drug in the body will increase and then plateau at a mean plasma level higher than the peak concentration (C_0). If the second dose is administered before the previous dose is entirely eliminated, drug accumulation will occur. This accumulation is quantified by the R index and is influenced by the elimination constant and the dosing interval, but it is independent of the dose itself (21, 42). For a drug administered in repeated oral doses, the time required to reach steady state depends on the elimination half-life of the drug. This time is independent of the size of the dose, the length of the dosing interval, and the number of doses (39). For instance, if the dose or dosing interval of a drug is modified, the time needed to reach steady state remains unchanged, but the final steady state plasma level adjusts proportionately. Consequently, the blood concentrations after the second, third, or nth dose will superimpose the blood concentrations attained after the $(n-1)^{th}$ dose.

The principle of superposition allows for the prediction of the plasma drug concentration-time profile after multiple consecutive doses by utilizing the plasma concentration-time data from a single dose. This method is based on two key assumptions: that the drug follows first-order elimination kinetics, and that its pharmacokinetics remains unchanged with repeated dosing. As a result, plasma concentrations after multiple doses can be forecasted from those observed after an initial dose. The first-order pharmacokinetics can apply to multiple dosing, consider equation 9 to describe the plasma

concentration at any time after a single IV bolus drug administration dose that follows linear pharmacokinetics.

$$\boldsymbol{C(t) = \sum_1^n A_i e^{-t/\tau j} = \sum_1^m A_i e^{-ajt}} \qquad \textbf{(equation 9)}$$

Where, A_i is the concentration coefficient, τ_j is a time constant and a_j is a rate constant ($a_j = 1/\tau_j$).

The concentration at the end of the first dosing interval (tau) is described in equation 10. Equation 11 describes the concentration at the start of the second interval, while equation 12 describes the concentration at the end of the second dose interval.

$$\boldsymbol{C_{p1}^{\tau} = C_{p1}^{0} e^{-k_{el}t}} \qquad \textbf{(equation 10)}$$

$$\boldsymbol{C_{p2}^{0} = C_{p1}^{\tau} + C_{p1}^{0} = C_{p1}^{0} e^{-k_{el}t} + C_{p1}^{0}} \qquad \textbf{(equation 11)}$$

$$\boldsymbol{C_{p2}^{\tau} = \left[C_{p1}^{0} e^{-k_{el}t} + C_{p1}^{0}\right] e^{-k_{el}t}} \qquad \textbf{(equation 12)}$$

As described in Table 1 there is fraction of the initial plasma concentration remaining at the end of the dosing interval. Intuitively there is both a fraction lost (R) and a fraction remaining in the body (1-R) every dosing interval. The remaining fraction in the body before the next dose depends only on the first order rate constant of elimination and the time after the dose as described in equation 13.

$$\boldsymbol{R = e^{-k_{el}t}} \qquad \textbf{(equation 13)}$$

Thus, replacing R in equation 12 to describe the concentration at the end of the second dose interval is shown in equation 14. Equation 15 describes the concentration at the start of the third dose interval.

$$C_{p2}^{\tau} = C_{p1}^{0}R + C_{p1}^{0}R^2 \qquad \textbf{(equation 14)}$$

$$C_{p2}^{0} = C_{p1}^{0} + C_{p1}^{0}R + C_{p1}^{0}R^2 \qquad \textbf{(equation 15)}$$

These fractions of drug that remain in the body before the next dose mathematically form a geometric series of remaining concentrations with each term R times the preceding term. This leads to drug accumulation. In the case of multiple dosing, it appears that the concentration profiles of the individual doses can be totaled or summed up over time (**Figure 4**). The steady-state can then be calculated by addition of areas, without the need to use any pharmacokinetic model, provided that first-order linearity holds (34)

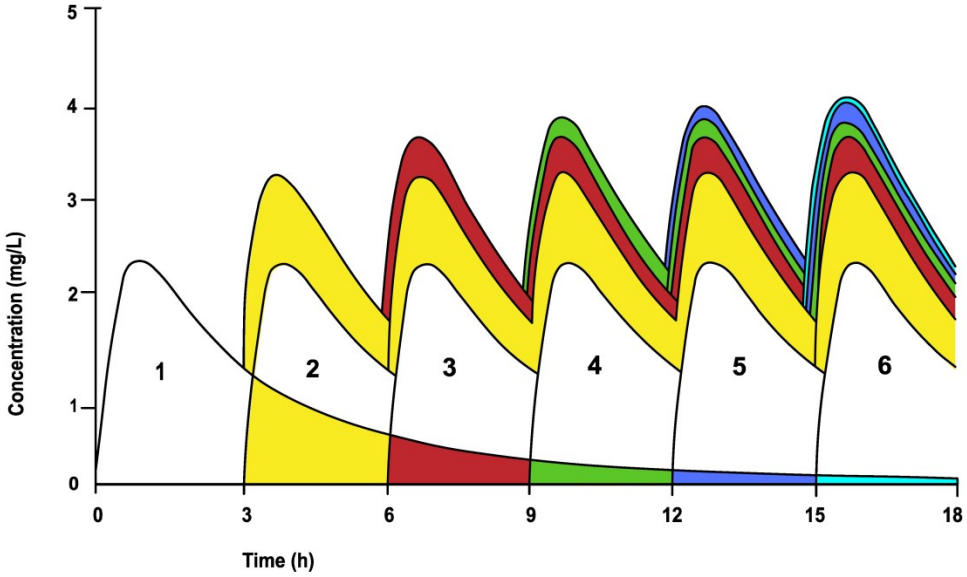

Figure 4. The Law of Superposition used to generate the concentration profile of multiple dosing from profile of the single dose. The area of the first dose in the interval of the second dose adds to the area of the second dose, and so on. Modified from Van Rossum and de Bie (34) with permission.

2.2 Pharmacokinetics After Multiple Intravenous Dosing:

In linear pharmacokinetic systems, the drug concentrations achieved by a second dose are comparable to those produced by the first dose. For instance, when a second 100

mg IV dose of Canadamycin is administered at the 8-hour mark, 5 mg/L of the drug remains from the first dose, as shown in **Table 1**. Consequently, the plasma concentration (Cp) immediately after the second dose would be 25 mg/L, consisting of the 5 mg/L remaining from the initial dose and an additional 20 mg/L from the new dose. This results in a combined concentration of 25 mg/L. In linear systems, each subsequent 100 mg dose will generate concentrations similar to those of the first dose. However, the resulting concentrations will be the sum of the residual concentrations from all prior doses and the concentration from the most recent dose. For example, administering a third dose at the 16-hour mark will also produce an initial concentration of 20 mg/L. The concentration remaining from the second dose would be 5 mg/L, and the concentration remaining from the first dose would be 1.25 mg/L. When these concentrations are combined, the observed total concentration will be approximately 26.25 mg/L, calculated as 20 mg/L (from the third dose) + 5 mg/L (remaining from the second dose) + 1.25 mg/L (remaining from the first dose). This additive process of combining concentrations from multiple doses to determine the observed concentration exemplifies the principle of superposition (21, 42).

The described pattern of superposition assumes that each dose behaves similarly despite increasing concentrations. While simple additive superposition is generally applicable to most drugs, it is important to note that the superposition of exposures can become more complex if the pharmacokinetic behavior of each dose changes with increasing concentrations. This complexity arises in drugs with saturable clearance, such as phenytoin, where the pharmacokinetics does not remain consistent as concentrations increase (44). For the remainder of this review, the simple additive superposition scenario will be used.

Consecutive multiple doses of a drug will lead to increasing concentrations in the body until a plateau, known as steady state, is reached. At steady state, the amount of drug administered with each dose is balanced by an equivalent amount of drug eliminated from the body between doses, resulting in a constant rate of drug input and output (rate in = rate out) (39). For the majority of drugs, reaching steady state typically takes about five half-lives. The time required to attain steady state in a repeat-dose regimen is governed exclusively by the half-life of the drug and the dosing interval, as accumulation and the remaining fraction are influenced by specific pharmacokinetic equations. Although changing the dose or dosing interval can influence the concentrations at steady state, it does not affect the time needed to reach steady state. Some drugs have prolonged half-lives, ranging from days to weeks or even longer. In such cases, waiting for five half-lives to achieve the desired steady-state concentration may not be necessary. When time is critical, as in the administration of antibiotics for critically ill patients, a loading dose can be used to reach steady state more quickly (39).

For our hypothetical drug, Canadamycin the C_{max} and C_{min} values using equation 16 and 17, respectively, can be estimated taking into consideration the following calculations:

$$\boldsymbol{C_{max} = \frac{C_{p1}^{0}}{(1-R)} = \frac{20}{(1-0.257)} = 26.92\ mg/L} \qquad \textbf{(equation 16)}$$

$$\boldsymbol{C_{min} = \frac{C_{p1\,R}^{0}}{(1-R)} = C_{\max}\ R = 26.92\ x\ 0.257 = 6.92\ mg/L} \qquad \textbf{(equation 17)}$$

Dose = 100 mg

V_d = 5 L

t½ = 4 hr

τ = 8 hr

C_0 = 20 mg/L

kel = 0.693 / t½ = 0.693 / 4 h = 0.17 h^{-1}

$R = e^{-k_{el}t} = e^{-0.17\ x\ 8} = 0.257$

Therefore, the plasma concentration will fluctuate between 26.92 mg/L and 6.92 mg/L during each dosing interval when steady state was reached.

2.3 Pharmacokinetics After Multiple Oral Dosing:

For oral dosing, the equations are more complex, but it is possible to model and predict concentrations with repeated doses and to estimate plasma concentrations and dosing regimens using superposition. The C_{max} value corresponds to the concentration at the peak time (t_{peak}) after reaching steady state. In the case of C_{min} is estimated based on the assumption that the plasma concentration has peaked and $e^{-ka\ t}$ is close to zero and that the next dose is administered once the absorption phase is complete, which is described in equation 18 and a simplified version in equation 19.

$$\boldsymbol{C_{min} = \frac{F\ x\ Dose\ x\ k_a}{V\ x\ (k_a - k_{el})}\left[\frac{e^{-k_{el}\tau}}{1 - e^{-k_{el}\tau}}\right]} \qquad \textbf{(equation 18)}$$

$$\boldsymbol{C_{min} = A\left[\frac{R}{1-R}\right]} \qquad \textbf{(equation 19)}$$

The relationship between loading dose and maintenance dose and thus drug accumulation during multiple dose administration can be examined by analyzing the ratio between the minimum concentration at steady state and the concentration one dosing interval (τ) after the first dose, as demonstrated in equation 20.

$$\frac{C_{min}}{C_{p1}^{\tau}} = \frac{1}{1-e^{-k_{el}\tau}} = \frac{1}{(1-R)} \qquad \textbf{(equation 20)}$$

Equations have been developed which facilitate calculation of the plasma concentration achieved following multiple oral administration. To start the plasma concentration achieved following a single oral dose that does not have flip flop kinetics (45) can be described by equation 21.

$$C_p = \frac{F\ x\ Dose\ x\ k_a}{V\ x\ (k_a - k_{el})}\left[e^{-k_{el}\tau} - e^{-k_a\tau}\right] \qquad \textbf{(equation 21)}$$

An intriguing outcome of this equation is that the average plasma concentration remains the same whether the dose is given as a single dose every dosing interval (τ) or divided into shorter dosing intervals. .

For multiple oral dosing we will use our hypothetical drug, Canadamycin, with an oral dose of 300 mg every 12 hours, bioavailability (F) of 100%, volume of distribution of 30 liters and half-life of 6 hours.

Dose = 300 mg

V_d = 30 L

t½ = 6 hr

τ = 12 hr

kel = 0.693 / t½ = 0.693 / 6 h = 0.116 h^{-1}

We will estimate the required dose (maintenance dose) to be administered every 12 hours to achieve an average plasma concentration of 15 mg/L using equations 22 and 23.

$$C_p = \frac{F \; x \; Dose}{V \; x \; k_{el} \; x \; \tau} \qquad \textbf{(equation 22)}$$

$$Dose = \frac{C_p \; x \; V \; x \; k_{el} \; x \; \tau}{F} = \frac{15 \; x \; 30 \; x \; 0.116 \; x \; 12}{1} = 624 \; mg \quad \textbf{(equation 23)}$$

The loading dose can be calculated using equation 24, with the use of the R value.

$R = e^{-k_{el}t} = e^{-0.116 \; x \; 12} = 0.25$

$$Loading \; Dose = \frac{Maintenance \; Dose}{1-R} = \frac{624}{1-0.25} = 832 \; mg \quad \textbf{(equation 24)}$$

To estimate the fluctuations in plasma concentration, the C_{min} can be calculated using equation 25.

$$C_{min} = \frac{F \; x \; Dose}{V}\left[\frac{e^{-k_{el}\tau}}{1-e^{-k_{el}\tau}}\right] = \frac{1 \; x \; 624}{30}\left[\frac{0.25}{1-0.25}\right] = 6.93 \; mg/mL \quad \textbf{(equation 25)}$$

Therefore, the plasma concentration would likely fluctuate between approximately 7 and 23 mg/L with an average concentration of around 15 mg/L. In this case, the average concentration can be estimated using an approximation of $C^{max} = [C_{av} + (C_{av} - C_{min})]$ or [23 = 15 + (15-7)].

Alternatively, half the maintenance dose (312 mg) could be administered more frequent (half the original tau) every 6 hours, as calculated using equation 25.

$$C_{min} = \frac{F \; x \; Dose}{V}\left[\frac{e^{-k_{el}\tau}}{1-e^{-k_{el}\tau}}\right] = \frac{1 \; x \; 312}{30}\left[\frac{0.5}{1-0.5}\right] = 10.4 \; mg/mL \quad \textbf{(equation 25)}$$

Thus, the plasma concentration would fluctuate between about 10.4 to 20 with an average of 15 mg/L.

3. Breaking the Law of Superposition:

Law of Superposition applies when all disposition processes are linear or first order, this include absorption, distribution, metabolism, and elimination (ADME) (23, 32, 34, 42, 43). Thus, concentrations after multiple doses can be calculated by adding together the concentrations from each dose. The assumptions underlying the Law of Superposition are:

1. The dosing is in a range where the pharmacokinetics are linear and dose proportional.
2. The rate and extent of absorption and average clearance are the same for each dosing interval.
3. Each dose acts independently of one another, and the sum of all these dosing events provides the total concentration of the drug in circulation.

There are many situations, however, in which the superposition principle does not apply. In these cases, the pharmacokinetics of the drug change after multiple dosing due to various factors, including (changing pathophysiology in the patient, saturation of a drug carrier system, enzyme induction, and enzyme inhibition) (43). Drugs that follow non-linear pharmacokinetics generally do not have predictable plasma drug concentrations after multiple doses using the superposition principle. When the Law of Superposition is broken prediction of pharmacokinetics, efficacy and toxicity can become more complicated (23, 32, 34, 42, 43). As described above the underlying theorem is that AUC single dose will equal AUC at steady state. However, the AUC after an oral dose can be affected not only by absorption but also by protein binding and elimination (43). Therefore, the AUC at steady state (AUC_{SS}) can either be higher or lower than the AUC after single dose ($AUC_{Single\ Dose}$). **Figure 5** demonstrates the linearity of pharmacokinetics and the validity of superposition, as well as instances where non-linearity in pharmacokinetics causes the

breakdown of the superposition principle. An overview of possible causes related to various ADME processes, along with examples, is provided in **Table 2**.

Table 2. Primary potential causes for deviations from the Law of Superposition in various ADME processes, with examples.

ADME Process		Main related causes of non-linearity		Examples
Elimination	Absorption	Carrier-mediated transport		Gabapentin (46), Metformin (47)
		Saturable pre-systemic loss	Gut metabolism	Verapamil (48)
			First-pass metabolism	Propranolol (49)
	Distribution	Saturable plasma protein binding		Paclitaxel (50)
		Saturable tissue binding		Imipramine (51)
	Metabolism	Saturable metabolism		Theophylline (52)
		Enzyme induction		Carbamazepine (53)
	Excretion	Saturable renal excretion	Saturable active secretion	Zidovudine (54)
			Saturable reabsorption	Methotrexate (55)
		Saturable biliary excretion		Tetracycline (56)

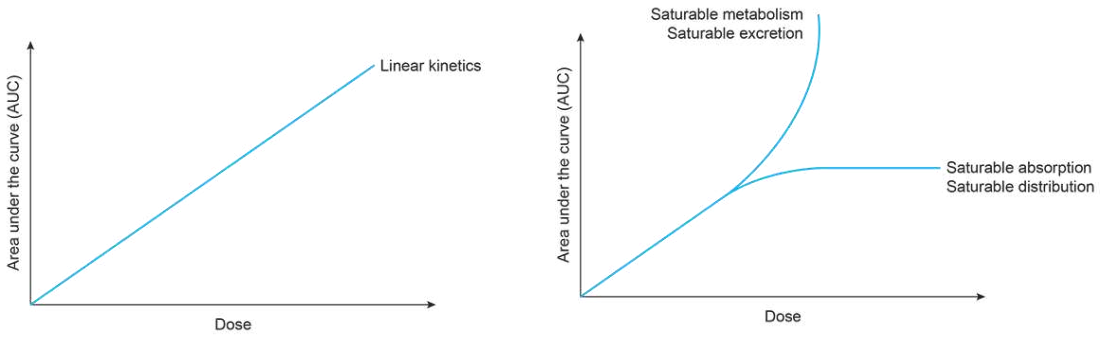

(a) (b)

Figure 5. Linearity of pharmacokinetics and the validity of the superposition principle, along with scenarios where non-linearity in pharmacokinetics leads to the breakdown of this principle.

3.1 Less than proportional increase in AUC ($AUC_{SS} < AUC_{Single\ Dose}$):

We first consider saturable processes such as absorption, distribution and elimination. There are at least three processes that can affect drug absorption to saturate; dissolution rate, GI transit time, and the ability or inability of drugs to cross intestinal barriers (43). While most drugs are absorbed through passive diffusion, some utilize specific transport processes in the small intestine. When passive diffusion plays a minor role, a less than proportional increase in the area under the curve (AUC) may occur due to saturation of the active transport process. Drug absorption can be described by a combination of Michaelis-Menten kinetics and first-order kinetics (23, 32, 34, 42, 43). This situation does not always hold. It remains that absorption of most drugs follow linear kinetics, and pharmacokinetic parameters describing absorption of a drug do not change over the therapeutic dose range. However, there are cases where transporters are involved in absorption and when high doses are utilized (or in overdose situations) the linear range may be exceeded (43). Sorafenib is an oral tyrosine kinase inhibitor that has been approved for treating advanced renal cell carcinoma and hepatocellular carcinoma. It has been found that the administration of sorafenib at doses exceeding 800 mg/day would result in a less than proportional increase in the area under the curve (AUC) of sorafenib with respect to repeated doses. This phenomenon was attributed to the saturation of the absorption of sorafenib at higher doses. This study has systematically considered and excluded all plausible contributing factors. It has also been demonstrated that partitioning of the daily dose into three discrete administrations would ameliorate the absorption saturation and lead to higher drug exposure at higher drug doses compared with once or twice daily doses at which the absorption saturation was more notable (57).

Since the concentration of a drug after oral dosing depends on both absorption and elimination, the area under the curve (AUC) represents the combined outcome of these processes. Elimination (clearance) influences this relationship, as a less than proportional increase in AUC at steady state may result from both increased elimination and decreased absorption. It is generally accepted that only the unbound drug can diffuse across membranes, enabling distribution between the vascular and tissue compartments. Accordingly, changes in drug-protein binding in plasma and tissues can impact the distribution of drugs within the body (32, 34, 43). Drug distribution is often measured by the volume of distribution, usually defined as the ratio of amount of drug in the body to its plasma concentration. The most basic quantitative expression relating the volume Vd of distribution to binding in plasma and tissue is provided by equation 26.

$$\boldsymbol{V_d = V_p + \sum V_t \frac{f_u}{f_t}} \qquad \textbf{(equation 26)}$$

Where, V_d is the volume of distribution to plasma, V_p is the plasma volume, V_t is the tissue volume, and f_u and f_t are the fraction of unbound drug in the plasma and tissue, respectively.

It is clear that the volume of distribution depends on plasma protein binding but also on tissue binding. For drugs with low-clearance, protein binding significantly influences drug elimination, and total body clearance is directly proportional to the unbound fraction in plasma (23, 34, 39, 43). A drug can exhibit concentration-dependent protein binding, with the unbound fraction changing (43). A less than proportional increase in AUC due to saturation of protein binding sites in plasma, may result in an in-crease in free fraction will resulting in enhanced clearance. The AUC_{SS} would be in-creased less than proportionally and the bioavailability reduced; thus, AUC_{SS} would be

less than $AUC_{Single\ Dose}$. Assuming a drug binds to n discrete sites on a protein molecule, with all sites having the same affinity for the drug and acting independently, the fraction of unbound drug, fu, can be described by equation 27.

$$f_u = \frac{K_d + D_f}{np_t + K_d + D_f} \qquad \textbf{(equation 27)}$$

Where K_d is the dissociation constant at equilibrium, D_f and *pt* are concentrations of unbound drug and total protein (bound and unbound), respectively, and n is number of binding sites on the protein molecule. The binding of a drug to a protein is determined by four factors: the drug concentration, protein concentration, the number of binding sites per protein molecule, and the dissociation constant (43). Irrespective of the affinity, the maximum possible binding capacity is the product of the molar concentration of protein and the number of binding sites per protein molecule. Mathematically, it can be observed that with multiple dosing, an elevated unbound fraction in plasma, *fu*, becomes apparent in plasma. This results in an increased volume of distribution, lowered plasma concentrations, and a less than proportional increase in AUC. Vismodegib (Erivedge™, GDC-0449; Genentech, South San Francisco, CA, USA) is an approved drug in the United States for the treatment of advanced basal cell carcinoma (BCC). An evaluation of intravenous pharmacokinetic (PK) parameters following both single and multiple oral dosing regimens showed increased clearance and volume of distribution, with values 81% and 63% higher, respectively, following repeated dosing. Moreover, a significant reduction in bioavailability (77% lower) was observed with multiple doses. Intriguingly, continuous daily dosing of Vismodegib led to a 2.4-fold increase in the unbound fraction compared to a single dose (58).

In tissues, drugs can bind to non-specific binding proteins, enzymes, and receptors (43). Enzymes and receptors are particularly important pharmacologically, as they contribute to the therapeutic effect. However, distinguishing these from non-specific binding sites is challenging because the binding capacities of enzymes and receptors are often low and overshadowed by non-specific binding. Similar to plasma protein binding, tissue protein binding can become saturated as drug concentrations increase over time, resulting in changes in the volume of distribution. However, saturation of tissue binding and of plasma protein binding can occur simultaneously (43).

The volume of distribution is directly related to plasma protein binding and inversely related to tissue binding, so changes in one type of binding can counterbalance the other. This complexity is further compounded by the fact that different tissues may not become saturated to the same extent. Consequently, the volume of distribution of a drug may not be significantly affected by changes in tissue binding, depending on the degree of non-linear tissue binding. Thus, it is essential to evaluate the non-linearity of tissue binding by examining the ratio of the drug concentration in a given tissue to that in plasma. At equilibrium, the tissue/plasma concentration ratio should match the ratio of unbound fraction in plasma to the unbound fraction in a non-eliminating tissue (43). In eliminating tissues, it is more complex; the ratio may be influenced by blood flow to the tissue and the eliminating process. Moreover, elimination could also be impacted by changes in intrinsic clearance (CLint'). Enzyme autoinduction is a time-dependent phenomenon where the elimination of a drug increases with multiple doses (43). Thus, an AUC_{SS} less than $AUC_{Single\ Dose}$ may be observed. One such example is the anticonvulsant carbamazepine (CBZ), that is known to auto-induce its own metabolism. Throughout the

course of multiple 200mg doses of CBZ, the daily trough CBZ levels consistently declined, reaching their lowest point after two weeks. Notably, the observed CBZ concentration was only 53.9% of what had been predicted under the assumption of no autoinduction. Furthermore, the total CBZ clearance following multiple doses was higher than after a single dose. Digging deeper into CBZ pharmacokinetics, considerable increase in the AUCs of CBZ metabolites during multiple-dose administration were noted. These changes were accompanied by increased urinary excretion of these metabolites compared to CBZ, all due to the phenomenon of autoinduction (59).

Phenytoin serves as another illustrative case, akin to carbamazepine. Like carbamazepine, phenytoin, an antiepileptic medication, also exhibits violation of the Law of Superposition due to enzyme autoinduction. In the case of phenytoin, after the third dose, the calculated AUC was found to be statistically significantly smaller than that observed after the initial dose. This phenomenon was attributed to the ability of phenytoin to induce its own metabolism. Consequently, this autoinduction led to an increased rate of elimination, which in turn resulted in a reduction in AUC following multiple doses (60).

3.2 More than proportional increase in AUC ($AUC_{SS} > AUC_{Single\ Dose}$):

A pharmacokinetic situation in which an increase in AUC at steady state is greater than after a single dose is also possible. In this case, lack of proportionality is more likely due to a decrease in elimination than to an increase in absorption (43). However, in certain instances, absorption can increase with higher doses due to specific mechanisms.

The more than proportional increase in AUC is likely due to non-linear clearance. This disproportionate increase in the AUC is most likely attributable to

decreased elimination clearance after multiple doses (32, 43). For drugs with a high extraction in the liver, a significant first-pass effect occurs. If this first pass effect diminishes with multiple dosing, it can lead to a disproportionate increase in AUC. This increase is due to both a decrease in elimination and an increase in bioavailability, the latter resulting from the saturation of hepatic metabolism during the initial passage of the drug through the liver (43). The disproportionate increase in AUC with multiple oral doses can be linked to enhanced bioavailability resulting from a reduced first-pass effect. The effects of capacity-limited metabolism are more apparent under steady-state conditions than after a single dose. This is exemplified by the relationship between the plasma phenytoin concentration at steady state and the administered dose. At steady-state, plasma concentration of phenytoin increases more than proportionally to the rate of input (29, 44). Verapamil, a drug used to treat cardiovascular conditions, exhibits low oral bioavailability, primarily due to extensive pre-systemic (first-pass) liver elimination. When the pharmacokinetics of verapamil was assessed, it was observed that the AUC at the steady state (1999 ± 435 ng/mL • hr) exceeded that recorded after the initial dose (788 ± 224 ng/mL • hr). That increase in AUC was attributed to the saturation of the first-pass effect that occurred with multiple dosing. As the first-pass effect became saturated, a greater proportion of the drug managed to evade pre-systemic elimination. That, in turn, led to the accumulation of verapamil and an increase in its AUC with multiple doses (61, 62).

Drugs are eliminated from the body through various processes, including biotransformation and excretion. The efficiency with which the body eliminates a drug is commonly expressed as total clearance, which is the sum of the individual clearances of different organs, occurring simultaneously. CLint is the intrinsic clearance, a measure of

the intracellular removal of drug, described by the Michaelis-Menten equation where V, is the capacity of the enzyme or carrier systems, K, is the Michaelis constant and C, is the unbound drug concentration (39). It is evident that the CLint remains constant when the concentration is lower than K, with a limited value of V/K. However, non-linearity arises when the drug concentration approaches the value of K. Since drug elimination typically involves multiple processes, determining whether elimination is linear or non-linear becomes increasingly complex as the number of these processes increases (43). Depending on the relative contribution of saturable pathways to overall elimination, non-linearity may not be easily discernible.

When saturation occurs, we will get accumulation of the drug greater at steady state than predicted from a single dose (21, 42, 43). Drug elimination often exhibits zero-order kinetics at high concentrations and first-order kinetics at low concentrations, a phenomenon known as concentration-dependent kinetics. At multiple doses, which lead to higher plasma concentrations, zero-order kinetics are observed. Conversely, at lower doses, the kinetics are linear, or first-order. This pattern is particularly common with drugs that are extensively metabolized (43). A typical characteristic of enzymatic reactions and active transport is their limited capacity. The liver has a finite amount of enzymes, establishing a maximum rate at which metabolism can occur. Additionally, the rate of metabolism can be further constrained by the limited availability of co-substances or co-factors necessary for the enzymatic process (43).

Most of our understanding of enzyme kinetics comes from *in vitro* studies, where the concentrations of substrate, enzyme, and co-factor are meticulously controlled. *In vivo* numerous factors are involved, making it difficult to isolate each one in detail.

Nevertheless, the fundamental principles of enzyme kinetics are applicable to pharmacokinetics. At single dose concentrations, where $K_m > C_p$, $K_m + C_p$ is approximately equal to Km as described in equation 28.

$$\frac{\partial C_p}{\partial t} = \frac{V_m}{K_m} C_p \qquad \textbf{(equation 28)}$$

Where, the V_m/K_m is a first order elimination rate constant and the whole equation now looks like that for first order elimination.

Therefore, at low plasma concentrations following a single dose, first-order kinetics would be expected. This is a typical situation for most drugs, as the K_m is usually larger than the plasma concentrations achieved. However, a high concentration at multiple dosing is achieved that is $C_p > K_m$, then $K_m + C_p$ is approximately equal to C_p leading to a zero-order elimination process as described in equation 29.

$$\frac{\partial C_p}{\partial t} = \frac{V_m \, x \, C_p}{C_p} = V_m \qquad \textbf{(equation 29)}$$

At high steady state plasma concentrations, zero order or concentration independent kinetics occurs. The presence of saturation kinetics can be significant when multiple doses of certain drugs are given, or in cases of overdose. At steady state, the effective elimination rate constant is reduced, leading to excessive drug accumulation if saturation kinetics is not properly understood.

The renal excretion of drugs usually involves three processes: glomerular filtration, renal tubular secretion, and reabsorption from the renal tubular lumen (43). Glomerular filtration is a passive process that depends on the unbound concentration of drug in plasma.

The relationship between renal clearance CLR and these processes is described in equation 30.

$$\boldsymbol{CLR = f_u x\, GFR + CL} \qquad \textbf{(equation 30)}$$

Where GFR, CL, and CLR are glomerular filtration rate, secretion clearance, and reab-sorption clearance, respectively; and f_u is the unbound fraction of drug in plasma.

When the CLR and GFR of a drug is much greater than one, it indicates that renal tubular se-cretion of the drug is occurring (43). Conversely, when the ratio is much less than one, it suggests reabsorption of the drug from the tubular lumen. Renal tubular secretion is a specialized and saturable process, whereas tubular reabsorption can occur through passive diffusion or active transport, while active reabsorption being also saturable (43). In addition, there are processes whose rates are affected by pharmacological actions of the drug itself. Elimination could also be affected through changes in intrinsic clearance (CLint'). Enzyme inhibition can be a time-dependent phenomenon in which the elimination clearance of a drug decreases following multiple doses and the decrease in clearance is significant compared to a single dose (43). Thus, AUC_{SS} would be higher than $AUC_{Single\ Dose}$. Propranolol and itraconazole provide examples of how changes in intrinsic clearance (CLint') can affect elimination. When administered in multiple doses, these drugs have been found to inhibit their own metabolizing enzymes. That inhibition resulted in a decrease in their hepatic clearance and led to an increase in their AUC at the steady state (63, 64).

3.3. Other Factors Affecting Adherence to the Law of Superposition:

The reasons discussed in the previous two sections pertain to situations where the Law of Superposition may not accurately characterize drug behavior due to drug-related factors. However, in other instances, a variety of factors can play a role. Patient-related causes that can lead to deviations from the Law of Superposition include non-compliance, irregular dosing schedules, and inconsistent dosing amounts (19, 20, 65). If the patient does not take the prescribed dosing amount or does not adhere to the dosing schedule, the drug concentration time curve can exhibit an increase in fluctuation. Similarly, variations in the dosage amount taken by the patient may result in varying drug levels in the body which can impact the pharmacokinetic behavior of some drugs. Inconsistent dosing sizes may result in varying drug levels in the body, which can lead to appearance of the Superposition principle not being upheld. In all described cases, the variability in drug administration may cause deviations from the expected linear pharmacokinetic behavior described by the Law of Superposition.

When patients take medications, some drugs may interact with specific components in the food they ingest or those released during the digestive process, leading to a reduction in their anticipated absorption (66, 67). When patients deviate from prescribed dosage instructions, these interactions can impact the expected pharmacokinetic behavior of drugs, especially when multiple doses are involved. The impact of meals on drug absorption is multifaceted. In particular, the concurrent administration of certain drugs with food has been shown to enhance their absorption. This phenomenon is particularly relevant for drugs that rely on surfactants to facilitate their absorption (66). Also, lipophilic drugs when taken with a fatty meal can follow another absorption pathway, bypassing the traditional portal

vein route and instead entering the systemic circulation via the lymphatic system, alongside absorbed dietary fats (68, 69).

Drug-drug interactions stand as another influential factor that can disrupt the adherence to the Law of Superposition for certain drugs. When certain drugs are co-administered with others, several intricate interactions can come into play, ultimately impacting their pharmacokinetic behavior. One common scenario involves competitive interactions, where co-administered drugs may compete for the same transporters responsible for drug absorption or elimination (70). This competitive struggle for transporters can lead to deviations from the expected linear pharmacokinetics of the involved drugs. Furthermore, drug interactions can also affect metabolizing enzymes (71). Some drugs may induce or inhibit these enzymes, which play critical roles in processes like pre-systemic first-pass metabolism and overall liver clearance (72, 73). These enzyme-related changes can significantly influence the pharmacokinetic profile of drugs, causing it to deviate from the anticipated linear behavior described by the Law of Superposition. Another intricate effect arises from the interaction between co-administered drugs with high plasma protein binding affinity (74, 75). When two drugs that both extensively bind to plasma proteins are taken together, they can engage in what is known as protein binding substitution. This process can influence the distribution and clearance of both drugs as they essentially compete for available protein-binding sites.

4. Conclusion:

The pharmacokinetics and area under the concentration time curve of the majority of drugs after administration of a single dose can be described by first-order or linear processes and can be used to predict a similar steady state area under the concentration time

curve exposure and thus follow the Law of Superposition. However, there are a number of scenarios and situations where drugs could display behaviors after multiple dosing that leads to capacity-limited or saturation non-linear kinetics and the Law of Superposition is overruled and not followed. As a consequence, when ADME processes are saturated, the AUC at steady-state may result in substantial changes in plasma concentrations leading possibly to changes in pharmacodynamics effect or a toxic effect. Thus, a sound understanding of the principles and influence of dosing (single or multiple dosing) on pharmacokinetics is important in the analysis of pharmacokinetic data by analysts in drug development.

References

1. Garza, I.; Swanson, J.W. Prophylaxis of migraine. Neuropsych. Dis. Trea. 2006, 2(3), 281-291. DOI: 10.2147/nedt.2006.2.3.281

2. Ong, J.J.Y.; De Felice, M. Migraine treatment: Current acute medications and their potential mechanisms of action. Neurother. 2018, 15(2), 274-290. DOI: 10.1007/s13311-017-0592-1

3. Diener, H-C.; Holle-Lee, D.; Nägel, S.; Dresler, T.; Gaul, C.; Göbel, H.; et al. Treatment of migraine attacks and prevention of migraine: Guidelines by the German Migraine and Headache Society and the German Society of Neurology. Clin. Transl. Neurosci. 2019, 3(1), 3. DOI: 10.1177/2514183X18823377

4. Do, T.P.; Guo, S.; Ashina, M. Therapeutic novelties in migraine: new drugs, new hope?. J Headache Pain 2019, 20(1), 37. DOI: 10.1186/s10194-019-0974-3

5. Borbély, A.A.; Mattmann, P.; Loepfe, M.; Fellmann, I.; Gerne, M.; Strauch, I.; et al. A single dose of benzodiazepine hypnotics alters the sleep EEG in the subsequent drug-free night. Eur. J. Pharmacol. 1983, 89(1-2), 157-161. DOI: 10.1016/0014-2999(83)90622-2

6. Johnson, L.C.; Chernik, D.A. Sedative-hypnotics and human performance. Psychopharmacol. 1982, 76(2), 101-113. DOI: 10.1007/BF00435262

7. Malpas, A.; Rowan, A.J.; Boyce, C.R.; Scott, D.F. Persistent behavioural and electroencephalographic changes after single doses of nitrazepam and amylobarbitone sodium. Br. Med. J. 1970, 2(5712), 762-764. DOI: 10.1136/bmj.2.5712.762

8. Kornetsky, C.; Vates, T.S.; Kessler, E.K. A comparison of hypnotic and residual psychological effects of single doses of chlorpromazine and secobarbital in man. J. Pharmacol. Exp. Ther. 1959, 127, 51-54.

9. Eckburg, P.B.; Jain, A.; Walpole, S.; Moore, G.; Utley, L.; Manyak, E.; et al. Safety, pharmacokinetics, and food effect of tebipenem pivoxil hydrobromide after single and multiple ascending oral doses in healthy adult subjects. Antimicrob. Agents Chemother. 2019, 63(9), 10-128. DOI: 10.1128/AAC.00618-19

10. Chua, H.C.; Tse, A.; Smith, N.M.; Mergenhagen, K.A.; Cha, R.; Tsuji, B.T. Combatting the rising tide of antimicrobial resistance: pharmacokinetic/pharmacodynamic dosing strategies for maximal precision. Int. J. Antimicrob. Agents 2021, 57(3), 106269. DOI: 10.1016/j.ijantimicag.2020.106269

11. Xie, J.; Roberts, J.A.; Lipman, J.; Cai, Y.; Wang, H.; Zhao N.; et al. Pharmacokinetic/pharmacodynamic adequacy of polymyxin B against extensively drug-resistant Gram-negative bacteria in critically ill, general ward and cystic fibrosis patient populations. Int. J. Antimicrob. Agents 2020, 55(6), 105943. DOI: 10.1016/j.ijantimicag.2020.105943

12. Bunke, C.M.; Aronoff, G.R.; Luft, F.C. Pharmacokinetics of common antibiotics used in continuous ambulatory peritoneal dialysis. Am. J. Kidney Dis. 1983, 3(2), 114-117. DOI: 10.1016/S0272-6386(83)80025-0

13. Kang, W.Y.; Lee, H.W.; Gwon, M.R.; Cho, S.; Shim, W.S.; Lee, K.T.; et al. A Pharmacokinetic drug interaction between fimasartan and linagliptin in healthy

volunteers. Drug Des. Devel. Ther. 2020, 14, 2101-2111. DOI: 10.2147/DDDT.S248205

14. Moon, S.J.; Yu, K.S.; Kim, M.G. An assessment of pharmacokinetic interaction between lobeglitazone and sitagliptin after multiple oral administrations in healthy men. Clin. Ther. 2020, 42(6), 1047-1057. DOI: 10.1016/j.clinthera.2020.04.005

15. Ghim, J.L.; Phuong, N.T.T.; Kim, M.J.; Kim, E.J.; Song, G.S.; Ahn, S.; et al. Pharmacokinetics of fixed-dose combination of atorvastatin and metformin compared with individual tablets. Drug Des. Devel. Ther. 2019, 13, 1623-1632. DOI: 10.2147/DDDT.S193254

16. Sheng, L.; Cao, W.; Lin, P.; Chen, W.; Xu, H.; Zhong, C.; et al. Safety, tolerability and pharmacokinetics of single and multiple ascending doses of benfotiamine in healthy subjects. Drug Des. Devel. Ther. 2021, 15, 1101-1110. DOI: 10.2147/DDDT.S296197

17. Kim, J.R.; Kim, S.; Huh, W.; Ko, J.W. No pharmacokinetic interactions between candesartan and amlodipine following multiple oral administrations in healthy subjects. Drug Des. Devel. Ther. 2018, 12, 2475-2483. DOI: 10.2147/DDDT.S172568

18. Vaidyanathan, S.; Jarugula, V.; Dieterich, H.A.; Howard, D.; Dole, W.P. Clinical pharmacokinetics and pharmacodynamics of aliskiren. Clin. Pharmacokinet. 2008, 47(8), 515-531. DOI: 10.2165/00003088-200847080-00002

19. Wang, W.; Husan, F.; Chow, S.C. The impact of patient compliance on drug concentration profile in multiple doses. Stat. Med. 1996, 15(6), 659-669. DOI: 10.1002/(SICI)1097-0258(19960330)15:6<659::AID-SIM207>3.0.CO;2-E

20. Wang, W. Patient Compliance and its Impact on Steady State Pharmacokinetics. In: Applied Statistics in the Pharmaceutical Industry: With Case Studies Using S-Plus. 1st ed.; Millard, S.P., Krause, A., Eds.; Springer: New York, United States, 2001; pp. 217-236. DOI: 10.1007/978-1-4757-3466-9_9

21. Van Rossum, J.M. Pharmacokinetics of accumulation. J. Pharm. Sci. 1968, 57(12), 2162-2165. DOI: 10.1002/jps.2600571230

22. Wang W, Ouyang SP. The formulation of the principle of superposition in the presence of non-compliance and its applications in multiple dose pharmacokinetics. J. Pharmacokinet. Biopharm. 1998, 26(4), 457-469. DOI: 10.1023/A:1021016218536

23. Lin, J.H. Dose-dependent pharmacokinetics: Experimental observations and theoretical considerations. Biopharm. Drug Dispos. 1994, 15(1), 1-31. DOI: 10.1002/bdd.2510150102

24. Cutler, D.J. Numerical deconvolution by least squares: use of prescribed input functions. J. Pharmacokinet. Biopharm. 1978, 6(3), 227-241. DOI: 10.1007/BF01312264

25. Cutler, D.J. Numerical deconvolution by least squares: use of polynomials to represent the input function. J. Pharmacokinet. Biopharm. 1978, 6(3), 243-263. DOI: 10.1007/BF01312265

26. Fernández-Campos, F.; Ferrero, C.; Colom, H.; Jiménez-Castellanos, M.R. *In-vivo* absorption behaviour of theophylline from starch-methyl methacrylate matrix tablets in beagle dogs. Int. J. Pharm. 2015, 478(2), 684-692. DOI: 10.1016/j.ijpharm.2014.11.071

27. Chiou, W.L. Rapid compartment- and model-independent estimation of times required to attain various fractions of steady-state plasma level during multiple dosing of drugs obeying superposition principle and having various absorption or infusion kinetics. J. Pharm. Sci. 1979, 68(12), 1546-1547. DOI: 10.1002/jps.2600681222

28. Gupta, P.; Hutmacher, M.M.; Frame, B.; Miller, R. An alternative method for population pharmacokinetic data analysis under noncompliance. J. Pharmacokinet. Pharmacodyn. 2008, 35(2), 219-233. DOI: 10.1007/s10928-008-9085-5

29. Ma, L. Analysis of nonlinear pharmacokinetic systems and the nonlinear disposition of phenylbutazone in equine (horses) Ph.D. Thesis, Oregon State University, United States, June 13, 2013.

30. McCoy, A.T.; Bartels, M.J.; Rick, D.L.; Saghir, S.A. TK Modeler version 1.0, a Microsoft® Excel®-based modeling software for the prediction of diurnal blood/plasma concentration for toxicokinetic use. Regul. Toxicol. Pharmacol. 2012, 63(2), 333-343. DOI: 10.1016/j.yrtph.2012.04.002

31. Mengozzi, G.; Intorre, L.; Bertini, S.; Giorgi, M.; Soldani, G. Comparative bioavailability of two sustained-release theophylline formulations in the dog. Pharmacol. Res. 1998, 38(6), 481-485. DOI: 10.1006/phrs.1998.0394

32. Thron, C.D. Linearity and superposition in pharmacokinetics. Pharmacol. Rev. 1974, 26(1), 3-31.

33. Tuntland, T.; Ethell, B.; Kosaka, T.; Blasco, F.; Zang, R.X.; Jain, M.; et al. Implementation of pharmacokinetic and pharmacodynamic strategies in early research phases of drug discovery and development at Novartis Institute of Biomedical Research. Front. Pharmacol. 2014, 5, 174. DOI: 10.3389/fphar.2014.00174

34. Van Rossum, J.M.; de Bie, J.E. Systems dynamics in clinical pharmacokinetics. An introduction. Clin. Pharmacokinet. 1989, 17(1), 27-44. DOI: 10.2165/00003088-198917010-00003

35. Peletier, L.A.; de Winter, W. Impact of saturable distribution in compartmental PK models: dynamics and practical use. J. Pharmacokinet. Pharmacodyn. 2017, 44(1), 1-16. DOI: 10.1007/s10928-016-9500-2

36. Gabrielsson, J.; Meibohm, B.; Weiner, D. Pattern Recognition in pharmacokinetic data analysis. AAPS J. 2016, 18(1), 47-63. DOI: 10.1208/s12248-015-9817-6

37. Mehrotra, N.; Gupta, M.; Kovar, A.; Meibohm, B. The role of pharmacokinetics and pharmacodynamics in phosphodiesterase-5 inhibitor therapy. Int. J. Impot. Res. 2007, 19(3), 253-264. DOI: 10.1038/sj.ijir.3901522

38. Shen, J.; Boeckmann, A.; Vick, A. Implementation of dose superimposition to introduce multiple doses for a mathematical absorption model (transit compartment

model). J. Pharmacokinet. Pharmacodyn. 2012, 39(3), 251-262. DOI: 10.1007/s10928-012-9247-3

39. Siwale, R.C.; Sani, S. N. Multiple-Dosage Regimens. In: Applied Biopharmaceutics & Pharmacokinetics, 8th ed.; Ducharme, M.P., Shargel, L., Eds.; McGraw Hill Education, 2022; pp. 205-228.

40. Mehvar, R. Dependence of time to reach steady-state on the length of dosage interval. Ann. Pharmacother. 2008, 42(10), 1518-1519. DOI: 10.1345/aph.1L251

41. Hieb, B.R.; Shrewsbury, B. Consecutive intravenous infusions: simulation of two compartment pharmacokinetic drugs. Comput. Methods Programs Biomed. 1980, 12(2-3), 96-104. DOI: 10.1016/0010-468X(80)90055-0

42. Brocks, D.R.; Mehvar, R. Rate and extent of drug accumulation after multiple dosing revisited. Clini. Pharmacokinet. 2010, 49(7), 421-438. DOI: 10.2165/11531190-000000000-00000

43. Van Rossum, J.M.; Van Lingen, G.; Burgers, J.P.T. Dose-dependent pharmacokinetics. Pharmacol. Ther. 1983, 21(1), 77-99. DOI: 10.1016/0163-7258(83)90068-2

44. Nation, R.L.; Evans, A.M.; Milne, R.W. Pharmacokinetic drug interactions with phenytoin (Part I). Clini. Pharmacokinet. 1990, 18(1), 37-60. DOI: 10.2165/00003088-199018010-00003

45. Yáñez, J.A.; Remsberg, C.M.; Sayre, C.L.; Forrest, M.L.; Davies, N.M. Flip-flop pharmacokinetics--delivering a reversal of disposition: challenges and opportunities during drug development. Ther. Deliv. 2011, 2(5), 643-672. DOI: 10.4155/tde.11.19

46. Stewart, B.H.; Kugler, A.R.; Thompson, P.R.; Bockbrader, H.N. A saturable transport mechanism in the intestinal absorption of gabapentin is the underlying cause of the lack of proportionality between increasing dose and drug levels in plasma. Pharm Res. 1993, 10, 276-81. DOI: 10.1023/A:1018951214146

47. Proctor, W.R.; Bourdet, D.L.; Thakker, D.R. Mechanisms underlying saturable intestinal absorption of metformin. Drug Metab. Dispos. 2008, 36(8), 1650-1658. DOI: 10.1124/dmd.107.020180

48. Hanada, K.; Ikemi, Y.; Kukita, K.; Mihara, K.; Ogata, H. Stereoselective first-pass metabolism of verapamil in the small intestine and liver in rats. Drug Metab. Dispos. 2008, 36(10), 2037-2042. DOI: 10.1124/dmd.107.020339

49. Kalam, M.N.; Rasool, M.F.; Rehman, A.U.; Ahmed, N. Clinical pharmacokinetics of propranolol hydrochloride: a review. Curr. Drug Metab. 2020, 21(2), 89-105. DOI: 10.2174/1389200221666200414094644

50. Karlsson, M.O.; Molnar, V.; Freijs, A.; Nygren, P.; Bergh, J.; Larsson, R. Pharmacokinetic models for the saturable distribution of paclitaxel. Drug Metab. Dispos. 1999, 27(10), 1220-1223.

51. Eling, T.E.; Pickett, R.D.; Orton, T.C.; Anderson, M.W. A study of the dynamics of imipramine accumulation in the isolated perfused rabbit lung. Drug Metab. Dispos. 1975, 3(5), 389-399.

52. Ha, H.R.; Chen, J.; Freiburghaus, A.U.; Follath, F. Metabolism of theophylline by cDNA-expressed human cytochromes P-450. Br. J. Clin. Pharmacol. 1995, 39(3), 321-326. DOI: 10.1111/j.1365-2125.1995.tb04455.x

53. Bernus, I.; Dickinson, R.G.; Hooper, W.D.; Eadie, M.J. Dose-dependent metabolism of carbamazepine in humans. Epilepsy Res. 1996, 24(3), 163-172. DOI: 10.1016/0920-1211(96)00011-3

54. Patel, B.A.; Chu, C.K.; Boudinot, F.D. Pharmacokinetics and saturable renal tubular secretion of zidovudine in rats. J. Pharm. Sci. 1989, 78(7), 530-534. DOI: 10.1002/jps.2600780704

55. Hendel, J.; Nyfors, A. Nonlinear renal elimination kinetics of methotrexate due to saturation of renal tubular reabsorption. Eur. J. Clin. Pharm. 1984, 26, 121-124. DOI: 10.1007/BF00546719

56. Babu, E.; Takeda, M.; Narikawa, S.; Kobayashi, Y.; Yamamoto, T.; Cha, SH, et al. Human organic anion transporters mediate the transport of tetracycline. JPN. J. Pharmcol. 2002, 88(1), 69-76. DOI: 10.1254/jjp.88.69

57. Hornecker, M.; Blanchet, B.; Billemont, B.; Sassi, H.; Ropert, S.; Taieb, F.; et al. Saturable absorption of sorafenib in patients with solid tumors: a population model. Invest. New Drug. 2012, 30, 1991-2000. DOI: 10.1007/s10637-011-9760-z

58. Graham, R.A.; Hop, C.E.C.A.; Borin, M.T.; Lum, B.L.; Colburn, D.; Chang, I.; et al. Single and multiple dose intravenous and oral pharmacokinetics of the hedgehog pathway inhibitor vismodegib in healthy female subjects. Br. J. Clin. Pharmacol. 2012, 74(5), 788-796. DOI: 10.1111/j.1365-2125.2012.04281.x

59. Yoon, Y-R.; Shin, J-G.; Cha, I-J.; Kim, K-A.; Shim, J-C.; Kim, Y-H.; et al. Pharmacokinetic analysis on autoinduction of carbamazepine metabolism. J. Korean Soc. Clin. Pharmacol. Ther. 1996, 4(2), 139-147. DOI: 10.12793/jkscpt.1996.4.2.139

60. Chetty, M.; Miller, R.; Seymour, M.A. Phenytoin auto-induction. Ther. Drug Monit. 1998, 20(1), 60-62. DOI: 10.1097/00007691-199802000-00011

61. Shand, D.G.; Hammill, S.C.; Aanonsen, L.; Pritchett, E.L.C. Reduced verapamil clearance during long-term oral administration. Clin. Pharmacol. Ther. 1981, 30(5), 701-703. DOI: 10.1038/clpt.1981.223

62. Abernethy, D.R.; Wainer, I.W.; Anacleto, A.I. Verapamil metabolite exposure in older and younger men during steady-state oral verapamil administration. Drug Met. Dispos. 2000, 28(7), 760-765.

63. Lalonde, R.L.; Pieper, J.A.; Straka, R.J. Bottorff, M.B.; Mirvis, D.M. Propranolol pharmacokinetics and pharmacodynamics after single doses and at steady-state. Eur. J. Clin. Pharmacol. 1987, 33, 315-318. DOI: 10.1007/BF00637569

64. Barone, J.A.; Koh, J.G.; Bierman, R.H.; Colaizzi, J.L.; Swanson, K.A.; Gaffar, M.C.; et al. Food interaction and steady-state pharmacokinetics of itraconazole capsules in

healthy male volunteers. Antimicrob. Agents and Chemother. 1993, 37(4), 778-784. DOI: 10.1128/AAC.37.4.778

65. Vrijens, B.; Goetghebeur, E. The impact of compliance in pharmacokinetic studies. Stat. Methods Med. Res.1999, 8(3), 247-262. DOI: 10.1177/096228029900800305

66. Martinez, M.N.; Amidon, G.L. A mechanistic approach to understanding the factors affecting drug absorption: a review of fundamentals. J. Clin. Pharmacol. 2002, 42(6), 620-643. DOI: 10.1177/00970002042006005

67. Singh, B.N. Effects of food on clinical pharmacokinetics. Clin. Pharmacokinet. 1999, 37(3), 213-255. DOI: 10.2165/00003088-199937030-0000368.

68. Gershkovich, P.; Hoffman, A. Effect of a high-fat meal on absorption and disposition of lipophilic compounds: the importance of degree of association with triglyceride-rich lipoproteins. Eur. J. Pharm. Sci. 2007, 32(1), 24-32. DOI: 10.1016/j.ejps.2007.05.109

69. Yousef, M.; Silva, D.; Bou-Chacra, N.; Davies, N.M.; Löbenberg R. The lymphatic system: A sometimes forgotten compartment in pharmaceutical sciences. J. Pharm. Pharm. Sci. 2021, 24, 533-547. DOI: 10.18433/jpps32222

70. König, J.; Müller, F.; Fromm, M.F. Transporters and drug-drug interactions: important determinants of drug disposition and effects. Pharmacol. Rev. 2013, 65(3), 944-966. DOI: 10.1124/pr.113.007518

71. Tornio, A.; Filppula, A.M.; Niemi, M.; Backman, J.T. Clinical studies on drug–drug interactions involving metabolism and transport: methodology, pitfalls, and

interpretation. Clin. Pharmacol. Ther. 2019, 105(6), 1345-1361. DOI: 10.1002/cpt.1435

72. Hall, S.D.; Thummel, K.E.; Watkins, P.B.; Lown, K.S.; Benet, L.Z.; Paine, M.F.; et al. Molecular and physical mechanisms of first-pass extraction. Drug Met. Dispos. 1999, 27(2), 161-166.

73. Bachmann, K. Drug–drug interactions with an emphasis on drug metabolism and transport. In: Pharmacology Principles and Practice, Hacker, M., Messer, W., Bachmann, K., Eds.; Academic Press: Massachusetts, United States, 2009; pp. 303-325. DOI: 10.1016/B978-0-12-369521-5.00012-9

74. DeVane, C.L. Clinical significance of drug binding, protein binding, and binding displacement drug interactions. Psychopharmacol. Bull. 2002, 36(3), 5-21.

75. Heuberger, J.; Schmidt, S.; Derendorf, H. When is protein binding important? J. Pharm. Sci. 2013, 102(9), 3458-3467. DOI: 10.1002/jps.2355

Appendix 4

Revisiting the Biopharmaceutics Classification System (BCS) for More Representative Bioequivalence Determination

According to the Biopharmaceutics Classification System (BCS) developed by Amidon *et al.*, drugs are categorized into four classes based on their solubility and permeability characteristics: Class I (high solubility and high permeability), Class II (low solubility and high permeability), Class III (high solubility and low permeability) and Class IV (low solubility and low permeability) (A4.1). According to this system, the key drug-related parameters controlling oral absorption and thus bioavailability are the solubility/dissolution of the drug in gastrointestinal (GI) fluid and the ability of the drug to traverse the GI membrane. It is a rule of thumb that for the drug to be absorbed, it has to dissolve first (A4.2); therefore poor aqueous solubility has been linked to limited oral bioavailability. Additionally, challenges related to poor stability and membrane permeability exacerbate the problem of poor bioavailability (A4.3).

As a result, several formulation strategies have been devised for class II drugs to increase their dissolution rate or sustain solubilization, thereby enhancing their bioavailability. These strategies encompass techniques such as nanosizing, complexation and crystal engineering among others (A4.4, A4.5).

However, for a long time, the most effective solution to improve the bioavailability of BCS class IV drugs has been to revisit the lead optimization phase of drug discovery. This is because techniques used for BCS class II drugs generally have little impact on the absorption of class IV drugs due to their limited membrane permeability. Yet, various strategies have been developed to enhance the bioavailability of BCS class IV drugs. These include lipid-based drug delivery systems (LBDD), polymeric nanoparticulate systems, liquisolid technology, self-emulsifying solid dispersions, and P-gp efflux inhibition strategies to name a few (A4.6, A4.7).

LBDD represents a promising strategy due to its capacity to improve both gastrointestinal solubilization and absorption. This is achieved through a pathway that promotes selective intestinal lymphatic uptake via chylomicrons, as demonstrated in Chapter 5 (Figures 5.1, 5.2 and 5.4). Moreover, this approach has been proposed to address additional challenges associated with BCS class IV drug absorption, such as presystemic drug metabolism related to gut cytochrome P-450 enzymes and the P-glycoprotein efflux transporters (A4.6, A4.8). LBDD have also been employed to improve the bioavailability of class II drugs as well, again taking advantage of the lymphatic pathway of absorption and specifically though the chylomicrons pathway (A4.9, A4.10).

The BCS and its derived classification systems, such as the Biopharmaceutical Drug Disposition and Classification System (BDDCS), Extended Clearance Classification System (ECCS), and Extended Clearance Concept Classification System (ECCCS or EC3S), have demonstrated practical utility in bioequivalence determination and early prediction of clearance mechanisms. These systems, as detailed by Amidon *et al.* (A4.1), Benet (A4.11), Kunze *et al.* (A4.12), and Varma *et al.* (A4.13), respectively, have been instrumental during drug development in formulating approaches to enhance drug bioavailability and reduce the likelihood of drug-drug interactions.

In Chapter 9, the developed lymph-focused dissolution test highlighted that standard performance tests and compendia have traditionally focused on the portal absorption pathway, neglecting the lymphatic pathway and thereby missing a potential absorption pathway. The equations presented in Chapter 5, Section 5.1.2, demonstrated that a more representative general bioavailability equation would incorporate the absorption constants of both the portal and lymphatic pathways. It is now crucial to revisit the BCS and

reconsider its parameters to include one that reflects the lymphatic absorption pathway, particularly via chylomicrons. Introducing a subclass that reflects potential lymphatic affinity would encompass all possible absorption pathways, thereby enhancing the reliability of this classification in bioequivalence determination. Since lipid solubility is not the sole factor influencing drug uptake through the lymphatic pathway, and the association of drugs with chylomicrons is a reliable indicator of this process (A4.14, A4.15).

Using various molecular descriptors that have been correlated with *in-vivo* lymphatic uptake can assist in subclassifying drugs based on their potential for lymphatic absorption via the chylomicron pathway. The significance of these descriptors in influencing lymphatic uptake follows this order: hydrogen bond acceptors (HBA) > polar surface area (PSA) > solubility in long-chain triglycerides (SLCT) > logP > melting point (MP) > logD > molar volume (MV) > density > pKa > molecular weight (MW) > freely rotatable bonds (FRB) > hydrogen bond donors (HBD). While SLCT, logP, logD, MV, and MW positively influence drug association with chylomicrons, other molecular descriptors tend to reduce this association (A4.15). Also, establishing a standardized test to measure this parameter would be a significant advancement. The developed *in-vitro* model (Chapters 7 wand 8) serves as a starting point for this endeavor.

References

A4.1. Amidon GL, Lennernäs H, Shah VP, Crison JR. A theoretical basis for a biopharmaceutic drug classification: The correlation of *in-vitro* drug product dissolution and *in-vivo* bioavailability. Pharmaceutical Research. 1995;12(3):413-20.

A4.2. Mudie DM, Amidon GL, Amidon GE. Physiological parameters for oral delivery and *in-vitro* testing. Molecular Pharmaceutics. 2010;7(5):1388-405.

A4.3. Avdeef A. Physicochemical profiling (solubility, permeability and charge state). Current Topics in Medicinal Chemistry. 2001;1(4):277-351.

A4.4. Krishnaiah YSR. Pharmaceutical technologies for enhancing oral bioavailability of poorly soluble drugs. Journal of Bioequivalence & Bioavailability. 2010;2(2):28-36.

A4.5. Bhalani DV, Nutan B, Kumar A, Singh Chandel AK. Bioavailability enhancement techniques for poorly aqueous soluble drugs and therapeutics. Biomedicines. 2022;10(9):2055.

A4.6. Ghadi R, Dand N. BCS class IV drugs: Highly notorious candidates for formulation development. Journal of Controlled Release. 2017;248:71-95.

A4.7. Kumari L, Choudhari Y, Patel P, Gupta GD, Singh D, Rosenholm JM, et al. Advancement in solubilization approaches: A step towards bioavailability enhancement of poorly soluble drugs. Life. 2023;13(5):1099.

A4.8. Chakraborty S, Shukla D, Mishra B, Singh S. Lipid–an emerging platform for oral delivery of drugs with poor bioavailability. European Journal of Pharmaceutics and Biopharmaceutics. 2009;73(1):1-15.

A4.9. Elmowafy M, Al-Sanea MM. Nanostructured lipid carriers (NLCs) as drug delivery platform: Advances in formulation and delivery strategies. Saudi Pharmaceutical Journal. 2021;29(9):999-1012.

A4.10. Sri RM, Sangeetha S, Seetha DA. Solid lipid nanoparticles: A potential option for enhancing oral bioavailability of highly soluble and poorly permeable (BCS Class III) drugs. Current Drug Delivery. 2023;20(3):223-36.

A4.11. Benet LZ. Predicting drug disposition via application of a biopharmaceutics drug disposition classification system. Basic & clinical pharmacology & toxicology. 2010;106(3):162-7.

A4.12. Kunze A, Poller B, Huwyler J, Camenisch G. Application of the extended clearance concept classification system (ECCCS) to predict the victim drug-drug interaction potential of statins. Drug Metabolism and Personalized Therapy. 2015;30(3):175-88.

A4.13. Varma MV, Steyn SJ, Allerton C, El-Kattan AF. Predicting clearance mechanism in drug discovery: Extended clearance classification system (ECCS). Pharmaceutical Research. 2015;32:3785-802.

A4.14. Yousef M, Park C, Henostroza M, Bou Chacra N, Davies NM, Löbenberg R. Development of a novel *in-vitro* model to study lymphatic uptake of drugs via artificial chylomicrons. Pharmaceutics. 2023;15(11):2532.

A4.15. Lu Y, Qiu Y, Qi J, Feng M, Ju D, Wu W. Biomimetic reassembled chylomicrons as novel association model for the prediction of lymphatic transportation of highly lipophilic drugs via the oral route. International Journal of Pharmaceutics. 2015;483(1-2):69-76.